Trends in Mathematics

Valentin Bertsch
Wolf Fichtner
Vincent Heuveline
Thomas Leibfried
Editors

Advances in Energy System Optimization

Proceedings of the First International Symposium on Energy System Optimization

Birkhäuser

Trends in Mathematics

Trends in Mathematics is a series devoted to the publication of volumes arising from conferences and lecture series focusing on a particular topic from any area of mathematics. Its aim is to make current developments available to the community as rapidly as possible without compromise to quality and to archive these for reference.

Proposals for volumes can be submitted using the Online Book Project Submission Form at our website www.birkhauser-science.com.

Material submitted for publication must be screened and prepared as follows:

All contributions should undergo a reviewing process similar to that carried out by journals and be checked for correct use of language which, as a rule, is English. Articles without proofs, or which do not contain any significantly new results, should be rejected. High quality survey papers, however, are welcome.

We expect the organizers to deliver manuscripts in a form that is essentially ready for direct reproduction. Any version of TEX is acceptable , but the entire collection of files must be in one particular dialect of TEX and unified according to simple instructions available from Birkhäuser.

Furthermore, in order to guarantee the timely appearance of the proceedings it is essential that the final version of the entire material be submitted no later than one year after the conference.

More information about this series at http://www.springer.com/series/4961

Advances in Energy System Optimization

Valentin Bertsch · Wolf Fichtner
Vincent Heuveline · Thomas Leibfried
Editors

Proceedings of the First International Symposium on Energy System Optimization

Birkhäuser

Editors
Valentin Bertsch
Economic Analysis
The Economic and Social Research Institute
Dublin
Ireland

Wolf Fichtner
Karlsruhe Institute of Technology
Karlsruhe
Germany

Vincent Heuveline
University of Heidelberg
Heidelberg
Germany

Thomas Leibfried
Institute of Electric Energy Systems
and High-Voltage Technology
Karlsruhe Institute of Technology
Karlsruhe
Germany

ISSN 2297-0215 ISSN 2297-024X (electronic)
Trends in Mathematics
ISBN 978-3-319-51794-0 ISBN 978-3-319-51795-7 (eBook)
DOI 10.1007/978-3-319-51795-7

Library of Congress Control Number: 2016963161

Printed on acid-free paper

This book is published under the trade name Birkhäuser (www.birkhauser-science.com)
The registered company is Springer International Publishing AG
The registered company address is: Gewerbestrasse 11, 6330 Cham, Switzerland

Preface

This volume on *Advances in Energy System Optimization* contains a selection of peer-reviewed papers related to the presentations given at the first *International Symposium on Energy System Optimization (ISESO 2015)*. The symposium was held on November 9 and 10, 2015 at the Heidelberg Institute for Theoretical Studies (HITS) and was organized by HITS, Heidelberg University (Engineering Mathematics and Computing Lab, EMCL) and Karlsruhe Institute of Technology (Institute for Industrial Production, IIP, and Institute of Electric Energy Systems and High-Voltage Technology, IEH). The organizing institutes are working together within a research project funded by the DFG (Deutsche Forschungsgemeinschaft), in the context of which the symposium was initiated. Under the title "New Approaches to Integrated Energy Systems and Grid Modeling", the respective research groups from mathematics, energy economics and electrical engineering develop new algorithms designed to efficiently solve real-world energy problems. More than 50 international participants attended 21 international presentations from both, industry and academia, including 3 keynote presentations and 18 contributed papers in 7 sessions. The sessions focused on diverse challenges in energy systems, ranging from operational to investment planning problems, from market economics to technical and environmental considerations, from distribution grids to transmission grids and from theoretical considerations to data provision concerns and applied case studies. The papers in this volume are structured according to the order of the sessions within the symposium as outlined below:

- Demand Response and Distribution Grids
- Optimizing Transmission Grid Operation
- Flexibility, Storage and Uncertainty Quantification
- Challenges in Microgrids
- Renewable Energy and Power Grid Expansion Planning
- Data Provision for Power Grid Modeling
- Convex versus Nonconvex Approaches for Power Flow Analysis

ISESO was designed to bring together experts from different disciplines, such as mathematics, electrical engineering, economics and operations research with the

objective of fostering interdisciplinary discussions on how to tackle the many challenges facing today's and tomorrow's energy systems. Beyond the presentations, the symposium offered ample time for discussion and reflection, which was perceived very positively by all participants.

The editors of this volume served as the organizing committee. We wish to thank all reviewers as well as all individuals and institutions who worked hard, often invisibly, for their tremendous support. In particular, we thank Philipp Gerstner for the coordination of the local organization. Finally, we also wish to thank all participants and speakers for their contributions to making ISESO a success.

Dublin, Ireland — Valentin Bertsch
Karlsruhe, Germany — Wolf Fichtner
Heidelberg, Germany — Vincent Heuveline
Karlsruhe, Germany — Thomas Leibfried

Contents

Part I
Demand Response and Distribution Grids

An Evolutionary Algorithm for the Optimization of Residential Energy Resources

Ana Soares, Álvaro Gomes and Carlos Henggeler Antunes

Abstract Important changes are currently underway in electric power systems, namely concerning the integration of distributed generation based on renewables to cope with Green-House Gas (GHG) emissions and external energy dependency. Moreover, the introduction of new loads such as electric vehicles and other storage systems, as well as local micro-generation and the possibility of using demand as a manageable resource create new challenges for the overall power system optimization. The deployment of smart metering and advanced communications capabilities will allow power systems to be managed more in accordance with generation availability, demand needs, and network conditions. A key issue for this optimal management is the existence of dynamic tariffs, according to the availability of several resources, congestion situations, generation scheduling, etc. Dynamic tariffs foreshadow a more active role for the consumer / prosumer concerning electricity usage decisions (consumption, storage, generation, and exchanges with the grid), namely in the residential sector. Demand Response (DR) can be used in this context by residential end-users to make the most of energy price information, weather forecasts, and operational requirements (e.g., comfort) to minimize the electricity bill. Nevertheless, the implementation of DR actions require the time availability of residential end-users, data processing capability, and the need to anticipate the corresponding impacts on the electricity bill and end-users satisfaction regarding the quality of energy services in use. Energy management systems (EMS) capable of offering decision support should be used to assist end-users optimizing the integrated usage of all energy resources. A multi-objective model has been developed aimed at minimizing the electricity bill and the possible dissatisfaction caused to the end-user

A. Soares (✉) · Á. Gomes · C. Henggeler Antunes
Department of Electrical and Computer Engineering, University of Coimbra, Coimbra, Portugal
e-mail: argsoares@inescc.pt

Á. Gomes
e-mail: agomes@deec.uc.pt

C. Henggeler Antunes
e-mail: ch@deec.uc.pt

A. Soares · Á. Gomes · C. Henggeler Antunes
INESC Coimbra, Coimbra, Portugal

V. Bertsch et al. (eds.), *Advances in Energy System Optimization*,
Trends in Mathematics, DOI 10.1007/978-3-319-51795-7_1

by the implementation of DR actions. An evolutionary algorithm to cope with the multi-objective and combinatorial nature of the model has been developed, which is tailored to the physical characteristics of the problem, namely using adequate solution encoding schemes and customized operators. Simulation results show that significant savings might be achieved by optimizing load scheduling, local micro-generation, and storage systems including electric vehicles (EVs) in both grid-to-vehicle (G2V) and V2G (vehicle-to-grid) modes.

Keywords Evolutionary algorithm · Demand response · Load management · Multi-objective optimization

1 Introduction

Electric power systems are currently witnessing important changes concerning the evolution to smart(er) grids, which are expected to accommodate the output variability associated with large-scale distributed generation based on renewables and the requirements of new loads such as EVs, both in G2V and V2G modes, and other storage systems, as well as local micro-generation. Pervasive Information and Communication Technologies (ICT) will allow a better monitoring of all system components, including demand-side resources. Bidirectional flows of information between the utility and end-users endowed with smart metering, with dynamic tariffs as the pricing mechanism, anticipate a more active role for the consumer / prosumer concerning energy usage behaviors and decisions (consumption, storage, generation, and exchanges with the grid) [6]. These decisions entail determining electricity flows between the grid, end-use loads, storage systems (either stationary or the EV), and local micro-generation. The aim is minimizing the electricity bill without jeopardizing the quality of the energy services provided by end-use loads. DR [1, 7] can be used in this setting to make the most of energy price information, weather forecasts, and operational requirements (e.g., comfort) to minimize the electricity bill.

Nonetheless, the implementation of DR actions is not straightforward to residential end-users mainly due to their necessary availability to engage in such actions, processing requirements of data originated from several sources, and the need to anticipate the corresponding impacts both on the electricity bill and the end-users satisfaction regarding the quality of energy services in use. EMS capable of offering decision support should then be used to assist end-users making optimal decisions on the integrated usage of all energy resources.

For this purpose a multi-objective model has been developed aimed at minimizing the electricity bill and the possible dissatisfaction caused to the end-user due to the implementation of DR actions, and exploring the trade-offs between these competing objectives. An evolutionary algorithm (EA) [4, 5] to cope with the multi-objective and combinatorial nature of the model has been designed. This EA has been tailored to the physical characteristics of the problem, namely using adequate solution encoding

schemes and customized operators that fit the type of load being managed and the corresponding DR actions.

In addition to the technical restrictions associated with the manageable loads [11], operational and quality of service constraints are also included into the model, namely time slots for allocating shiftable loads, temperature bounds for thermostatically controlled loads, desired state of charge (SoC) of the EVs battery and stationary storage system. The cost objective function takes into account dynamic tariffs. The dissatisfaction objective function encompasses penalties associated with:

- allocating the working cycles of the shiftable loads in less preferred time slots;
- not respecting the desired level of the SoC of the EVs battery when using the EV in V2G mode;
- assessing the temperature deviation caused by the DR actions when compared to the reference case with no DR actions implemented in thermostatically controlled loads;
- preventing the interruption of energy supply due to overcoming the contracted power.

Simulation results show that significant savings might be achieved by such EMS comparing to a reference case without an EMS installed. These savings are due to the optimized management of end-use loads, local micro-generation, and storage systems including the EV in V2G mode.

The remainder of the paper is structured as follows. Section 2 focuses on methodology issues, namely the customization of the EA, the solution encoding and the operators. Section 3 presents some simulation results. Conclusions are drawn in Sect. 4.

2 Methodology

Optimization algorithms have been extensively used to manage energy resources [12]. Although a considerable number of works focus on the end-users perspective aiming at reducing electricity costs [2, 9], other point of views recognize the need of an aggregator to optimize the use of energy resources according to the objectives of multiple entities [1, 3, 8]. The aggregator is mostly used for dealing with energy flows associated with EVs either in V2G and G2V modes.

This work differs from previous ones since it aims at an integrated optimization of multiple residential energy resources [11] through the implementation of a wide range of DR actions. The impact of the DR actions is assessed through the use of:

- physically based models to reproduce the power profile of thermostatically controlled loads;
- a generic dynamic model parameterized to represent the stationary storage system;
- real data for shiftable loads;
- set of rules based on real data for EVs when used in the G2V mode.

The EV can be used under two different modes: either as a load that only consumes energy (G2V) or as a stationary system that can sell stored energy to the grid or use it for self-consumption when kWh prices are high (V2G). In this latter option the EV is expected to be fully charged by a certain hour; otherwise, there is a dissatisfaction penalty associated with not meeting this requirement.

The flowchart of the optimization approach is displayed in Fig. 1. The underlying mathematical model is based on the one presented in [10]. The objective functions are:

- the minimization of the energy acquisition cost from the grid, which includes the revenue from injecting energy into the grid whenever possible and the revenue associated with responding to grid request signals (either for rising or decreasing demand in a given time slot);
- the minimization of the end-users potential dissatisfaction caused by the implementation of DR actions. This dissatisfaction includes normalized:
  - time slot penalties associated with the allocation of shiftable loads in the planning period (similar to what is presented in [10]);
  - temperature penalties for DR actions implemented over a given thermostatically controlled load causing an increase/decrease of temperature outside the range associated with the regular working cycle. These penalties increase exponentially with the absolute difference between the controlled temperature, in a given interval, and the maximum/minimum expected temperature during the regular working cycle;
  - penalty associated with the use of the EV in V2G mode and the desired requirement of achieving a minimum SoC by the end of the planning period;
  - penalty for the peak of the resulting load diagram being too close to the contracted power (as a surrogate to reduce risk of supply interruptions);
  - penalty for exceeding the contracted power.

Although the model does not include the cost of the power component and thus the associated savings are not accounted for, the algorithm is also able to reduce peak power. This means that higher savings can be achieved by reducing the level of the contracted power, according to the Portuguese pricing scheme. Therefore, a penalty for being too close to the contracted power and other one for exceeding this threshold are considered. This latter penalty exponentially increases with the number of algorithm iterations and is extremely high to exclude combinations of DR actions leading to exceed the contracted power. Thus, during the fitness assessment process, solutions exceeding the contracted power will have their rank strongly penalized and will hardly be considered for the next generation.

The set of constraints include:

- end-users time slot preferences for allocating shiftable loads;
- end-users temperature thresholds for thermostatically controlled loads;
- end-users desired SoC for the EVs battery in the V2G mode (not mandatory);
- the value of the contracted power.

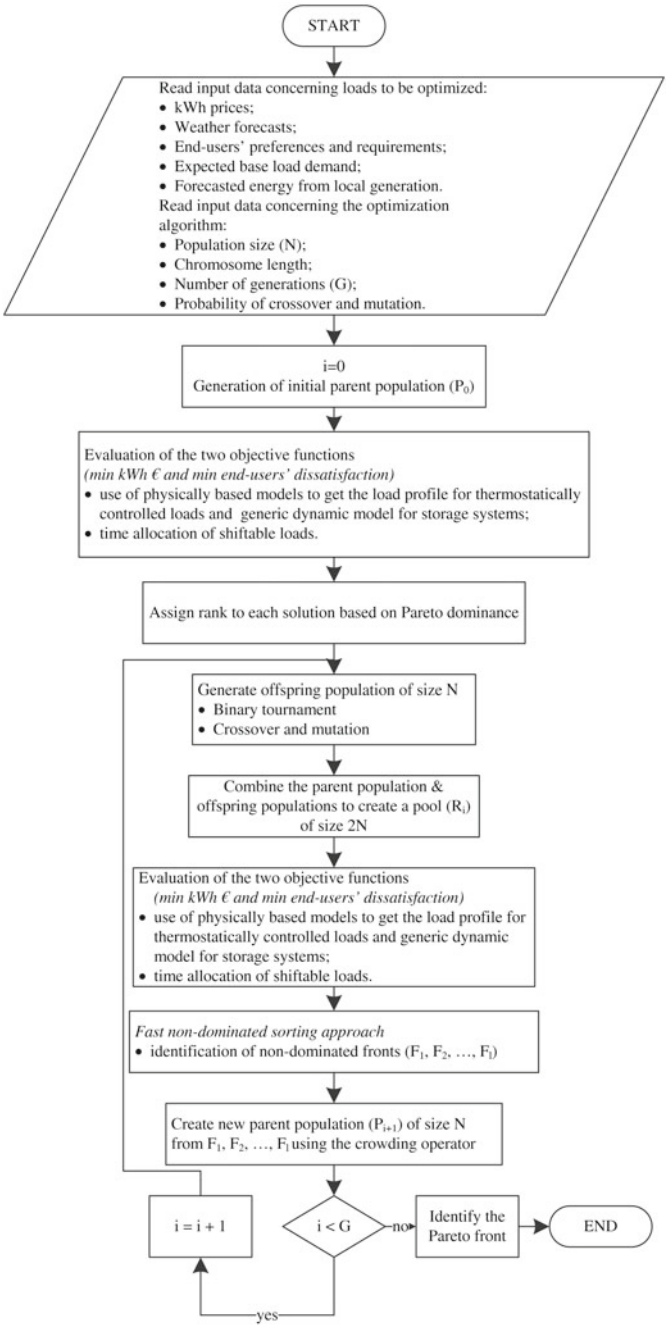

Fig. 1 Flowchart

Time slots preferences are dealt with either as hard constraints or soft constraints. The choice depends on the flexibility to be allowed in the model and the residential end-users profile. When using time slot preferences as hard constraints, it is assumed that the end-user has some knowledge of the duration of the working cycle to be scheduled and, therefore, time slots with a shorter duration than the working cycle of the load to be allocated are excluded. This option, although assuring that end-users dissatisfaction is minimized, may also reduce the number of time slots available for scheduling shiftable loads and consequently also lead to lower savings. On the other hand, using time slot preferences as soft constraints allows shaping time slots by increasing their duration when this is not adequately set. This may lead to higher savings but the end-users dissatisfaction may also increase.

Technical restrictions are also considered in the model and influence the way evolutionary operators are used. Therefore, operators are specialized and customized according to the segment of the chromosome (i.e., load) where they are applied and represent different DR actions over different loads. Since the solution encoding respects the different nature of manageable loads (by segmenting the chromosome according to the type of DR actions allowed), the customized operators act independently for each segment (Fig. 2).

The initial population is randomly generated, although a certain diversity is induced in the population at the outset by forcing the existence of "extreme" individuals concerning the chromosome segments corresponding to thermostatically

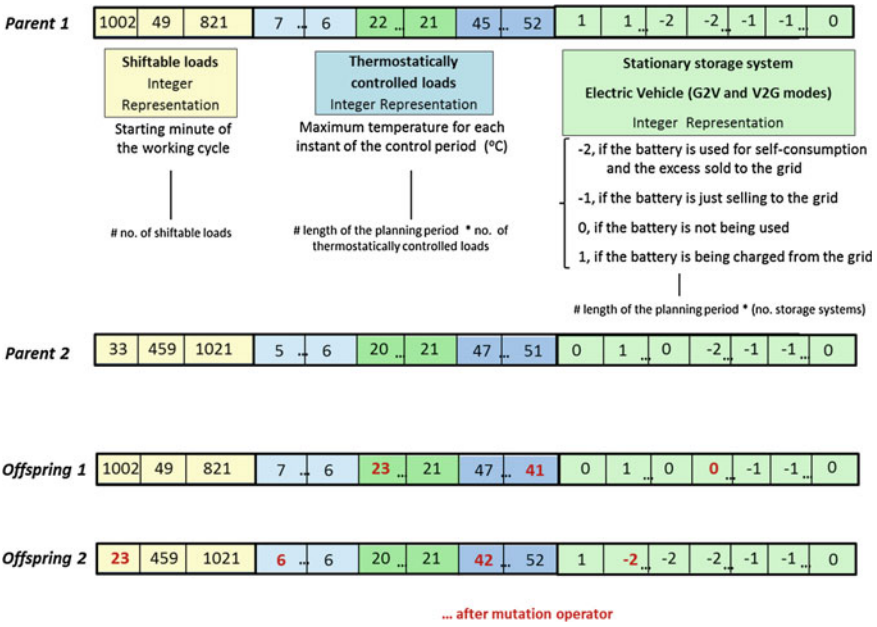

Fig. 2 Example of the solution encoding and use of the crossover and mutation operators [13]

controlled loads. Two dissimilar individuals are generated, one with the maximum and the other with the minimum allowable temperatures according to the regular working cycles of those loads. Concerning the storage system (including the EV in the V2G mode), the decisions are made based on price information. When the kWh price is below the average within the planning period, then the decision is charge from the grid. In kWh price peaks the decision is self-consumption and the remaining energy is injected into the grid. The storage system decision is randomly generated when the kWh price is above the average value within the planning period.

For the sake of preserving the physical characteristics of the loads being managed, the crossover operator never splits the segments of the chromosome corresponding to each load. Accordingly, each segment of the chromosome has its own probability for the crossover operator.

The mutation operator was also customized to the physical characteristics of loads in the following way:

- in shiftable loads it modifies the starting minute of the working cycle;
- in thermostatically controlled loads it slightly changes the maximum temperature allowable within the end-user's preferences;
- in the EVs battery in both G2V and V2G modes it modifies the integer representation within the range [−2;1], which encodes the type of battery usage (Fig. 2).

The probability of the mutation operator was tuned by experimentation and according to the physical characteristics of the managed loads. Therefore, the probability of the mutation operator is higher for thermostatically controlled loads than for shiftable loads.

It is important to note that this strategy is able to deal with unexpected changes of the input information (including a sudden increase in the base load, i.e. the uncontrollable load that cannot be the target of DR actions) or requests from the grid. Thus, if for some reason the end-user changes the loads to be scheduled, or the set point temperatures of any thermostatically controlled load, or the time slot preferences for shiftable loads, the evolutionary approach will swiftly re-compute new solutions from that point in time to the end of the planning period taking into account the loads that have already run and the current state of loads running (e.g. temperatures and SoC). If there is a sudden rise of the base load, which might cause the interruption of the energy supply due to exceeding the contracted power, then the optimization process reacts by interrupting the working cycle of any shiftable or thermostatically controlled load and turning them back on as soon as the base load is back to a lower value that does not compromise the energy supply.

Concerning grid signals, incentives are offered to the end-user to positively react to them. Thus, if the end-user allows the EMS to make automated decisions concerning these signals, higher savings may be achieved. Depending on the nature of these signals, the optimization process may decrease or increase demand in the time slot corresponding to the request signal. However, if the incentive is not economically attractive from the end-users point of view, then the decision of the EMS may just be "disregard the request" and no re-computation would be needed.

3 Simulation Results

For simulation purposes a case study including multiple manageable loads was designed. Three shiftable loads and three thermostatically controlled loads were considered, as well as an EV operating in V2G and G2V modes. A local PV micro-generation system was also considered. The energy locally produced is firstly used for self-consumption and the remainder, if any, is injected into the grid with a revenue of 80% of the kWh buying price. Dynamic tariffs are known one day and a half in advance, as well as weather forecasts for temperature and expected local generation.

The time step used for simulation purposes is 1 minute in a planning period of 36 hours. A short time step is crucial to assure the integrated optimization accounting for situations in which there is a sudden rise of (uncontrollable) demand and consequently power peaks that may lead to the interruption of energy supply (due to overcoming the contracted power).

The evolutionary algorithm was tuned through extensive experimentation and the parameters are summarized in Table 1. Statistics concerning the results obtained for the solutions that individually optimize each objective function are summarized in Table 2 and Fig. 3. As it was already mentioned in Sect. 2, the operators are customized according to the technical features of the manageable loads and are used over the specific segment of the chromosome associated with each load.

The case study considers the management of a dishwasher, a laundry machine, a tumble dryer, a fridge, an air conditioner, an electric water heater and an EV. The EV is used in both V2G and G2V modes and a dissatisfaction penalty is assigned if a minimum SoC of 80% is not achieved. Weather and local generation forecasts, kWh price information, contracted power value, usage of hot water and end-user's preferences and requirements are used as inputs.

Table 1 EA parameters - 50 individuals; 1000 generations

Loads	Mutation	Crossover
Shiftable	0.2	0.5
Thermostatically controlled	0.6	0
EV (V2G and G2V modes)	0.9	0.3

Table 2 Results obtained for the solutions that individually optimize each objective function (30 EA runs, 50 individuals, 1000 generations)

	Energy Cost (€)	Dissatisfaction
Best	1.916	0.042
Worst	2.050	0.064
Average	1.980	0.050
Median	1.982	0.049

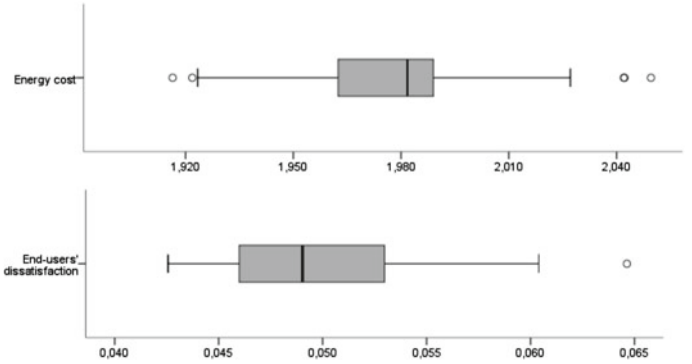

Fig. 3 Box plots for the solutions that individually optimize each objective function (30 EA runs, 50 individuals, 1000 generations). The *circles* denote outliers

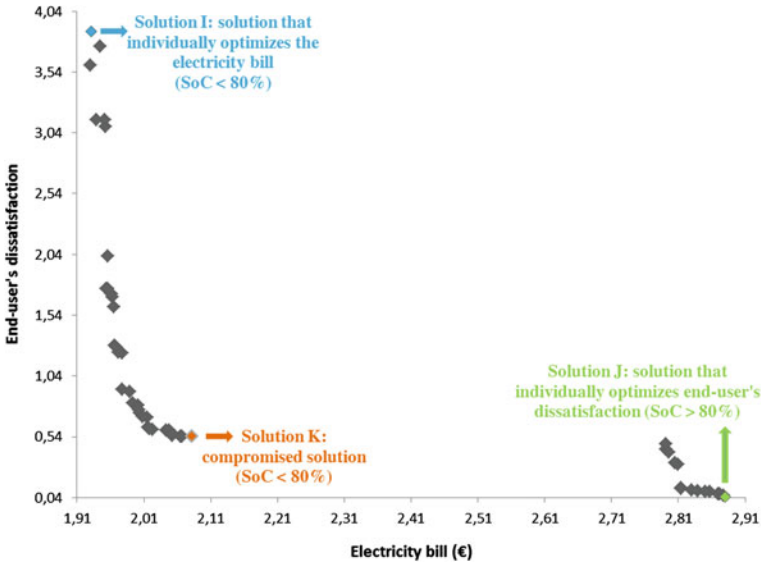

Fig. 4 Pareto optimal front

The Pareto optimal front obtained for this case study is displayed in Figs. 4 and 5. Three distinct regions can be identified in this front. Solutions with a lower electricity bill make an intensive use of the EV in V2G and G2V modes but do not achieve the minimum SoC of 80% and thus present a high dissatisfaction value. The SoC evolution is displayed in Fig. 6 for the solutions that individually optimize each objective function (solutions I and J) and for a compromise solution K. Although the SoC evolution looks similar in solutions I and K, the SoC by the end of the planning period in solution K is slightly higher.

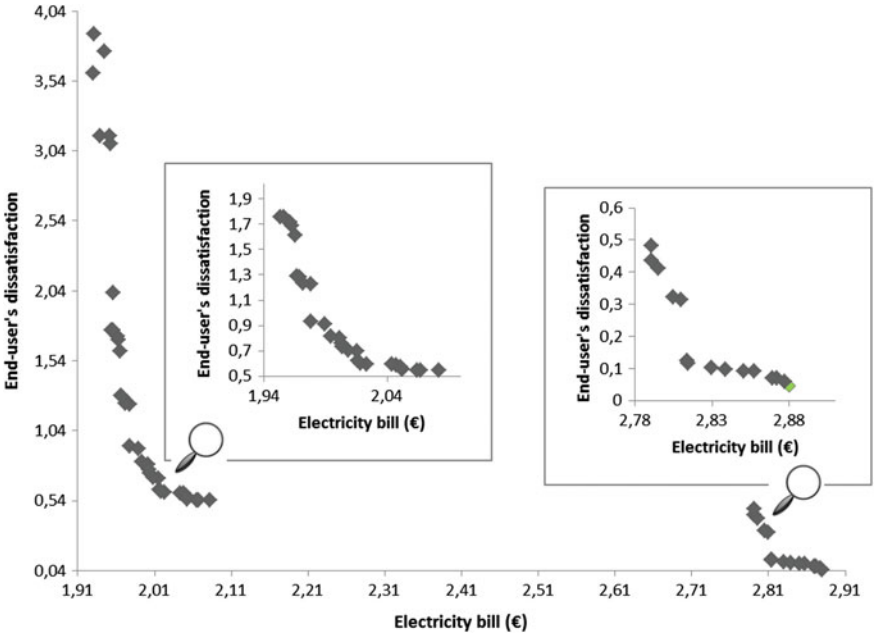

Fig. 5 Zoom of the Pareto optimal front

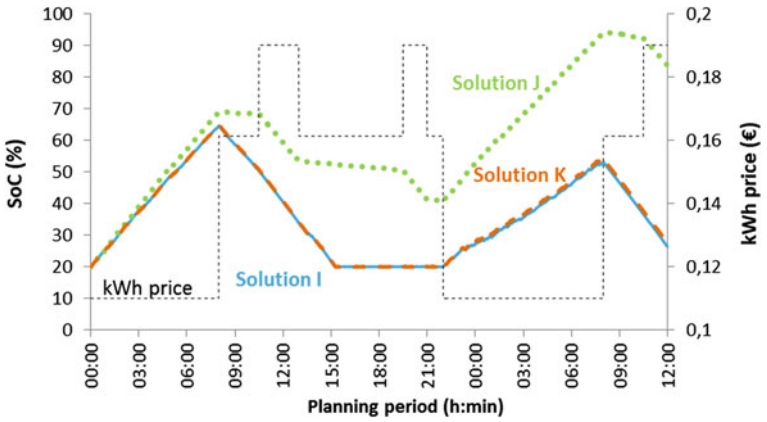

Fig. 6 Variation of SoC of the EV in the V2G and G2V modes

End-user's preferences for shiftable loads and their time allocation for solutions I and J are displayed in Figs. 7 and 8. Solution K is similar to solution J concerning the allocation of shiftable loads and therefore it is not displayed. It can be seen that the evolutionary algorithm allocates these loads in time slots with no penalty associated and simultaneously with the lower kWh price.

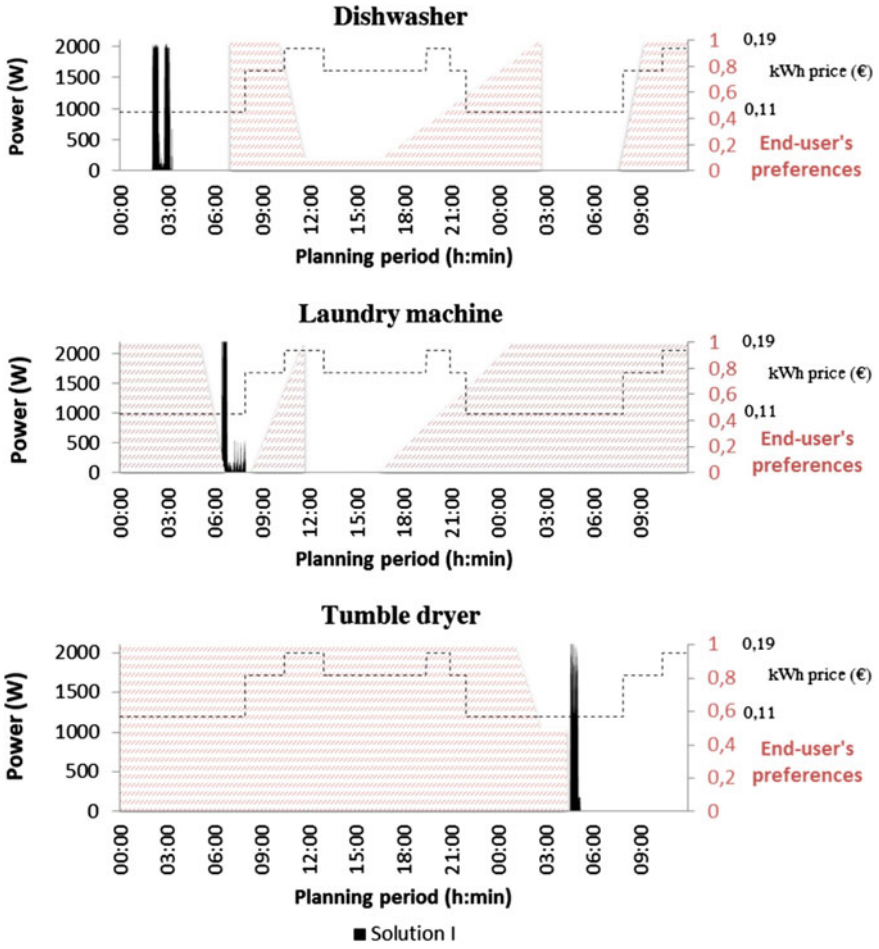

Fig. 7 Shiftable loads time slot preferences and time allocation for solution I

The impact of the DR actions over thermostatically controlled loads for solutions I, J and K is displayed in Fig. 9. Although there is a difference of about 0.95 € in objective function electricity bill between solutions I and J, it is important to note that this is mainly due to:

- not achieving the minimum SoC of 80% for the EV in solution I (less energy consumed for attaining the desired SoC and consequently a lower energy acquisition cost);

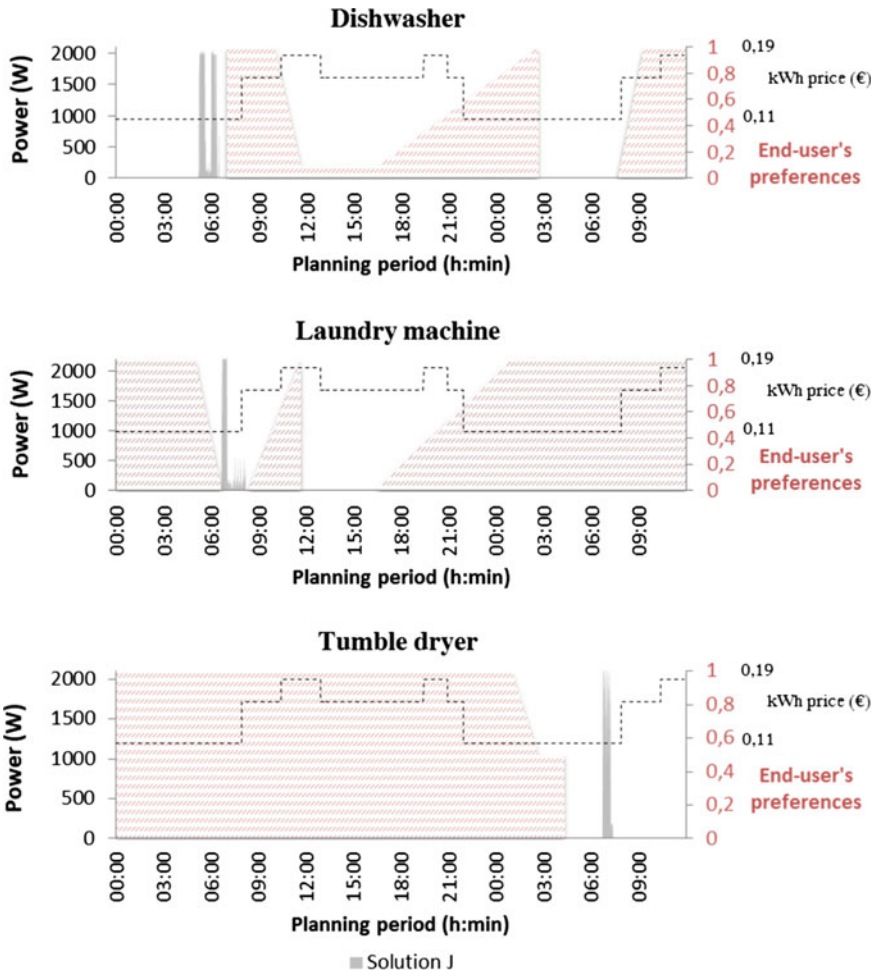

Fig. 8 Shiftable loads time slot preferences and time allocation for solution J

- letting the hot water temperature fall to about 48 °C average instead of 53 °C (average for solution J), which also represents less energy consumed and consequently a lower energy acquisition cost;
- letting indoor temperature rise to an average of 22 °C instead of 20 °C (average for solution J). Once again this situation leads to less energy consumed and consequently a lower energy acquisition cost.

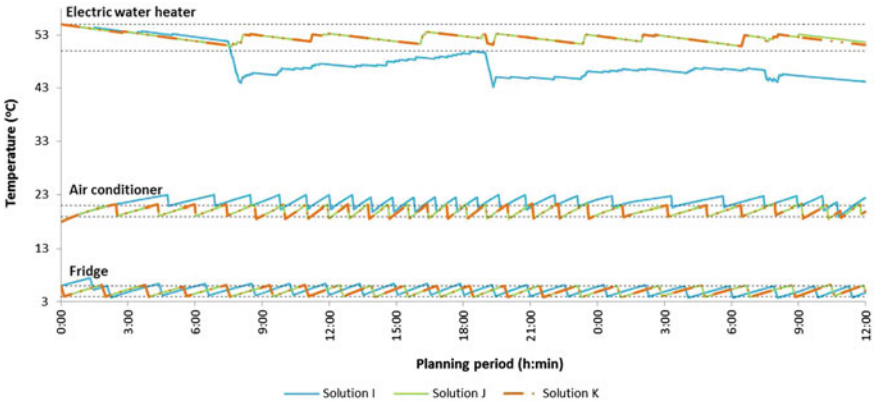

Fig. 9 Impact of DR actions over thermostatically controlled loads

4 Conclusion

This paper proposes a customized evolutionary algorithm to be embedded in a residential EMS to offer end-users an integrated management of energy resources balancing economic and quality of service evaluation dimensions. Customized solution encoding and operators were designed, which play a significant role in the optimization process of DR actions.

This approach operates in a near-real time environment and is able to swiftly obtain solutions when input information is changed or grid signals are received. In the case study herein presented, the day and a half electricity bill resulting from the optimization process varies between 1.93 and 2.88 €, trading-off with the dissatisfaction objective function. Comparing these results with a reference case study, a minimum saving of 10% can be easily achieved. This is mainly due to the use of the EV in the V2G mode, which is hardly achievable in a scenario where no energy management systems with adequate optimization algorithms are installed.

Future work will focus on robustness issues (i.e. guaranteeing that results are consistent when the input data including user's preferences slightly changes), the integration of the system intelligence in a hardware prototype displaying sensing and actuation capabilities to perform the DR actions, and the study of the end-user willingness to accept this type of automated control.

Acknowledgements This work has been developed under the Energy for Sustainability Initiative of the University of Coimbra and supported by Energy and Mobility for Sustainable Regions Project CENTRO-07-0224-FEDER-002004 and Fundação para a Ciência e a Tecnologia (FCT) under grant SFRH/BD/88127/2012 and project grants UID/ MULTI/00308/2013 and MITP-TB/CS/0026/2013.

References

1. Barbato A, Capone A, Carello G, Delfanti M, Falabretti D, Merlo M (2014) A framework for home energy management and its experimental validation. Energy Efficiency 7(6):1013–1052, doi:10.1007/s12053-014-9269-3, http://link.springer.com/10.1007/s12053-014-9269-3
2. Boaro M, Fuselli D, Angelis FD, Liu D, Wei Q, Piazza F (2012) Adaptive Dynamic Programming Algorithm for Renewable Energy Scheduling and Battery Management. Cognitive Computation 5(2):264–277, doi:10.1007/s12559-012-9191-y, http://link.springer.com/10.1007/s12559-012-9191-y
3. Carreiro AM, Oliveira C, Antunes CH, Jorge HM (2015) An Energy Management System Aggregator Based on an Integrated Evolutionary and Differential Evolution Approach. In: Applications of Evolutionary Computation - 18th European Conference, EvoApplications 2015, Copenhagen, Denmark, April 8-10, 2015, Proceedings, Springer International Publishing, pp 252–264, doi:10.1007/978-3-319-16549-3_21, http://link.springer.com/10.1007/978-3-319-16549-3_21
4. Deb K, Pratap A, Agarwal S, Meyarivan T (2002) A fast and elitist multiobjective genetic algorithm: NSGA-II. IEEE Transactions on Evolutionary Computation 6(2):182–197, doi:10.1109/4235.996017
5. Eiben AE, Smith JE (2003) Introduction to Evolutionary Computing. Springer, Berlin
6. Faruqui A, Sergici S, Akaba L (2013) Dynamic pricing of electricity for residential customers: the evidence from Michigan. Energy Efficiency 6(3):571–584, doi:10.1007/s12053-013-9192-z, http://link.springer.com/10.1007/s12053-013-9192-z
7. Gellings CW, Samotyj M (2013) Smart Grid as advanced technology enabler of demand response. Energy Efficiency 6(4):685–694, doi:10.1007/s12053-013-9203-0, http://link.springer.com/10.1007/s12053-013-9203-0
8. Gkatzikis L, Koutsopoulos I, Salonidis T (2013) The role of aggregators in smart grid demand response markets. IEEE Journal on Selected Areas in Communications 31(7):1247–1257, doi:10.1109/JSAC.2013.130708
9. Silva M, Morais H, Vale Z (2012) An integrated approach for distributed energy resource short-term scheduling in smart grids considering realistic power system simulation. Energy Conversion and Management 64:273–288, doi:10.1016/j.enconman.2012.04.021, http://linkinghub.elsevier.com/retrieve/pii/S0196890412002087
10. Soares A, Antunes CH, Oliveira C, Gomes A (2014) A multi-objective genetic approach to domestic load scheduling in an energy management system. Energy 77:144–152, doi:10.1016/j.energy.2014.05.101, http://linkinghub.elsevier.com/retrieve/pii/S0360544214006689
11. Soares A, Gomes A, Antunes CH (2014) Categorization of residential electricity consumption as a basis for the assessment of the impacts of demand response actions. Renewable and Sustainable Energy Reviews 30:490–503, doi:10.1016/j.rser.2013.10.019, http://linkinghub.elsevier.com/retrieve/pii/S1364032113007181
12. Soares A, Gomes A, Antunes CH (2015) Soft Computing Applications for Renewable Energy and Energy Efficiency. In: Cascales MdSG, Lozano JMS, Arredondo ADM, Corona CC (eds) Soft Computing Applications for Renewable Energy and Energy Efficiency, IGI Global, doi:10.4018/978-1-4666-6631-3, http://services.igi-global.com/resolvedoi/resolve.aspx?doi=10.4018/978-1-4666-6631-3
13. Soares A, Oliveira C, Gomes A, Antunes CH (2015) Integrated optimization of energy resources in a residential setting development of an energy management system. In: eceee 2015 Summer Study on energy efficiency, Belambra Presquîle de Giens, France

Comparison of Control Strategies for Electric Vehicles on a Low Voltage Level Electrical Distribution Grid

Simon Marwitz, Marian Klobasa and David Dallinger

Abstract If electrical energy demand is not balanced with electricity generation the results are additional electrical power grid investments and system stability risks. An increasing energy demand caused by charging plug-in electric vehicles (PEVs) is expected to affect distribution grid levels in the future. Uncontrolled PEV charging causes additional grid stress but PEVs are also capable of balancing the demand to the present supply situation via charging control strategies. Different control strategies for PEVs have been tested to address this issue. They can be classified as indirect, direct and autonomous control strategies. However, it is still under discussion, which charging strategy is best suited to integrate PEVs into feature dependent power generation on a distribution grid level. We investigated the advantages and weaknesses of autonomous control via local voltage measurement compared to direct and indirect charging control. Here we found that autonomous control of PEVs can counteract voltage dips caused by simultaneous charging. This is of great benefit for smart grids because autonomous control realised with PEVs internal systems can reduce the investment in communication technology on the infrastructure side. Nevertheless, this research also shows the limits of autonomous control. It can be concluded that a mix of different control strategies is necessary to realise PEVs demand response opportunities. Autonomous control will play an important role supporting the control of PEVs to stabilise smart grids.

Keywords Smart grid · Plug-in electric vehicles (PEVs) · Control strategies · Direct control · Indirect control · Autonomous control

S. Marwitz (✉) · M. Klobasa · D. Dallinger
Fraunhofer Institute for Systems and Innovation Research (ISI),
Competence Center Energy Technology and Energy Systems, Karlsruhe, Germany
e-mail: simon.marwitz@isi.fraunhofer.de

M. Klobasa
e-mail: marian.klobasa@isi.fraunhofer.de

V. Bertsch et al. (eds.), *Advances in Energy System Optimization*,
Trends in Mathematics, DOI 10.1007/978-3-319-51795-7_2

1 Introduction

With high penetration rates of plug-in electric vehicles (PEVs) an increasing electricity demand especially at low voltage distribution grid level occurs. This could overcharge the grid if these additional consumers are not sufficiently controlled [1–4].

Therefore a high number of different control strategies were recently introduced to manage PEVs charging behaviour. The goal of these strategies is to integrate PEVs into electrical distribution grids by utilising low electricity prices and/or by providing ancillary services for stable grid operation. Furthermore, control strategies are used to minimise power losses, avoid thermal overstress of grid assets and voltage violations [5–8].

Control strategies differ primarily in terms of user acceptance, complexity of information and communications technology (ICT) and final decision-making authority over the charging process [9].

In [10, 11] control strategies are categorised into direct and indirect methods. Within direct control, a central aggregation unit is allowed to control the charging of the PEVs. For indirect control the end user decides on the basis of (price)-incentives and is therefore finally in control of the PEV charging process [12]. Reference [9] adds an autonomous category where the PEV itself manages its charging process based on grid signals.

Direct control strategies require bidirectional ICT to provide PEV driver information to the aggregator and to allow the aggregator remote charging control over the PEV [1, 4, 13]. The goal of direct control can be efficient market integration as well as frequency and local voltage control [10, 14, 15].

Within indirect control strategies PEV users receive price incentives to schedule charging. These incentives are transported statically via time of use (TOU) or dynamic via critical peak pricing (CPP) and real-time pricing (RTP) [11, 16, 17]. These pricing methods are also referred to as price-based demand response [12]. For indirect control PEV users receive information but do not provide information to a central unit in contrast to direct control, hence only unidirectional ICT is required. Within the indirect control strategy PEV users decide whether they react to the price incentives, and therefore have final control over the charging process [9, 12].

Autonomous control strategies take only the information of available sensors[1] into consideration to schedule real and reactive power demand [6, 7]. Therefore, PEVs controlled by this strategy need a device to measure node voltage and power electronics, which are capable of responding; ICT is not required. If PEVs are additionally equipped with ICT, this approach has to be considered as direct or indirect control strategy with grid monitoring.

Which type of control strategy should be used in a future smart grid is still under discussion. The literature lacks comparisons between direct, indirect and autonomous control. Here we compare these strategies by focusing on the capability to avoid grid

[1] E.g. frequency or voltage measurement at the grid connection point.

overstress in terms of voltage violations. Therefore, we build a computer model, which simulates these control strategies and evaluates their grid impact.

In Sect. 2 we describe a grid topology with connected consumers where we test the control strategies introduced in Sect. 3. In particular we describe a direct strategy with perfect charging control via a central aggregator, an indirect strategy using a static TOU tariff to schedule PEV charging and an autonomous control strategy which feeds in reactive power as a function of the node voltage. In Sect. 4 we show the impact of these strategies on grid voltages within our model. Additionally, we present a reference case, where the grid operates without connected PEVs. Conclusions are given in Sect. 5.

2 Network Model and Load Profiles

Within our alternating current (AC) simulation model we compare a direct, an indirect and an autonomous control strategy (see Sect. 3) on a single 10 node low voltage (LV)[2] test feeder by only varying PEVs control strategies. The test feeder is taken from [18]. With respect to DIN EN 50160 grid voltage should not be above or below 0.1 p.u more often than in 5% of all 10 min time intervals for one week at medium voltage (MV) and LV distribution grid level [19]. Here we contribute 30% (±0.03 p.u) to LV level.

For each control strategy every node is connected via a 30 m long cable of type NAYY-J 35 mm^2 to the next node. We assume symmetric load and a connected single dwelling unit (SDU) with a yearly electrical energy demand of 5000 kWh, without space heating, on very node. This refers to the average yearly electricity demand for a four person family home in Germany [20]. The simulation runs from Monday to Sunday for the transition season on a fine weather day. Therefore we use typical household profiles from reference [21] and aggregate them to a 15 min base. SDUs on node 4, 5, 6 and 9 cover their space heat demand by NSHs of type AEG 3 kW WSP 3010 [22] with a constant power demand of 6 kW from 10 pm to 4 am in the morning. This refers to an average space heating demand of approximately 190 m^2 net dwelling area for a newly built house [23]. For the indirect control strategy introduced in Sect. 3.2 we assume a TOU tariff with a low price period between 11 pm and 6 am for each day and high electricity prices for the rest of the time (see Fig. 1).

Furthermore, we assume a very high PEV penetration rate (50%) by connecting a separate PEV to node 2, 3, 6, 8 and 10 (see Fig. 2).

For each day and simulation run every PEV arrives at 7 pm with an empty battery on the same node and departs at 7 am the next morning fully charged. Furthermore, every PEV requires 25 kWh electrical energy a day, charges with 95% efficiency and provides a high maximal charging power of 18 kVA. The scenario is based on reference [18].

[2] 400 V phase to phase refers to 1-Volt-p.u.

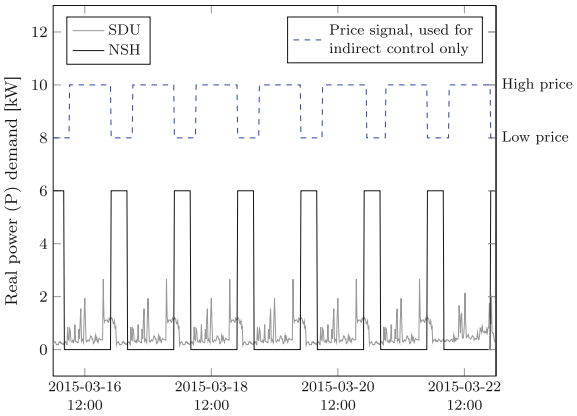

Fig. 1 Power profiles for single dwelling units (SDUs) [21] and night storage heaters (NSHs) [18] (*left axis*), as well as assumed high and low price time periods (*right axis*), both from Monday to Sunday during transition season

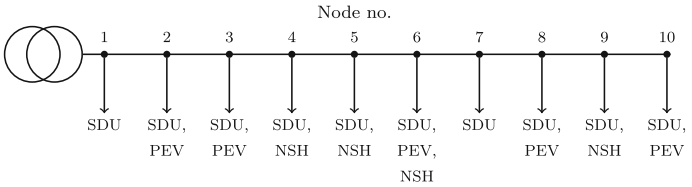

Fig. 2 Low voltage 10 node test feeder, with connected single dwelling units (SDUs), plug-in electric vehicles (PEVs) and night storage heaters (NSHs) (scenario base on [18])

3 Control Strategies

As reference [9] shows, control strategies for PEVs can be classified into direct, indirect and autonomous control. Here we describe how we implement these strategy types in an alternating current (AC) distribution grid simulation by schedule PEVs electrical power demand.

3.1 Direct Control with a Central Aggregator

For our direct charging control strategy the charging behaviour for all connected PEVs is controlled by a central aggregator with perfect foresight.

Here the aggregator defines a maximal allowed power demand ($P_{max,n,t}$) for every node n and and every time step t to avoid grid overstress. The aggregator finds $P_{max,n,t}$ by rising monotonously the combined nodal power $P_{n,t}$ just before the voltage on node 10 violates the 0.97 p.u boundary. Furthermore, we assume that the aggregator

knows the preferences of all PEVs users and can therefore prioritise PEVs charging by putting them into an ordered charging queue. In this study the aggregator orders PEVs priority by their connected node number in ascending order, hence the PEV on node 2 has the highest priority. After PEVs are prioritised, the aggregator evaluates for every t if there are one or more PEVs with less than 100% state of charge (SOC) connected to the grid. If this is true, he picks the highest prioritised PEV with SOC below 100%.

Within our perfect control assumption the aggregator knows the maximal charging power, as well as the time of arrival and departure for every PEV. Furthermore, he is aware of SDUs and NSHs power demand ($P_{SDU,n,t}$, $P_{NSH,n,t}$) on every n and for every t. Therefore the real power demand ($P_{PEV,n,t}$) for the picked PEV is limited with respect to Eq. 1.

$$P_{PEV,n,t} = P_{max,n,t} - (P_{SDU,n,t} + P_{NSH,n,t}) \tag{1}$$

The PEV with the highest priority starts charging with respect to the maximal allowed charging power until it reaches 100% SOC. Afterwards the remaining PEVs are charged with respect to their priority by the same procedure (see Fig. 3).

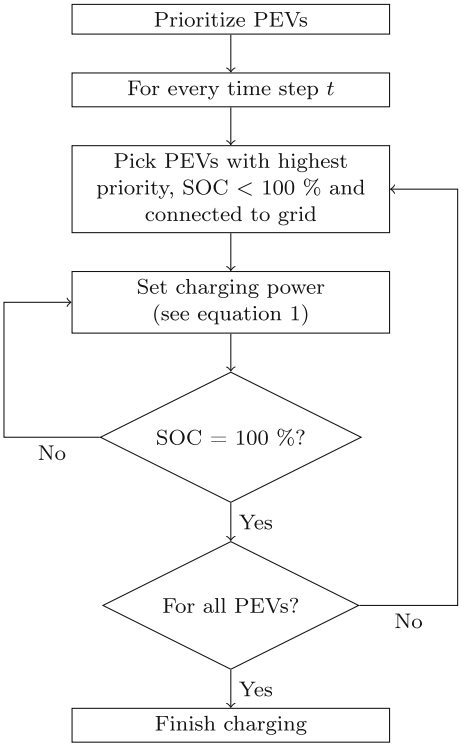

Fig. 3 Direct control strategy, coordinates plug-in electric vehicle (PEV) charging via a central aggregator

3.2 Indirect Control via a Static Time of Use (TOU) Tariff

For the indirect control strategy PEV users schedule charging individually to minimise their costs for electricity consumption based on an electricity price tariff and without the consideration of other PEVs charging behaviour and grid constraints. Like reference [24], which provides a TOU tariff give an incentive to charge at low price times, we use one static TOU tariff which is assigned to every PEV (see Fig. 1).

At the moment a PEV is connected to the grid the energy which should be charged into the battery, until the PEV departs, is evaluated. Depending on the PEV's charging power and energy demand, the number of time steps, which are necessary to charge the PEV battery, are calculated. For the grid connection time (GCT) in between (see Eq. 2) the price tariff is ordered to evaluate these time steps with the lowest possible electricity costs.

$$T_{GCT} = t_{departure} - t_{arrival} \tag{2}$$

If there are multiple possibilities for the same low price, PEV users prefer the earlier charging possibility (see also Fig. 4).

In our scenario all PEVs receive the same tariff and arrive before the low price time begins at 10 pm. Therefore charging begins simultaneously at 10 pm with maximal charging power until every PEV's battery reaches 100% SOC (see also Sect. 2).

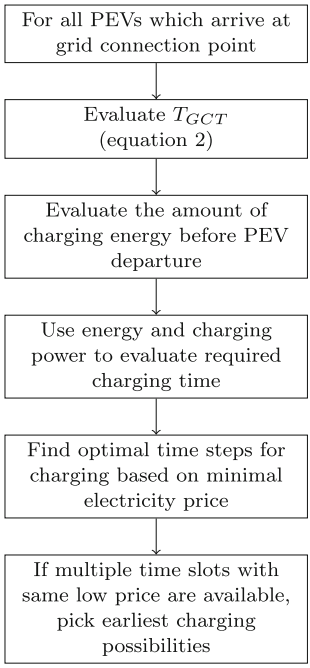

Fig. 4 Indirect control strategy via a time of use (TOU) tariff

3.3 Autonomous Control Implementing Reactive Power to Voltage Control

Local supply[3] and local demand[4] influence grid voltage which can be used as a control signal for PEVs. Furthermore, reactive power can be used to influence grid voltage positively. Within our autonomous control strategy this mechanism is used.

Here every PEV schedules the charging power based on the node voltage on the PEV grid connection point. We use a reactive power to grid voltage relationship by raising reactive power linearly between nominal grid voltage and a 0.03 p.u boundary (see Fig. 5). Reference [6] shows that the linear approach fits into the power dependencies, where reactive power demand leads to increasing and reactive power supply to decreasing node voltages. The reference uses a partly linear relationship where reactive power supply is not used to stabilise grid voltages around 1 p.u. We adapt this with a fully linear voltage to reactive power relationship between 0.97 and 1.03 p.u. This approach leads to higher inverter losses, but allows a wider range to stabilises grid voltages. Nevertheless, the evaluated amount of reactive power limits real power demand with respect to Eq. 3. Both effects, reactive power supply as well as reduced real power demand have a positive effect on grid voltages [25].

For our approach every PEV measures for every time step the node voltage if it is connected on a grid connection point. Afterwards it uses the measured node voltage and the reactive power to voltage relation to evaluate its reactive power for that time step (see Fig. 5).

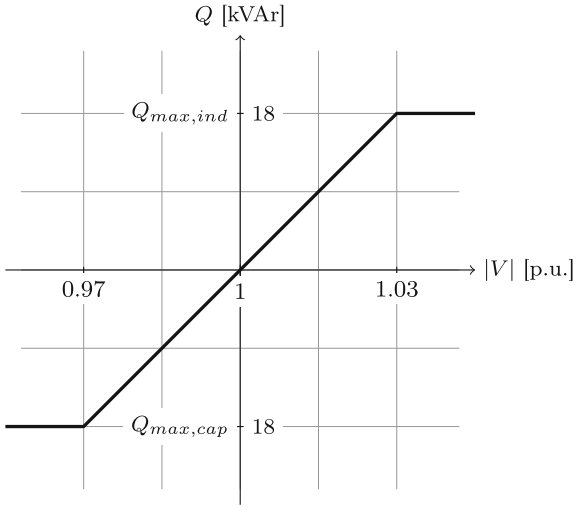

Fig. 5 Reactive power (Q) on all three phases as a function of node voltage absolute value (V) for autonomous control. Capacitive power demand if node voltage is below 1 per unit (p.u.), inductive if node voltage is above 1 p.u.

[3] E.g. renewable energy technologies like wind turbines and photovoltaic.

[4] E.g. PEVs and NSHs.

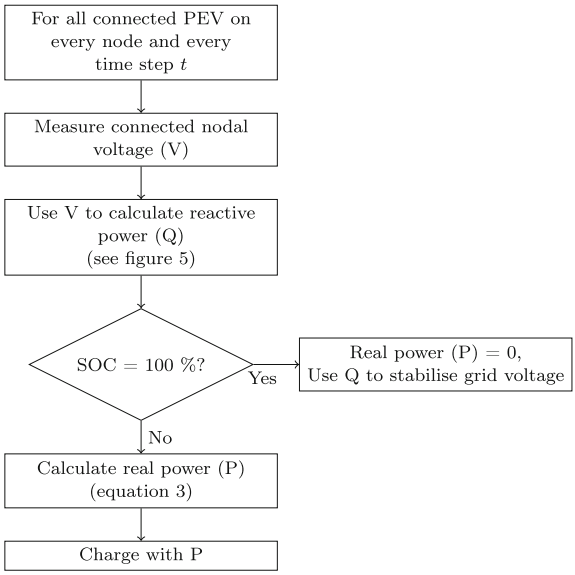

Fig. 6 Autonomous control strategy, implementing reactive power to voltage control

If the PEV battery is already fully charged, only reactive power Q_t is used to stabilise grid voltages. If not, Q_t and the maximal PEV inverter power $|\underline{S}_{max}|$ is used to evaluate the PEV's real power demand P_t (see Eq. 3).

$$P_t = \sqrt{|\underline{S}_{max}|^2 - Q_t^2} \tag{3}$$

With respect to the maximal battery storage the PEV battery gets charged by the evaluated real power (see Fig. 6).

4 Results and Discussion

In Fig. 7 we show the individual node voltages of our 10 node feeder (see Fig. 2) for the direct, indirect and autonomous control strategy (see Sect. 3). The voltages are recorded over simulation time and presented within quartiles. Additionally we present a case without connected PEVs, where only SDU and NSHs consume electrical power.

Due to the fact, that we do not consider local electrical power generation, power demand is higher than electrical generation for all time steps and nodes. Hence, for each case the highest voltage dips occur on the last node of the power grid, i.e. node 10.

As described in Sect. 2, all connected SDU exhibit the same power profile, therefore high voltage dips occur at peak demand (19 pm on weekdays) even without

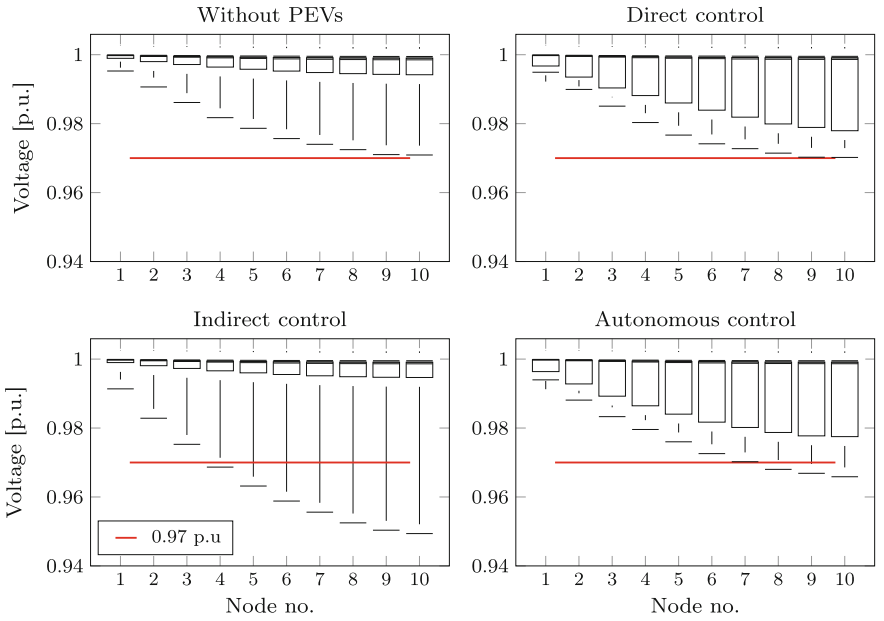

Fig. 7 Node voltages without connected plug-in electric vehicles (PEVs) to the 10 node test feeder and with connected PEVs implementing direct-, indirect- and autonomous control

connected PEVs (see Sect. 4.1). We use these improbable circumstances to emphasise that electrical grids are designed for peak electrical power demand. Furthermore, in all cases we assume symmetric load on all three grid phases; unsymmetric load would lead to even higher voltage dips.

Here we simulate these control strategies for just one week during the transition season on a rather small 10 node feeder. For other grids, seasons and PEV penetration rates the occurring voltage dips would probably be less extreme, but the results should show the same tendency.

4.1 Without Connected Plug-In Electric Vehicles (PEVs)

If there are no PEVs connected to the grid, the highest voltages dips occur on node 10. On this node for 75 percent of all time steps voltages do not dip below 0.987 p.u. Even for peak demand node voltages do not fall below 0.97 p.u, hence no voltage bound violations occur (see Fig. 7, Without PEVs).

4.2 Direct Control with Perfect Foresight

For the direct control scenario PEVs' charging process follows the algorithm described in Sect. 3.1. For 75% of all time steps voltages do not dip below 0.98 p.u from node 1–7. Voltages on node 8, 9 and 10 are slightly deeper compared to node 7.

Here voltages remain above 0.97 p.u on all nodes (see Fig. 7, Direct control). This is because we assume that an aggregator, which manages all PEVs' charging process, has perfect foresight. Therefore he knows the maximal allowed feed-in power, the actual power demand of every consumer, PEV driver's preferences, daily arrival and departure times and can therefore perfectly coordinate PEVs' charging behaviour.

4.3 Indirect Control via a Single Time of Use (TOU) Tariff

Here PEVs' charging follows the indirect strategy introduced in Sect. 3.2, where every PEV uses the same TOU tariff. Therefore every PEV receives the same price and consequently all PEVs start charging simultaneously. At that high demand time high voltage dips occur especially on node 10 (below 0.94 p.u). For 75% of the simulation time voltages do not dip below 0.994 p.u on every node. Consequently, voltages vary more often compared to direct control (see Fig. 7, Indirect control).

As differentiated at [26] and shown at [4] purely market orientated approaches lead to high grid overstress. We demonstrate this once more with our indirect control strategy. Nevertheless, much better results could be achieved if PEVs receive different price signals and therefore do not react simultaneously.

4.4 Autonomous Control via Reactive Power to Voltage Control

Within our autonomous control strategy grid voltages can be held above 0.965 p.u for all nodes over the entire simulation time. On node 8, 9 and 10 voltages violations occur at high demand times, but they stay above the 0.97 p.u boundary for the rest of the week, while voltages on node 1–7 remain in the allowed interval. Like for our direct control strategy voltages do not dip below 0.98 p.u at node 1–7 for 75% of all time steps. Hence, autonomous control can significantly reduce 0.97 p.u voltage bound violations compared to our indirect approach, but does not eliminate them completely (compare Fig. 7, Autonomous control with Indirect control).

Within our approach PEVs react simultaneously for each 15 min simulation step, which is an improbable case. Controlling the PEVs one after another by updating grid voltages every time, would be a more realistic approach. Additionally, PEVs measure grid voltages only once for every time step. This could be improved by a control loop. The control loop could monitor grid voltage on a PEV grid connecting

point while the PEV increases its power demand continuously until the allowed voltage boundary is reached for that simulation step.

5 Conclusion

We set up a computer model for a simple power grid structure to compare different control strategies for plug-in electric vehicle (PEV) charging. In particular we investigated a direct, an indirect and an autonomous control strategy with respect to the resulting grid voltages.

Within our model direct control works best in terms of voltage stability, because no 3% boundary violations occur (see Sect. 4.2). This is because we assume that for direct control our aggregator has perfect foresight and therefore can realise optimal control. However, such an approach is probably related to extensive information and communications technology (ICT) and therefore high financial investments. The indirect control strategy, which uses a static time of use (TOU) tariff, can be realized by a timer function with most PEVs on the market today. Costs for the technical implementation are low but the strategy can result in opposite effects. Instead of relieving the stress on the grid TOU tariffs can cause strong voltage dips. Our autonomous control strategy can achieve good results in terms of voltage control while using PEVs internal ICT and sensors. This study shows that TOU tariffs are not sufficient to reach good grid integration of PEVs in the future. The autonomous control strategy used leads to much better results and should therefore be part of future strategies integrating PEVs into the grid.

Also user acceptance, required investments into ICT and grid extension have to be taken into account in order to evaluate which control strategy is best suited for future smart grids. These aspects are not addressed here, but should be considered in future research.

Acknowledgements This work has been financed by the "Stiftung Energieforschung Baden-Wrttemberg". We thank the foundation members for their support. We also thank Barbara Sinnemann and two anonymous reviewers for critically reading the manuscript.

References

1. Sara Deilami et.al., Real-Time Coordination of Plug-In Electric Vehicle Charging in Smart Grids to Minimize Power Losses and Improve Voltage Profile, IEEE Transactions on Smart Grid, 456–467, (2011)
2. Amir S et.al., Impacts of battery charging rates of Plug-in Electric Vehicle on smart grid distribution systems, 2010 IEEE PES Innovative Smart Grid Technologies Conference Europe (ISGT Europe), 1–6, (2010)
3. J.A Peas Lopes et.al., Identifying management procedures to deal with connection of Electric Vehicles in the grid, PowerTech, 2009 IEEE Bucharest, 1–8, (2009)

4. Else Veldman and Remco A. Verzijlbergh, Distribution Grid Impacts of Smart Electric Vehicle Charging From Different Perspectives, IEEE Transactions on Smart Grid, 333–342, (2015)
5. K. Clement-Nyns et.al., The Impact of Charging Plug-In Hybrid Electric Vehicles on a Residential Distribution Grid, IEEE Transactions on Power Systems, 371–380, (2010)
6. Kilian Dallmer-Zerbe et.al., Analysis of the Exploitation of EV Fast Charging to Prevent Extensive Grid Investments in Suburban Areas, Energy Technology, 54–63, (2014)
7. Mehrdad Ehsani et.al., Vehicle to Grid Services: Potential and Applications, Energies, 4076–4090, (2012)
8. Shaojun Huang et.al., Voltage support from electric vehicles in distribution grid, Power Electronics and Applications (EPE), 2013 15th European Conference on, 1–8, (2013)
9. David Dallinger et.al., Plug-in electric vehicles automated charging control, http://www.isi.fraunhofer.de/isi-wAssets/docs/e-x/working-papers-sustainability-and-innovation/WP04-2015_PEV-automated-charging-control_marwitz_dallinger_wesche-et-al.pdf, (2015)
10. David Dallinger, Plug-in electric vehicles integrating fluctuating renewable electricity, PhD thesis, Universität Kassel, (2012)
11. Lutz Hillemacher, Lastmanagement mittels dynamischer Strompreissignale bei Haushaltskunden, PhD thesis, Karlsruhe, Karlsruher Institut für Technologie (KIT), (2014)
12. DOE, Benefits of demand response in electricity markets and recommendations for achieving them, (2006)
13. Lunci Hua et.al., Adaptive Electric Vehicle Charging Coordination on Distribution Network, IEEE Transactions on Smart Grid, 2666–2675, (2014)
14. S. Iacovella et.al., Double-layered control methodology combining price objective and grid constraints, 2013 IEEE International Conference on Smart Grid Communications (SmartGridComm), 25–30, (2013)
15. Sekyung Han et.al., Development of an Optimal Vehicle-to-Grid Aggregator for Frequency Regulation, IEEE Transactions on Smart Grid, 65–72, (2010)
16. David Dallinger and Martin Wietschel, Grid integration of intermittent renewable energy sources using price-responsive plug-in electric vehicles, Renewable and Sustainable Energy Reviews, 3370–3382, (2012)
17. Frank A. Wolak, An experimental comparison of critical peak and hourly pricing: the PowerCentsDC program, Department of Economics Stanford University, (2010)
18. Der Verband kommunaler Unternehmen, Stellungnahme zur Ausgestaltung des §14a EnWG auf Basis der Aufgabenstellung des BMWi vom 26.03.2013, (2013)
19. European Committee for Electrotechnical Standardization, Voltage characteristics of electricity supplied by public distribution systems: English version, Draft May 2005
20. Energie Argentur NRW, Erhebung: Wo im Haushalt bleibt der Strom? Anteile, Verbrauchswerte und Kosten von 12 Verbrauchsbereichen in Ein- bis Sechs-Personen-Haushalten, (2011), http://www.energieagentur.nrw.de/presse/singles-verbrauchen-strom-anders-15327.asp
21. Verein Deutscher Ingenieure e.V., Referenzlastprofile von Ein- und Mehrfamilien-häusern für den Einsatz von KWK-Anlagen: VDI 4655, Mai 2008,
22. AEG Nachtspeicherofen 3 kW WSP 3010, http://www.hme-technik.de/aeg-nachtspeicherofen-3-kw-wsp-3010.html, last checked: 2015–08–27
23. I. Sartori and A. G. Hestnes, Energy use in the life cycle of conventional and low-energy buildings: A review article, Energy and Buildings, 249–257, (2007)
24. Pacific Gas and Electric, Electric vehicle time of the use tariff, http://www.sdge.com/clean-energy/ev-rates, (2014)
25. Martin Braun, Provision of Ancillary Services by Distributed Generators: Technological and Economic Perspective, PhD thesis, (2008)
26. J. G. Slootweg et.al. Sensing and control challenges for Smart Grids, 2011 International Conference on Networking, Sensing and Control (ICNSC), 1–7, (2011)

Part II
Optimizing Transmission Grid Operation

Optimal Storage Operation with Model Predictive Control in the German Transmission Grid

Nico Meyer-Hübner, Michael Suriyah, Thomas Leibfried, Viktor Slednev, Valentin Bertsch, Wolf Fichtner, Philipp Gerstner, Michael Schick and Vincent Heuveline

Abstract In this paper, a model predictive control approach is presented to optimize generator and storage operation in the German transmission grid over time spans of hours to several days. In each optimization, a full AC model with typical OPF constraints such as voltage or line capacity limits is used. With given RES and load profiles, inter-temporal constraints such as generator ramping and storage energy are included. Jacobian and Hessian matrices are provided to the solver to enable a fast problem formulation, but the computational bottleneck still lies in solving the linear Newton step. The deviation in storage operation when comparing the solution over the entire horizon of 96 h against the model predictive control is shown in the German

N. Meyer-Hübner (✉) · M. Suriyah · T. Leibfried
Institute of Electric Energy Systems and High-Voltage Technology, Karlsruhe Institute of Technology, Karlsruhe, Germany
e-mail: nico.meyer-huebner@kit.edu

M. Suriyah
e-mail: michael.suriyah@kit.edu

T. Leibfried
e-mail: thomas.leibfried@kit.edu

V. Slednev · V. Bertsch · W. Fichtner
Institute for Industrial Production, Karlsruhe Institute of Technology, Karlsruhe, Germany
e-mail: viktor.slednev@kit.edu

V. Bertsch
e-mail: valentin.bertsch@kit.edu

W. Fichtner
e-mail: wolf.fichtner@kit.edu

P. Gerstner · M. Schick · V. Heuveline
Engineering Mathematics and Computing Lab, Heidelberg University, Heidelberg, Germany

P. Gerstner · M. Schick · V. Heuveline
Heidelberg Institute for Theoretical Studies, Heidelberg, Germany
e-mail: philipp.gerstner@h-its.org

M. Schick
e-mail: michael.schick@h-its.org

V. Heuveline
e-mail: vincent.heuveline@h-its.org

V. Bertsch et al. (eds.), *Advances in Energy System Optimization*,
Trends in Mathematics, DOI 10.1007/978-3-319-51795-7_3

transmission grid. The results show that horizons of around 24 h are sufficient with today's storage capacity, but must be extended when increasing the latter.

Keywords Time constrained optimal power flow · OPF · Storage · Model predictive control · Receding horizon · Transmission grid

1 Introduction

In today's energy system, the expansion of renewable energy sources (RES) leads to an increasingly uncertain, volatile and decentralized power generation, pushing the grid ever more frequently towards its limitations. If those limits are not considered during the dispatch of the generators, expensive re-dispatch will be necessary to avoid outages. However, the limits can be integrated into the search for the most economic generator dispatch, meaning the distribution of the demanded power to a pre-defined set of generators considering their individual costs. This is called an Optimal Power Flow (OPF), which was introduced by Carpentier in 1962 [1]. Voltages should not be neglected to ensure secure operation. It is therefore necessary to include an entire AC load flow instead of a linearized model. Yet, the OPF for one time step is not sufficient in today's electricity distribution. Energy storage will be a crucial piece of the puzzle for a successful integration of renewable energy. If the wind or solar power is higher than the demand, it shall be stored to supply the loads in times of low RES in-feed. Information of wind or solar in-feed must be provided to the storage device in order to guarantee free capacity or stored energy for the future. The problem, whether a storage device should load or feed into the grid, leads to a time-constrained optimal power flow (TCOPF), in literature also called Dynamic or multi-period OPF [3, 9, 10, 13]. Time-dependent constraints like stored energy or generator ramping can be considered and a detailed formulation is presented in [6]. To take into account real-time operation, a model predictive control [11] or receding horizon control has already been applied to power systems in [4] or [8]. So far, only smaller test systems have been optimized, whereas a realistic large-scale system is applied in this paper. Additionally, different horizon lengths and sample rates are tested in order to investigate the different storage behavior and the impact on the overall system costs.

2 Problem Formulation

A general OPF problem can be described as

$$\min_x F(x) \tag{1}$$

s.t.

$$g(x) = 0 \tag{2}$$
$$h(x) \leq 0, \tag{3}$$

where a cost function $F(x)$ is minimized while respecting equality constraints $g(x)$ and inequality constraints $h(x)$.

2.1 Time-Constrained Optimal Power Flow

In the time-constrained OPF formulation, the state vector becomes

$$x = \left[(x^1)^\mathsf{T} \ \ldots \ (x^\mathrm{t})^\mathsf{T} \ \ldots \ (x^\mathrm{T})^\mathsf{T}\right]^\mathsf{T} \tag{4}$$

The constraints $g(x)$ and $h(x)$ can be split into two types of constraints: non-linear constraints $g_\mathrm{nl}(x)$, $h_\mathrm{nl}(x)$ and linear constraints $g_\mathrm{l}(x)$, $h_\mathrm{l}(x)$:

$$g(x) = \begin{bmatrix} g_\mathrm{nl}(x) \\ g_\mathrm{l}(x) \end{bmatrix} \qquad h(x) = \begin{bmatrix} h_\mathrm{nl}(x) \\ h_\mathrm{l}(x) \end{bmatrix} \tag{5}$$

Further, the constraints can be divided into the groups of time-decoupling (intra-temporal) constraints $\overline{g}(x)$, $\overline{h}(x)$ and constraints depending additionally on the previous time step $\tilde{g}(x)$, $\tilde{h}(x)$. The non-linear constraints are entirely time-decoupling and are therefore formed to

$$g_\mathrm{nl}(x) = \begin{bmatrix} \overline{g}^1_\mathrm{nl}(x^1) \\ \vdots \\ \overline{g}^\mathrm{t}_\mathrm{nl}(x^\mathrm{t}) \\ \vdots \\ \overline{g}^\mathrm{T}_\mathrm{nl}(x^\mathrm{T}) \end{bmatrix} \qquad h_\mathrm{nl}(x) = \begin{bmatrix} \overline{h}^1_\mathrm{nl}(x^1) \\ \vdots \\ \overline{h}^\mathrm{t}_\mathrm{nl}(x^\mathrm{t}) \\ \vdots \\ \overline{h}^\mathrm{T}_\mathrm{nl}(x^\mathrm{T}) \end{bmatrix} \tag{6}$$

The linear constraints may contain time-coupling equations:

$$g_l(x) = \begin{bmatrix} \overline{g}_l^1(x^1) \\ \tilde{g}_l^1(x^0, x^1) \\ \vdots \\ \overline{g}_l^t(x^t) \\ \tilde{g}_l^t(x^t, x^{t-1}) \\ \vdots \\ \overline{g}_l^T(x^T) \\ \tilde{g}_l^T(x^T, x^{T-1}) \end{bmatrix} \quad h_l(x) = \begin{bmatrix} \overline{h}_l^1(x^1) \\ \tilde{h}_l^1(x^0, x^1) \\ \vdots \\ \overline{h}_l^t(x^t) \\ \tilde{h}_l^t(x^t, x^{t-1}) \\ \vdots \\ \overline{h}_l^T(x^T) \\ \tilde{h}_l^T(x^T, x^{T-1}) \end{bmatrix} \tag{7}$$

The state vector x^0 describes the initial state for inter-temporal constraints like the SOC of storage or the power output of generators with ramping limits. The separation of non-linear and linear constraints simplifies the calculation of the constant Jacobians of the linear constraints, which have to be computed only once in the first iteration:

$$g_l(x) = A_g^T \times x + b_g \tag{8}$$

$$h_l(x) = A_h^T \times x + b_h, \tag{9}$$

where

$$A_g = \begin{bmatrix} \overline{A}_{g,t} & \tilde{A}_{g,t} & & \tilde{A}_{g,t-1} & \\ & \overline{A}_{g,t} & \tilde{A}_{g,t} & \ddots & \\ & & \ddots & \ddots & \tilde{A}_{g,t-1} \\ & & & \overline{A}_{g,t} & \tilde{A}_{g,t} \end{bmatrix} \tag{10}$$

$$A_h = \begin{bmatrix} \overline{A}_{h,t} & \tilde{A}_{h,t} & & \tilde{A}_{h,t-1} & \\ & \overline{A}_{h,t} & \tilde{A}_{h,t} & \ddots & \\ & & \ddots & \ddots & \tilde{A}_{h,t-1} \\ & & & \overline{A}_{h,t} & \tilde{A}_{h,t} \end{bmatrix} \tag{11}$$

Each column in A_h and A_g contains the gradients of one constraint with respect to all optimization variables x. $\overline{A}_{h,t}$ and $\overline{A}_{g,t}$ denominate the blocks of the Jacobian where the function depends only on the very same time step. The additional entries related to inter-temporal functions depending on the same time step are set in $\tilde{A}_{g,t}$ and $\tilde{A}_{h,t}$; the ones depending on the previous time step are set in $\tilde{A}_{g,t-1}$ and $\tilde{A}_{h,t-1}$. Note that these blocks are constant throughout all time steps.

The components of vector b in the linear system $Ax + b$ are shown in (12). Contrarily to the blocks in the A-matrix, the blocks in b differ with every time step, e.g. containing the fluctuating power limits of the RES. They also contain an offset in the first time step through inter-temporal constraints depending on the initial state x^0.

$$b_{\mathrm{g}} = \begin{bmatrix} \overline{b}_{\mathrm{g}}^{1} \\ \tilde{b}_{\mathrm{g}}^{1} + (\tilde{A}_{\mathrm{g}}^{\mathrm{t-1}})^{\mathsf{T}} \times x^{0} \\ \overline{b}_{\mathrm{g}}^{2} \\ \tilde{b}_{\mathrm{g}}^{2} \\ \vdots \\ \overline{b}_{\mathrm{g}}^{\mathrm{T}} \\ \tilde{b}_{\mathrm{g}}^{\mathrm{T}} \end{bmatrix} \quad b_{\mathrm{h}} = \begin{bmatrix} \overline{b}_{\mathrm{h}}^{1} \\ \tilde{b}_{\mathrm{h}}^{1} + (\tilde{A}_{\mathrm{h}}^{\mathrm{t-1}})^{\mathsf{T}} \times x^{0} \\ \overline{b}_{\mathrm{h}}^{2} \\ \tilde{b}_{\mathrm{h}}^{2} \\ \vdots \\ \overline{b}_{\mathrm{h}}^{\mathrm{T}} \\ \tilde{b}_{\mathrm{h}}^{\mathrm{T}} \end{bmatrix} \tag{12}$$

The costs of each time step only depend on the generated power and the total costs sum up to

$$F(x) = \sum_{\mathrm{t}=1}^{\mathrm{T}} F^{\mathrm{t}}(x^{\mathrm{t}}) \tag{13}$$

The cost function can be a piecewise linear or polynomial function.

2.2 Model Constraints

A detailed description of the model can be found in [7].

The state variables x consist of the busbar voltages (real and imaginary part); active and reactive power of all kinds of generating units such as conventional and renewable generators, pump storages, HVDC converters and connections to neighboring countries; load shedding variables; energy states of storages or contracts.

The linear, intra-temporal inequality constraints $\overline{h}_{\mathrm{l}}$ include all variable limitations except the voltage limits, which are found together with the branch flow limits in the nonlinear, intra-temporal inequality constraints $\overline{h}_{\mathrm{nl}}$. The ramp rates of conventional generators are set in $\tilde{h}_{\mathrm{l}}$. The nonlinear equality constraints $\overline{g}_{\mathrm{nl}}$ only consist of the load flow equations. The linear equality constraints $\overline{g}_{\mathrm{l}}$ contain the model of the bidirectional point-to-point HVDC connections and the setting of a reference angle. The calculation of energy states always depends on the previous time step, and thus can be found in the inter-temporal part of the linear equality constraints $\tilde{g}_{\mathrm{l}}$.

2.3 Solving the Problem

The problem is solved with a Primal-Dual Interior Point Method, assigning a Lagrangian multiplier to each constraint. The equality constraints are represented by λ, and the inequality constraints by μ. To include the inequalities in a function which shall be minimized, slack variables $Z > 0$ are introduced. With $h(x) + Z = 0$, the inequalities are transformed to equality functions and the Lagrangian is formed to

$$\mathscr{L}(x, \lambda, \mu, Z) = F(x) + \mu^{\mathsf{T}}(h(x) + Z) + \lambda^{\mathsf{T}} g(x) \tag{14}$$

In the Interior Point Method, the slack variables are weighted with the barrier coefficient γ to keep the inequality constraints away from zero in the first iterations. Eventually, γ is reduced to zero and the problem approaches the original one. The Lagrangian is built up to be minimized, while maximizing the multipliers. This leads to a minimization of the cost function F, while $h(x)$ is kept below and $g(x)$ close to zero. Common Newton steps are applied to solve the KKT-conditions [5]. The main effort lies in solving the linear system

$$\begin{bmatrix} M & g_{\mathrm{x}}^{\mathsf{T}} \\ g_{\mathrm{x}} & 0 \end{bmatrix} \begin{bmatrix} \Delta x \\ \Delta \lambda \end{bmatrix} = \begin{bmatrix} -N \\ -g(x) \end{bmatrix} \tag{15}$$

with

$$M = \nabla^2_{\mathrm{xx}} \mathscr{L}(x, \lambda, \mu, Z) + h_{\mathrm{x}}^{\mathsf{T}} [Z]^{-1} [\mu] h_{\mathrm{x}} \tag{16}$$

$$N = \nabla_{\mathrm{x}} \mathscr{L}(x, \lambda, \mu, Z) + h_{\mathrm{x}}^{\mathsf{T}} [Z]^{-1} (\gamma e + [\mu] h(x)) \tag{17}$$

Note that $[A]$ creates a diagonal matrix with the vector A on its diagonal, e is a vector of ones and the Jacobian and the Hessian of a function f with respect to x is given by f_{x} and f_{xx} respectively. It is therefore necessary to provide first and second order derivatives of the cost function and all constraints with respect to the optimization variables x. A detailed description of the Primal-Dual Interior Point Method can be found in [12].

3 The German Transmission Grid

A detailed description of the applied model is presented in [7]. The network is shown in Fig. 1, where pump storages are marked with red circles and HVDC connections with blue lines. In Fig. 2, the profiles for both wind and PV generation are shown. They are chosen with relatively large gradients in order to challenge the storage operation and then scaled with the corresponding installed power. The total load and RES curve can be seen in Fig. 3.

3.1 Costs

Linear costs are used in this model, though it is possible to also include non-linear or piece-wise linear costs. The conventional fuel costs are assumed to range between 40–55 €/MWh. RES as well as pumped hydro do not have any variable costs in the macro economic sense, but if RES had zero costs, there would be no incentive of

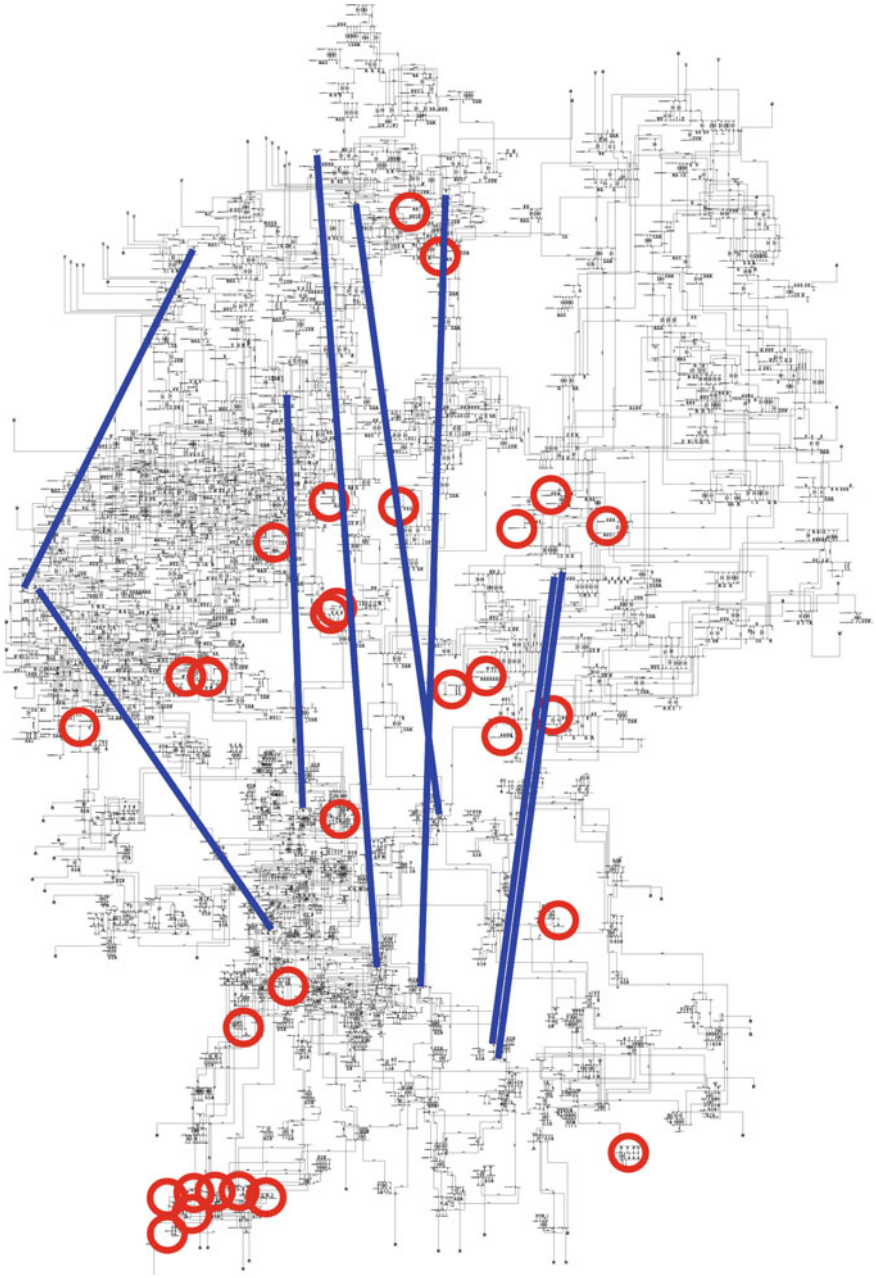

Fig. 1 German transmission grid with HVDC lines and locations of pump storages

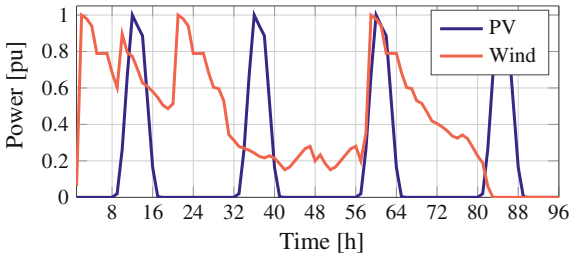

Fig. 2 RES profiles

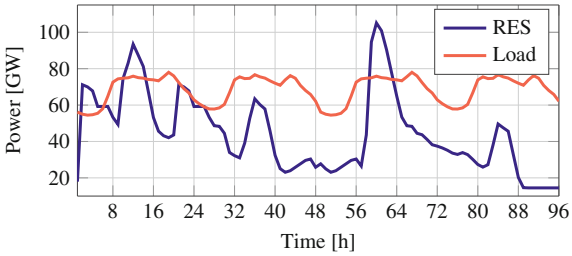

Fig. 3 Total load and RES in-feed

feeding the power into the grid once the load is covered. As it is political will in Germany to privilege energy from RES, even if the demand is already covered, an export to neighboring countries must be forced by giving the RES negative costs. As a result, the optimization tries to integrate as much RES power as possible into the grid, which means that high losses would actually be preferable once the load is covered. This should not be the goal and as a consequence, the export costs also need to be negative. By trying to export as much of the available RES as possible, the losses are minimized. Obviously, the absolute value of the export costs must be lower than the costs of conventional generation in order to avoid export of the latter. Import, however, is assumed to be more expensive than any generator within the grid. Shedding a load should be the very last possibility to ensure secure system operation and therefore has the highest costs. An overview of the different costs is shown in Table 1.

Table 1 Generation and load shedding costs

		Costs (€/MWh)
RES		−10
Pump storage		0
Conventional	Coal	40
	Gas	50
	Oil	55
Export		−10
Import		60
Load shedding		100

4 Reference Solution

First, a reference solution for the entire time interval of 96 h is shown. In the next section, the model predictive control scheme is explained and applied.

4.1 Computation

There are $n_x = 612384$ decision variables, $n_h = 1501056$ inequality constraints and $n_g = 240384$ equality constraints considered. The calculation of one Newton step, which means solving the linear system (15) of the size $(n_x + n_g) \times (n_x + n_g)$ with 6591872 non-zeros, is executed with the Matlab Backslash operator (MA57 [2]) and takes an average of 4 min with an Intel Xeon E5-2687W at 3.40 GHz and 128 GB RAM. For the calculation of the presented scenario in this paper, it took 59 iterations to achieve the convergence criteria of 2e-5, which are defined in [12].

4.2 Results

It can be seen in Fig. 3 that there are some hours of the first day in which the RES power exceeds the demand. This is also the case between hour 60 and 64, which is reflected in the exported power shown in Fig. 5. The conventional generation is ramped down to the minimum generated power during these periods, which can be seen in Fig. 5 as well. The usage of storage is shown in Fig. 4. Two macro cycles can be identified, with a complete discharge at hour 58, where an interval of high demand ends and an interval of RES exceed starts. Interestingly, even when the demand exceeds the RES in-feed again in hour 64, the storages are charged until hour 78. This is due to binding ramping constraints of the conventional generators, needing power support in the following hours.

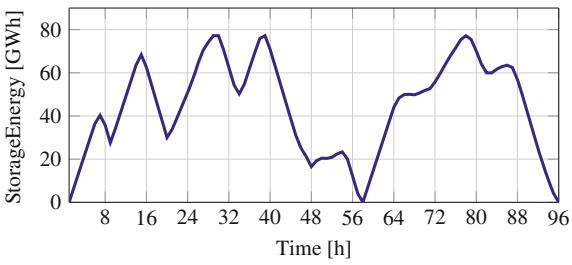

Fig. 4 Cumulated storage energy

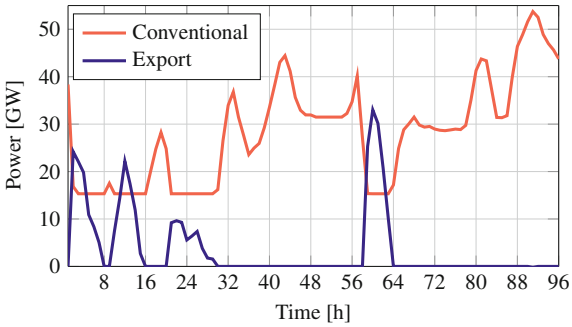

Fig. 5 Exported power and conventional generation

5 Model Predictive Control

To reduce the computational effort as well as the forecast error, model predictive control (MPC) [11] is used now to operate the system. The optimal control sequence is calculated over a certain horizon H by executing a TCOPF. The sequence is then applied for a shorter sample rate only and a new starting point for the next TCOPF calculation is shifted to the end of the sequence. The offset O is the overlap between horizon and sample rate, determining the additional forecast information we receive for that sequence. If an optimization is done with a horizon of $H = 24\,\text{h}$ and an offset of $O = 14\,\text{h}$, the operation scheme is called "MPC 24/14". The scheme is shown in Fig. 6.

5.1 Computation

Even though the problem size increases linearly with the optimized horizon, the computation time increases superlinearly. In Fig. 7 the average time for calculating the Newton step and the total computation time can be seen on the same architecture as described above. While the computation time for shorter horizons from 12–36 h

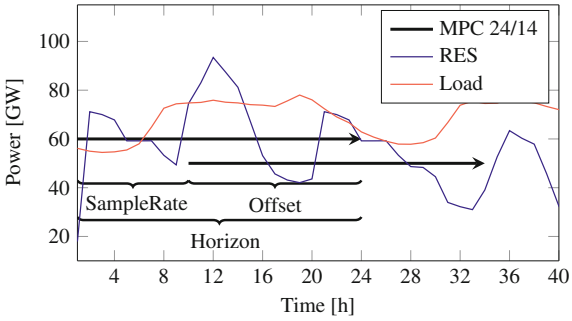

Fig. 6 Optimization scheme for MPC 24/14

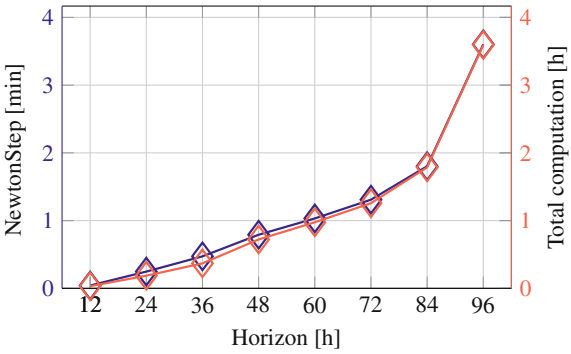

Fig. 7 Computation time

ranges between 2 and 20 min, it grows more than linearly up to several hours for horizons larger than 84 time steps. This requires an examination of the cost increase when using shorter optimization horizons.

5.2 Scenarios

The offset is crucial for storage operation. It provides the additional information beyond the sample rate which enables the storage to either guarantee available energy or free capacity to compensate time spans with an excess of RES or insufficient RES. It is varied between 6 and 18 h by using the parameter sets 12/6, 24/12 and 36/18. The extent of storage use also depends on the relationship of in-feed and demand. Therefore, a second RES profile is used, where wind and PV in-feed is set to zero after the second day, i.e. hour 48. The original profile in Fig. 2 is called profile "A" and the reduced profile is called profile "B". Last, the storage size has a strong impact on the relationship between overall costs and MPC offset. In the scenario "large storage" a storage capacity increased by 50% (from 80 to 120 GWh) is assumed.

5.3 Results

In Fig. 8, the schemes are shown for profile A and normal storage size. Compared to the reference solution, MPC 36/18 shows very similar storage operation and thus very similar costs (Table 2). Increased costs are generated by a shorter update interval with MPC 24/12, but the deviation is only 0.67%. When the update interval and offset is further reduced to MPC 12/6, the effect is remarkable and only half of the available storage capacity can be used. This results in a cost increase of 2.55%. A similar

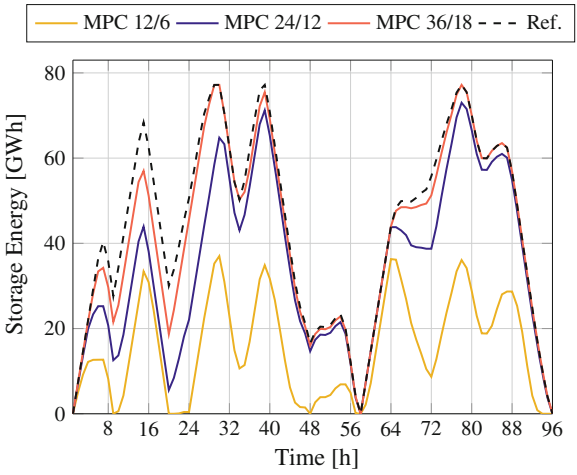

Fig. 8 Profile A, normal storage

Table 2 Relative generation costs [%] compared to reference solution

	12/6	24/12	36/18	Ref.
Profile A, normal Stor.	102.55	100.85	100.01	100.00
Profile B, normal Stor.	101.74	100.67	100.00	100.00
Profile A, large Stor.	103.69	101.97	100.90	100.00
Profile B, large Stor.	102.74	101.66	100.61	100.00

result is obtained with the same storage sizes and profile B, see Fig. 9. Even though the loading behavior is quite different from hour 40 on, the deviation between the different MPC schemes shows a comparable effect on the overall costs. In Fig. 10, profile A and large storages are applied. The cost increase is already notable with MPC 36/18. A further degradation is achieved with even smaller horizon and offset. A similar result for profile B can be seen in Fig. 11.

6 Critical Review

As stated before, perfect forecast is assumed and the implemented profiles of RES are synthetic. The results are therefore meaningful, but not yet complete. Additionally, the system boundaries lead to uncertainties in relation to the conclusions. The European system cannot be considered entirely, which would lead to the highest accuracy.

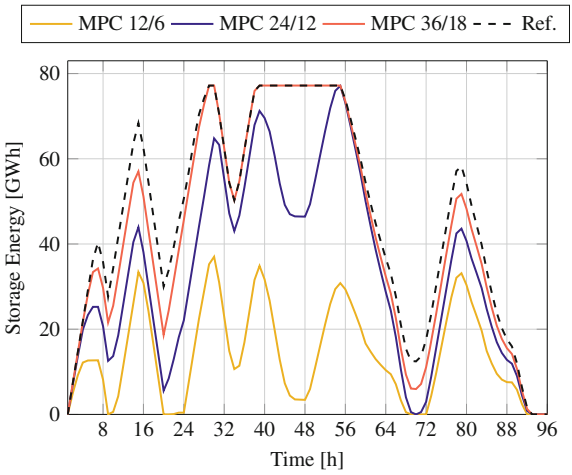

Fig. 9 Profile B, normal storage

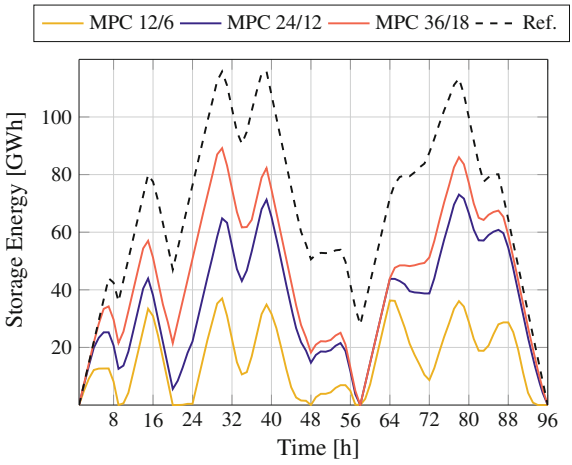

Fig. 10 Profile A, large storage

7 Conclusion

A TCOPF framework was presented and a model of the German transmission grid was created from data of the BNA. An optimization over 96 h was achieved to show the functionality of the methodology. The resulting reference solution was compared to a real-time operation scheme, the Model Predictive Control. It can be seen that the storage size has a strong impact on how close one can get to the optimum with certain MPC parameter sets. With an assumed capacity of 80 GWh, horizons around 30 h are sufficient to nearly reach the reference optimum, whereas larger horizons are necessary for larger storage sizes. This indicates an upper bound of useful foresight, but in reality other parameters need to be considered as well. It will always be a trade-off between the ability to frequently provide forecast updates with reasonable effort

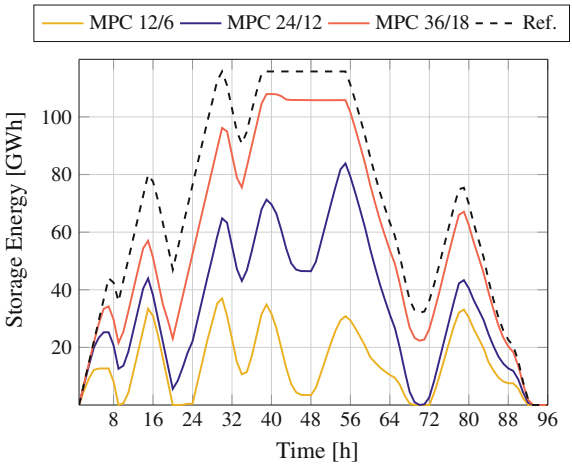

Fig. 11 Profile B, large storage

on one hand and the actual forecast error with the resulting costs due to necessary balancing energy on the other hand.

8 Outlook

An integration of forecast errors will deliver more realistic conclusions about preferable parameters, even though the effect will not be as crucial as on lower voltage levels due to the aggregated profiles. The improvement of RES profiles forms a major part of current work and will be integrated in the future. Large potential can be seen in the improvement of solving the Newton step. A new solving technique is currently being studied to strongly reduce the computation time. In this work, DC lines are modeled as point-to-point connections with linear efficiency. Future models will include non-linear converter losses and an entire DC-side load flow, enabling also multi-terminal operation.

Acknowledgements The authors kindly acknowledge the support for this work from the German Research Foundation (DFG) under the Project Number LE1432/14-1.

References

1. Carpentier J (1962) Contribution a l'etude du dispatching economique. Bull Soc Francaise des Electriciens 3:431–447
2. Duff IS (2004) Ma57—a code for the solution of sparse symmetric definite and indefinite systems. ACM Trans Math Softw 30(2):118–144

3. Gill S, Kockar I, Ault G (2014) Dynamic optimal power flow for active distribution networks. IEEE Transactions on Power Systems 29(1):121–131
4. Glavic M, Hajian M, Rosehart W, Van Cutsem T (2011) Receding-horizon multi-step optimization to correct nonviable or unstable transmission voltages. Power Systems, IEEE Transactions on 26(3):1641–1650
5. Kuhn HW, Tucker AW (1951) Nonlinear programming. In: Proceedings of the Second Berkeley Symposium on Mathematical Statistics and Probability, University of California Press, Berkeley, Calif., pp 481–492
6. Meyer-Huebner N, Suriyah M, Leibfried T (2015a) On efficient computation of time constrained optimal power flow in rectangular form. In: IEEE PowerTech conference, Eindhoven
7. Meyer-Huebner N, Suriyah M, Leibfried T, Slednev V, Bertsch V, Fichtner W, Gerstner P, Schick M, Heuveline V (2015b) Time constrained optimal power flow calculations in the german transmission grid. In: International ETG Congress, Bonn
8. Olivares D, Lara J, Canizares C, Kazerani M (2015) Stochastic-predictive energy management system for isolated microgrids. Smart Grid, IEEE Transactions on 6(6):2681–2693
9. Qin Z, Yang Y (2008) Vectorization implementation of optimal power flow in rectangular form based on interior point method. In: IEEE Power and Energy Society General Meeting - Conversion and Delivery of Electrical Energy in the 21st Century, pp 1–8
10. Qin Z, Hou Y, Lu E, Luo C, Cheng S (2014) Solving long time-horizon dynamic optimal power flow of large-scale power grids with direct solution method. IET Generation, Transmission Distribution 8(5):895–906
11. Rawlings J (2000) Tutorial overview of model predictive control. Control Systems, IEEE 20(3):38–52
12. Wang H, Murillo-Sanchez C, Zimmerman R, Thomas R (2007) On computational issues of market-based optimal power flow. IEEE Transactions on Power Systems 22(3):1185–1193
13. Xie K, Song Y (2001) Dynamic optimal power flow by interior point methods. IEE Proceedings-Generation, Transmission and Distribution 148(1):76–84

Security-Constrained Optimization Framework for Large-Scale Power Systems Including Post-contingency Remedial Actions and Inter-temporal Constraints

Jonas Eickmann, Christian Bredtmann and Albert Moser

Abstract To cope with a growing amount of congestion in the transmission grid, decision support systems for transmission system operation have to be developed. Thus, this paper presents a security-constrained optimization framework including post-contingency control for the application in transmission grid operation with excellent applicability to large-scale power systems and outstanding computational performance.

Keywords SCOPF · Post-contingency control

1 Introduction

Increasing power flows in the transmission grid lead to a growing amount of congestions and an increased number of implemented remedial measures [2]. To cope with this challenge in daily transmission grid operation, decision support systems have to be developed to support the transmission system operators. Within this context, the previous developments provide room for enhancements, especially when it comes to computational effort [11, 12]. Thus, this paper aims at presenting a framework for solving continuous Security Constrained Optimal Power Flow (SCOPF) problems to support transmission grid operation and focusing on applicability in transmission grid operational planning and real time transmission grid operation.

J. Eickmann (✉) · C. Bredtmann · A. Moser
Institute of Power Systems and Power Economics, RWTH Aachen University, Aachen, Germany
e-mail: am@iaew.rwth-aachen.de

J. Eickmann
e-mail: Jonas.Eickmann@rwth-aachen.de

C. Bredtmann
e-mail: br@iaew.rwth-aachen.de

V. Bertsch et al. (eds.), *Advances in Energy System Optimization*, Trends in Mathematics, DOI 10.1007/978-3-319-51795-7_4

2 Modeling

Functional core of the developed optimization framework is a model for a security constrained optimal power flow.

2.1 Area Definitions

To match the functional requirements for the application in parts of a large interconnected network, different areas are defined. The determination of import, export, transit and loop flows is carried out on a full network model. Considered as constraints are only components in the observation area of the network model. This can, e.g., be one control block and the respective tie lines. To comply with theses constraints, the components located in a separate control area are taken into account. In practical applications, the control area is typically larger than the observation area to enable the relieve of overloading on tie lines.

2.2 Power Flows

The modeling of power flows is based on the complex power flow equations given by the nodal power balances and system. Security constraints are considered by a set of situations Ω that contains the situations of undisturbed operation s_0 and the situations after contingencies Ω_a. The power flow equations have to be solved for all situations $s \in \Omega$.

$$\underline{\mathbf{S}}^s = \mathrm{diag}(\underline{\mathbf{V}}^s) \cdot \underline{\mathbf{Y}}^{s*} \cdot \underline{\mathbf{V}}^{s*} \qquad \forall\, s \in \Omega \tag{1}$$

To enable time coupling optimization problems, the set of situations Ω is extended to one situation of normal operation per timestep Ω_0^t and a set of situations after contingencies per time step Ω_a^t. Additionally, the modeling of post-contingency control is enabled by the definition of different post-contingency situations at a duration τ after the appearance of the contingency. These situations are given by a set $\Omega_{a,\tau}^t$ per time step.

2.3 Constraints

The currents on all branches need to be below the current limits at the beginning (I_{beg}) and the end of the branch (I_{end}).

Fig. 1 Current limits

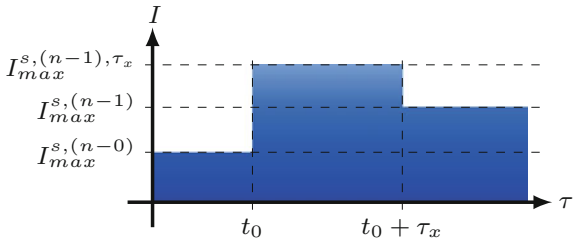

$$\mathbf{I}_z^s = \begin{pmatrix} \left|\underline{I}_{beg}^s\right| \\ \left|\underline{I}_{end}^s\right| \end{pmatrix} \leq \mathbf{I}_{max,z}^s \qquad \begin{matrix} \forall\, s \in \Omega \\ \forall\, z \in B_b \end{matrix} \tag{2}$$

The current limits depend on the type of situation.

$$I_{max}^s = \begin{cases} I_{max}^{s,(n-0)} & \text{if } s \in \Omega_0 \\ I_{max}^{s,(n-1),\tau} & \text{if } s \in \Omega_{a,\tau} \\ I_{max}^{s,(n-1)} & \text{if } s \in \Omega_a \end{cases} \tag{3}$$

The different current limits for a single post-contingency time stamp τ_x and a contingency at t_0 are shown exemplarily in Fig. 1.

To secure voltage stability and avoid increased equipment aging, voltage limits need to be observed.

$$V_{min,i}^s \leq \left|\underline{V}_i^s\right| \leq V_{max,i}^s \qquad \begin{matrix} \forall\, s \in \Omega \\ \forall\, i \in N \end{matrix} \tag{4}$$

The voltage limits differ dependent on the type of operational situation.

$$V_{min/max}^s = \begin{cases} V_{min/max}^{(n-0)} & \text{if } s \in \Omega_0 \\ V_{min/max}^{(n-1)} & \text{if } s \in \{\Omega_a \cup \Omega_{a,\tau}\} \end{cases} \tag{5}$$

For the consideration of physical limits outside of the observation area, additional constraints are considered for the import/export power on sets of tie lines.

$$P_{min,g}^s \leq \sum_{z \in \Upsilon_g} P_{beg,z}^s \leq P_{max,g}^s \begin{matrix} \forall\, s \in \Omega_0 \\ \forall\, g \in \Theta \end{matrix} \tag{6}$$

where Υ_g is the set of tie lines on border g from the set of all relevant borders with import/export limitations Θ.

In real world applications, the compliance with all technical constraints cannot be guaranteed. Thus, the solution space of the optimization problem needs to be enlarged. This is implemented by a relaxation of technical constraints using slack variables ν in the Eqs. 2, 4, and 6.

$$\mathbf{I}_z^s \leq \mathbf{I}_{max,z}^s + \nu_{I,z}(s) \qquad \begin{array}{l} \nu_{I,z}(s) \in \mathbb{R}_0^+ \\ \forall\, s \in \Omega \\ \forall\, z \in B_b \end{array} \tag{7}$$

$$\begin{array}{l} V_{min,i}^s - \nu_{V,i}^-(s) \leq \left|\underline{V}_i^s\right| \\ \leq V_{max,i}^s + \nu_{V,i}^+(s) \end{array} \qquad \begin{array}{l} \nu_{V,i}^{+/-}(s) \in \mathbb{R}_0^+ \\ \forall\, s \in \Omega \\ \forall\, i \in N \end{array} \tag{8}$$

$$\begin{array}{l} P_{min,g}^s - \nu_{\Upsilon,g}^-(s) \leq \sum_{z \in \Upsilon_g} P_{beg,z}^s \\ \leq P_{max,g}^s + \nu_{\Upsilon,g}^+(s) \end{array} \qquad \begin{array}{l} \nu_{\Upsilon,g}^{+/-}(s) \in \mathbb{R}_0^+ \\ \forall\, s \in \Omega_0 \\ \forall\, g \in \Theta \end{array} \tag{9}$$

2.4 Degrees of Freedom

The impact of control actions on the power flows are modeled as a change of admittance matrixes as well as a change of nodal power balances. To distinguish between preventive measures and measures to be used preventively and correctively, there are the following denominations. Preventive measures have to be set identically for all situations of one time step Ω^t and are written as a function of a set of situations $X_f(\Omega^t)$. Corrective measures can be chosen individually per situation s and are written as a function of the individual situations $X_f(s)$. The following holds for the intermediate state.

$$\Delta \underline{S}_k(s_{a,\tau}) = \begin{cases} \Delta \underline{S}_k(s_0) & \text{if } \tau < \tau_k \\ \Delta \underline{S}_k(s_a) & \text{if } \tau \geq \tau_k \end{cases} \tag{10}$$

where τ_k is the required time for the activation of a corrective measure k.

The reactive power provision by shunt elements is modeled by tap position dependent admittances.

$$\begin{aligned} \check{\underline{Y}}_\kappa(\Omega^t) &= \check{\underline{Y}}_\kappa(\gamma_\kappa(\Omega^t)) \\ &= \check{\underline{Y}}_\kappa(\gamma_{0,\kappa}^{\Omega^t} + \Delta\gamma_\kappa(\Omega^t)) \qquad \gamma \in \Psi_\kappa \subset \mathbb{Z} \end{aligned} \tag{11}$$

where Ψ_κ is the set of possible tap positions for shunt element κ. The modeling of Flexible AC Transmission Systems (FACTS) is implemented by a voltage dependent, continuous controllable reactive power source.

$$\Delta \underline{S}_f(s) = \mathrm{j}\, \Delta Q_f(s) \tag{12}$$

$$Q_{min,f}(\underline{\mathbf{V}}) \leq Q_{0,f}^s + \Delta Q_f(s) \leq Q_{max,f}(\underline{\mathbf{V}}) \tag{13}$$

A change of transformer tap positions is projected in the change of the transformer quadripole parameters.

$$\begin{aligned}\check{\underline{\mathbf{Y}}}_r(s) &= \check{\underline{\mathbf{Y}}}_r(\gamma_r(s)) \\ &= \check{\underline{\mathbf{Y}}}_r(\gamma_{0,r}^{\Omega^t} + \Delta\gamma_r(s)) \qquad \gamma \in \Psi_r \subset \mathbb{Z}\end{aligned} \tag{14}$$

The modeling of HVDC-lines is carried out by an explicit modeling of two converters and one line. The line has the series resistance R_{hbr} to model ohmic losses. The converters are considered to have no-load and transmission losses given by shunt and series resistances $R_{hc,q}$ and $R_{hc,l}$. Converter 1 is considered to control the DC voltage.

The reactive power limits depend on the active power feed-in of the respective converter.

$$\begin{aligned}\underline{S}_{hc}(s) &= P_{hc}(s) + \mathrm{j}\, Q_{hc}(s) \\ &= \underline{S}_{0,hc}^{\Omega^t} + \Delta\underline{S}_{hc}(s) \leq \underline{S}_{max,hc}(\underline{\mathbf{V}})\end{aligned} \tag{15}$$

$$P_{hc2}(s) = P_{hc2}(P_{hc1}(s)) \tag{16}$$

where the operator $\leq$ is defined for the field of complex numbers in a way, that the converter set-point has to be inside of the area of admissible apparent power provision. The adjustment of the active power transmission as a corrective measure is limited.

$$|P_{hc}(s_a) - P_{hc}(s_0)| \leq \Delta P_{max,\tau_x,hc} \tag{17}$$

The adjustment of generator feed-ins is modeled by a change of power injections. The apparent power limits of generators are modeled by the simplified operational diagram shown in Fig. 2.

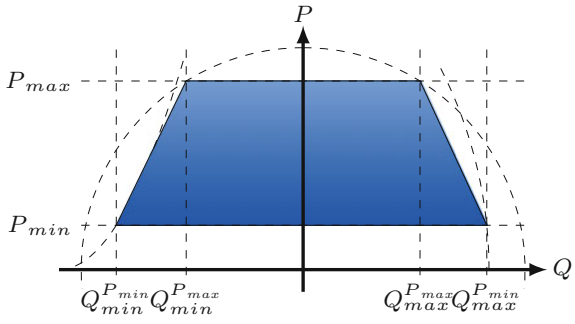

Fig. 2 Generator apparent power limits

$$b_k(\Omega^t) \in \{0, 1\} \tag{18}$$

$$\underline{S}_k(s) = P_k(s) + \mathrm{j}\, Q_k(s) \leq b_k(s) \cdot \underline{S}_{max,k} \tag{19}$$

where $b_k(\Omega^t)$ is the operating state of generator k at time step t. The adjustment of active power feed-in as a corrective measure is limited by power gradients.

$$|P_k(s_a) - P_k(s_0)| \leq b_k(s_0) \cdot \frac{\partial P}{\partial \tau}_{max,k} \cdot \tau_x \tag{20}$$

The same holds for the change of active power feed-in in normal operation in subsequent time steps.

$$\frac{\partial P}{\partial t}_{min,k} \cdot \Delta t \leq P_k(s_0^{t+1}) - P_k(s_0^t) \leq \frac{\partial P}{\partial t}_{max,k} \cdot \Delta t \tag{21}$$

Additionally, the consideration of hydro power plants including interlinked basins is possible, see [4]. A future publication will also cover the available models to consider minimum uptimes and downtimes of thermal power plants.

Feed-in from renewable energy sources can be reduced by the transmission system operators, if there are no more conventional generation units available for reduction.

$$0 \leq P_{res}(s) = P_{0,res}^{\Omega^t} + \Delta P_{res}(s) \leq P_{0,res}^{\Omega^t} \tag{22}$$

2.4.1 Load Shedding

In emergency situations, if there are no more other remedial measures available, there is a possibility to shed consumer loads.

$$P_{0,v}^{\Omega^t} \leq P_v(s) = P_{0,v}^{\Omega^t} + \Delta P_{0,v}(s) \leq 0 \tag{23}$$

2.5 Objective Function

The different operational requirements are modeled by a multi-objective optimization. In a first step, the active power losses in normal operation are to be reduced. Thus, they are weighted with an objective coefficient c_{loss}.

$$C_{loss} = \sum_{s_0^t \in \Omega_0} c_{loss} \cdot \Big(\sum_{z \in B} P_{loss,z}(s_0^t) + \sum_{hbr \in B_{DC}} P_{loss,hbr}(s_0^t) \Big) \tag{24}$$

To maintain security margins for real time operation, the use of network based remedial measures is to be minimized.

$$\begin{aligned} C_{net} = & \sum_{s_0^t \in \Omega_0} \sum_{\kappa \in K} \quad c_\kappa \cdot \left| \Delta \gamma_\kappa(s_0^t) \right| \\ & + \sum_{s \in \Omega} \Big(+ \sum_{f \in F} \quad c_f^s \cdot \left| \Delta Q_f(s) \right| \\ & \qquad + \sum_{hc \in H} \quad \Big(c_{|P|,hc}^s \cdot |\Delta P_{hc}(s)| \\ & \qquad\qquad + c_{|Q|,hc}^s \cdot |\Delta Q_{hc}(s)| \Big) \Big) \end{aligned} \tag{25}$$

If the feed-in of generators has to be adjusted, the costs of the respective measures given by their marginal costs c_P have to be considered. Beyond these physical costs, additional cost components $c_{|P|/|Q|}$ for the absolute changes in feed-in are integrated to increase the robustness against imperfections in cost modeling. The different priorities of remedial measures are projected to the relation of cost coefficients $c_{|P|,k} < c_{|P|,res} < c_{|P|,v}$.

$$\begin{aligned} C_{ma} = & + \sum_{s \in \Omega} \Big(+ \sum_{k \in G} \quad \Big(c_{P,k}^s \cdot \Delta P_k(s) \\ & \qquad\qquad + c_{|P|,k}^s \cdot |\Delta P_k(s)| \\ & \qquad\qquad + c_{|Q|,k}^s \cdot |\Delta Q_k(s)| \Big) \\ & \qquad + \sum_{res \in RES} \quad c_{|P|,res}^s \cdot |\Delta P_{res}(s)| \\ & \qquad\qquad + \sum_{v \in L} \quad \Big(c_{P,v}^s \cdot \Delta P_v(s) \\ & \qquad\qquad\qquad + c_{|P|,v}^s \cdot |\Delta P_v(s)| \Big) \Big) \end{aligned} \tag{26}$$

To ensure the compliance with the technical limits, the use of slack variables has to be avoided.

$$\begin{aligned} C_\nu = & \sum_{s_0^t \in \Omega_0} + \sum_{g \in \Theta} \left(c_{\Upsilon,g}^{+,s_0^t} \cdot \nu_{\Upsilon,g}^+(s_0^t) + c_{\Upsilon,g}^{-,s_0^t} \cdot \nu_{\Upsilon,g}^-(s_0^t) \right) \\ & + \sum_{s \in \Omega} \Big(+ \sum_{z \in B} c_{I,z}^{\ s} \cdot \nu_{I,z}(s) \\ & \qquad + \sum_{i \in N} \left(c_{V,i}^{+,s} \cdot \nu_{V,i}^+(s) + c_{V,i}^{-,s} \cdot \nu_{V,i}^-(s) \right) \Big) \end{aligned} \tag{27}$$

The objective function values of non-slack variables are weighted with the probability of occurrence $p(s)$ of the respective situation. Within this context, a rough estimate of $p(s)$ based on outage statistics is sufficient.

$$c^s = \begin{cases} c_0 & \text{if } s \in \Omega_0 \\ p(s) \cdot c_0 & \text{if } s \in \Omega_a \\ 0 & \text{if } s \in \Omega_{a,\tau} \end{cases} \tag{28}$$

The objective function is given by the sum of the different components.

$$o(\chi) = C_{loss} + C_{net} + C_{ma} + C_{\nu} \tag{29}$$

3 Solution Methodology

There are two main types of algorithms available to solve the given type of SCOPF problem. On the one hand, the problem can be solved with an interior-point-method, e.g. a Lagrange method. On the other hand, a piecewise linear formulation can be used [6, 14]. A special situation in the given problem formulation compared to other OPF formulations, e.g., for the estimation of nodal prices like [1], is given by the quality of the initial solution. In many situations, especially if there are no technical limits violated, there is no need to implement remedial measures and the initial solution is very similar to the solution of the optimization problem. This makes the utilization of a piecewise linear algorithm favourable, especially in terms of computational effort.

3.1 Successive Linear Algorithms for OPF Problems

Successive linear algorithms separate the solution of power flow equations from the solution of the optimization problem [6]. This is shown in Fig. 3. The power flow equations are solved for all considered grid use cases.

Using the estimated solution, the power flow equations are linearized in the respective operating point. Typically, this is implemented by use of an inversion of the Jacobian matrix of the power flow equations.

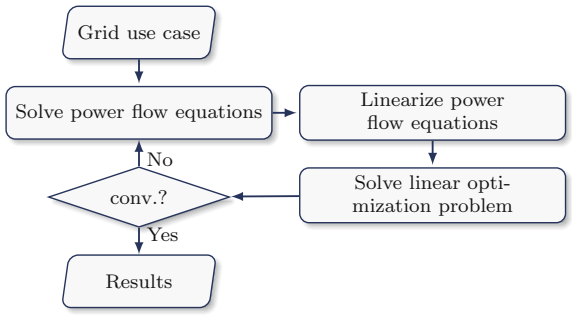

Fig. 3 Basic successive linear approach for OPF-problems

$$\mathbf{J}(\mathbf{x}_n) = \left(\begin{array}{cc} \frac{\partial P(\mathbf{x})}{\partial V} & \frac{\partial P(\mathbf{x})}{\partial \theta} \\ \frac{\partial \underline{Q}(\mathbf{x})}{\partial V} & \frac{\partial \underline{Q}(\mathbf{x})}{\partial \theta} \end{array} \right) \Bigg|_{\mathbf{x}=\mathbf{x}_n} \tag{30}$$

Based on the power flow solutions and the linearization, an optimization problem with linear constraints is built. The objective function can be linear or quadratic.

$$\begin{array}{ll} \min\limits_{\mathbf{u}} & o(\mathbf{u}) \\ \text{subject to} & \mathbf{A} \cdot \mathbf{u} \leq \mathbf{b} \end{array} \tag{31}$$

The solution of the optimization problem provides updated nodal balances for the power flow equations that can be used for a new solution of the power flow equations and an iterative update of the whole algorithm.

3.2 Linearization of Variable Quadripole Parameters

The direct application of the Jacobian matrix for the calculation of first order derivatives is only possible for degrees of freedom that are modeled as a change of nodal power balance. For those degrees of freedom modeled by a change of quadripole parameters, an extension of the Jacobian matrix is required.

$$\mathbf{J}_Y(\mathbf{x}_n) = \left(\begin{array}{cc} \frac{\partial P(\mathbf{x})}{\partial V} & \frac{\partial P(\mathbf{x})}{\partial \theta} \\ \frac{\partial \underline{Q}(\mathbf{x})}{\partial V} & \frac{\partial \underline{Q}(\mathbf{x})}{\partial \theta} \\ \frac{\partial Y(\mathbf{x})}{\partial V} & \frac{\partial Y(\mathbf{x})}{\partial \theta} \end{array} \right) \Bigg|_{\mathbf{x}=\mathbf{x}_n} \tag{32}$$

This extension of the Jacobian matrix increases the matrix dimension and hereby the computational effort in the linearization of power flow equations. To avoid this extension, an intermediate step by use of the nodal balance equations is used.

$$\frac{\partial \underline{V}(\mathbf{x})}{\partial \underline{Y}} \Bigg|_{\mathbf{x}=\mathbf{x}_n} = \frac{\partial \underline{V}(\mathbf{x})}{\partial \underline{S}(\mathbf{x})} \Bigg|_{\mathbf{x}=\mathbf{x}_n} \cdot \frac{\partial \underline{S}(\mathbf{x})}{\partial \underline{Y}} \Bigg|_{\mathbf{x}=\mathbf{x}_n} \cdot \frac{\partial \underline{Y}}{\partial \kappa} \tag{33}$$

The linearization relating to the apparent power $\frac{\partial \underline{V}}{\partial \underline{S}}$ can be directly taken from the inverted Jacobian matrix. The linearization with respect to the variable quadripole parameters can be concluded from the power flow equations $\frac{\partial \underline{S}}{\partial \underline{Y}}$. In addition, the derivative of the quadripole parameters with respect to the tap position $\frac{\partial \underline{Y}}{\partial \kappa}$ need to be considered. This formulation enables an efficient consideration of variable quadripole parameters without an increased size of the respective Jacobian matrix. The linearization is performed efficiently based on a linear combination of derivatives.

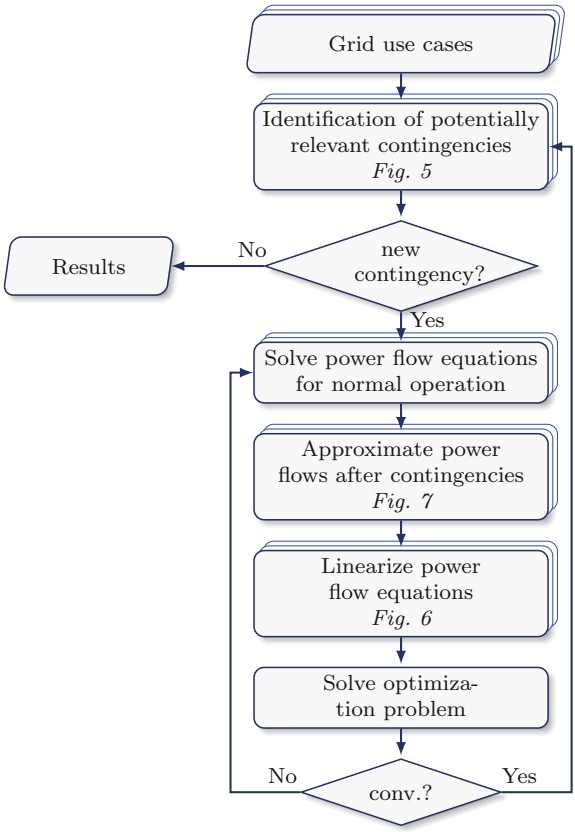

Fig. 4 Successive linear optimization procedure to solve large SCOPF problems

3.3 Optimization Problem Speed-Up

The solution of the developed optimization model by use of the method depicted in Fig. 3 is computationally very expensive. The computational effort is mostly determined by the solution of power flow equations and the linearization process. The actual solving process has only a minor influence. To enable the solution in limited computational time, a number of methodologies to reduce the problem size and speed up the solving process have been developed and are presented in the following. An overview of the extended method is given in Fig. 4.

3.3.1 Problem Size Reduction

Main driver of the computational effort is the large number of different power flow situations. This large number is caused by the number of considered grid use cases within the time coupling optimization on the one hand and the large number of

considered contingencies on the other hand. A direct neglecting of grid use cases is not possible. Different from this, there are a number of simplifications that can be applied to reduce the number of contingencies.

Relevant for the optimization problem are only contingencies that cause violations of technical constraints. All other contingencies can be neglected without any impact on the optimal solution. To benefit from this, a heuristic multistage reduction scheme is developed.

Starting point for this scheme are the solutions of power flow equations in normal operation for all grid use cases. Based on this solution, potentially critical contingencies are identified. For current limits, these are outages of branches that are loaded significantly in normal operation. For voltage limits, these are large reactive power sources in the surrounding of nodes with an absolute value of voltage close to the operational limits.

The power flow equations are solved for the set of potentially critical contingencies. For all grid components, the impact of all contingencies is ordered descendent by impact and only N_{asf} (typical value $N_{asf} = 3$) contingencies per component are considered further. In addition, only components with a loading above a critical limit Ξ_{crit} (typical value $\Xi_{crit} = 0.8$) are considered in the optimization problem.

As the optimization leads to a change of the operating point, there can be a change in critical contingencies. Thus, the identification is repeated iteratively as shown in Fig. 5. Even in this reduced solution scheme, the largest part of the computational time is consumed by calculations for contingency situations. Nevertheless, the objectives of the contingency analysis calculations differ. The first solution of power flow equations after contingencies only aims at the estimation of critical elements. It does not need to estimate the exact element loading. This enables the identification of critical elements by an efficient power flow approximation method (see [5]). The accuracy of this method furthermore enables the application to estimate the power flows for contingencies that do not generate any violated voltage constraints. This reduces the computational effort for solving the power flow equations in contingency situations by up to two orders of magnitude.

3.3.2 Linearization of Power Flow Equations

As can be seen in Eq. 30, the linearization of power flow equations can be performed by an inversion of the Jacobian matrix. Nevertheless, from a computational perspective, there is no need for a full inversion of the Jacobian matrix. In a successive linear approach sensitivities are only required for those electrical nodes where a controllable element is directly connected. Thus an inversion is only required for parts of the control area. Reducing the matrix inversion to these relevant parts reduces the computational effort in real world network models significantly.

The same approach could be used to reduce the output of the matrix inversion to the observation area. This can be done using a Sparse-Right-Hand-Side-Solver [8]. Nevertheless, different from the reduction on the control area, using a Sparse-Right-Hand-Side-Solver did not reduce the computational effort.

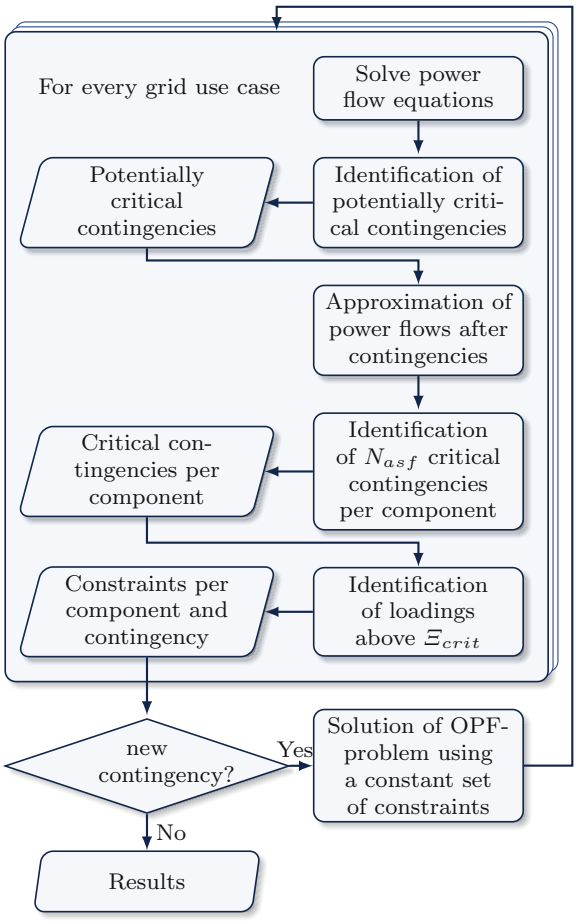

Fig. 5 Method to reduce the number of calculated contingencies

Even with these considerations, linearization remains the computationally most expensive part of the solution algorithm. Thus, there are a couple of approximation methodologies available to speed-up this process [1, 7, 9]. Within this paper, the power flow approximation methodology presented in [5] is extended to enable the efficient calculation of power flow linearizations. Compared to existing methods, it can be applied to any kind of contingency (e.g. two independent outages, outage of a tripod line, busbar outage) and it is faster and/or more accurate than other methods having this property.

Starting point for the methodology is the linearization in normal operation. The linearization enables the calculation of the change of power flows on the outaged elements due to an incremental change in the network topology of the normal operating state. These power flow changes on the outaged elements can be injected in the topology of the network model with the respective contingency considered and the outaged elements removed. The linearization of the power flow equations

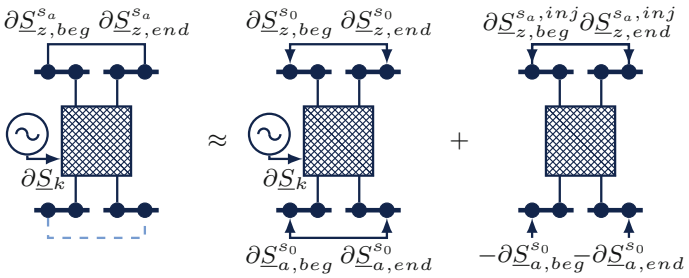

Fig. 6 Approximation methodology for power flow linearization after contingencies

after the contingency can then be estimated as the superposition of the linearization in normal operation and the changes due to the redistribution of power flows on the outaged elements as shown in Fig. 6.

$$\left.\frac{\partial \underline{\mathbf{V}}}{\partial \underline{\mathbf{S}}}\right|_{s=s_a} = \left.\frac{\partial \underline{\mathbf{V}}}{\partial \underline{\mathbf{S}}}\right|_{s=s_0} - \left.\frac{\partial \underline{\mathbf{V}}}{\partial \underline{\mathbf{S}}}\right|_{s=s_a} \cdot \sum_{z \in B_a^{s_a}} \underline{\mathbf{V}} \cdot \mathbf{A}_z \cdot \left(\check{\underline{\mathbf{Y}}}_z \cdot \mathbf{A}_z{}^T \cdot \left.\frac{\partial \underline{\mathbf{V}}}{\partial \underline{\mathbf{S}}}\right|_{s=s_0} \right)^* \tag{34}$$

The computational benefit of this approach is caused by a reduction of the number of sets of linear equations that need to be solved. Within the direct formulation, there are two sets of linear equations per node with a controllable element connected, that need to be solved. Using the developed approximation, there is only the need to solve two sets of linear equations per node where an outaged element is connected. This reduces the computational effort by up to two orders of magnitude.

3.3.3 Prediction of Power Flows After Contingencies

To further reduce the computational effort, the adaptive prediction scheme shown in Fig. 7 is used. For all considered constraints, the respective power flow solution and power flow linearization are estimated in the first iteration step.

$$\left.\underline{V}\right|^0_{s=s_a} = \left.\underline{V}\right|_{s=s_a} \tag{35}$$

$$\left.\frac{\partial \underline{V}}{\partial \underline{S}}\right|^0_{s=s_a} = \left.\frac{\partial \underline{V}}{\partial \underline{S}}\right|_{s=s_a} \tag{36}$$

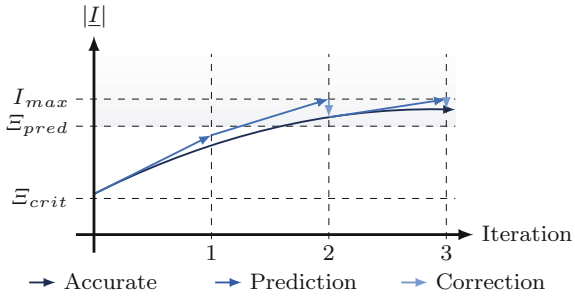

Fig. 7 Prediction scheme for constraints after contingencies

After the optimization step of the initial iteration, the linear optimization problem itself provides a prediction of the expected component loadings. This expected loading is used as an indicator for the impact of the respective constraint on the optimization problem. If the component loading is below a prediction threshold Ξ_{pred} (typical value $\Xi_{pred} = 0.9$), the predicted loading is used within the subsequent iteration and the linearization of the power flow equations is considered constant. If the loading is above the threshold, power flow equations for the respective contingency are solved in the new operating point and the linearization is also recalculated.

$$\tilde{I}_z^{s_a} = I_z^{s_a,m-1} + \left.\frac{\partial I_z^{s_a}}{\partial \underline{S}}\right|_{s=s_a}^{m-1} \cdot \Delta \underline{S}^{m-1} \tag{37}$$

$$\left.\underline{V}\right|_{s=s_a}^{m} = \begin{cases} \left.\underline{V}\right|_{s=s_a}^{m-1} + \left.\frac{\partial \underline{V}}{\partial \underline{S}}\right|_{s=s_a}^{m-1} \cdot \Delta \underline{S}^{m-1} \\ \quad \text{if } \tilde{I}_z^{s_a} \leq \Xi_{pred} \; \forall \, z \in B_b^{s_a} \\ \left.\underline{V}\right|_{s=s_a} \quad \text{else} \end{cases} \tag{38}$$

$$\left.\frac{\partial \underline{V}}{\partial \underline{S}}\right|_{s=s_a}^{m} = \begin{cases} \left.\frac{\partial \underline{V}}{\partial \underline{S}}\right|_{s=s_a}^{m-1} & \text{if } \tilde{I}_z^{s_a} \leq \Xi_{pred} \; \forall \, z \in B_b^{s_a} \\ \left.\frac{\partial \underline{V}}{\partial \underline{S}}\right|_{s=s_a} & \text{else} \end{cases} \tag{39}$$

This prediction scheme reduces the computational effort but does not affect the results, if the prediction threshold is chosen adequately.

4 Exemplary Results

To evaluate the capabilities of the developed optimization framework, it is applied to an exemplary day ahead congestion forecast (DACF) data-set of the european transmission grid. The network model has 7496 electrical nodes and 10709 branches. The observation and control area are limited to Germany, Poland, the Czech Republic, Austria, Slovenia, Switzerland and the Netherlands with an overall number of 3312

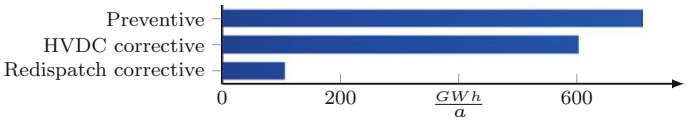

Fig. 8 Amount of redispatch assuming different preventive/corrective control strategies

nodes. To evaluate the performance of the optimization framework, a simulation of congestion management is performed considering current constraints in normal operation and after contingencies, phase-shifting-transformers and redispatch measures. All branch outages are considered as contingencies. The simulation considering only preventive remedial measures takes 18 seconds on an Intel i7-4810 notebook processor. The additional consideration of corrective remedial measures increases the computational time to 36 seconds. Considering the fact that the size of the linear optimization problem increases from $7.6 \cdot 10^6$ elements to $1.7 \cdot 10^9$ elements by more than a factor of 200, the developed optimization framework appears to be well suitable to cope with the dimensions and requirements of real world network models and operational requirements. A further evaluation on the impact of corrective remedial measures is carried out on a model for the european transmission grid for the year 2024 based on publicly available data [13] and the assumptions of the German network development plan 2014 [3]. The power plant schedules are based on a market simulation based on [10]. All simulations are performed for the 8760 individual grid use cases assuming a temporary admissible transmission loading of 120% on all lines. It can be seen in Fig. 8 that the corrective control of HVDC line power transmission reduces the required amount of preventive redispatch by 19%. A further use of corrective redispatch measures even reduces the amount of preventive redispatch under the given assumptions by 86%. This demonstrates the potential benefits that might be achievable by an increased implementation of corrective remedial measures.

5 Critical Review

The presented methodology for solving continuous SCOPF problems based on successive linear programming using different approximation methodologies shows excellent performance and plausible results within the application to real world test cases. Nevertheless, the impact of the proposed solution methodology on the accuracy of results should be kept in mind. A successive linear approach is not able to estimate the global optimum of the optimization problem. But keeping in mind that the proposed approach is similar to the successive linear approach used within the Newton-Raphson methodology, it will very likely be sufficiently accurate for most practical applications. Unfortunately, there is no possibility to provide an absolute figure on the accuracy of results of the successive linear algorithm, as there is no

solution methodology available to estimate the global optimum on real world test cases using finite computational resources.

Considering the convergence properties of the developed algorithm, the convergence for most test cases is very robust. Nevertheless, especially when it comes to disadvantageous cost parametrization and voltage constraints, additional computational steps to ensure algorithm convergence might be required.

The approximation and reduction methodologies applied on top of the piecewise linearization do not have a significant influence on results. Due to the fact, that all results are verified by a final contingency analysis, potential inaccuracies of the reduction methodologies are compensated in an additional iteration step. The approximation methodology for power flow equation linearization is found to be sufficiently accurate so that no significant influence on results could be identified.

6 Conclusions

A piece-wise linear approach to solve SCOPF problems using a number of different approximation and reduction methodologies has been presented in this paper. The presented methodology shows excellent computational performance and plausible results. Although the methodology is not capable to warrant solution optimality, it is expected to be sufficiently accurate for most practical applications.

Future publications will also cover the integration of binary power plant start-up decisions in the presented approach and additional computational aspects within the implementation of the presented methodology into a modular optimization framework.

Acknowledgements This research work has been carried out within the scope of the project UMBRELLA, supported under the 7th Framework Programme of the European Union, grant agreement 282775.

References

1. Breuer C (2014) Optimale Marktgebietszuschnitte und ihre Bewertung im europäischen Stromhandel. PhD thesis, RWTH Aachen, Aachen
2. Bundesnetzagentur, Bundeskartellamt (14.11.2014) Monitoringbericht 2014
3. Deutsche Übertragungsnetzbetreiber (04.11.2014) Netzentwicklungsplan Strom 2014: Zweiter Entwurf der Über-tragungsnetzbetreiber
4. Eickmann J, Drees T, Sprey JD, Moser A (2014) Optimizing storages for transmission system operation. Energy Procedia 46
5. Eickmann J, Kellermann J, Moser A (2015) Efficient power flow approximation methodology for topology optimization algorithms in transmission system operation. In: 5th International Conference on Clean Electric Power 2015
6. Glavitsch H, Bacher R (1991) Optimal power flow algorithms. Analysis and Control System Techniques for Electric Power Systems, ACADEMIC Press Inc (41)

7. Hug-Glanzmann G, Andersson G (14-18.07.2008) An accurate and efficient current injection method for the determination of the system state during line outages
8. Intel Corporation (2014) Reference manual for intel® math kernel library 11.1 update 4
9. Linnemann C, Echternacht D, Breuer C, Moser A (2011) Modeling optimal redispatch for the european transmission grid. In: PowerTech, 2011 IEEE Trondheim, pp 1–8
10. Mirbach T (2009) Marktsimulationsverfahren zur untersuchung der preisentwicklung im europäischen markt für elektrische energie. PhD thesis, RWTH Aachen, Aachen
11. Pegase Consortium (2011) D3.2: Development of prototype software for steady state optimizsation of the etn
12. Platbrood L, Capitanescu F, Merckx C, Crisciu H, Wehenkel L (2014) A generic approach for solving nonlinear-discrete security-constrained optimal power flow problems in large-scale systems. IEEE Transactions on Power Systems 29(3):1194–1203
13. Ringelband T (2011) Unsicherheit witterungsabhängiger Übertragungskapazitäten bei der Netzbetriebsplanung. PhD thesis, RWTH Aachen, Aachen
14. Zhu J (2009) Optimization of power system operation. IEEE Press series on power engineering, Wiley-IEEE and John Wiley [distributor], Piscataway, N.J. and Chichester

Part III
Flexibility, Storage and Uncertainty Quantification

Dispatch of Flexibility Options, Grid Infrastructure and Integration of Renewable Energies Within a Decentralized Electricity System

Results from Two Scenario Based Research Projects

Matthias Koch, Franziska Flachsbarth, Dierk Bauknecht, Christoph Heinemann, David Ritter, Christian Winger, Christof Timpe, Malin Gandor, Thole Klingenberg and Martin Tröschel

Abstract We present results of two model based scenario analysis focussing on the future German power sector which is characterized by a rising share of renewable energies and an associated higher demand for flexibility. Case study 1 is based on a general comparison between a decentrally and a centrally orientated electricity system. The research question of case study 2 is whether flexibility should be centrally balanced by a national market-based dispatch or dispatched in a decentralized manner

M. Koch (✉) · F. Flachsbarth · D. Bauknecht · C. Heinemann · D. Ritter · C. Winger · C. Timpe
Öko-Institut e.V., Freiburg, Germany
e-mail: m.koch@oeko.de

F. Flachsbarth
e-mail: f.flachsbarth@oeko.de

D. Bauknecht
e-mail: d.bauknecht@oeko.de

C. Heinemann
e-mail: c.heinemann@oeko.de

D. Ritter
e-mail: d.ritter@oeko.de

C. Winger
e-mail: c.winger@oeko.de

C. Timpe
e-mail: c.timpe@oeko.de

M. Gandor · T. Klingenberg · M. Tröschel
OFFIS e.V., Oldenburg, Germany
e-mail: gandor@offis.de

T. Klingenberg
e-mail: klingenberg@offis.de

M. Tröschel
e-mail: troeschel@offis.de

V. Bertsch et al. (eds.), *Advances in Energy System Optimization*,
Trends in Mathematics, DOI 10.1007/978-3-319-51795-7_5

within regional balancing areas. The combined results of these two case studies offer the possibility to show the differences between a decentralized and a centralized electricity system regarding the dispatch of generation, storage and flexibility options as well as resulting effects on variable costs, CO_2 emissions, grid usage and RE integration. Decentralization as control strategy leads to higher variable generation costs due to more expensive generation and less efficient flexibility options that come into the market, while the majority of demand and supply still needs a transmission grid for balancing.

Keywords Decentralized electricity system · RE integration · Flexibility options

1 Introduction

Germany as well the European Union aim to decrease their emissions of climate gases in order to reduce negative effects on climate change. The energy sector plays a major role within this strategy, especially concerning the substitution of electricity generation from fossil fuel fired power plants by renewable energy sources (RE) and higher energy efficiency.

With an increasing share of RE in the German electricity system, more flexibility is needed to balance demand and supply. Especially the concentration of wind turbines in the North of Germany in contrast with load centres in the western and southern part leads to a higher demand for transmission capacity, complementary to flexibility options like storage capacity. Until now, flexibility is mainly provided by thermal and pump storage power plants. Due to an expected decreasing dispatch of conventional power plants, new players also have to offer flexibility in the future, like demand side management (DSM) or combined heat and power plants (CHP) with thermal storages which is a question of the design of the future electricity system.

This design is still an open question in terms of scientific assessment, and diverging societal ideas do pose additional difficulties. One key question is whether the new infrastructure should be planned according to a centralized or decentralized concept. While there are efficiency losses in a decentralized concept which can be quantified, there are expected qualitative gains, e.g. like a higher acceptance of the transformation process of the electricity systems, coming along with the more diverse ownership structure and a broader participation in a decentralized market [1]. In fact, the decision between following a centralized or a decentralized concept is the basis for any further planning as it comprises several dimensions, including the geographical location and the grid level of new power plants, the role flexibility options have to fulfill and system coordination.

The focus of this paper is on the dimension of system coordination. Coordination between generation and demand is currently mainly located on the transmission grid level rather than on lower grid levels. At the same time, an increased share of decentralized generation and flexibility may also entail the development of coordination mechanisms on lower grid levels, including the arise of decentralized markets [2].

With larger shares of decentralized production, the question arises whether and how responsibility for system coordination should be decentralized as well. As proposed in [3], this could mean that more system services, especially the balancing of demand and supply, should be organized in cells on the lowest possible level. By combining them to larger cells representing urban districts, industrial areas or regions, the remaining imbalances can be balanced on a higher level [4, 5].

In terms of costs, there is a potential trade-off between decentralized coordination on the one hand that requires larger capacities of local resources and tends to dispatch them in a less efficient way and on the other hand centralized coordination, that requires a larger grid infrastructure. Due to the centralized coordination of the grid infrastructure today, Germany currently consists of a powerfull grid infrastructure. But for the future, strenghtening and extension of the exisiting grid infrastructure is necessary depending on the design of the electricity system.

The aim of this paper is to show the differences between a decentralized and a centralized electricity system regarding the dispatch of generation, storage and flexibility options based on a scenario analysis supported by the dispatch model PowerFlex-Grid developed by Öko-Institut. The presented results, like effects on variable generation costs, CO_2 emissions, transmission grid usage and RE integration, have been calculated and analyzed within two research projects:

- Transparency of Transmission Grid Planning[1] funded by the BMBF and realized in cooperation with E-Fect (Berlin) (case study 1)
- D-Flex[2] funded by the BMWi and realized in cooperation with OFFIS e.V. (Oldenburg) (case study 2).

2 Scenario Definition and Methodology of the Two Case Studies

2.1 Consideration of Grid Restricitons in Electricity System Modeling

Electricity system models that focus on transmission expansion planning may consider grid restricitions either as AC power flows including reactive power, ohmic losses, frequency and voltage constraints or as a linearized DC model approach, disregarding nonlinearities of AC power flow simulation [6]. Using a mixed-integer

[1]Project title "Erhöhung der Transparenz über den Bedarf zum Ausbau der Strom-Übertragungsnetze", project term: 2013–2015, funded within the BMBF reserach programm "Sozial-ökologische Forschung zum Themenschwerpunkt Umwelt- und gesellschaftsverträgliche Transformation des Energiesystems".

[2]Project title "Dezentral und zentral gesteuertes Energiemanagement auf Verteilnetzebene zur Systemintegration erneuerbarer Energien", project term: 2013–2015, funded within the BMWi reserach programm "Förderung von Forschung und Entwicklung im Bereich erneuerbare Energien".

formulation, grid restrictions can also be considered as linear disjunctive constraints [7].

Due to the increasing complexity of solving the transmission expansion planning problem including the AC power flow approach, the problem is often solved within two steps: the schedules of power plants, storages and other flexibility options are calculated with a market based dispatch model disregarding grid restrictions. Based on these dispatch results, load flows and the need for transmission expansion are determined by a AC power flow simulation [8, 9].

Uncertainty is another relevant topic for transmission expansion planning, to get an impression of the robustness of the solution and to indentify the most sensitive assumptions and input parameters. Van der Weijde and Hobbs propose a stochastic two-stage optimisation model for transmission planning under uncertaintity, formulated as a MILP. Within this approach, generators may react to decisions in transmission expansion and vice versa [10].

Because of the interaction of transmission expansion planning and generation planning, this combined planning problem is also solved within one model. Munoz, Hobbs and Watson therefore developped a two-phase bounding and decomposition approach, which provides information for optimal and near-optimal investment decisions in new grid and generation infrastrucutre [11].

In contrast to investments models for expansion planning, grid restrictions may be considered in pure dispatch models calculating unit commitment and redispatch. A three-phase algorithmic scheme is therefore developped in [12]. Another research topic for dispatch models including grid restricitions is nodal pricing, especially in the context of renewable energy integration [13].

2.2 Methodology of the Dispatch Model PowerFlex-Grid

PowerFlex-Grid is based on a linear optimization problem in hourly resolution (perfect foresight) and covers various generation and supply side technologies like thermal power plants and RE as well as different flexibility and storage options (e.g. DSM or pump storage power plants) [14]. DSM is considered in the model as a storage, with a time depending charging (capability for load increase), discharging (capability for load decrease) and storage capacity (depending on accumulated capability for load increase and corresponding time shift). The German transmission grid is implemented using the DC-approach on the underlying grid [15]. The resulting power flows are calculated based on dispatch results which may include redispatch. The PowerFlex model can be used in different configurations depending on the research question and available computation time.

In case study 1 the transmission grid in Germany is covered in detail in the PowerFlex model with about 500 nodes and 1000 transmission lines (see Fig. 2). The used grid data is mainly based on a data set provided by the German Federal Network Agency (BNetzA) regarding §12f(2) of the law on the energy industry (EnWG). The other countries of the ENTSO-E area are implemented as one node in the

PowerFlex model, linked with each other by interconnectors which can be used up to their hourly net transfer capacities (NTCs). Due to the high complexity of the optimization problem in this model configuration, thermal power plants are modeled without consideration of minimum load restrictions. This leads to a linear optimization problem. Furthermore a rolling horizon approach is used with an optimization horizon of 72 h and an overlap of 24 h.

In case study 2 the transmission grid in Germany is represented in a simplified and highly aggregated way. There are five nodes each representing a characteristic area in Germany:

- The region Northern Germany including Lower Saxony, Bremen, Schleswig-Holstein, Hamburg and Mecklenburg-West Pomerania is mainly characterized by a high share of wind energy, which often exceeds local demand.
- The region Western Germany including North Rhine-Westfalia, Rhineland-Palatinate and Saarland represents industrial load centres as well as a fossil fuel fired generation system.
- The region Eastern Germany including Brandenburg, Berlin, Saxony and Saxony-Anhalt may be characterized by a high share of wind onshore energy and lignite power plants combined with a demand on a low level.
- The region Southern Germany comprising Bavaria and Baden-Württemberg has the characteristics of a high share of photovoltaics and pump storage power plants combined with many load centres.
- The region Central Germany including Hessen and Thuringia is characterized as a transfer zone with local demand exceeding local RE supply.

The simplified transmission grid as implemented in the model is based on the VDE grid map [16] and consists of 42 existing interregional power lines, 1 interregional power line under construction and 5 power lines projected. Due to this simplification, the decentralized producers and consumers as well as thermal power plants can be modeled in more detail, e.g. thermal power plants are modeled regarding minimum load and specific ramp rate restrictions for uptime and downtime. This leads to a mixed-integer optimization problem. Due to the rolling horizon approach minimum uptime and downtime restrictions are not considered. As it is not in the focus of case study 2, interactions with other European countries are neglected. The optimization horizon is 120 h with an overlap of 24 h.

2.3 Description of the BMBF Project "Transparency of Transmission Grid Planning" and Scenario Definition

The aim of the project "Transparency of Transmission Grid Planning" is to support stakeholders in understanding and evaluating the calculations of the transmission system operators (TSOs) and the BNetzA which lead to the definition of the need of grid extension. The stakeholders involved represent non-governmental organizations such as World Wide Fund For Nature (WWF) or Deutsche Umwelthilfe e.V. (DUH)

as well as members from action groups in the context of local projects on transmission grid extension. In several workshops, the Öko-Institut and the stakeholders discussed the model-based results of different scenarios which were defined in advance by the stakeholders. A scenario highly requested by the stakeholders creates a decentralized electricity market in 2024. Compared to the scenario B2024 of the Grid Development Plan [8], the following variations of the assumptions were considered to point out the decentralized character of the scenario:

- In a decentralized world, consumers are more aware of the need of energy savings and measures on energy efficiency lead to a decrease of 2%/a in one decade. On the other hand the rising level of electrification leads to an increase of 1%/a in the same decade. As a consequence, electricity demand decreases by approximately 10% from 535 to 480 TWh/a.
- Furthermore, the consumers' willingness in terms of load shifting is higher and might be implemented in policy instruments, so that industry, trade and commerce and households are enabled to shift demand up to 4.7 GW.
- It is also assumed that in a decentralized setting, there is a higher share of RE distributed according to the federal targets. Hence, RE supply is increased and distributed as proposed in the scenario C2024 of the Grid Development Plan (+80 TWh) [8].
- To boost decentralized thermal production, it is assumed that the installed capacity of lignite and hard coal power plants decreases significantly until 2024 (lignite: −9.1 GW, hard coal: −11.7 GW). The order of decomissioning depends on the year of installation. To substitute the shortage of thermal capacity, there is an investment in natural gas fired power plants mainly CHP and gas turbines (+8 GW) at locations with residual demand peaks.
- It is assumed that the price of CO_2 certificates rise from 29 €/t to 40 €/t CO_2.
- Concerning the assumed underlying future transmission grid, grid extension is realized according to the defined needs in scenario B2024 of the Grid Development Plan and might be overestimated. In contrast, the NTCs are assumed to remain as present.

To model a decentralized scenario, a two-step approach is realized. In the first step, each node has to supply its own demand. As a consequence, the maximum transfer capacity of each power line is set to 0, and cross-border electricity exchange is disabled. If local electricity production by RE, thermal power plants and stored electricity cannot cover demand at any time step, a generic backup power plant will start to produce the shortfalls at very high costs.

On the other hand, in case of nodal electricity surpluses due to RE, must-run or heat production, there is the possibility to curtail production. To reduce the need for curtailment, demand can be shifted in time up to a certain amount and heat-storage facilities can be used. As a result of step 1, one can analyze the cost-minimal unit commitment as well as the need for capacity building in 2024 under highly decentralized assumptions.

In step 2 an internodal electricity exchange is enabled after each node has tried to cover its demand as much as possible. While all existing power plants have to produce the resulting supply of step 1 as a minimum, the nodal production of backup

power plants should be substituted with excess energy from other nodes. For this purpose, the capacities of the power lines (including cross-border lines) are set to their physical maximum, so that the grid can be used as a flexibility option.

2.4 Description of the BMWi Project "D-Flex" and Scenario Definition

Many of the new flexibility options, especially micro combined heat and power plants (engines) with thermal storages and DSM of heat pumps, households or electric vehicles are small-scaled and distributed. This leads to the main question of the research project D-Flex (case study 2) whether supply and demand should be centrally balanced by a national market-based oriented dispatch, or better be dispatched in a decentralized manner within regional balancing areas at the distribution grid level. For this purpose, demand and generation utilities have been assigned either to the decentralized or to the centralized level of the electricity system according to their installed capacity. Generation utilities with a capacity of more than 5 MW as well as the industrial electricity demand are allocated to the centralized level. All other players are allocated to the decentralized level of the electricity system.

To answer the question, the project combines the co-simulation platform mosaik from OFFIS for the decentralized sector with the dispatch model PowerFlex-Grid developed by Öko-Institut for the centralized sector.

2.4.1 Scenario Definition

The scenario analysis includes the years 2020 and 2030. Most of the input data refers to scenario A' of the BMU "Leitszenario" [17] or scenario B of the Grid Development Plan [8]. In scenario 2020 the conventional generation capacity is mainly located on the centralized level, while 60% of demand and 70% of RE supply are allocated to the decentralized level (see Table 1).

In scenario 2030 a decrease of about 5% from 2020 to 2030 is assumed for the electricity demand due to efforts in energy efficiency and demand reduction. The conventional generation capacity decreases due to phasing out coal fired power

Table 1 Allocation of generation capacity, RE supply and demand to the decentralized and centralized level of the electricity system in the scenario 2020

	Decentral	Central	Total
Conventional capacity	8 GW	74 GW	82 GW
RE supply	118 TWh	52 TWh	170 TWh
Demand	307 TWh	220 TWh	527 TWh

Table 2 Allocation of generation capacity, RE supply and demand to the decentralized and centralized level of the electricity system in the scenario 2030

	Decentral	Central	Total
Conventional capacity	10 GW	51 GW	61 GW
RE supply	145 TWh	92 TWh	237 TWh
Demand	290 TWh	208 TWh	498 TWh

plants. It is still mainly allocated to the centralized level, but less than in scenario 2020. Due to a strong increase in wind offshore capacity, 40% of RE supply is allocated to the centralized level in scenario 2030. Demand at the decentralized level slightly increases due to an increasing share of heat pumps and electric vehicles (see Table 2).

As flexibilized generation technologies located at the decentralized grid level CHP engines fired with biogas and combined with a 6 h biogas storage as well as CHP engines fired with natural gas and combined with a 2 h heat storage are considered in the scenario analysis. The so like flexibilized generation comprises about 52 TWh in 2020 and 60 TWh in 2030. The flexibilized demand at decentralized grid level is assumed to be 12 TWh in 2020 and 35 TWh in 2030 and consists of heat pumps, electric vehicles and DSM for trade and commerce as well as private households.

Each scenario year consists of three subscenarios, which represent the balancing and dispatch strategy:

- In the reference scenario, decentralized flexibility is not available at all. CHP engines and heat pumps are controlled by heat demand only, and the charging of electric vehicles as well as the electricity consumption from other consumers are only driven by their inelastic demand.
- In the scenario with a decentralized balancing strategy, the flexibility options are coordinated on the distribution grid level. They are dispatched in order to smooth the local residual loads (see Sect. 2.4.2).
- In the scenario with a market-oriented dispatch strategy from a central perspective, the commitment of the flexibility options coordinated on the distribution grid level is optimized under consideration of minimizing overall dispatch costs (see Sect. 2.4.2).

2.4.2 Dispatch Simulation at Distribution Grid Level

The co-simulation platform mosaik provides an AC power flow simulation at the distribution grid level with a resolution of 15 min. It includes various typical producers and consumers as well as a grid topology modeled by combining several typical topologies of rural and urban topologies of the low and medium voltage level. Based on real grid data from distribution system operators, these models differ in the number of nodes, line lengths and number of inhabitants. Each of the 5 regions considered

is represented by an urban and a rural distribution grid model with characteristic amount of installed power per technology.

During the simulation, the behavior of each individual producer and consumer in the grid is simulated individually. Furthermore, each flexible unit (producer or consumer) can be controlled by the coordination algorithm. To determine the number of units of different technologies (like photovoltaics or wind power units), the scenario-design process for regionally-specific scenario definition from [18] was used. The process maps assumptions about future changes in decentralized electricity generation and consumption into a grid model, such that this model reflects the real-world structure of a specific region. These scenarios are used to compare the impact of the following two coordination strategies on the transmission grid.

Decentralized Balancing

The PowerMatcher algorithm [19] is an agent-based coordination algorithm. It is organized in a hierarchical manner and tries to balance the generation and demand in the distribution grid. It thereby smooths the residual load. Each flexible and inflexible unit in the grid is represented by a software agent. During every simulation step, the agents inform an assigned parent agent (a so called concentrator agent) about the available flexibilities for the next 15 min. These so called bids are send to the auctioneer agent, which calculates a nearly optimal coordination of generation and demand in order to smooth the residual load for the next time interval. The result is sent back to the unit agents and they control the generation or consumption accordingly. Note that this algorithm is implemented to coordinate the units only for the next simulation step, or the next 15 min in this case and predictions about flexibilities are only given for the next 15 min. In each simulation step, the agents repeat this coordination process until the simulation of one year is finished.

Market-Oriented Dispatch

The second algorithm coordinates the flexible units in the grid, such that their aggregated power profile approximates a given target profile. The target profiles are calculated by PowerFlex-Grid, which balances generation and consumption through a cost minimal approach. As a result, each area gets a target profile for each flexible technology. Based on these target profiles, an optimization calculates an aggregated operation schedule for the flexible technologies. The implemented algorithm executes the following steps for each flexible technology in every simulation grid:

1. In a preparation step the target profile is downscaled to fit the installed capacity per technology in the simulation grid. The next steps are executed for each unit in the pool of simulated units.
2. The algorithm removes a unit from the pool and calculates a possibly fitting target profile for this specific unit. Note that this target profile may not be practical for the unit, so the next steps are necessary to generate a technically valid profile of the unit.
3. This target profile is used as input for the scheduler of the simulation model of the unit and the model generates a valid profile that approximates the target profile, but may deviate from it if the unit is not capable to provide a perfect fit.

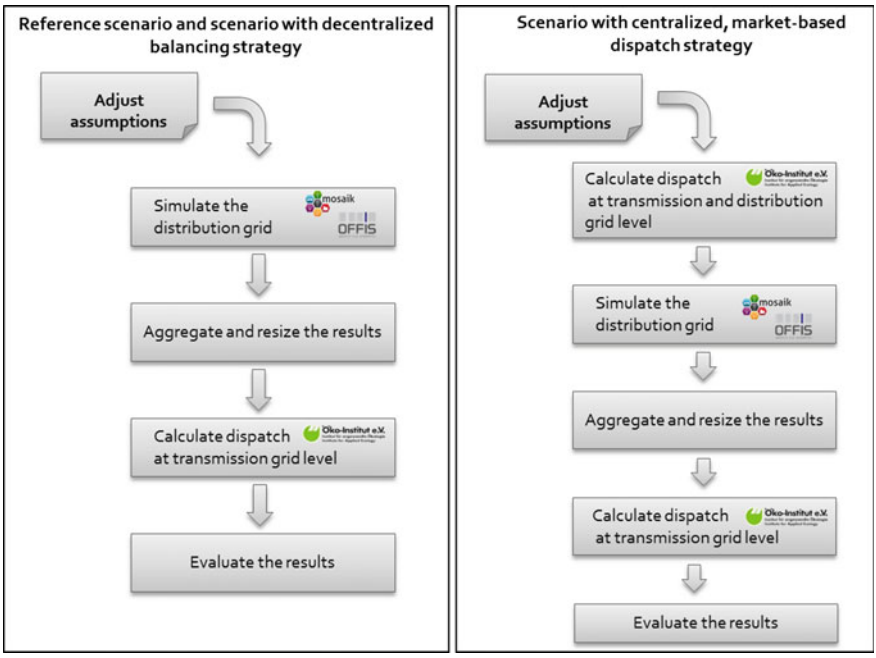

Fig. 1 Combination of the two simulation approaches (*left*: *reference scenario and decentralized balancing* and *right*: *centralized, market-based dispatch*, *source* OFFIS)

4. A new target profile for the technology is calculated by subtracting the new unit profile from the aggregated target profile.
5. If there are more units in the pool, the algorithm starts again at step 1. Otherwise the optimization finishes and with the unit profiles, an aggregated profile for the technology can be calculated.

2.4.3 Dispatch Modeling at Transmission and Distribution Grid Level by Combination of the Simulation Tools

This section gives a short overview of the used combination approach. A different order of the transmission grid and distribution grid simulation is used for each coordination approach. Figure 1 shows both combination methods. Both methods need a thorough adjustment of the assumptions in terms of installed power, typical unit sizes in the distribution grids and power profiles of the inflexible units.

In the reference scenario and in the scenario with decentralized balancing strategy the co-simulation platform mosaik is used to simulate the dispatch of supply and demand at the distribution grid level. As a result, the residual load which still has to be provided by the transmission grid level as well as the remaining surplus of RE at

the distribution grid level, serves as input for dispatch modeling at transmission grid level using the PowerFlex-Grid model.

The model PowerFlex-Grid is used twice in the scenario with market-oriented dispatch strategy. First it calculates the optimal schedules for all generation and storage units as well as DSM from a perspective of overall cost minimization, including all nodes and the decentralized and centralized grid level. Afterwards, the resulting technology profiles are used as target profiles for the decentralized units in order to optimize their schedules accordingly. Since these new profiles do not match the target profiles perfectly, the dispatch optimization at transmission grid level needs to be repeated.

3 Results of the Two Case Studies

3.1 Results of the BMBF Project "Transparency of Transmission Grid Planning"

As described above, the decentralized scenario analyzed in case study 1 is a multi-parameter variation compared to scenario B2024 of the Grid Development Plan. The results discussed do not directly reveal the effects of decentralization only, but the effects of a possible development in the energy sector if we aimed at achieving a decentralized electricity supply in Germany. To answer the question posed in this paper, it is helpful to first isolate the effects caused by decentralization only and in a second step to present the results of the multi-parameter variation.

Assuming a highly decentralized world as realized in step 1 where no assistance from other nodes is allowed to fulfill the nodal energy balance, the results show that a significant amount of RE production cannot be integrated and 188 TWh of RE notably produced by wind energy turbines have to be curtailed. Furthermore, there is excess energy from must-run and CHP units (43 TWh/a). On the other hand, at nodes where electricity production does not cover demand at each time step, backup power plants have to supply energy at very high costs. Over the year, the shortage of electricity reaches 158 TWh which corresponds to a capacity shortage of 38 GW distributed over 380 nodes. Corresponding to the existence of capacity shortages, Fig. 2 illustrates that the flexibility option of DSM is used at most of the nodes. The size of the circles indicate the amount of positive load shifting.

Over the year, a total amount of only 2 TWh of load is shifted from one time step to another which is low compared to the given potential. Also the flexibility option provided by pump storage power plants cannot be deployed significantly (0.9 TWh) as it can only be used at the one node where the power plant is situated. Load shifting and flexibility need the impulse of a price gap between two time steps in order to minimize costs as illustrated in Fig. 3. There are 3 demand curves d at 3 different time steps and a supply curve which is not changing over time in this example.

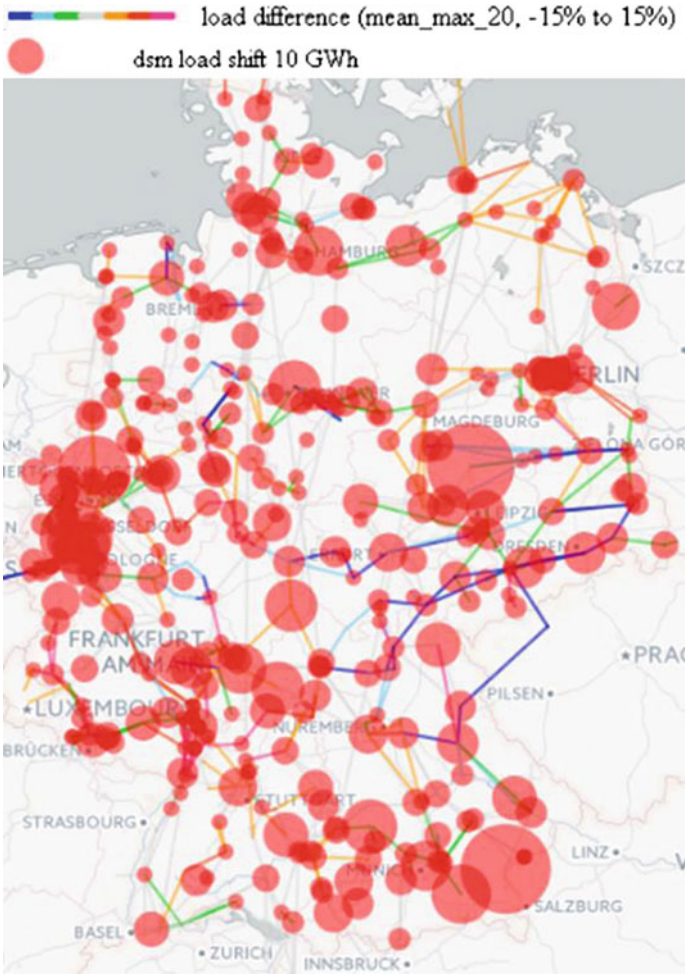

Fig. 2 Nodal utilization of DSM-potentials in the decentralized scenario per year (*source* Öko-Institut e.V.)

Furthermore, there is the possibility to shift demand up to the amount x from one time step to another, where $\Delta D \leq x$.

As $p_{t=1} = p_{t=2}$ and cannot be changed by lowering demand by x, a reduction or increase of demand in t=1 would not reduce costs. In t = 2, it is helpful to reduce demand in order to minimize costs as the quantity which has to be bought at the price of $p_{t=2}$ decreases, and in t = 3, demand can be increased, but still be bought at the lower price $p_{t=3}$.

Compared to a German or European merit order, a nodal merit order shows a more extreme specific characteristic with less time steps where such price gaps can be used (e.g. longer periods with electricity oversupply or deficit). Providing potential alone

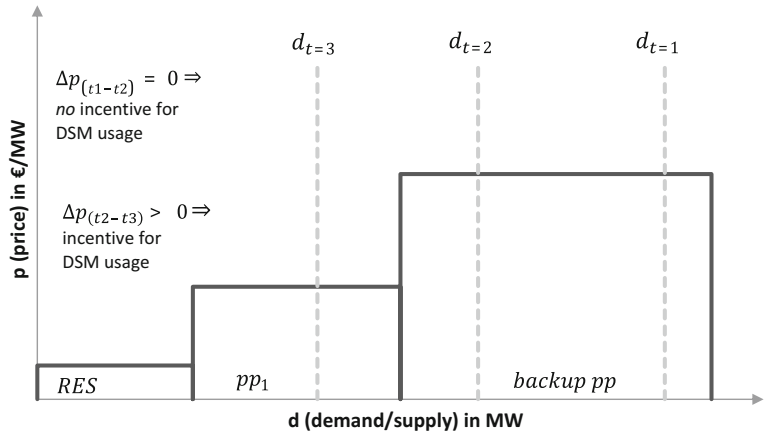

Fig. 3 Price gaps between time steps are necessary to give an incentive for load shifting (*source* Öko-Institut e.V.)

does not imply its utilization: There is also the need to give an incentive. Concerning CHP production, thermal storages are used at times where price gaps can be used to minimize costs and at times where RE can be additionally integrated in the market. A detailed evaluation of flexible CHP plants is part of an ongoing research project[3] and it is out of the scope of this paper.

In step 2 electricity supply provided by backup power plants in step 1 is completely substituted and production from must-run and CHP facilities are completely capitalized showing that there was a lack of a flexibility option having the characteristics of the transmission grid.[4] Furthermore RE curtailment drops to the amount of 38 TWh, proving that the underlying power grid increases RE integration. But as there is still RE curtailment, it has to be stated that decentralization of power supply does also reduce RE integration: By fixing the production level of thermal power plants according to step 1, local thermal power plants are preferred to RE surpluses from adjacent nodes.

Looking at the effects of a multi parameter variation, Fig. 4 shows the resulting fuel mix of the decentralized scenario (blue) compared to the scenario B2024 of the Grid Development Plan (green). The total electricity production decreases in the decentralized scenario by about 70 TWh due to the assumed decrease of demand in Germany. The electricity supplied by lignite and coal power plants decreases significantly by 220 TWh while electricity generated by natural gas power plants increases by 110 TWh based on a fuel shift in the merit order from natural gas to coal at a price of 40 €/t CO_2. In Germany, the fuel switch is intensified by the partial

[3]Project title "Einbindung des Wärme- und Kältesektors in das Strommarktmodell PowerFlex zur Analyse sektorübergreifender Effekte auf Klimaschutzziele und EE-Integration", project term 2014–2016, funded by Federal Ministry for Economic Affairs and Energy.

[4]The enlargement of the electricity market is a second factor favoring RE integration and reducing the supply of backup power plants.

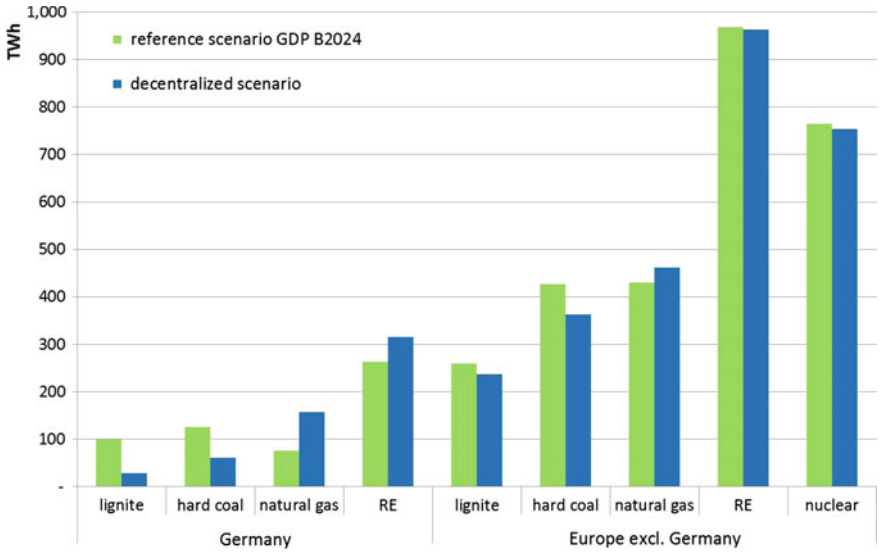

Fig. 4 Comparison of the fuel mix between the reference scenario and the decentralized scenario (*source* Öko-Institut e.V.)

phase out of coal power plants and the additional installation of gas power plants. Furthermore some oil power plants which would otherwise not be able to enter the market are covering local demand due to decentralization. A higher level of RE production might substitute lignite and coal electricity production as well.

The total CO_2 emissions in Europe are decreased by 100 million tons in the decentralized scenario compared to the scenario B2024 of the Grid Development Plan. This positive effect comes along with additional variable generation costs. Although demand is significantly reduced (−70 TWh) and integrated RE supply is much higher (+50 TWh), which both lowers the overall variable generation costs, there is an increase in costs of 8.7 billion € mainly caused by the higher price of CO_2 certificates. The impact of decentralization itself cannot be isolated properly due to multi-parameter variation. However, decentralization leads to higher costs due to more expensive generation units used for local supply primarily.

The stakeholders' interest in a decentralized solution for the transformation of the energy sector is linked to the assumption that, in a decentralized world, the need for grid extension should be reduced, as there is the incentive to consume production locally. The need for grid extension depends, among other criteria, on a grid load of at least 20% once a year. Concerning the grid extension projects within scenario B2024 of the Grid Development Plan, the maximum grid load decreases only for two projects below the 20% level. This leads to reduced investments of about 0.2 billion €.

In contrast to the maximum gird load, the average grid load in the decentralized scenario is reduced by 11.5% compared to the reference scenario. Figure 5 illustrates

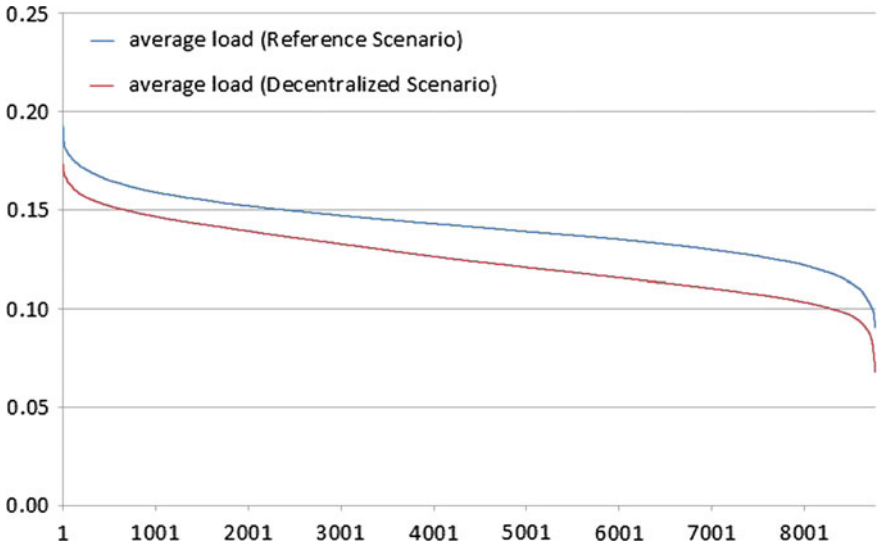

Fig. 5 Comparison of the annual load duration curves averaged over all power lines at each time step between the reference scenario and the decentralized scenario (*source* Öko-Institut e.V.)

the load duration curves of the average grid usage in both scenarios. All workloads of a certain time step are averaged and then put in a decreasing order. The distance between both curves is constant, which shows that decentralization reduces the average grid usage in general.

Assuming a linear correlation between transmission losses and grid load, transmission losses decrease by 17% in the decentralized scenario. As transmission losses decrease above average compared to the grid usage, one can conclude that in the decentralized scenario the average transport distances decrease.

Furthermore, we are interested in detecting relevant changes concerning the grid usage of single power lines. Such differences might show regional changes of the electricity market which could lead to deviant recommendations concerning grid extension plans. Therefore, the top 20% of workloads of each power line are aggregated to an indicator ("mean max 20"). The differences of that indicator between both scenarios are visualized in Fig. 2.

If the averaged usage of a power line increases (decreases) in the decentralized scenario compared to the reference scenario, the power line turns pink (blue). Due to the decreased production of lignite power plants, in the decentralized scenario the workload of power lines directing from the east to the west is significantly lowered. On power lines directing from Thuringia to Bavaria the maximum capacity is only achieved in the reference scenario.[5] The grid usage of cross border power lines as well

[5]There are more power lines which operate at their maximum capacity compared to the reference scenario which is an indicator for possible bottlenecks and further need for grid extension. On the other hand, some bottlenecks of the scenario B2024 disappeared.

Table 3 Trade balance of electricty generation, demand, import and export from some country's perspective (*source* Öko-Institut e.V.)

	Reference (TWh)	Decentralized (TWh)	Import/export
Germany	−37	−109	More export
Belgium	7	6	Less import
Poland	7	19	More import
Czech Rep.	−19	−8	Less export
Sweden	−30	−20	Less export
France	−44	−38	Less export
Austria	4	10	More import

as the power lines close to neighboring countries is increased. German exports rise from 37 to 109 TWh/a, while especially the production in Poland, Czech Republic, Sweden, France and Austria is reduced which can be seen in Table 3.

Decentralization supports export because of power plants at high costs get into the market in step 1 and as a consequence, cheap German power plants can still supply electricity at low costs for European countries in step 2, which also effects the workload of the German transmission grid and the reduction stays beyond the stakeholders' expectations.

3.2 Results of the BMWi Project "D-Flex"

Concerning the results from case study 2, we focus on effects from different balancing and dispatch strategies illustrated in the example of the flexibilized CHP engines (see Sect. 2.4.1). Figure 6 shows the calculated schedule of all CHP engines on a decentralized grid level. In the reference scenario (blue), the generation profile is quite flat due to the dominance of biogas CHP engines, but it increases during winter due to the heat demand which has to be covered by natural gas fired CHP engines.

In the scenario with the market-oriented dispatch, the result of the unit commitment according to the model PowerFlex-Grid (purple) shows the highest fluctuations as well as the highest amplitude which means that the flexibilty potential of the decentralized CHP engines is utilized most. This optimal profile from a centralized perspective is used as a target profile for the model mosaik (green) which tries to realize it including local restrictions. Although the amplitude is getting smaller, the original pattern of the profile is visible. The deviations between both curves show, that unit specific restrictions which come into account by discrete unit simulation lead to an overestimation of flexibility from the centralized perspective, where these restrictions are not visible.

The efficiency losses caused by following a decentralized balancing strategy (red) may be quantified by comparison with the green profile. Both curves demonstrate a

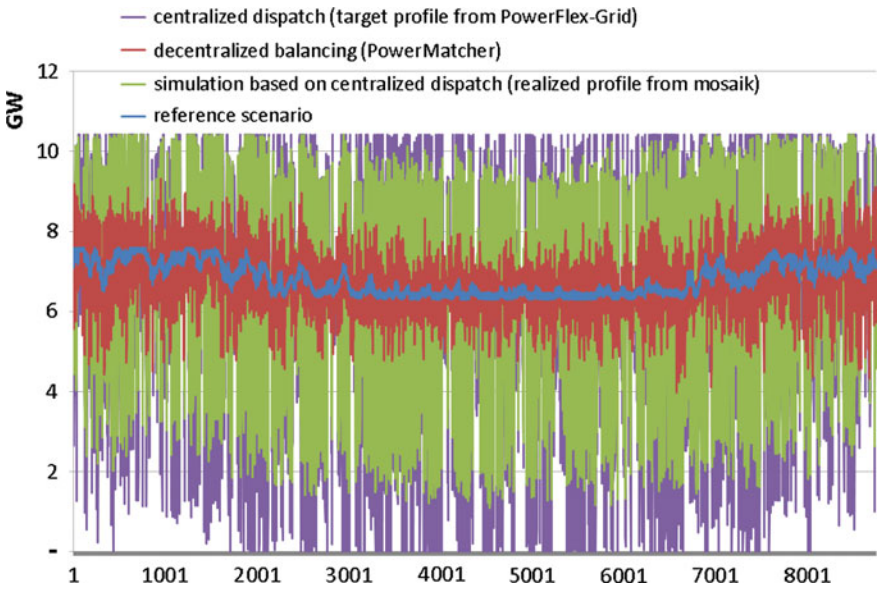

Fig. 6 Dispatch of decentralized CHP engines in different balancing strategies (*source* Öko-Institut e.V.)

similiar pattern of fluctuation. Regardless of the balancing strategy, the frame conditions provoke a concurrent impulse on how to use of the flexibility potential. However, following a decentralized balancing strategy leads in all D-Flex subscenarios of a specific scenario year to a decreased utilization of the flexibility potential, as the amplitude is scaled down. As a result, one can conclude that there are efficiency losses due to the lack of knowlegde caused by the decentral perspective and the used modeling approach. While demand for flexibility outside of the local system boundary is not visible due to the decentralized balancing strategy, the PowerMatcher algorithm has to make up its decision based on the knowledge about one time step in contrast to the perfect foresight of the centralized dipatch algorithm.

4 Critical Review

The analysis carried out in the two projects as described in this paper focuses on a comparison between a centrally and a decentrally balanced electricity market. In case study 1 it is assumed that the introduction of decentralized balancing is combined with several other variations, such as the share of renewables. Due to this multi parameter variation, it is difficult to isolate the effects of decentralized balancing. In case study 2 the balancing strategy is the only variation between the scenarios, but it is realized in different approaches with different models. In this case it is

difficult to decide whether the effect is caused by decentralized balancing or by differing algorithms. The scenario analysis in this paper is based on the dispatch model PowerFlex-Grid (case study 1 and 2) and on the AC power flow simulation plattform mosaik (case study 2). Effects concerning investment decisions in grid, generation or flexibility infrastructure are therefor not part of the model results. These effects have to be derived indirectly from dispatch profiles and other indicators (e.g. back-up generation).

5 Conclusions

In both case studies, we could verify that decentralized balancing causes welfare losses in terms of system operation due to the fact that a global minimum is smaller or equal than the sum of all local minima. From a central perspective where all information is accessible a more profound decision can be taken compared to the result of a couple of regional decisions based on limited knowledge about the respective region only. Decentralised balancing increases the need for flexibility because the interregional smoothing effects of supply and demand are not exploited, and the flexibility provided by the transmission grid has to be partially substituted by other flexibility options.

At the same time we found that in a decentralized scenario, in which DSM can be used only locally, the dispatch of the available flexibility from DSM decreases. The reason for this is that in local markets with only a limited number of market participants, there is a lower number of price differences between adjacent time steps and thus longer time periods with equal prices. This reduces the incentive to shift demand in order to reduce costs. It can therefore be concluded that DSM and even small-scale DSM resources that seem to lend themselves to decentralized balancing should be integrated in centralized markets as well.

There is a potential trade-off between a higher need for investments in local capacity and flexibility resources in a decentralized scenario and a higher need for investments in grid infrastructure in a centralized scenario. We found that in a decentralized scenario, the grid usage decreases only slightly, which indicates that the effect on transmission expansion requirements is only limited. This is partly due to the fact that Germany is embedded in the European market. The increased dispatch of more expensive gas and oil fired power plants for covering demand locally in a scenario with decentralized balancing, frees up less expensive coal fired power plant capacity that can be used for increasing exports. The resulting cross-border power flows increase grid usage.

6 Outlook

Within further case studies we will develop the decentralized scenario further. For example, by selecting only small scale electricity producers and consumers for local balancing in step 1 or by an extension of the areas of local balancing from a nodal to a regional perspective including several nodes, it is assumed to realize a more efficient concept of decentralization.

Acknowledgements We thank the Federal Ministry of Education and Research and the Federal Ministry for Economic Affairs and Energy for funding the two research projects and E-Fect and OFFIS for excellent cooperation.

References

1. Funcke, Simon; Bauknecht, Dierk, Typology of centralised and decentralised approaches for the electricity infrastructure, accepted for publication in Utilities Policy (2015).
2. Agsten, M.; Bauknecht, D.; Becker, A.; Brinker, W.; Conrads, R.; Diebels, V.; Erge, T.; Feuerhahn, S.; Heinemann, C.; Hermsmeier, J.; Hollinger, R.; Klose, T.; Koch, M.; Mayer, C.; Pistoor, G.; Rosinger, C.; Rüttinger, H.; Schmedes, T.; Stadler, M.; eTelligence. New energy sources require a new approach, Oldenburg (2013)
3. Benz, Thomas; Dickert, Jörg; Erbert, Maik; Erdmann, Niels; Johae, Christopher; Katzenbach, Burkhard; Glaunsinger, Wolfgang; Müller, Holger; Schegner, Peter; Schwarz, Jürgen; Speh, Rainer; Stagge, Hanno; Zdrallek, Markus, Der zelluläre Ansatz, Grundlage einer erfolgreichen, regionenübergreifenden Energiewende, 96. VDE Verband der Elektrotechnik Elektronik Informationstechnik e.V., Frankfurt am Main (2015)
4. Schmitt, Frieder, E-Energy-Projekt Modellstadt Mannheim. Nachhaltigkeit und Partizipation mit regionalen Energiekonzepten, E-Energy Abschlusskongress, Themenblock 2: Dezentrale Systeme für sichere Versorgung, Bundesministerium für Wirtschaft und Technologie, Berlin, (17.01.2013)
5. Smart Grids-Plattform Baden-Württemberg e.V., Schaufenster für intelligente Energieversorgung geht an den Start, Länderübergreifendes Modellprojekt initiiert, Pressemitteilung vom 27.08.2015, http://www.smartgrids-bw.net/csells/csells-ueberblick/
6. Reza Hemmati; Rahmat-Allah Hooshmand; Amin Khodabakhshian, State-of-the-art of transmission expansion planning: Comprehensive review, Renewable and Sustainable Energy Reviews, Volume 23, p. 312–319 (2013)
7. Özge Özdemir; Francisco D. Munoz; Jonathan L. Ho; Benjamin F. Hobbs, Economic Analysis of Transmission Expansion Planning With Price-Responsive Demand and Quadratic Losses by Successive LP, IEEE TRANSACTIONS ON POWER SYSTEMS, 0885–8950 (2015)
8. 50Hertz Transmission GmbH; Amprion GmbH; TenneT TSO GmbH; TransnetBW GmbH, Netzentwicklungsplan Strom 2024, Zweiter Entwurf (2014)
9. Carsten Pape; Philip Härtel; Angela Scholz; Rainer Schwinn; Tim Drees; Andreas Maaz; Normann Gerhardt; Jens Sprey; Christopher Breuer; Albert Moser; Frank Sailer; Simon Reuter; Thorsten Müller, Roadmap Speicher. Speicherbedarf für Erneuerbare Energien – Speicheralternativen - Speicheranreiz - Überwindung rechtlicher Hemmnisse. Endbericht. Hg. v. Bundesministerium für Wirtschaft und Energie (BMWI). IWES; IAEW; Stiftung Umweltenergierecht. Kassel, Aachen, Würzburg, 2014.
10. Adriaan Hendrik van der Weijde; Benjamin F. Hobbs, The economics of planning electricity transmission to accommodate renewables: Using two-stage optimisation to evaluate flexibility and the cost of disregarding uncertainty, Energy Economics, Volume 34, p. 2089–2101 (2012)

11. F. D. Munoz; B. F. Hobbs; J.-P. Watson, New bounding and decomposition approaches for MILP investment problems: Multi-area transmission and generation planning under policy constraints, European Journal of Operational Research, Volume 248, p. 888–898 (2016)
12. Chung-Li Tseng; Shmuel S. Oren; Carol S. Cheng; Chao-an Li; Alva J. Svoboda; Raymond B. Johnson, A transmission-constrained unit commitment method in power system scheduling, Decision Support Systems, Volume 24, p. 297–310 (1999)
13. Karsten Neuhoff; Julian Barquin; Janusz W. Bialek; Rodney Boyd; Chris J. Dent; Francisco Echavarren; Thilo Grau; Christian von Hirschhausen; Benjamin F. Hobbs; Friedrich Kunz; Christian Nabe; Georgios Papaefthymiou; Christoph Weber; Hannes Weigt, Renewable electric energy integration: Quantifying the value of design of markets for international transmission capacity, Energy Economics, Volume 40, p. 760–772 (2013)
14. Koch, Matthias; Bauknecht, Dierk; Heinemann, Christoph; Ritter, David; Vogel, Moritz; Tröster, Eckehard, Modellgestützte Bewertung von Netzausbau im europäischen Netzverbund und Flexibilitätsoptionen im deutschen Stromsystem im Zeitraum 2020 – 2050, Zeitschrift für Energiewirtschaft, Volume 39, Issue 1, p. 1–17, (2015)
15. Stigler, Heinz; Todem, Christian, Optimization of the austrian electricity sector (control zone of verbund apg) by nodal pricing, Central European Journal of Operations Research, Volume 13, Issue 2, p. 105 (2005)
16. VDE-Netzkarte des Forums Netztechnik / Netzbetrieb im VDE (Stand: 01.01.2012)
17. Nitsch, Joachim; Pregger, Thomas; Naegler, Tobias; Heide, Dominik; de Tena, Diego Luca; Trieb, Franz; Scholz, Yvonne; Nienhaus, Kristina; Gerhardt, Norman; Sterner, Michael; Trost, Tobias; von Oehsen, Amany; Schwinn, Rainer; Pape, Carsten; Hahn, Henning; Wickert, Manuel; Wenzel, Bernd, Langfristszenarien und Strategien für den Ausbau der erneuerbaren Energien in Deutschland bei Berücksichtigung der Entwicklung in Europa und global, BMU - FKZ 03MAP146 (29.03.2012)
18. Blank, M.; Gandor, M.; Nieße, A.; Scherfke, S.; Lehnhoff, S.; Sonnenschein, M., Regionally-Specific Scenarios for Smart Grid Simulations, 5th International Conference on Power Engineering, Energy and Electrical Drives (POWERENG2015)
19. Kok, JK, The PowerMatcher: Smart Coordination for the Smart Electricity Grid, PhD Thesis, Amsterdam: Vrije Universiteit (2013)

Dynamic Decision Making in Energy Systems with Storage and Renewable Energy Sources

Stephan Meisel and Warren B. Powell

Abstract We model an energy system with a storage device, a renewable energy source and with market access as a Markov decision process. We have identified four classes of pure policies (PFAs, CFAs, VFAs and lookaheads), each of which may work best depending on the characteristics of the system (volatility of prices, stationarity, accuracy of forecasts). We demonstrate that each of the four classes can work best on a particular instance of the problem. We describe the problem characteristics that bring out the best of each policy.

Keywords Energy storage · Stochastic optimization · Sequential decision making

1 Introduction

The combination of renewable energy sources and energy storage plays an increasingly important role in modern energy systems [2, 11]. Operating a system with storage and renewables over time requires making dynamic (sequential) decisions about energy flows. At each point in time system operators, such as utilities, can decide about how much energy to store or retrieve from storage, and about how much energy to buy or sell at the markets. These decisions typically need to be made in the presence of uncertainty about both future energy prices and future amounts of generated energy. Making the right decisions that take into account the remaining decision process is a key to increasing economic efficiency of such an energy system [12].

In order to ensure economic efficiency, system operators need policies, i.e., decision rules, that inform about which decisions to make at any possible state of the

S. Meisel (✉)
Department of Information Systems, University of Münster, Münster, Germany
e-mail: stephan.meisel@uni-muenster.de

W.B. Powell
Department of Operations Research and Financial Engineering, Princeton University, Princeton, NJ, USA
e-mail: powell@princeton.edu

V. Bertsch et al. (eds.), *Advances in Energy System Optimization*,
Trends in Mathematics, DOI 10.1007/978-3-319-51795-7_6

system. There are four classes of policies that have been identified that may be used [13]: policy function approximations (PFAs), cost function approximations (CFAs), policies based on value function approximations (VFAs), and lookahead policies. Each class is suited to handle specific problem characteristics. In this paper, we create different problem settings which bring out the best of each class of policy, which helps us identify when each policy might work best.

Energy systems with renewable sources have been a field of application of optimization methods since a few years ago [1]. Throughout this period of time a number of authors have used stochastic optimization techniques to derive policies for systems with energy storage. Optimal policies could only be considered in very few particular cases. Reference [7] derives an optimal energy commitment policy for a system with wind farms, storage and a mean-reverting price process. Optimality is subject to the fairly strong hypothesis of wind energy being uniformly distributed. Reference [5] models a system with renewables, conventional generation and storage device over an infinite time horizon. They prove the existence of an optimal stationary policy for this system, and use the optimal policy to derive a number of structural results about the value of storage.

The optimal policies of both [5, 7] rely on modeling the considered energy storage problem as a stochastic dynamic program [16]. The same modeling approach is used by [9, 10, 18] to derive approximations of optimal policies. Reference [9] models the problem of a renewable energy producer who trades on a day-ahead market under supply and price uncertainty. They compare an approximately optimal policy for their model with an optimal policy of a discretized version of the model and conclude that the former outperforms the latter. Reference [10] derive an approximation of the optimal policy for operation of hydro storage systems with multiple connected reservoirs. Their problem formulation integrates short-term intraday decisions with long-term interday decisions, and their solution approach combines different stochastic optimization techniques. Reference [18] considers operation of a storage device with multiple competing demands subject to various sources of market and system uncertainty. They use different optimization techniques to derive feasible policies that allow for statement of lower and upper bounds on the value of an optimal policy. Similarly, [8] relies on stochastic dynamic programming to compute upper and lower bounds on the value of natural gas storage. They optimize inventory trading decisions subject to capacity constraints in the presence of uncertain gas prices.

A different modeling approach to approximating an optimal policy is applied by [4]. The authors propose a two-stage stochastic program [6] for making both bidding decisions on the day-ahead market and operating decisions with a pumped storage facility. They consider the energy system of a generating company with a wind farm and uncertain market prices. The work of [3] also considers an energy system with pumped storage. Relying on scenario-based linear programs, the authors answer the question of whether and how much pumped storage to include in an energy system on a small island with abundant renewable energy.

Reference [14] provides an overview of solution strategies that can be applied to energy systems with storage and renewables. They propose a canonical modeling framework for dynamic decision problems and show that any of the solution strategies

corresponds to one class of policy. The different classes of policies are discussed in Sect. 3.

The remainder of this paper is organized as follows. In Sect. 2 we present a model of the energy storage problem that we use for illustrating the challenge of policy class selection. In Sect. 3 we introduce the four classes of elementary policies that may be applied, and in Sect. 4 we propose one policy from each class. In Sect. 5 we introduce different variations of the problem introduced in Sect. 2, and show numerically how the policies of Sect. 4 perform with these variations. Section 6 concludes the paper.

2 Problem Formulation

We consider an energy system over a finite period of time. The system includes an intermittent source of renewable energy, a storage device and the option to buy and sell energy at the market. Generated energy, price, loads and forecasts may be subject to uncertainty. The system operator aims at maximizing profits from energy sales.

In order to represent the dynamic decision problem of the system operator as a Markov decision process, we use the modeling framework proposed in [14]. We refer to [15] for a detailed illustration of how to apply this framework to energy storage problems.

2.1 State and Exogenous Information

The energy system is operated over a continuous period of time, starting at time $t = 0$ and ending at $t = T$. Within this period, decisions about energy flows are made at discrete points in time $t \in \{0, \ldots, T\}$. In a real-world application the time interval between t and $t + 1$ may, e.g., be 15 minutes. At each decision time t the system is at a state $S_t = (L_t, E_t, P_t, R_t, f_t)$, where the variables of the state are defined as follows:

Load: L_t denotes the energy load at time t in MWh. We assume that the load occurring between points in time t and $t + 1$ is known at t.
Renewable energy: E_t denotes the amount of renewable energy (in MWh) available at time t.
Price: P_t denotes the unit price of energy at time t in Dollars. We assume that both selling price and purchase price of energy are equal at any possible decision time.
Energy in storage: R_t denotes the amount of energy in storage at time t in MWh.
Forecasts: $f_t = (f_t^L, f_t^E, f_t^P)$ denotes forecasts of the future loads, amounts of generated energy and prices. Each of the three elements of f_t is a vector of length $T - t$, where each component represents the forecasted quantity at a future point in time t' with $t < t' \leq T$.

We assume that forecasts are provided by a third party company and that they are therefore not subject to the decision maker's control. Similarly, load, generated energy and market price result from uncontrolled exogenous processes that evolve over time.

From the decision maker's point of view, each of the uncontrolled processes is random. At each point in time t he receives new exogenous information in terms of changes of L_t, E_t, P_t and f_t. We denote these changes as $\hat{L}_t$, $\hat{E}_t$, $\hat{P}_t$ as well as $\hat{f}_t$, and represent the exogenous information arriving at time t as $W_t = (\hat{L}_t, \hat{E}_t, \hat{P}_t, \hat{f}_t)$.

2.2 Decisions

At each point in time the system operator decides about the energy flows of the system. We assume that he may use the generated energy either for satisfying the current load or for charging the storage device. Any amount of generated energy that is not used for one of these two purposes is lost. The operator must always fully satisfy the current load. In order to do so he can both retrieve energy from storage and buy energy at the market, in addition to relying on generated energy. Apart from satisfaction of loads, the operator has the additional option of trading energy at the market. At each point in time he may sell stored energy at the market or charge the storage device by buying energy from the market.

We represent the operator's decision at time t as $x_t = (x_t^{EL}, x_t^{RL}, x_t^{ML}, x_t^{ER}, x_t^{MR}, x_t^{RM})$, where the elements of x_t denote energy flows between renewable energy source (E), load (L), market (M) and storage device (R). E.g., x_t^{EL} represents the amount of generated energy that is used for load satisfaction at time t. The maximum set $\mathcal{X}_t$ of feasible decisions x_t at a point in time t is defined by the following constraints.

$$
\begin{aligned}
x_t^{EL} + \eta^d x_t^{RL} + x_t^{ML} &= L_t + E_t^- && (1)\\
\eta^c (x_t^{ER} + x_t^{MR}) &\leq R^C - R_t && (2)\\
x_t^{RL} + x_t^{RM} &\leq R_t && (3)\\
x_t^{EL} + x_t^{ER} &\leq E_t^+ && (4)\\
x_t^{ER} + x_t^{MR} &\leq \delta^c && (5)\\
x_t^{RL} + x_t^{RM} &\leq \delta^d && (6)\\
x_t^{EL}, x_t^{RL}, x_t^{ML}, x_t^{ER}, x_t^{MR}, x_t^{RM} &\geq 0 && (7)
\end{aligned}
$$

Constraint (1) enforces a decision that fully satisfies the currently required amount of energy. Note that we take into account the fact that E_t may be negative, as units such as wind turbines typically consume energy if they do not generate. Consequently, the required energy consists of the sum of current load L_t and the amount E_t^- of consumed energy, where $E_t^- = -1 * \min(0, E_t)$.

Constraint (2) makes sure that the amount of energy that is stored at time t does not exceed the storage device's remaining capacity. We denote the maximum capacity of the device as R^C, and include its (dis-)charge efficiencies η^d and η^c into constraints (1) and (2).

Constraint (3) guarantees decisions that do not take more energy than currently available out of the storage device. Similarly, constraint (4) ensures that no decision is made that uses more renewable energy than currently generated. We define $E_t^+ = max(0, E_t)$.

Constraints (5) and (6) make sure that both charge rate and discharge rate of the storage device are not violated by the energy flows that go in and out of storage at time t. Constraint (7) guarantees nonnegativity of all energy flows.

2.3 State Transition

The evolution of the system over time is determined by the initial system state, the sequence of decisions as well as the exogenous information that is arriving randomly over time. At each state S_t the transition to successor state S_{t+1} follows the transition function $S^M(S_t, x_t, W_{t+1}) = S_{t+1}$. This function is defined by the following equations:

$$L_{t+1} = L_t + \hat{L}_{t+1}, \tag{8}$$

$$P_{t+1} = P_t + \hat{P}_{t+1}, \tag{9}$$

$$E_{t+1} = E_t + \hat{E}_{t+1}, \tag{10}$$

$$f_{t+1}^L = f_t^L + \hat{f}_{t+1}^L, \tag{11}$$

$$f_{t+1}^P = f_t^P + \hat{f}_{t+1}^P, \tag{12}$$

$$f_{t+1}^E = f_t^E + \hat{f}_{t+1}^E. \tag{13}$$

$$R_{t+1} = R_t + \eta^c(x_t^{ER} + x_t^{MR}) - (x_t^{RL} + x_t^{RM}). \tag{14}$$

Equations (8), (9) and (10) show the transitions of the variables representing load, price and generated energy. Each of these variables changes its value according to the exogenous information arriving at $t + 1$. The transitions of the variables representing the forecasts are given by Eqs. (11), (12) and (13). They are executed in a similar way as the transitions of load, price and generated energy. The exogenous information, as e.g., $\hat{f}_{t+1}^L$, is given in terms of a vector of length $T - t$. Each element of the vector represents the change of the current forecast of the corresponding quantity, as, e.g. the change of the current forecast of load, for a specific point in time t'.

Only the transition from R_t to R_{t+1} is not due to exogenous influences. Equation (14) shows that the amount of energy in storage at time $t+1$ merely depends on the amount at time t as well as on the (dis)charged amount of energy at t.

2.4 Objective

As the processes governing the evolutions of generated energy, price, load and forecasts are random, the system operator's goal is maximization of expected profits over time.

At each point in time he makes money by satisfying the current load as well as by possibly selling energy to the market. Costs incur from buying energy at the market. The resulting profit at time t is given in terms of the contribution function

$$C(S_t, x_t) \;=\; P_t\,(D_t \;+\; \eta^d\, x_t^{RM} \;-\; x_t^{ML} \;-\; x_t^{MR}\,). \tag{15}$$

In order to formulate the optimization problem of the system operator, we define a policy as a set of decision functions $\{X_t^\pi(S_t)|t \in \{0,\ldots,T\}\}$. Given the set $\mathcal{S}_t$ of possible states at t, we let $X_t^\pi(S_t) : \mathcal{S}_t \mapsto \mathcal{X}_t$.

The problem of maximization of the expected sum of contributions over the entire time horizon can now be stated as

$$\max_{\pi\in\Pi} \mathbb{E}^\pi \sum_{t=0\ldots T} C\big(S_t, X_t^\pi(S_t)\big)\;, \tag{16}$$

where π is the abbreviation for the policy given by $X_t^\pi(S_t)$, Π is the set of all policies, and $\mathbb{E}^\pi$ is the expected value with fixed policy π.

3 Fundamental Classes of Policies

The formulation we derived in the preceding section fully captures the sequential and stochastic nature of the system operator's decision problem. In this section we present the possible approaches to deriving a policy that solves the problem.

Note that due to the well-known curses of dimensionality [13] deriving a provably optimal policy typically is computationally infeasible for a real-world application. As a consequence the challenge is to derive a best possible policy. In [14] we illustrate that the different approaches to deriving a policy fall into four fundamental classes of policies. We briefly summarize these classes in the following:

- Policy function approximations (PFAs): PFAs are analytical functions that map states to decisions without deriving the decisions by solution of an optimization problem. However, a PFA may, e.g., be a decision rule with tunable parameters,

where tuning may be done by use of optimization techniques. An example of a PFA for an energy storage problem is represented by the simple rule of charging the storage device as much as possible, if P_t falls below a certain threshold value θ_l, and discharging as much energy as possible if P_t is above threshold θ_u. The values of the tunable parameters θ_l and θ_u need to be set by the decision maker.

- Cost function approximations (CFAs): CFAs start with deterministic optimization models, which are then modified to achieve robust behaviors over time. One example is to start with a myopic policy

$$X_t^{\pi}(S_t) = \arg\max_{x_t \in \mathcal{X}_t} C(S_t, x_t). \tag{17}$$

The modifications may either affect the objective function or the set of feasible decisions of the myopic policy. As in case of PFAs, tunable parameters may be involved. Examples of CFAs include adding a weighted correction term to the contribution function in order to encourage use of storage, or adding an additional constraint in order to restrict the set of feasible decisions to decisions allowing for a certain amount of reserve capacity.

- Value function approximations (VFAs): A value function represents the values $V_t(S_t)$ of states, and consequently provides information about how desirable a state is. In our energy storage example the value of a state is given by the expected remaining profits to be made from the current point in time on until the end of the time horizon, provided that the decision maker follows an optimal policy from the current state on. The resulting policy is given by

$$X_t^{\pi}(S_t) = \arg\max_{x_t \in \mathcal{X}_t} \big(C(S_t, x_t) + \mathbb{E}\{V_{t+1}(S_{t+1})|S_t\}\big).$$

Value functions can usually not be computed for real-world energy storage problems. Instead one may find a computationally feasible approximation $\bar{V}_t$ of V_t and use the approximation to define the VFA based policy

$$X_t^{\pi}(S_t) = \arg\max_{x_t \in \mathcal{X}_t} \big(C(S_t, x_t) + \mathbb{E}\{\bar{V}_{t+1}(S_{t+1})|S_t\}\big).$$

The definition of a value function approximation often includes parameters that are optimized by statistical learning and optimization techniques. We refer to [13] for detailed description of techniques for value function approximation.

- Lookahead policies (LAs): LAs are policies that solve a lookahead model of the dynamic decision problem. The models can be deterministic or stochastic, and solving them results in decisions for both the current point in time and a number of future time steps. The lookahead horizon H determines the number of time steps to be considered, and forecasts are often used as point estimates of the data that is needed for model formulation. As the model is solved, the decision for the current point in time is implemented.

4 The Competing Policies

In this section we propose four alternative policies for making decisions with the energy system modeled in Sect. 2. We propose one policy from each of the fundamental policy classes discussed in Sect. 3. In Sect. 5 we compare the qualities of these policies with respect to different instances of the model of Sect. 2.

4.1 Policy Function Approximation

The PFA based policy $X_t^{PFA}(S_t|\theta)$ we propose maps the current state S_t to a decision x_t by applying the following logic: As much as possible of E_t is used for load satisfaction. If P_t is above a given upper bound θ^U and if there is enough energy in storage, the load that cannot be satisfied from E_t is satisfied by stored energy as much as possible. Any remaining load is satisfied by buying energy at the market. And any remaining generated energy is stored if possible. Additionally, the storage device is charged as much as possible, if P_t is below a certain lower bound θ^L. We refer to [15] for a formal statement of this policy. Note that the policy has two tunable parameters $\theta^{PFA} = (\theta^L, \theta^U)$.

4.2 Cost Function Approximation

We propose a CFA based policy $X_t^{CFA}(S_t|\theta)$ that modifies the myopic policy provided in Eq. (17). The modification consists of adding a tunable correction term to the contribution function. The idea of the correction term is to encourage use of the storage device in terms of charge or discharge operations. The extent of encouragement is determined by the value of a parameter $\theta^{CFA} = \theta$. The CFA based policy is defined as $X_t^{CFA}(S_t|\theta) =$

$$\arg\max_{x_t \in \mathcal{X}_t} \left(C(S_t, x_t) \; + \; \theta \, (x_t^{ER} + x_t^{MR} + x_t^{RL} + x_t^{RM}) \right).$$

We note that this is a very simple example of a CFA with a cost function correction term, but it actually works quite well in certain settings.

4.3 Value Function Approximation

A common approach to deriving VFA based policies is approximation of the value function around the post-decision states. A post-decision state S_t^x is the system state that results immediately from applying decision x_t to state S_t. In case of the model

introduced in Sect. 2, we get to the post-decision state by defining $R_t^x = R_{t+1}$ and $S_t^x = (L_t, P_t, E_t, R_t^x, f_t)$. Note that the transition from a state S_t to post-decision state S_t^x is fully determined by Eq. (14).

Relying on post-decision states and using a piece-wise linear architecture for value function approximation allows for formulating our VFA based policy as

$$X_t^{VFA}(S_t) = \arg\max_{x_t \in \mathcal{X}_t} \big(C(S_t, x_t) \; + \; \bar{V}_t(S_t^x) \big).$$

The piece-wise linear value function $\bar{V}_t(S_t^x)$ approximates the marginal value of the post-decision resource state R_t^x. $\bar{V}_t(S_t^x)$ needs to be derived by simulation and statistical learning techniques. We refer to [17] for a detailed introduction into the algorithm for deriving value function approximations around the post-decision states with a piecewise-linear approximation architecture.

4.4 Lookahead Policy

We propose a deterministic lookahead policy $X_t^{LA}(S_t|\theta)$ that uses the forecasts f_t to make decisions. The parameter to be selected for this type of policy is the lookahead horizon H, i.e., $\theta^{LA} = H$. With the forecasts, the lookahead policy makes decisions for each point in time t' with $t \le t' \le t + H$, but only implements the decisions for time t. We refer to the decisions resulting from the lookahead policy at time t as $\tilde{x}_t = (\tilde{x}_{tt}, \tilde{x}_{t,t+1}, \ldots, \tilde{x}_{t,t+H})$, where

$$\tilde{x}_{tt'} = (\tilde{x}_{tt'}^{EL}, \tilde{x}_{tt'}^{RL}, \tilde{x}_{tt'}^{ML}, \tilde{x}_{tt'}^{ER}, \tilde{x}_{tt'}^{MR}, \tilde{x}_{tt'}^{RM}),$$

and where the decision to be implemented is $\tilde{x}_{tt} = x_t$. Defining $f_{tt}^L = L_t$, $f_{tt}^P = P_t$ and $f_{tt}^E = E_t$, the lookahead policy can be formulated as $X_t^{LA}(S_t|\theta) \;=$

$$\arg\max_{\tilde{x}_t} \sum_{t'=t}^{t+H} f_{tt'}^P \big(\, f_{tt'}^L \; + \; \eta^d \, \tilde{x}_{tt'}^{RM} \; - \; (\, \tilde{x}_{tt'}^{ML} \; + \; \tilde{x}_{tt'}^{MR}) \, \big)$$

$$\text{subject to} \quad \forall t' \text{ with } t \le t' \le t + H :$$

$$\begin{aligned}
\tilde{x}_{tt'}^{EL} + \eta^d \tilde{x}_{tt'}^{RL} + \tilde{x}_{tt'}^{MD} &= f_{tt'}^L + f_{tt'}^{E^-} \\
\eta^c (\tilde{x}_{tt'}^{ER} + \tilde{x}_{tt'}^{MR}) &\le R^C - \tilde{R}_{tt'} \\
\tilde{x}_{tt'}^{RL} + \tilde{x}_{tt'}^{RM} &\le \tilde{R}_{tt'} \\
\tilde{x}_{tt'}^{EL} + \tilde{x}_{tt'}^{ER} &\le f_{tt'}^{E^+} \\
\tilde{x}_{tt'}^{ER} + \tilde{x}_{tt'}^{MR} &\le \delta^c
\end{aligned}$$

$$\begin{aligned} \tilde{x}^{RL}_{tt'} + \tilde{x}^{RM}_{tt'} &\leq \delta^d \\ (\tilde{x}^{RL}_{tt'} + \tilde{x}^{RM}_{tt'}) - \eta^c(\tilde{x}^{ER}_{tt'} + \tilde{x}^{GR}_{tt'}) + \tilde{R}_{t,t'+1} &= \tilde{R}_{tt'} \\ \tilde{x}^{EL}_{tt'}, \tilde{x}^{RL}_{tt'}, \tilde{x}^{ML}_{tt'}, \tilde{x}^{ER}_{tt'}, \tilde{x}^{MR}_{tt'}, \tilde{x}^{RM}_{tt'}, \tilde{R}_{tt'} &\geq 0 \end{aligned}$$

Note that for each t' the set of feasible decisions is defined along the lines of constraints (1)–(7). The additional constraint represents the storage balance equation at each point in time. $\tilde{R}_{tt}$ is the current amount of energy in storage at time t, whereas for all $t' > t$, $\tilde{R}_{tt'}$ is a decision variable in the resulting linear program.

5 Selecting the Best Policy

We now compare the policies proposed in the previous section numerically. In Sect. 5.1 we introduce a number of variations of the dynamic decision problem of Sect. 2. Each of the policies is then evaluated with respect to each of the variations in Sect. 5.2.

5.1 Problem Variations

We design four variations of our energy storage problem. For the sake of comparability of results, we leave part of the problem characteristics unchanged across all variations. We always let the time horizon be equal to one week with decisions being made every 15 min, i.e., we always let $T = 672$. Additionally, the storage device has maximum capacity $R^C = 40$ MWh and (dis)charge efficiencies $\eta^c = \eta^d = 0.85$. Beyond this, we vary the following problem characteristics:

- Process type of load, energy and price
- Noise level of load, energy and price
- Presence of price jumps
- Forecast accuracy
- Charge rate of storage device

We use truncated normal distributions $\mathcal{N}(\mu_t, \sigma^2, l, u)$ for definition of the processes that determine the evolution of load, energy and price over time. Parameters l and u make sure that the corresponding process evolves within realistic bounds, σ^2 sets the noise level of the process, and the sequence $\mu_0, \mu_1, \ldots, \mu_T$ determines the general type of the process. We distinguish between the three general process types.

- stationary: means remain constant over time, i.e., $\mu_0 = \mu_1 = \ldots = \mu_T$.
- daily pattern: means change according to a oscillating function, i.e., $\mu_t = a + b\sin(ct)$.
- no pattern: means are determined by predecessor state, e.g., $\mu^E_t = E_{t-1}$.

Table 1 Characteristics of the four problem variations

ID	Type	Noise	Jumps	Forecasts	Storage
1	Stationary	Low	Yes	Medium	Normal
2	Patterns	Low	No	Good	Normal
3	Patterns	High	No	Bad	Normal
4	No patterns	Medium	Yes	Bad	Fast

Price jumps occur with a probability of 0.06, if the problem variant allows for them. Forecasts of generated energy, loads and prices are simulated with a parameterized heterogeneous first-order autoregressive covariance structure. The (dis)charge rate of the storage device may be "normal" ($\delta^c = \delta^d = 20\,\text{MW}$) or "fast" ($\delta^c = \delta^d = 100\,\text{MW}$).

With these parameters we define the four problem variations summarized in Table 1:

- **Problem 1** serves as our baseline problem with all processes being stationary, and with the price process featuring jumps. Sample paths of the three processes are shown in Figs. 1a, 2a and 3a. The forecast accuracy is set to medium in order to reflect the combination of stationarity and hardly predictable price jumps.
- **Problem 2** has similar noise levels and storage device as Problem 1, but no price jumps and the exogenous processes feature daily patterns. Sample paths of the three processes are shown in Figs. 1b, 2b and 3b. Figure 3b shows two load peaks at each day, and Figs. 1b and 2b illustrate that both generated energy and price oscillate with one peak a day.
- **Problem 3** differs from Problem 2 in terms of both noise level and forecast accuracy. As the noise level is significantly higher for all three processes, we assume bad forecast quality.
- **Problem 4** represents a non-stationary problem with no daily patterns in both the price process and the energy generating process. As loads rarely occur without patterns, we assign Problem 4 the load Process of Problem 2. Sample paths of generated energy and prices (with jumps) are displayed in Figs. 1c and 2c. Due to the characteristics of these two processes we assume bad quality of forecasts, but allow for a faster storage device.

5.2 Computational Results

In order to be able to evaluate a given policy, we randomly generated $n = 100$ sample paths for the exogenous processes of each of the four problem instances proposed in the previous subsection. We use these sample paths for simulating the policies. Based on the 100 simulation runs, we estimate the quality

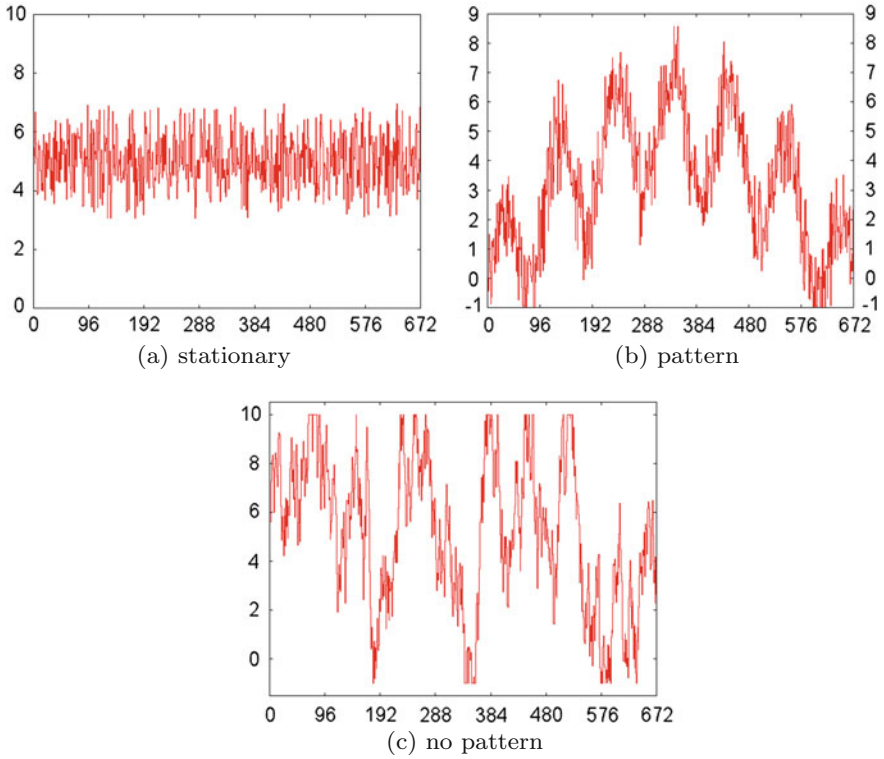

Fig. 1 Sample paths of generated energy for different types of generating processes. Time steps are shown on the x-axes of the graphs, generated power in MW is shown on tht y-axes of the graphs

Table 2 Optimal parameter values

ID	θ^{PFA}	θ^{LA}	θ^{CFA}
1	(20,30)	192	18
2	(15,35)	48	12
3	(22.5,27.5)	96	18
4	(15,35)	80	9

$$\mathbb{E}^{\pi} \sum_{t=0}^{T} C\left(S_t, X_t^{\pi}(S_t)\right)$$

of the corresponding policy X^{π} by sample average, where $S_{t+1} = S^M(S_t, X_t^{\pi}(S_t), W_{t+1})$.

The first step in our computational experiments is determination of the best policy of each class, i.e., identification of the optimal parameter values of each of the policies with each of the problems. We did this by tuning the parameters of the

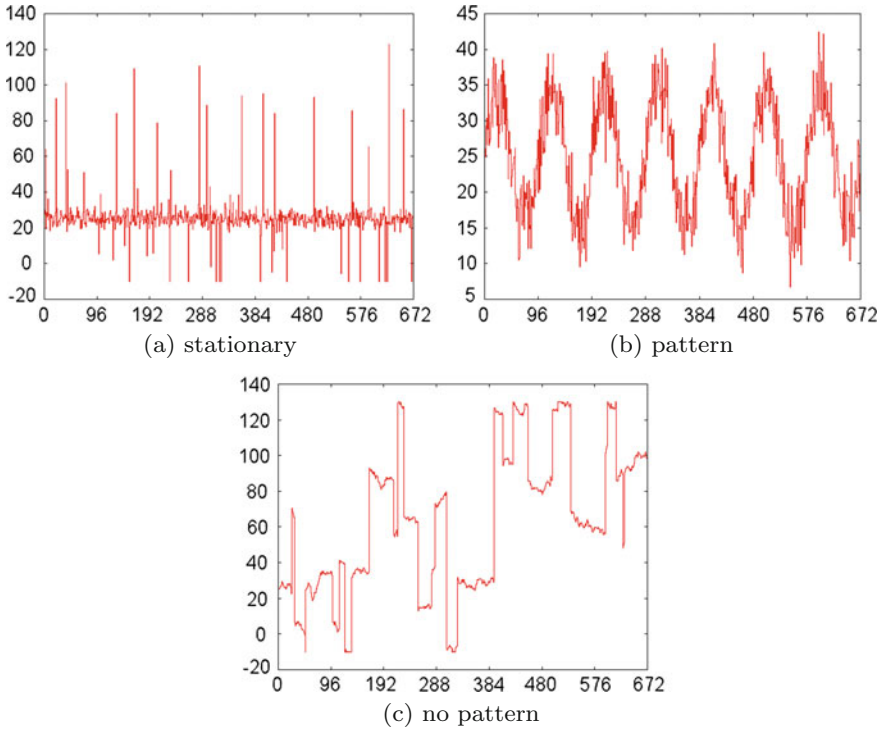

Fig. 2 Sample paths of market price for different types of price processes. Time steps are shown on the x-axes of the graphs, market price in $ is shown on the y-axes of the graphs

policies manually. Table 2 shows the resulting values for X^{PFA}, X^{CFA} and X^{LA} and Problems 1–4. Note that in case of X^{VFA} the process of finding the optimal parameters is embedded into an offline learning process.

We are now ready to compare the best policies of each class with each other. Table 3 shows the improvements of each of the best policies with respect to the quality achieved by the myopic policy. Obviously all policies are outperforming the myopic policy on each of the considered problems. However, the relative performance of the four policies varies significantly between the problems. In particular, each of the policies performs best on one of the problems.

The PFA performs best with the stationary Problem 1, whereas LA is best as we switch to having patterns in the processes (Problem 2). As we then increase the noise and transition to Problem 3 the VFA performs better than all other policies. The quality of CFA is relatively low with Problems 1–3. However, CFA is the policy that outperforms all others on the particularly hard Problem 4 without patterns and stationarity.

We conclude that the upper and lower bounds of the PFA are able to introduce a certain robustness with respect to price jumps in case of a stationary problem. With

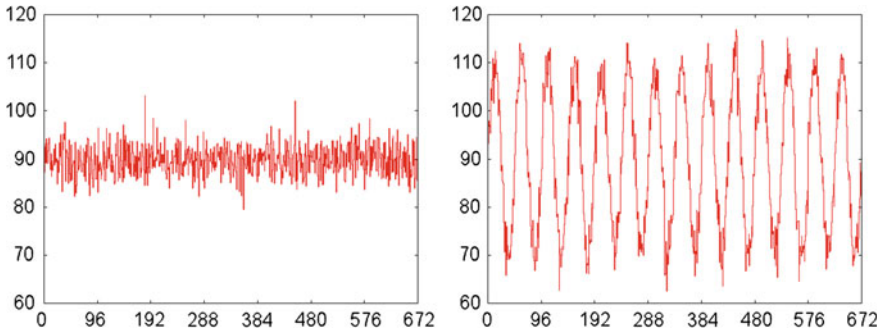

Fig. 3 Sample paths of loads for different types of load processes. Time steps are shown on the x-axes of the graphs, demanded power in MW is shown on tht y-axes of the graphs

Table 3 Improvement (%) over myopic policy

ID	PFA	LA	VFA	CFA
1	**15.4**	6.7	12.7	1.0
2	29.7	**34.4**	30.9	1.0
3	72.0	76.1	**81.7**	17.4
4	1.9	6.5	1.7	**7.4**

lower noise and accurate forecasts LA is able to take advantage of forecasts, whereas the statistical learning techniques behind the VFA policy are able to cope with high uncertainty and a regular problem type.

6 Conclusions

We illustrate the challenge of selecting the best policy for making decisions about energy flows in energy systems with storage and a source of renewable energy. First we modeled the sequential decision problem of the operator of such a system as a Markov decision process. Then we discussed the four fundamental classes of policies that may be considered for solving the problem. We proposed a policy from each class and compared their performances with respect to different problem variations.

Our computational results show that the best policy heavily depends on the characteristics of the energy storage problem at hand. In particular the nature of the processes that guide the evolutions of price, generated energy and loads over time is crucial.

The main point to be addressed in future work is development of approaches to algorithmic selection of the best policy for a given energy system.

Acknowledgements The work of the first author was supported by the German Academic Exchange Service (DAAD).

References

1. Banos R, Manzano-Agugliaro F, Montoya F, Gil C, Alcayde A, Gomez J (2011) Optimization methods applied to renewable and sustainable energy: A review. Renewable and Sustainable Energy Reviews 15(4):1753–1766
2. Beaudin M, Zareipour H, Schellenberglabe A, Rosehart W (2010) Energy storage for mitigating the variability of renewable electricity sources: An updated review. Renewable and Sustainable Energy Reviews 14(4):302–314
3. Brown PD, Lopes JAP, Matos MA (2008) Optimization of pumped storage capacity in an isolated power system with large renewable penetration. IEEE Transactions on Power Systems 23(2):523–531
4. Garca-Gonzalez J, Moraga Ruiz de la Muela R, Matres Santos L, Mateo Gonzalez A (2008) Stochastic joint optimization of wind generation and pumped-storage units in an electricity market. IEEE Transactions on Power Systems 23(2):460–468
5. Harsha P, Dahleh M (2015) Optimal management and sizing of energy storage under dynamic pricing for the efficient integration of renewable energy. IEEE Transactions on Power Systems 30(3):1164–1181
6. Kall P, Wallace S (1994) Stochastic programming. John Wiley & Sons
7. Kim JH, Powell W (2011) Optimal energy commitments with storage and intermittent supply. Operations Research 59(6):1347–1360
8. Lai G, Margot F, Secommandi N (2010) An approximate dynamic programming approach to benchmark practice-based heuristics for natural gas storage valuation. Operations Research 58(3):564–582
9. Löhndorf N, Minner S (2010) Optimal day-ahead trading and storage of renewable energiesan approximate dynamic programming approach. Energy Systems 1(1):61–77
10. Löhndorf N, Wozabal D, Minner S (2013) Optimizing trading decisions for hydro storage systems using approximate dual dynamic programming. Operations Research 61(4):810–823
11. Lund PD, Lindgren J, Mikkola J, Salpakari J (2015) Review of energy system flexibility measures to enable high levels of variable renewable electricity. Renewable and Sustainable Energy Reviews 45(C):785–807
12. Meisel S (2011) Anticipatory Optimization for Dynamic Decision Making, Operations Research/Computer Science Interfaces Series, vol 51. Springer New York
13. Powell W (2011) Approximate Dynamic Programming: Solving the curses of dimensionality. John Wiley & Sons, Hoboken, NJ
14. Powell W, Meisel S (2016) Tutorial on stochastic optimization in energy I: Modeling and policies. IEEE Transactions on Power Systems 31(2):1459–1467
15. Powell W, Meisel S (2016) Tutorial on stochastic optimization in energy II: An energy storage illustration. IEEE Transactions on Power Systems 31(2):1468–1475
16. Puterman M (2005) Markov Decision Processes: Discrete Stochastic Dynamic Programming. John Wiley & Sons, Hoboken, NJ
17. Salas D, Powell W (2015) Benchmarking a scalable approximate dynamic programming algorithm for stochastic control of multidimensional energy storage problems. Tech. rep., Department of Operations Research and Financial Engineering, Princeton University
18. Xi X, Sioshansi R (2014) A stochastic dynamic programming model for co-optimization of distributed energy storage. Energy Systems 5(3):474–505

Part IV
Challenges in Microgrids

An Optimal Investment Model for Battery Energy Storage Systems in Isolated Microgrids

Hisham Alharbi and Kankar Bhattacharya

Abstract In remote microgrids, the integration of renewable energy sources (RES) is essential to meet the demand in conjunction with the dispatchable fuel-based generation units. The need to facilitate RES efficiently and the very high cost of fuel transportation in these areas make installing battery energy storage system (BESS) an appealing solution. However, the high cost of BESS requires optimizing the BESS technology selection and size to increase their benefits to the microgrid. In this paper, the optimal BESS installation decisions are determined from the perspective of an investor with the objective of profit maximization. The maximum size of BESS that the investor is willing to install for a certain discharge price is determined for various BESS technologies. Also, a new approach to determine the minimum acceptable discharge price at which the installation would make profit for the investor is proposed. Thereafter, the optimal microgrid and BESS operation is determined to minimize the total microgrid costs while meeting its growing demand considering the installation decisions obtained from the proposed investment model.

Keywords Battery energy storage system · Remote microgrids · Investment model · Optimal sizing

Nomenclature

Indices

h Index for hours, $h = 1, 2, \ldots, H$
i Index for distributed generation (DG) units, $i = 1, 2, \ldots, I$
y Index for years, $y = 1, 2, \ldots, Y_T$

H. Alharbi (✉) · K. Bhattacharya
Department of Electrical & Computer Engineering, University of Waterloo, Waterloo, ON, Canada
e-mail: h3alharb@uwaterloo.ca

K. Bhattacharya
e-mail: kankar@uwaterloo.ca

V. Bertsch et al. (eds.), *Advances in Energy System Optimization*,
Trends in Mathematics, DOI 10.1007/978-3-319-51795-7_7

Parameters

B_0	Net present value (NPV) of budget allocation in year-0 ($)
C^f	Fixed installation cost of BESS ($)
Ce^v	Variable installation cost of BESS associated with energy capacity ($/kWh)
Cp^v	Variable installation cost of BESS associated with power rating ($/kW)
$\overline{DOD}$	Maximum depth of discharge (%)
Eff_{ch}	Charging efficiency (%)
$\underline{Eff_{dch}}$	Discharging efficiency (%)
$\overline{EPR}$	Maximum energy to power ratio
$\underline{EPR}$	Minimum energy to power ratio
OMC^f	Yearly fixed operations and maintenance (O&M) cost of BESS ($/kW-year)
OMC^v	Variable O&M cost of BESS ($/kWh)
$\overline{P_i}$	Maximum output power of DG unit i (kW)
$Pd_{y,h}$	Forecasted demand (kW)
$PV_{y,h}$	Forecasted photovoltaic (PV) output power (kW)
$Pw_{y,h}$	Forecasted wind output power (kW)
RC	Replacement cost of BESS ($/kW)
RR	Rate of return (%)
RY	Replacement year of BESS
SD_i	Shut-down cost of DG unit i ($)
SU_i	Start-up cost of DG unit i ($)
β	Fuel cost escalation rate (%)
δ_D	Error factor in forecasted demand (%)
δ_{PV}	Error factor in forecasted PV (%)
δ_W	Error factor in forecasted wind (%)
θ_{ch}	Price of energy at which BESS purchases from microgrid ($/kWh)
θ_{dch}	Price of BESS discharge energy, purchased by microgrid ($/kWh)
θ_{res}	Price of reserves provided by BESS ($/kW)
λ	Load growth rate (%)

Variables

CH	NPV of investor's cost or microgrid's revenue from BESS charging ($)
DCH	NPV of investor's revenue or microgrid's cost from BESS discharging ($)
E_{BESS_y}	Energy capacity of BESS (kWh)
INS	NPV of installation cost of BESS ($)
$MGOC$	NPV of microgrid operational cost ($)
OM	NPV of O&M cost of BESS ($)
$P_{y,h,i}$	DG output (kW)
$PB_{y,h}$	BESS power; negative when charging, and positive when discharging (kW)
P_{BESS_y}	Power rating of BESS (kW)
$RTH_{y,h,i}$	Reserve from DG units (kW)

$RESV$	NPV of investor's revenue or microgrid's cost from BESS reserve provision ($)
$RB_{y,h,i}$	Reserve from BESS (kW)
$SOC_{y,h}$	BESS state of charge (kWh)
$U_{y,h,i}$	Binary start-up decision of DG units, 1 or 0
$V_{y,h,i}$	Binary shut-down decision of DG units, 1 or 0
$W_{y,h,i}$	Binary commitment decision of DG units, 1 or 0
We_y	Energy capacity of BESS at year of installation and 0 otherwise (kWh)
Wp_y	Power rating of BESS at year of installation and 0 otherwise (kW)
Z_y	BESS installation decision, 1 or 0
$Zch_{y,h}$	Binary variable associated with BESS charging, 1 or 0
$Zdch_{y,h}$	Binary variable associated with BESS discharging, 1 or 0

1 Introduction

Microgrids are defined as small groups of customers and generating units which can be controlled independently and have the ability to manage the energy locally [1]. Remote microgrids mainly depend on dispatchable distributed generation (DG) units, such as diesel generators, since they can maintain the system reliability and operational flexibility in contrast to intermittent renewable energy sources (RES) such as photovoltaic (PV) and wind [2]. The need to facilitate RES efficiently and the very high cost of fuel transportation in these areas make installing battery energy storage system (BESS) an appealing solution. However, the high cost of BESS requires optimizing the BESS technology selection and size to increase their benefits to the microgrid.

The operational strategies of BESS differ from one application to another. Therefore, appropriate BESS technology, the optimal size, and the optimal operation strategy including charging/discharging cycles need to be chosen carefully, so as to result in the maximum benefit to the microgrid.

In one of the power quality applications of BESS [3] considering a PV/Battery system, the fluctuations of PV output power are mitigated by three methods including the installation of BESS. The optimal size of BESS is obtained to maximize the revenue generated from the PV/Battery system by reducing system fluctuations. The fluctuations of wind generation are taken into consideration for BESS sizing in [4] and [5]. The main objective of [4] is to find the optimal BESS size that maximizes the economic benefit while maintaining the output wind power constant. Also, the voltage across the DC link is required to be within a certain limit. However, since the capacity determined in [4] is based on peak wind generation, the determined BESS size may be higher than required. A stochastic optimization model is proposed in [5] to overcome this limitation and hence arrive at a more accurate BESS size to reduce power fluctuations from wind generation.

In the context of energy management applications, sizing BESS in a PV/Battery system is reported in [6, 7]. The optimal size of BESS is determined in [6] so as to

minimize the cost of net power purchased during peak hours as well as minimize the cost of capacity degradation after each discharging process, taking the advantage of time-of-use electricity pricing. Distributed BESS is also studied in a distribution system with high PV penetration in [7]. The optimal size of BESS is determined, at each bus, based on a cost-benefit analysis, considering voltage regulation and peak load shaving applications.

The optimal size of BESS that decreases the difference between the predicted and actual wind generation is investigated in [8]. Also, the integration of wind generation in a system that lacks generation units for reserve, is studied in [9]. The BESS is installed to provide the reserve required for such a system. The optimal power rating and energy capacity are determined using temporal and non-temporal methods. Although savings in cost of reserves is achieved in the aforementioned studies, since BESS costs are not considered in [8, 9], the proposed methods may lead to oversizing the BESS.

It is noted from the brief review of literature presented above, and also from microgrid developments around the world, that investments in resources have been primarily from the governments or utilities. However, there may be possibilities for third-party investors to invest in capacity resources in microgrids if the returns are justifiable. The main objective of this paper is to propose an investment planning framework to optimize the BESS installation decisions and operation in isolated microgrids, considering that the BESS investments are being made by a private party seeking to maximize its profit.

The outputs include the optimal BESS technology selection, power rating, energy capacity, and year of installation. Also, the minimum discharge price that would make profit for the investor based on the projected microgrid operation is determined. The optimal BESS operation is then studied from the microgrid operator (MGO) perspective of minimizing the total costs with an option of exchanging energy with the third-party owned BESS.

The rest of the paper is organized as follows: in Sect. 2, the proposed BESS investment framework is discussed. Section 3 presents the microgrid test system and the results. Finally, conclusions are provided in Sect. 4.

2 BESS Investment Framework

The BESS installation decisions including the optimal BESS technology, power rating, energy capacity, year of installation along with the energy exchange prices between the BESS and microgrid are determined from the investor's perspective in the optimal BESS investment model (Model I). The optimal BESS selection is then used in the microgrid operation model (Model II) to determine the optimal BESS and DG units operations schedules. It should be noted that the objective functions in the two models, shown in Fig. 1, are different because of the differing perspectives of the cost. Model I is from the investor's perspective seeking to maximize profit

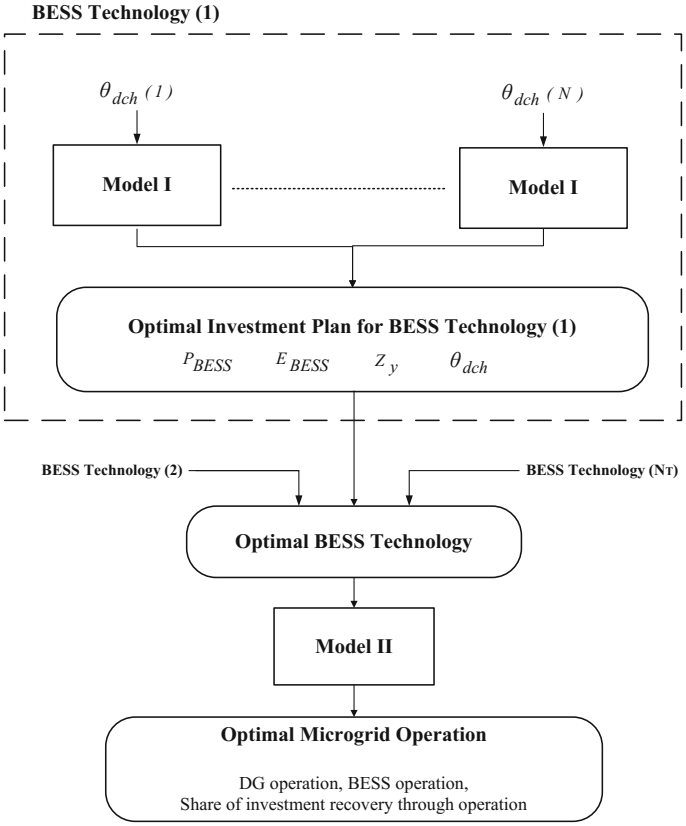

Fig. 1 Schematic for the proposed BESS operational-cum-investment planning framework

while determining the optimal BESS investments, while Model II is from the MGO's perspective minimizing operations cost.

The main assumptions of the proposed framework are as follows:

- The BESS investment is made by a third-party entity, but after installation, the BESS is scheduled and operated along side other resources by the MGO using a least-cost criterion. The MGO, however, is contractually obliged to ensure a specific profit margin to the third-party as determined from Model I.
- An average load profile of the microgrid for a given year is considered for the BESS planning in order to keep the computational burden within reasonable limits.
- Typical wind and solar generation profiles are considered in the work without taking into account the seasonal variations or other uncertainties.

2.1 Model I: Optimal BESS Investment

This model investigates the benefit accrued to an investor from installing BESS, with the objective to maximize the profit from the energy supplied to the microgrid. The investor is expected to bear the BESS installation cost and the O&M cost. Also, since the BESS is owned by the third party, the only way to charge the batteries is to purchase energy from the microgrid. It is assumed that the BESS investor balances the demand based on the most profitable unit commitment schedule. However, the microgrid is responsible for the thermal generation cost. The objective function for the optimal BESS investment model is to maximize the investor's profit, as follows:

$$J_1 = \big(DCH + RESV\big) - \big(CH + INS + OM\big) \tag{1}$$

Fixed charging and discharging energy prices are assumed in this model, θ_{ch} and θ_{dch} respectively, considering a higher discharge price to generate profit for the investor. Since this is an isolated microgrid, electricity market prices do not apply, and it is assumed that the MGO and the investor have contractual agreements for θ_{ch} and θ_{dch}. The BESS can also help in the provision of microgrid's reserve at a fixed price θ_{res}. The revenue from discharging and reserve services and the cost of charging can be expressed as a function of the BESS discharge energy, as follows:

$$DCH = 365 \times \sum_{y=1}^{Y_T} \sum_{h=1}^{H} \Big[\frac{1}{(1+RR)^y} \theta_{dch} \Big(\frac{Eff_{ch} Eff_{dch}}{1 - Eff_{ch} Eff_{dch}} \Big) \big(- PB_{y,h} \big) \Big] \tag{2}$$

$$RESV = 365 \times \sum_{y=1}^{Y_T} \sum_{h=1}^{H} \Big[\frac{1}{(1+RR)^y} \theta_{res} \, RB_{y,h} \Big] \tag{3}$$

$$CH = 365 \times \sum_{y=1}^{Y_T} \sum_{h=1}^{H} \Big[\frac{1}{(1+RR)^y} \theta_{ch} \Big(\frac{1}{1 - Eff_{ch} Eff_{dch}} \Big) \big(- PB_{y,h} \big) \Big] \tag{4}$$

As noted earlier, the model considers one typical day per year, and hence the discharging revenue as well as the charging cost are extrapolated to represent the revenue/cost of one year using a factor of 365.

The *INS* cost component of BESS in (1) comprises costs proportional to the installed power rating ($/kW) and energy capacity ($/kWh), and a fixed installation cost ($) irrespective of the size:

$$INS = \sum_{y=1}^{Y_T} \left[\frac{1}{(1+RR)^y} \left(Cp^v Wp_y + Ce^v We_y + C^f Z_y \right) \right] \tag{5}$$

The *OM* cost component in (1) comprises the fixed cost, variable cost, and replacement cost. The fixed and replacement costs are proportional to the BESS power rating, whereas the variable cost depends on the discharged energy from the BESS.

$$\begin{aligned} OM = & \sum_{y=1}^{Y_T} \left[\frac{1}{(1+RR)^y} OMC^f P_{BESS_y} \right] \\ & + 365 \times \sum_{y=1}^{Y_T} \sum_{h=1}^{H} \left[\frac{1}{(1+RR)^y} \, OMC^v \right. \\ & \left. \left(\frac{Eff_{ch}}{1 - Eff_{ch} Eff_{dch}} \right) \left(- PB_{y,h} \right) \right] \\ & + \left[\frac{1}{(1+RR)^{RY}} + \frac{1}{(1+RR)^{2RY}} + \ldots \right] RC \; P_{BESS_{y=1}} \\ & + \sum_{y=RY+1}^{Y_T} \left[\left(\frac{1}{(1+RR)^y} + \frac{1}{(1+RR)^{y+RY}} + \ldots \right) RC \right. \\ & \left. \left(P_{BESS_{y-RY+1}} - P_{BESS_{y-RY}} \right) \right] \end{aligned} \tag{6}$$

The first term of (6) represents the fixed O&M cost of the BESS. In the second term, the total energy discharged is used to compute the variable O&M cost. Since the model considers one typical day per year, the variable cost is also extrapolated to one year using a factor of 365. The replacement cost of BESS is applied when the BESS's years of operation reach its predefined life *RY*. The third term of (6) denotes the replacement cost for a BESS installed in the first year, while the last term represents the replacement cost if it is installed after the first year. The replacement cost may apply several times if the BESS life is reached more than once over the planning horizon.

The objective function above is subject to the following constraints:

2.1.1 Demand-Supply Balance

The demand-supply balance shall include both RES and BESS. This constraint ensures sufficient generation from dispatchable DG units and RES to meet the demand at an hour. The demand is assumed to increase annually by a constant rate, λ.

$$\sum_{i=1}^{I} P_{y,h,i} + PB_{y,h} + PV_{y,h} + Pw_{y,h} = \left(1+\lambda\right)^{y-1} Pd_h \qquad \forall y, \forall h \tag{7}$$

2.1.2 Dispatchable DG Units Constraints

These constraints include ramp up, ramp down, minimum up, minimum down, maximum and minimum output power, and coordination constraints, as per standard unit commitment models and are not presented here for the sake of conciseness.

2.1.3 Microgrid Reserve Requirements

The MGO ensures a minimum reserve level of 10% of the demand plus factors accounting for uncertainty in demand and RES forecasting errors [10, 11]. The reserve constraint is modeled as follows:

$$RTH_{y,h} + RB_{y,h} \geq \left(0.1 + \delta_D\right)\left(1+\lambda\right)^{y-1} Pd_h + \delta_{PV} PV_{y,h} + \delta_W Pw_{y,h} \qquad \forall y, \forall h \tag{8}$$

$$RTH_{y,h} \leq \sum_{i=1}^{I} \left(\overline{P_i} W_{y,h,i} - P_{y,h,i}\right) \qquad \forall y, \forall h \tag{9}$$

$$RB_{y,h} \leq -PB_{y,h} + \min\left\{\left[SOC_{y,h} - E_{BESS_y}(1 - \overline{DOD})\right] Eff_{dch}, P_{BESS_y}\right\} \qquad \forall y, \forall h \tag{10}$$

As shown in (8), *RB* is the reserve from BESS that supports the spinning reserve from DG units; denoted by *RTH*, and given by (9) in providing reserves for the microgrid. In (10), the BESS reserve contribution is defined either by its available energy (SOC), accounting for discharging efficiency, or its power rating. The lower value of the two, determines the maximum reserve that can be provided by the BESS. Note that, for the sake of dimensions, the available energy (SOC) and E_{BESS} (given in kWh) are considered for a one hour interval, thereby making them equivalent to be as a kW basis. The committed charging and discharging power of the BESS is included in modeling the BESS reserve. When the BESS is discharging, it supplies a portion of the demand, and hence the discharged power should not be reconsidered as reserve. However, the BESS can discharge part of its energy and use the remaining

as reserve. In case of charging, the charging power can be used as a reserve since the BESS can interrupt its charging instantaneously, which allows the DG that is committed to supply the BESS, to be used for supplying demand instead.

2.1.4 BESS Size Constraints

Power Size of BESS

In order to allow the model to optimize the power size of the BESS, the following constraints are considered:

$$P_{BESS_y} = Wp_y \quad ; y = 1 \tag{11}$$

$$P_{BESS_y} = Wp_y + P_{BESS_{y-1}} \quad \forall y; y \neq 1 \tag{12}$$

$$Wp_y \geq Z_y \quad \forall y \tag{13}$$

$$Wp_y \leq M\ Z_y \quad \forall y \tag{14}$$

To keep the linearity of the model, two variables are defined for BESS power size, P_{BESS_y} and Wp_y. The first denotes the power rating of BESS, and once the BESS is installed, it remains constant over the plan horizon. On the other hand, while Wp_y also denotes the installed BESS size, it is used to compute the installation cost, and is active only at the year of installation; otherwise, it is zero, as per (11). The constraints (13) and (14) are used to activate the binary variable Z_y when installing BESS using the big M method.

Energy Size of BESS

Similar to the power rating, two variables are defined for energy capacity E_{BESS_y} and We_y. The following constraints are considered:

$$E_{BESS_y} = We_y \quad ; y = 1 \tag{15}$$

$$E_{BESS_y} = We_y + E_{BESS_{y-1}} \quad \forall y; y \neq 1 \tag{16}$$

$$We_y \geq Z_y \quad \forall y \tag{17}$$

$$We_y \leq M\ Z_y \quad \forall y \tag{18}$$

Energy to Power Ratio (E/P)

The energy capacity of the BESS for a certain power rating, is determined based on its E/P ratio, as follows:

$$\underline{EPR}\ P_{BESS_y} \leq E_{BESS_y} \leq \overline{EPR}\ P_{BESS_y} \quad \forall y \tag{19}$$

$\overline{EPR}$ and $\underline{EPR}$ are the maximum and minimum possible E/P ratio for a certain BESS technology. The E/P ratio constraint also determines the maximum discharge time at rated power.

Coordination of Binary Variables

To ensure limiting the activation of the binary variable associated with the BESS installation, to only once over the planning horizon, the following constraint is considered:

$$\sum_{y=1}^{Y_T} Z_y \leq 1 \tag{20}$$

2.1.5 Budget Constraint

The NPV of the BESS installation cost should not exceed the NPV of the allocated budget for the year.

$$INS \leq B_0 \tag{21}$$

2.1.6 BESS Operational Constraints

BESS Power and SOC Relationship

The relationship between the charging and discharging power of BESS and its SOC can be described as follows:

$$\frac{PB_{y,h}}{Eff_{dch}} Zdch_{y,h} + PB_{y,h} Eff_{ch} Zch_{y,h} = SOC_{y,h} - SOC_{y,h+1} \forall y, \forall h; h \neq 24 \tag{22}$$

However, the equation (22) is not linear; therefore, the charging and discharging constraints are formulated in [12] to linearize it using the big M method.

(a) *Charging constraints:*

$$-PB_{y,h} Eff_{ch} - M\ Zdch_{y,h} \leq SOC_{y,h+1} - SOC_{y,h} \quad \forall y, \forall h; h \neq 24 \tag{23}$$

$$SOC_{y,h+1} - SOC_{y,h} \leq -PB_{y,h} Eff_{ch} + M\ Zdch_{y,h} \quad \forall y, \forall h; h \neq 24 \tag{24}$$

(b) *Discharging constraints:*

$$\frac{-PB_{y,h}}{Eff_{dch}} - M\left(Zch_{y,h} - Zdch_{y,h} + 1\right) \leq SOC_{y,h+1} - SOC_{y,h} \quad \forall y, \forall h; h \neq 24 \tag{25}$$

$$SOC_{y,h+1} - SOC_{y,h} \leq \frac{-PB_{y,h}}{Eff_{dch}} + M\left(Zch_{y,h} - Zdch_{y,h} + 1\right) \quad \forall y, \forall h; h \neq 24 \tag{26}$$

Since (23)–(26) do not force the binary variables $Zch_{y,h}$ and $Zdch_{y,h}$ associated with charging and discharging respectively, to be activated during the process, the following constraints are also considered:

$$-M\ Zch_{y,h} \leq PB_{y,h} \quad \forall y, \forall h \tag{27}$$

$$M\ Zdch_{y,h} \geq PB_{y,h} \quad \forall y, \forall h \tag{28}$$

Initial and Final SOC

The initial and final SOC of the BESS are assumed to be 50% of the installed BESS energy capacity. The initial SOC is formulated as follows:

$$SOC_{y,h} = 0.5\ E_{BESS_y} \quad \forall y, h = 1 \tag{29}$$

Similarly, (23)–(26) are adopted to the desired final SOC value, i.e.,

$$SOC_{y,h+1} = 0.5\ E_{BESS_y} \quad \forall y, h = 24 \tag{30}$$

Limits on BESS Power and SOC

The limits on BESS power and SOC are formulated respectively, as follows:

$$-P_{BESS_y} \leq PB_{y,h} \leq P_{BESS_y} \quad \forall y, \forall h \tag{31}$$

$$(1 - \overline{DOD})E_{BESS_y} \leq SOC_{y,h} \leq E_{BESS_y} \quad \forall y, \forall h \tag{32}$$

The minimum SOC limit is set based on the maximum DOD of the BESS. For example, if the DOD is 80%, the minimum SOC level is 20% of the energy size.

Coordination of Binary Variables

This constraint ensures that simultaneous charging and discharging of the BESS does not take place. Also, it ensures that there is no charging or discharging if the binary variable associated with BESS installation (Z_y) has not been activated yet.

$$Zch_{y,h} + Zdch_{y,h} \leq \sum_{1}^{y} Z_y \qquad \forall y, \forall h \tag{33}$$

2.2 Model II: Optimal Microgrid Operation

Once the optimal investment decisions are obtained, as per the model proposed in Sect. 2.1, it is assumed that the MGO will consider the BESS as one of its available resources in its energy management system (EMS) program, and determine its day-to-day operations. In this model, the microgrid has an option of exchanging energy with the BESS to reduce its costs and maintain the demand. The objective of this model is to minimize the total costs including the microgrid operational cost and energy purchasing costs. Installation cost and O&M cost are not included in the objective function because the BESS investor is responsible for them. However, the investor's profit should be ensured as a constraint.

The objective function in the microgrid operation model is to minimize the costs, as follows:

$$J_2 = \big(DCH + RESV + MGOC + N \times INS\big) - \big(CH\big) \tag{34}$$

The components *DCH*, *RESV*, *CH*, and *INS* are similar to the ones defined in (2), (3), (4), and (5), respectively, while the variable N denotes the fractional payment of BESS installation cost paid by the microgrid.

The *MGOC* component in (34) represents the operational cost of dispatchable DG units including their start-up and shut-down cost, taking into account the annual fuel cost escalation. The generation cost of one typical day in a year is extrapolated to represent the cost of the corresponding year.

$$MGOC = 365 \times \sum_{y=1}^{Y_T} \sum_{h=1}^{H} \sum_{i=1}^{I} \Bigg[\frac{1}{(1+\alpha)^y} \Big[(1+\beta)^{y-1} F_i\big(P_{y,h,i}\big) W_{y,h,i} + SU_i U_{y,h,i} + SD_i V_{y,h,i} \Big] \Bigg] \tag{35}$$

where $F_i(\cdot)$ is the operational cost function of a DG.

In addition to the constraints discussed above, the objective function is subject to constraints described in the following subsections.

2.2.1 Investor's Revenue Constraint

This constraint ensures the investor's profit, while minimizing the total microgrid costs, satisfied at the same level as determined from the investment model.

$$\left(DCH + RESV\right) - \left(CH + OM + (1 - N)INS\right) \geq 0 \tag{36}$$

$$\left(DCH + RESV + N \times INS\right) \geq R_0 \tag{37}$$

where R_0 is the total investor's revenue from the investment model.

2.2.2 Budget Constraint

The fractional payment of the BESS installation cost should not exceed the allocated budget for the year.

$$N \times INS \leq B_0 \tag{38}$$

3 Results and Analysis

The proposed models of the BESS investment framework are formulated as MILP problems and solved in GAMS using CPLEX solver. The solver uses branch and cut algorithm in which the main problem is divided into linear programming subproblems [13]. In the BESS investment model (Model I), there are 8,901 variables, which includes 4,130 integer and binary variables. In this model, four types of BESS are tested with 15 discharge prices, hence the model is solved 60 times. The total computation time is about 36.3 h. In the optimal microgrid operation model (Model II), the number of variables is 8,832 including 4,101 integer and binary variables. This model is solved once, after selecting the optimal BESS technology and discharge price from Model I, and the computation time is about 2.8 h.

3.1 Microgrid Test System

The proposed model is applied to the modified CIGRE medium voltage microgrid [14] to determine the optimal BESS plan. The controllable generating units in the microgrid are three diesel generators, one combined heat and power (CHP) diesel, and one CHP microturbine with a total capacity of 5,510 kW. The DG data are taken from [14]. The installed PV capacity is 840 kW, and wind capacity is 1,450 kW.

The planning period in the case study is 10 years. The peak demand of the microgrid in the first year is 5,290 kW, and is assumed to increase annually by 1%. The fuel cost is considered to increase by 3% every year [15].

The microgrid is required to maintain an operating reserve equivalent to 10% of its hourly demand plus a certain fraction of the forecasted RES generation and demand, to account for forecasting error. The forecasting error parameters δ_D, δ_{PV}, and δ_W are assumed to be 3, 9, 13%, respectively [10].

Table 1 BESS performance and cost parameters [16]

BESS Type	NaS	VRB	PbA	Li-ion
Cp^v ($/kW)	757	2133	1407	1859
Ce^v ($/kWh)	372	880	275	901
OMC^f ($/kW-year)	9.2	16.5	26.8	13.2
OMC^v ($/Wh)	0.8	1.6	1.1	1.4
RC ($/kW)	0	720	375	1560
RY (y)	15	8	8	5
Charging efficiency	87 %	83 %	95 %	95 %
Discharging efficiency	87 %	83 %	95 %	95 %
Maximum DOD	80 %	100 %	80 %	100 %
E/P ratio range	6–8	N/A	1–5	1–4

Four BESS technologies are examined, namely, NaS, VRB, PbA, and Li-ion BESS. The performance and cost parameters of different BESS technologies, shown in Table 1, are taken from [16]. The fixed installation cost, applicable to all technologies, is assumed to be $20,000. The maximum size for BESS is assumed as, $P_{BESS} =$ 6,500 kW, and $E_{BESS} =$ 6,500 kWh, the options are considered to be available in multiples of 50 and 50 kWh, respectively.

3.2 Optimal BESS Investment

The third-party investor seeks to determine the maximum amount of energy that can be exchanged with the microgrid for a certain discharge price θ_{dch}. The BESS size is determined from an optimistic viewpoint to capture the maximum profit for the investor. Although in reality, the BESS may not discharge this amount of energy to the microgrid, this study seeks to find the minimum acceptable discharge price for the investor that recovers the investment cost of the BESS.

The revenue is accrued from supplying energy to the microgrid and from providing reserve, while the installation and O&M cost is paid by the third party. Since the system is isolated, hourly market prices are not applicable, and it is assumed that θ_{ch} is fixed at 1 ¢/kWh, while θ_{dch} is varied in the range of 2.5 ¢/kWh and 37.5 ¢/kWh. The price of BESS reserve θ_{res} is assumed to be 0.6 ¢/kW [17]. The rate of return for the investor is considered to be 14%.

As shown in Fig. 2, different BESS technologies are considered to investigate the profit for the investor over a range of discharge prices. It is shown that the PbA BESS is the best choice for the third party since the minimum acceptable discharge price that generates profit is 12.5 ¢/kW, which is the lowest across the BESS technologies. The PbA BESS is followed by NaS, Li-ion, and VRB BESS with minimum acceptable discharge prices of 15 ¢/kWh, 20 ¢/kWh, and 25 ¢/kWh, respectively. The optimal

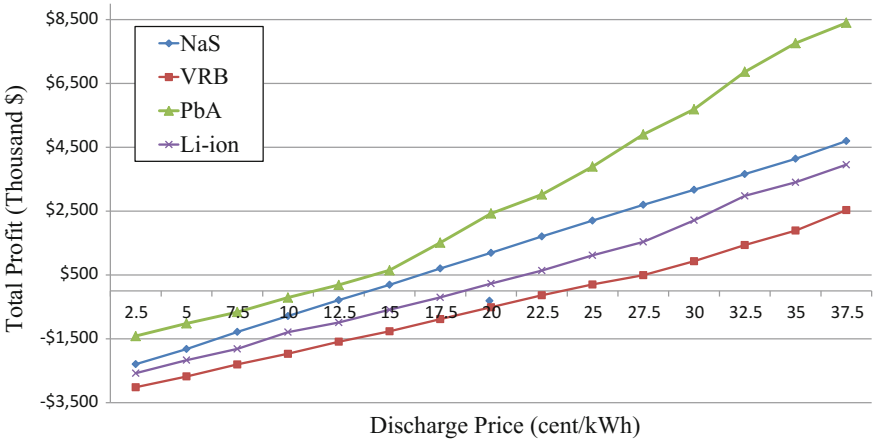

Fig. 2 Discharge price impact on total profit

Table 2 Optimal installation decisions at the minimum profit point

BESS Type	NaS	VRB	PbA	Li-ion
Year of Installation	Year 1	Year 1	Year 1	Year 1
P_{BESS}	1050 kW	1050 kW	1050 kW	1100 kW
E_{BESS}	6300 kWh	2050 kWh	2550 kWh	1500 kWh
θ_{dch}	15 ¢/kWh	25 ¢/kWh	12.5 ¢/kWh	20 ¢/kWh
DCH REV	$2,975,273	$3,870,797	$2,233,353	$3,304,285
Reserve REV	$317,816	$239,963	$245,932	$203,715
CH Cost	$262,058	$224,752	$197,970	$183,063
INS	$2,770,570	$3,564,605	$1,928,596	$2,996,842
OM	$68,627	$120,216	$167,469	$100,085
Total Profit	$191,834	$201,186	$185,249	$228,010

power and energy size of BESS and the installation year at the minimum discharge prices that generates profit, are presented in Table 2.

3.3 Optimal BESS and Microgrid Operations Schedule

Now, the BESS size, year of installation, and the selected BESS technology are determined by the investor, and the BESS charge, discharge, and reserve prices are fixed. Hence, the 1050 kW and 2550 kWh PbA BESS is installed in first year of the planning horizon. The discharge price is 12.5 ¢/kWh, while the charge and reserve prices are 1 ¢/kWh and 0.6 ¢/kWh, respectively.

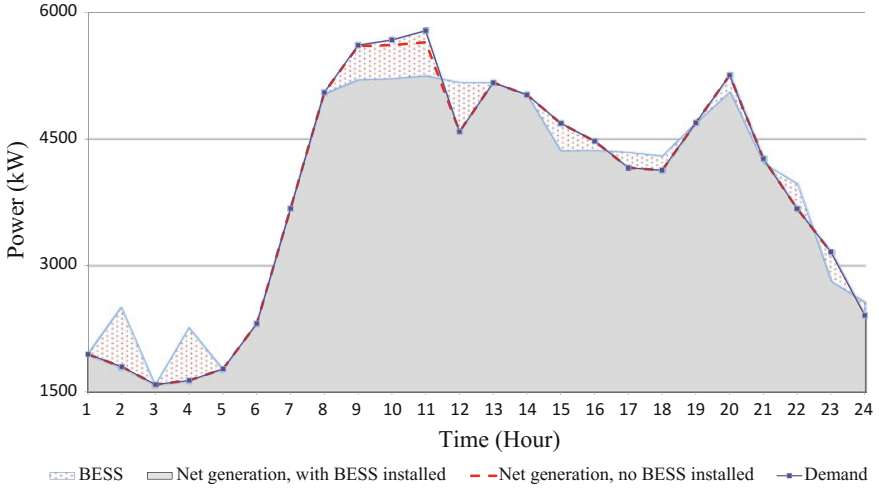

Fig. 3 Optimal operation of PbA BESS and microgrid in year 10

The microgrid schedules the BESS when it is required only to avoid a higher operational cost. The results show that in order to satisfy the investor's revenue constraints (36) and (37), the microgrid pays 80% of the installation cost in the year of installation, while the remaining of the investor's revenue is paid through the BESS operation. Figure 3 shows the BESS charging and discharging cycles and microgrid supply-demand balance in year 10 of the planning period. It is noted that since the DG capacity of the microgrid cannot supply the entire demand and provide reserve at peak hours, the microgrid is forced to use the high BESS energy costs to meet the demand and reserve requirements.

4 Conclusions

This paper proposed a new approach to determine the minimum acceptable discharge price for third-party investors in battery energy storage system. The optimal sizing and year of installation are determined considering investor profit maximization as the objective. Different battery energy storage technologies are examined, and the optimal technology is selected based on its minimum discharge price that generates investor's profit. After that, the microgrid and battery energy storage system operations are optimized from the perspective of the microgrid operator, while ensuring the same level of investor's revenue from the investment model. The results show the feasibility and effectiveness of the proposed investment framework. The work can be extended to consider detailed representation of the load profile and seasonal variations in renewable generation availability. There is also a need to consider uncertainty effects on the planning process.

Acknowledgements The first author wishes to acknowledge the funding support to carry out this work received from Taif University, Saudi Arabia, through the Saudi Arabian Cultural Bureau in Canada.

References

1. Lasseter, R.H., MicroGrids, IEEE Power Engineering Society Winter Meeting, 1, 305-308 (2002)
2. Arriaga, M., Cañizares, C.A., Kazerani, M., Northern Lights: Access to Electricity in Canada's Northern and Remote Communities, IEEE Power and Energy Magazine, 12, 50-59 (2014)
3. Omran, W.A., Kazerani, M., Salama, M.M.A., Investigation of Methods for Reduction of Power Fluctuations Generated From Large Grid-Connected Photovoltaic Systems, IEEE Transaction Energy Conversion, 26, 318-327 (2011)
4. Wang, X., Mahinda Vilathgamuwa, D., Choi, S.S., Determination of Battery Storage Capacity in Energy Buffer for Wind Farm, IEEE Transaction Energy Conversion, 23, 868-878 (2008)
5. Xiaoyu Wang, Meng Yue, Muljadi, E., Wenzhong Gao, Probabilistic Approach for Power Capacity Specification of Wind Energy Storage Systems, IEEE Transaction Industry Applications, 50, 1215-1224 (2014)
6. Yu Ru, Kleissl, J., Martinez, S., Storage Size Determination for Grid-Connected Photovoltaic Systems, IEEE Transaction Sustainable Energy, 4, 68-81 (2013)
7. Ye Yang, Hui Li, Aichhorn, A., Jianping Zheng, Greenleaf, M., Sizing Strategy of Distributed Battery Storage System With High Penetration of Photovoltaic for Voltage Regulation and Peak Load Shaving, IEEE Transaction Smart Grid, 5, 982-991 (2014)
8. Brekken, T.K.A., Yokochi, A., Von Jouanne, A., Yen, Z.Z., Hapke, H.M., Halamay, D.A., Optimal Energy Storage Sizing and Control for Wind Power Applications, IEEE Transaction Sustainable Energy, 2, 69-77 (2011)
9. Hartmann, B., Dan, A., Methodologies for Storage Size Determination for the Integration of Wind Power, IEEE Transaction Sustainable Energy, 5, 182-189 (2014)
10. Chen, S.X., Gooi, H.B., Wang, M.Q., Sizing of Energy Storage for Microgrids, IEEE Transaction Smart Grid, 3, (2012)
11. Zein Alabedin, A.M., El-Saadany, E.F., Salama, M.M.A., Generation Scheduling in Microgrids Under Uncertainties in Power Generation, IEEE Electrical Power and Energy Conference, London, ON, Canada, 133-138 (2012)
12. Ramos-gaete, F., Modeling and Analysis of Price-Responsive Loads in the Operation of Smart Grids, University of Waterloo (2013)
13. GAMS Documentation Center. [online]. Available: https://www.gams.com/help/index.jsp
14. Olivares, D.E., Cañizares, C.A., Kazerani, M., A Centralized Energy Management System for Isolated Microgrids, IEEE Transaction Smart Grid, 4, 1864-1875 (2014)
15. Viswanathan, V., Kintner-Meyer, M., Balducci, P., Jin, C., National Assessment of Energy Storage for Grid Balancing and Arbitrage:Phase 2, Volume 2: Cost and Performance Characterization, Pacific Northwest National Laboratory, PNNL-21388 (2013)
16. Akhil, A.A., Huff, G., Currier, A.B., Kaun, B.C., Rastler, D.M., Chen, S.B., Cotter, A.L., Bradshaw, D.T., Gauntlett, W.D., DOE / EPRI 2013 Electricity Storage Handbook in Collaboration with NRECA, Sandia National Laboratories, SAND2013-5131 (2013)
17. Eyer, J., Corey, G., Energy Storage for the Electricity Grid: Benefits and Market Potential Assessment Guide, Sandia National Laboratories, SAND2010-0815 (2010)

A Dynamic Programming Approach to Multi-period Planning of Isolated Microgrids

Benoît Martin, Emmanuel De Jaeger, François Glineur and Arnaud Latiers

Abstract An original methodology is presented to perform multi-period planning of isolated microgrids in a green field context. The aim is to build an isolated radial network to supply power to a set of initially unconnected loads whose consumption is growing through the planning horizon. The planning tool's outputs are: (1) network routing, (2) network sizing and (3) investments timing. These 3 steps are undertaken so that they minimize the total Net Present Value of the whole system. In this paper, the emphasis is put on the structure of the distribution planning problem. In particular, its optimal substructure allows to make use of a dynamic programming approach to tackle the time dimension of the optimization problem. Furthermore, several characteristics of radial networks are presented on the basis of which the main problem can be decoupled in independent subproblems. This reduces the size of the search space and consequently the computational burden. A non-linear and unbalanced triphase representation of the network is used to account for the effect of single-phase connected loads on the voltage profile. The effectiveness of the proposed method is illustrated through a case study.

Keywords Distribution planning · Dynamic programming · Microgrids · Unbalanced load-flow

B. Martin (✉) · E. De Jaeger
Center For Research in Energy and Mechatronics (CEREM), Université Catholique de Louvain (UCL), Louvain-la-Neuve, Belgium
e-mail: benoit.martin@uclouvain.be

E. De Jaeger
e-mail: emmanuel.dejaeger@uclouvain.be

F. Glineur · A. Latiers
Center for Operations Research and Econometrics (CORE), Université Catholique de Louvain (UCL), Louvain-la-Neuve, Belgium
e-mail: francois.glineur@uclouvain.be

A. Latiers
e-mail: arnaud.latiers@uclouvain.be

V. Bertsch et al. (eds.), *Advances in Energy System Optimization*,
Trends in Mathematics, DOI 10.1007/978-3-319-51795-7_8

1 Introduction

Electrification is considered today as an essential developing factor for emerging countries. However, the architecture of the power systems to be developed is strongly dependent on the geographic distribution of consumers on one side and existing infrastructures on the other side. As such, isolated microgrids are seen as efficient and economic solutions to electrify remote rural areas, i.e. areas located far from an existing transmission network, as they avoid costly investments in those transmission systems [1]. Isolated microgrids are thus only powered by locally installed generators and are operated in stand-alone, with no connection to any transmission network. A distribution planning study aims at giving an investment plan for a distribution network covering a certain planning area over a predefined planning horizon. It essentially consists of answering the three following questions:

- Which equipments to place?
- Where to place them?
- When to place them?

The planning objective is to come up with a system that ensures quality and reliability of the power supply at the lowest cost. In the present study, the focus is on the planning of isolated microgrids supplying a set of geographically dispersed loads. The rest of this paper is organized as follows. A review of the concerned literature is presented in Sect. 2. Section 3 is dedicated to the mathematical definition of the problem. In Sect. 4, the structure of the developed tool is presented based on the structure of the problem, along with the different subblocks. A case-study is presented in Sect. 5, and the boundaries of the proposed approach are discussed in Sect. 6.

2 State of the Art

A large amount of papers have already treated the distribution planning problem. In the vast majority, they deal with the following variables: feeder routing [2–11], branch conductor sizes [2–10, 12, 13], and substation location and size [6, 9, 11–14]. Most authors tend to consider only radial distribution networks, fewer consider looped or meshed networks [2, 7, 15–18]. There are two main objectives for planning studies. At first, all papers perform minimization of the total cost of the system. Secondly, more and more authors add an extra objective related to reliability maximization [3, 6–8]. Other objectives are also treated in literature, such as maximization of DG penetration [6, 8]. When more than one objective is considered, a multi-objective approach is used, either with multiple objective functions [2, 3, 6, 7] or a single weighted sum of different objective functions [8].

Optimization techniques employed for planning studies essentially belong to the following two categories [7]: deterministic algorithms [7, 10, 12, 13] and

heuristic-based algorithms [2–6, 8, 12]. The former always deliver the same solution to a particular problem while the latter may deliver different solutions to the same problem from one execution to another. Heuristic-based algorithms are mainly evolutionary algorithms such as Particle Swarm Optimization [6, 8], Genetic Algorithms [3, 9] or Immune System Inspired Algorithms [4]. The review of the aforementioned papers reveals three shortcomings. First, most of these perform a 'one-step planning', where all investments are made at the same time and there is no reinforcement afterwards. Nevertheless, some authors do consider the time schedule of investments [10, 12, 13]. Then, physical constraints of power distribution are often simplified. These are related to node voltages and cables ampacity. Load flow studies have to be run in order to verify those two types of constraints. However, most papers use simplified power flow representation such as linearized DC load flow and approximate formulas for voltage drops. Furthermore, in the vast majority, they don't consider the fundamentally unbalanced character of distribution networks and perform single-phase load flow. As a matter of fact, loads (residential and commercial) connected at low voltage level are often single-phase and randomly distributed on the three phases [19]. This unbalance may substantially worsen the voltage plan in comparison with perfectly balanced situation. A single-phase representation of distribution networks may thus lead to overoptimistic results regarding the respect of voltage constraints. Finally, reviewed papers seldom perform an exhaustive exploration of the search space, whether this is due to the nature of evolutionary algorithms or to heuristic rules imposed by the authors. The developed tool thus intends to tackle the aforementioned shortcomings. The proposed methodology makes use of graph theory and dynamic programming frameworks to efficiently and exhaustively explore the search space while using a three-phase load flow algorithm to properly model network constraints.

3 Problem Definition

3.1 Graph Formulation of the Problem

Formally, the problem of distribution planning may be expressed using graph theory. The aim is to connect a set of vertices or nodes $\mathcal{V}$(the loads) with a set of edges $\mathcal{E}$(network lines). Those two sets form the graph $\mathcal{G} = (\mathcal{V}, \mathcal{E})$. Graph $\mathcal{G}$ is undirected as power may flow in both directions. An important planning choice is to decide whether to build a meshed network or a radial one. Meshed networks, if well planned, may reduce losses, voltage constraints [2] and enhance reliability by providing alternative feeding routes in case of contingencies [16]. However, they are more complex to plan [2]. Furthermore, they require more sophisticated protection schemes, which renders the DSO's (Distribution system operators) reluctant to implement them. This work will thus focus on radial distribution network. Hence, graph $\mathcal{G}$ is a tree, where there is only one path from one vertex to another.

3.2 Objective Function and Constraints

The objective in this work is to minimize the Net Present Value of the system over the planning horizon T as expressed by (1).

$$\min_{u_{t,b,i,j}} \sum_{t=1}^{T} \sum_{i,j \in \mathcal{V}} \sum_{b \in \mathcal{B}} \frac{1}{(1+r)^t} (u_{t,b,i,j} \cdot l_{i,j} \cdot c_b + E^{loss}_{i,j,t} \cdot C_{en}) \tag{1}$$

There are two cost components: investments costs (CAPEX) to build new lines or reinforce existing ones and operational costs (OPEX) related to losses. Investments in lines are chosen among a set $\mathcal{B}$ of available branches. The discount rate is r, the decision variable $u_{t,b,i,j}$ is 1 if a line of type b is placed between nodes i and j at timestep t and is 0 otherwise. The length of the line between nodes i and j is $l_{i,j}$ (km), the cost of a type b branch is c_b (\$/km). The second term in the equation is the cost of losses, where $E^{loss}_{i,j,t}$ represent the losses in the line between nodes i and j during timestep t (kWh) and C_{en} the cost of energy (\$/kWh). There are three types of constraints. First, the graph must be a connected tree (2), meaning that every node is supplied at all times by a unique route. n is the amount of nodes to be supplied, with $n = |\mathcal{V}|$

$$|\mathcal{E}| = n - 1 \tag{2}$$

The following constraints are related to power flows, node voltages and branch currents. At first, balance of active and reactive power injections must be respected at all nodes, as stated by (3). P_k and Q_k are the active and reactive power injections at node k (positive if power is consumed) and $P_{l,k}$ and $Q_{l,k}$ are active and reactive power flows from node l to node k. For the rest of the paper, the complex power notation is used for more convenience: $\overline{S}_{t,k} = P_{t,k} + j\,Q_{t,k}$.

$$\overline{S}_k = \sum_{l \neq k} \overline{S}_{l,k} \qquad \forall k, l \in \mathcal{V} \tag{3}$$

Then, nodal voltages should be bound as in (4), V_n being the nominal voltage.

$$0.9 \cdot V_n \leq V_i \leq 1.1 \cdot V_n \qquad \forall i \in \mathcal{V} \tag{4}$$

Finally, branch currents are limited by the thermal rating of lines (5), $I_{max,b}$ being the ampacity of conductors of type b and $I_{i,j}$ the current flowing from node i to node j with $b_{i,j}$ the type of the branch linking i and j.

$$I_{i,j} \leq I_{max,b_{i,j}} \qquad \forall i, j \in \mathcal{V} \tag{5}$$

The last type of constraints concerns investment trajectory. As mentioned before, the load is considered to grow through the planning horizon. Voltage and ampacity constraints can thus only become worse with time with growing power flows on the

same network. This implies that investments cannot be unmade and the size of the lines may only be growing (6).

$$Size_{i,j,t} \leq Size_{i,j,t+1} \qquad \forall i, j \in \mathcal{V}, t = 1, \ldots, T-1 \tag{6}$$

A load flow is run to ensure constraints (3)–(5). The choice is made for a three-phase backward forward sweep algorithm. The main modelling features are the following: (1) loads are represented as one, two or three current sources depending on whether they are single-, two- or three-phase, (2) generators are considered as negative loads (i.e. they consume a negative current which is equivalent to inject a positive current) and (3) voltage drops (or rises in case of positive current injection towards the grid) on the three phases of a line are computed with the full impedance matrix and the three-phase currents, taking into account the mutual impedances effect. Comparative tests have been carried out to assess the loss of accuracy when using a single-phase load flow instead of a three-phase one to compute voltages on a distribution network with only single-phase loads. For this comparison, single-phase loads are replaced by three-phase loads with the same total power but evenly distributed on the three phases. Furthermore, intrinsic unbalance of the line impedances is neglected. These 2 hypotheses allow to draw an equivalent single-line diagram on which a single-phase load flow is run. It has been found that voltages errors up to 4% are introduced when using this single-phase approximation. Hence, it justifies the use of a full three-phase load flow calculation for distribution systems where there are many single-phase loads and generators. The backward forward sweep algorithm is proven to be faster than traditional Newton–Raphson or Gauss–Seidel methods for radial networks [20]. It is an iterative method in which currents (backward sweep) and voltages (forward sweep) are successively computed and updated with the result of previous iterations until convergence. The interested reader can refer to [20] for more details on this algorithm. The modelling of branches and loads, based on the work of [20, 21], has been slightly adapted to explicitly model 4-wires networks.

3.3 Input Data

There are three types of data for this planning study. First, there is the set of n cartesian coordinates (X, Y) (km) for each node. Then, the load consumption is given for each node and each timestep t of the planning horizon $\{\overline{S}_{t,1}, \ldots, \overline{S}_{t,n}\}$ (kVA). Finally, there is the set of available electric conductors $\mathcal{B}$, with their respective impedance matrices Z_b and costs c_b, $b \in 1, \ldots, n_{\mathcal{B}}$ with $n_{\mathcal{B}}$ the amount of different available conductor types.

4 Problem Decomposition and Tool Structure

The goal is to solve (1) subject to constraints (2)–(6). In (1), the decision variables $u_{t,b,i,j}$ aggregate three different decisions: place a line between nodes i and j, give it the size b and build it at timestep t. All these decisions are discrete by nature, making the problem subject to the curse of dimensionality. If 15 nodes are to be connected in a radial way with 3 different branch sizes available, there are $2 * 10^{15}$ possible trees connecting the nodes. For each of them, there are $5 * 10^{6}$ different possibilities for branch sizes. There are thus 10^{22} different possible networks, without even taking investment timing into account. To avoid this computational intractability, decision making is separated in three. Firstly, the architecture is determined. Then, all possible combinations of branch sizes are generated and constraints are evaluated for each alternative. The timing of investments is finally decided. The following subsections are dedicated to each subproblem.

4.1 Network Routing

In (1), OPEX and CAPEX are simultaneously minimized, which are conflicting objectives as the cheapest lines (the ones with smallest cross-sections) are also the ones that generate the highest losses. Nevertheless, preliminary tests have shown that the cost of losses is always an order of magnitude below the cost of investments. Investment minimization may thus be considered alone in first approximation. Cost of investment in new lines or reinforcement of existing ones depends on the cross-section of the conductor and the length of the line. As network sizing has not been done yet, only the total length of the lines can be minimized. The problem is thus reduced to a Minimum Spanning Tree (MST) problem. Kruskal algorithm is used to find the MST [22]. First, the $n * (n-1)/2$ possible branches between n nodes are defined. Then, Kruskal algorithm chooses the routes in a greedy way [22]. The center of the graph is defined as the node with the smallest eccentricity, that is, with the smallest maximum distance to any other node of the network. This node will be the feeding node of the network, i.e. where the necessary generation is placed. It is further called the source node. Data about graph connectivity is stored in a connectivity matrix $\mathcal{C}$ $[n \times n]$. Node i is said to be the feeding node of node j if there is a branch between both and i is upstream from j relative to the source node. $\mathcal{C}$ is a defined as follows (7):

$$\mathcal{C}_{i,j} = \begin{cases} 1 & \text{if } i \text{ is the feeding node of } j \\ -1 & \text{if } j \text{ is the feeding node of} i \\ 0 & \text{otherwise} \end{cases} \tag{7}$$

4.2 Network Sizing

The goal here is to enumerate the different possible network alternatives with branch sizes chosen among a set $\mathcal{B}$ of branches. Let $n_{\mathcal{B}}$ be the cardinality of this set. With $n-1$ branches, there are $n_{\mathcal{B}}^{n-1}$ choices for network sizing, which rapidly grows with an increase in the amount of available conductors or nodes. Again, a decomposition technique is proposed to reduce computational burden, which consists of three steps:

- Feeder decomposition
- Decreasing size of branches
- Section decomposition

First, the radial nature of the network can be exploited. Indeed, power flows on one feeder neither influence power flows nor voltage plan on adjacent feeders. Feeders can thus be considered as independent networks that can be optimized separately.

Then, as generation is located at the center of the network, power flows are always directed from the center to the extreme nodes of the network. This means that current flowing in the branches may only increase when getting closer to the center. This implies that a particular branch size should always be greater than or equal to the size of any branch located downstream. Finally, the search space is further reduced by specifying that branches located on the same section should have the same size. A section of a feeder is defined as a set of branches of this feeder with no junction. In the network shown on Fig. 3, there are 2 feeders. The 2 feeders connect the nodes $[1-10-11-12-13-14-15-16-17-18-19-20]$ and $[1-8-6-7-5-4-3-2-9]$ respectively. One section is for example $[1-8-6]$. The output of this subblock is a set $\mathcal{S}$ of n_{alt} matrices B_k, each one representing the branch size of each network alternative.

4.3 Constraints Verification and Transition Costs

There is now a set of n_{alt} network alternatives. A network alternative is characterized by its connectivity matrix, common to all alternatives, and its matrix B, which differs from one alternative to another. Constraint (2) is always respected with the Kruskal algorithm presented above. Remaining constraints may be divided in two types. *Static* constraints (3)–(5), related to power flows and equipment limits, must be ensured *at each timestep* while the *transition* constraint (6) must hold *between each two successive timesteps*. Let alternative k be considered at timestep t and alternative l at timestep t+1, $k, l \in 1, \ldots, n_{alt}$. This particular transition is written $k_t \rightarrow l_{t+1}$. There are three verifications to make:

1. Constraints (3)–(5) hold for alternative k at t
2. Constraints (3)–(5) hold for alternative l at $t+1$
3. Constraint(6) holds from k to l

If these three steps are respected, $i_t \rightarrow j_{t+1}$ is assigned a finite transition cost $C_{k_t \rightarrow l_{t+1}}$. It includes the reinforcement cost from i to j and the operational cost during timestep $t+1$. The former is the cost of additional conductor. The latter is the cost of losses on network l with particular load consumptions at all nodes during timestep $t+1$,$\{\overline{S}_{t+1,1}, \ldots, \overline{S}_{t+1,n}\}$. If one of the three steps is not respected, $C_{k_t \rightarrow l_{t+1}} = \infty$.

4.4 Investment Timing with Dynamic Programming

As mentioned in the introduction, the goal of this planning is to determine not only a network able to supply power demand at the beginning of the planning horizon, but also to decide the reinforcements that will be made afterwards to cope with a growing demand from the nodes. Transition costs between alternatives have been defined in the previous Sect. 4.3. A graph representation of these transitions is adopted (Fig. 1). On this graph $\mathcal{T}$, each node represents a network alternative at a given timestep. An edge between nodes k_t and l_{t+1} has a weight equal to $C_{k_t \rightarrow l_{t+1}}$, thus representing the evolution from alternative k to alternative l for branches sizes. Two additional nodes are defined: $Init$ corresponds to the initial situation before the beginning of planning horizon (timestep 0) when there is no network. $C_{Init \rightarrow k_1} \quad k \in 1, \ldots, n_{alt}$ thus comprises the total cost of building particular alternative k plus the cost of losses on this particular network at first timestep. Node $Last$ represents the situation after timestep T. $C_{k_T \rightarrow Last}$ is set to zero as there are no further investments considered after the end of planning horizon. Once this transition graph has been defined, the least-cost sequence of investment is still to be found. As mentioned in the beginning of this paper, a dynamic programming approach is chosen to handle this multistage problem, in a similar way to [23]. This approach is adapted to problems to which Bellman's principle of optimality applies. This principle states that at any timestep of a multistage decision making problem, the optimal decision policy for future timesteps should not depend on previously made decisions but only on the current state of the system [24]. This is the case for this problem as future investment and operational costs only depend on the current state of the system, not on the way it

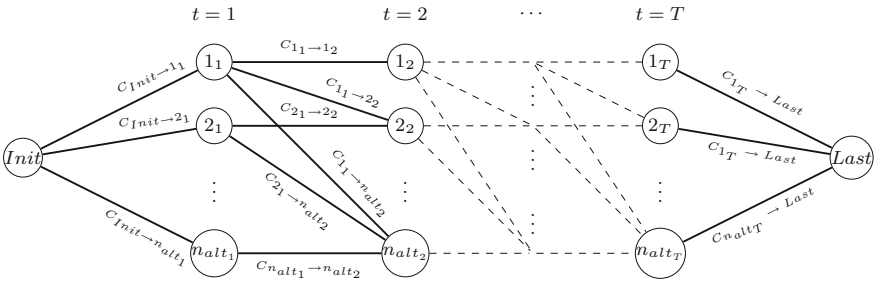

Fig. 1 Graph $\mathcal{T}$ of the transition costs between different network alternatives at successive timesteps

got at this current state. In this case, the state variables x_t of the system are the set of branches sizes at a given timestep $t \in 1, \ldots, T$ and the decision variables are the reinforcement decisions u_t. The state equation can be written in a compact form [25] (8).

$$x_t = x_{t-1} + u_t; \tag{8}$$

The minimization objective may be written as follows (9), with $C_{opt}(x_0)$ the optimal solution cost for the whole planning horizon given the initial state x_0 for which there is no network yet.

$$C_{opt}(x_0) = \min_{u_1,\ldots,u_T} \sum_{t\in 1,\ldots,T} \text{Cost}(u_t) \tag{9}$$

The idea behind dynamic programming is to make use of Bellman's principle of optimality to rewrite (9) in a recursive way by defining the function $f_{min}(x_t)$ as the optimal solution cost for all $\tau \geq t$ given the state x_t (10). This form is called *Bellman Optimality Equation* [25]. It can be interpreted as follows: at each timestep, the optimal solution cost for future timesteps is the minimum of the sum of current decision cost and the optimal solution cost at the next timestep given the state in which current decision will bring the system. x_{t+1} is obtained from state x_t and decision u_{t+1} with the state equation (8). $C_{x_t \to x_{t+1}}$ is the transition cost defined in Sect. 4.3. At the last timestep, $f_{min}(x_T) = 0$.

$$f_{min}(x_t) = \min_{u_{t+1}} [\ C_{x_t \to x_{t+1}} + f_{min}(x_{t+1})\ ] \tag{10}$$

The problem is thus solved in an iterative way. To do that, Dijkstra's algorithm [22] is applied to the previously defined transition graph $\mathcal{T}$. As a matter of fact, this algorithm is based on the same recursive principle as Bellman Optimality Equation.

4.5 Global Structure of the Planning Tool

In previous subsections, the four different subblocks of the planning tool have been defined. The following diagram (Fig. 2) summarizes the articulation of these subblocks, the three types of input data they use and the information they exchange. The output is the set $\mathcal{U}$ of investment decisions. As mentioned in Sect. 3, an investment decision mentions the reinforcement (conductor size increase), the line being concerned by this reinforcement and the timestep at which the investment is made.

5 Case-Study

The planning tool presented in Sect. 4 is applied to a 20-node dataset used in [3]. This dataset, including cartesian coordinates of nodes, power consumptions and conductor data, can be found in [26]. Network upgrading can be realized either

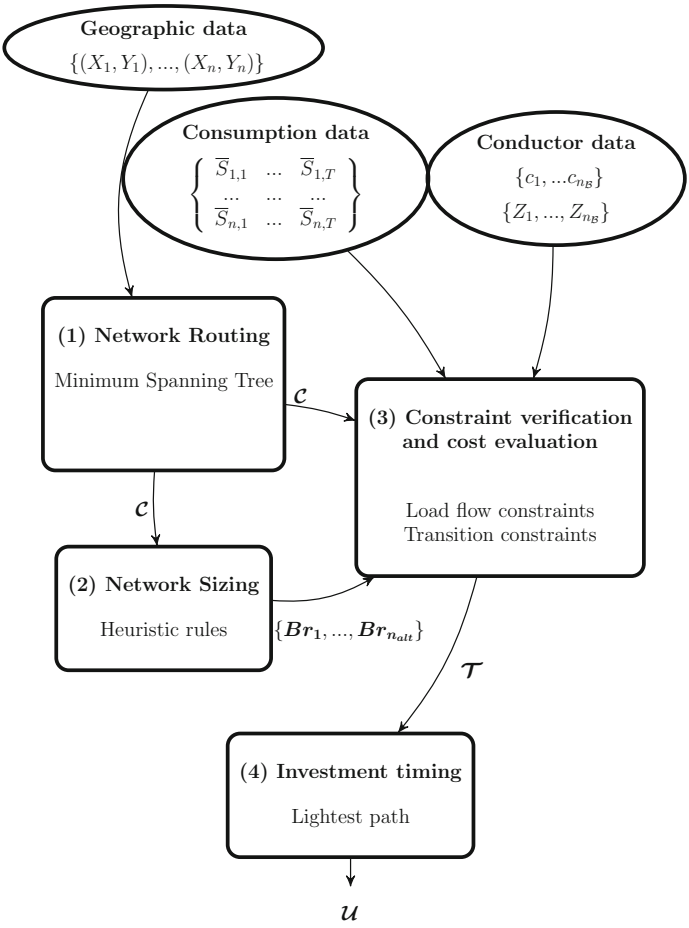

Fig. 2 The problem has 3 different types of data. There are 4 subblocks that perform the following functions: (*1*) Network routing, (*2*) Network sizing, (*3*) Constraint verification and cost evaluation and (*4*) Investment timing. The output is the set $\mathcal{U}$ of investment decisions with their respective timing

by reconductoring or reinforcement. In the former case, the existing conductor is removed and replaced by a conductor of bigger capacity. In the latter case, a conductor is added in parallel to the existing one to reduce the total impedance of the line and increase its ampacity. In this study, only reinforcement is considered. A single conductor type is used, and up to three such conductors can be placed in parallel, which gives three possible branch sizes, named hereafter 1, 2 and 3. In this case, the impedance of size 2 and 3 lines is thus half and a third of size 1 lines impedance respectively. In Sect. 4.2, a rule has been introduced to limit the size of the search space: every branch of a section of a feeder should have the same size. For this case

Table 1 Parameters used for the planning study

Planning horizon	20	(Years)
Interest rate	10%	
Cost of losses	60	($/MWh)
Yearly load growth	10%	
Base voltage	13.8	(kV)
Conductor resistance	0.64	(Ω/km)
Conductor reactance	0.45	(Ω/km)
Conductor ampacity	214	(A)
Building cost of line	23000	($/km)
Unit conductor cost	8220	($/km)

Table 2 Investment sequence: case 1

Branch	2–4	4–5	5–6	2–9	2–9
Year	6	6	6	9	10
Reinf.	2 → 3	2 → 3	2 → 3	1 → 2	2 → 3

Table 3 Investment sequence: case 2

B	2–4	6–8	5–6	4–5	2–9	2–4	2–9
Y	2	2	3	5	6	8	12
R	1 → 2	2 → 3	2 → 3	2 → 3	1 → 2	2 → 3	2 → 3

study, the relevance of this rule is tested by running 2 planning studies, one with this rule (case 1) and the other one without (case 2). The planning horizon is set to 20 years. Load consumption is growing at constant and uniform yearly rate of 10%, with consumptions at the beginning of the planning horizon being the same as in [26], for a total initial load of 4.9 (MVA). Relevant parameters for the planning study are presented in Table 1. The cost of lines is made of two components. The first one is a fixed one, called the building cost of line in Table 4. It is common to all lines and corresponds to pole installation. The second component is the cost of conductors. If is obtained by multiplying the unit conductor cost by the amount of lines in parallel (1, 2 or 3). Both cases have been run on a 2.7 Ghz Intel Core i7 processor with 8Go of memory.

Initial and final network (year 1 and year 20) are presented for cases 1 and 2 in Table 4. Tables 2 and 3 illustrate the differences in the sequences of investment for cases 1 and 2, with the third line of these tables representing the upgrade in the line size. Figure 3 shows the final network for case 2, with network graph and branch sizes.

Several observations can be made for results in Table 4. First, initial and final solutions are very close for both cases. Then, branch (16–17) can have a lower size

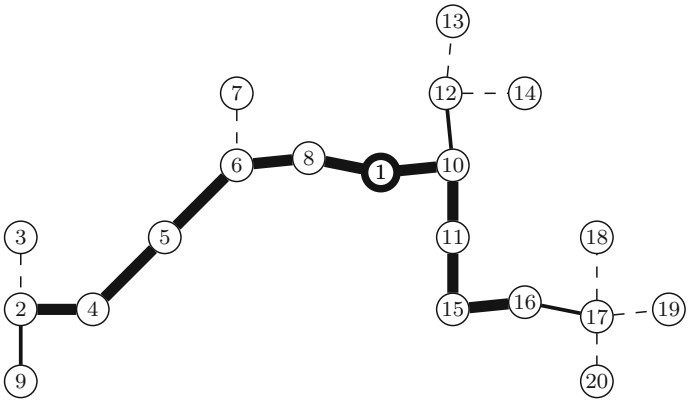

Fig. 3 Final network for case 2. Thick lines represent branches of size 3, normal lines branches of size 2 and dashed lines branches of size 1. Node 1 is the center of the network, where generation is placed

Table 4 Branches size at the beginning of years 1 and 20 where reinforcements take plac. Gray cells show differences between the 2 cases

	Case 1		Case 2	
Branch	Year 1	Year 20	Year 1	Year 20
1-8	3	3	3	3
8-6	3	3	2	3
6-7	1	1	1	1
6-5	2	3	2	3
5-4	2	3	2	3
4-2	2	3	1	3
2-3	1	1	1	1
2-9	1	3	1	3
1-10	3	3	3	3
10-11	2	2	2	2
11-15	2	2	2	2
15-16	2	2	2	2
16-17	2	2	1	1
17-18	1	1	1	1
17-19	1	1	1	1
17-20	1	1	1	1
10-12	1	1	1	1
12-13	1	1	1	1
12-14	1	1	1	1

by relaxing the aforementioned rule. Furthermore, the removal of this rule allows to have a more progressive investment sequence (Tables 3 and 4) for case 2. This means that some costs happen later in time. These costs thus contribute less to the total NPV of the system because of the time value of money. The cost for case 1 is 1393 (k$) while it is 1385 (k$) for case 2, which makes a 0.6% difference. Execution times are respectively 200 and 467 (s) for cases 1 and 2. This comparative case study thus shows that the rule that has been imposed to limit computational burden does not yield a significant error while substantially reducing execution time. However, it has to be confirmed for bigger problems with more nodes and longer feeder sections.

6 Discussion

The proposed approach has introduced some simplifications. As a matter of fact, network sizing and network routing have been decoupled to limit the computational burden. However, it may introduce a loss of optimality because the behaviour of a network depends not only on its graph but also on the size of its branches. By defining the graph first, other topologies are dismissed that may lead, with appropriate branch sizing, to better solutions. Limiting factors for the problem are mainly the amount of nodes and the amount of available conductors. The duration of the planning study is less critical regarding problem size as the number of evaluations to make grows linearly with the amount of planning steps, while a growing amount of nodes or available conductors produces a combinatorial explosion of the amount of network alternatives to evaluate at each timestep. For example, adding an extra conductor type (four instead of three types) multiplies the amount of network alternatives by a factor 5 in the case-study presented in the previous section.

7 Conclusion

An original planning tool for autonomous and radial microgrids has been presented in this paper. It is composed of 4 different subblocks that perform (1) Network Routing, (2) Network Sizing, (3) Constraints and costs evaluation and (4) Investment Timing. A dynamic programming approach has been proposed to solve the problem. The structure of the problem has been exploited to limit the search space to feasible solutions. An additional heuristic rule has been added for network sizing to further reduce the search space. Preliminary results have shown that the loss of optimality introduced by this rule was negligible, even though further tests have to be carried out to confirm it. Limitations of the proposed approach have been described in Sect. 6. The biggest limitation concerns the size of the problems that can be solved: this approach, in its current form, is hardly usable for problems with more than 40 nodes. However, the field of approximate dynamic programming gathers a set of approximation methods to cope with the traditional curse of dimensionality encountered

in dynamic programming. Further research thus includes the investigation of such methods to cope with problems of bigger size. Another axis of research is to include distributed generation placement and sizing to perform coordinated planning where generation and distribution are planned simultaneously.

Acknowledgements The first author is supported by a FRIA grant from the Belgian Fund for Scientific Research - FNRS.

References

1. Kaundinya DP, Balachandra P, Ravindranath NH (2009) Grid-connected versus stand-alone energy systems for decentralized power—A review of literature. Renewable and Sustainable Energy Reviews 13(8):2041–2050
2. Alvarez-Herault MC (2009) Architectures des reseaux de distribution du futur en presence de production decentralisee. PhD thesis, Institut National Polytechnique de Grenoble - INPG
3. Carrano EG, Soares LA, Takahashi RH, Saldanha RR, Neto OM (2006) Electric distribution network multiobjective design using a problem-specific genetic algorithm. Power Delivery, IEEE Transactions on 21(2):995–1005
4. Carrano EG, Guimaraes FG, Takahashi RHC, Neto OM, Campelo F (2007) Electric Distribution Network Expansion Under Load-Evolution Uncertainty Using an Immune System Inspired Algorithm. IEEE Transactions on Power Systems 22(2):851–861
5. Falaghi H, Ramezani M, Haghifam MR, Milani KR (2005) Optimal selection of conductors in radial distribution systems with time varying load. In: Electricity Distribution, 2005. CIRED 2005. 18th International Conference and Exhibition on, IET, pp 1–4
6. Ganguly S, Sahoo NC, Das D (2010) A novel multi-objective PSO for electrical distribution system planning incorporating distributed generation. Energy Systems 1(3):291–337
7. Ganguly S, Sahoo NC, Das D (2013a) Multi-objective particle swarm optimization based on fuzzy-Pareto-dominance for possibilistic planning of electrical distribution systems incorporating distributed generation. Fuzzy Sets and Systems 213:47–73
8. Ganguly S, Sahoo NC, Das D (2013b) Multi-objective planning of electrical distribution systems using dynamic programming. International Journal of Electrical Power & Energy Systems 46:65–78
9. Kalesar BM, Seifi AR (2011) Optimal substation placement and feeder routing in distribution system planning using genetic algorithm. Elixir International journal of Electrical Engineering pp 3908–3915
10. Nahman J, Spirić J (1997a) Optimal planning of rural medium voltage distribution networks. International Journal of Electrical Power & Energy Systems 19(8):549–556
11. Narasimhulu N, Sikindar babu T, Shiva Kumar T (2013) Focus on optimal feeder routing for radial distribution systems. ijareeie 2(8)
12. Falaghi H, Singh C, Haghifam MR, Ramezani M (2011) DG integrated multistage distribution system expansion planning. International Journal of Electrical Power & Energy Systems 33(8):1489–1497
13. Haffner S, Pereira L, Pereira L, Barreto L (2008) Multistage Model for Distribution Expansion Planning With Distributed Generation - Part I: Problem Formulation. IEEE Transactions on Power Delivery 23(2):915–923
14. Kersting W, Green RK (2011) The application of Carson's equation to the steady-state analysis of distribution feeders. In: Power Systems Conference and Exposition (PSCE), 2011 IEEE/PES, pp 1–6
15. Celli G, Pilo F, Pisano G, Allegranza V, Cicoria R, Iaria A (2004) Meshed vs. radial MV distribution network in presence of large amount of DG. In: Power Systems Conference and Exposition, 2004. IEEE PES, IEEE, pp 709–714

16. Celli G, Pilo F, Pisano G, Allegranza V, Cicoria R (2005) Distribution network interconnection for facilitating the diffusion of distributed generation. In: Electricity Distribution, 2005. CIRED 2005. 18th International Conference and Exhibition on, IET, pp 1–5
17. Ruben B, Cross A, Strickland D, Aten M, Ferris R (2011) Meshing radial networks at 11kv. In: Innovative Smart Grid Technologies (ISGT Europe), 2011 2nd IEEE PES International Conference and Exhibition on, IEEE, pp 1–8
18. Zidan A, Shaaban MF, El-Saadany EF (2013) Long-term multi-objective distribution network planning by DG allocation and feeders' reconfiguration. Electric Power Systems Research 105:95–104
19. Navarro-Espinosa A, Gozel T, Ochoa L, Shaw R, Randles D (2015) Data Analysis of LV networks: key parameters from one year of monitoring over hundreds ok UK LV feeders. In: 23nd International Conference and Exhibition on Electricity Distribution (CIRED 2015), Lyon
20. Demirok E, Kjĕr SBe, Sera D, Teodorescu R (2013) Three-Phase Unbalanced Load Flow Tool for Distribution Networks. In: 2nd International Workshop on Integration of Solar Power Systems
21. Zimmerman RD (1995) Comprehensive distribution power flow: modeling, formulation, solution algorithms and analysis. PhD thesis, Cornell University
22. Bondy JA, Murty US (2008) Graph theory, volume 244 of Graduate Texts in Mathematics. Springer, New York
23. Nahman J, Spirić J (1997b) Optimal planning of rural medium voltage distribution networks. International Journal of Electrical Power & Energy Systems 19(8):549–556
24. Boulaxis N, Papadopoulos M (2002) Optimal feeder routing in distribution system planning using dynamic programming technique and GIS facilities. IEEE Transactions on Power Delivery 17(1):242–247
25. Newham N (2008) Power System investment planning using stochastic dual dynamic programming. PhD thesis, University of Canterbury, Christchurch, New Zealand
26. Carrano EG, Soares LA (2006) Data Used in Simulations of Paper Electric Distribution Network Design Using a Problem-Specific Genetic Algorithm

Part V
Renewable Energy and Power Grid Expansion Planning

Curtailing Renewable Feed-In Peaks and Its Impact on Power Grid Extensions in Germany for the Year 2030

A Load Ow Model Using an Enhanced Benders Decomposition Approach

David Gunkel and Dominik Möst

Abstract Transmission grid extension is a central aspect of the future energy system transition. This is due to the diverging occurrence of renewable energy feed-in and consumption. The existing layout of the German grid was not designed to accommodate this divergence. To analyze the most cost-effective grid extensions, efficient methods for techno-economic analysis are required. The challenge of conducting an analysis of grid extensions involves the lumpy investment decisions and the nonlinear character of several restrictions in a real-data environment. The addition of new lines makes the grid characteristic variable for approximately load flow calculations. The following paper presents an application of the Benders Decomposition, dividing the problem into an extension and a dispatch problem combined with a Karush–Kuhn–Tucker-system. This combination enables one to solve the problem within reasonable time by using the favorable conditions contained in the sub-problem. The method is applied to the analysis of the integration of renewable energy within the context of German transmission grid extension planning for the year 2030. It can be shown that curtailing feed-in peaks of renewables can significantly reduce the extent of grid extensions necessary to sustain the energy system in Germany.

Keywords Transmission grid extensions · Germany · Integration of renewable energy sources

1 Introduction

The German energy system is expected to be faced with a significant increase in the share of renewable energy sources (RES) in the near future. This development has brought about an ever-increasing amount of research into redesigning the

D. Gunkel (✉) · D. Möst
Chair of Energy Economics, TU Dresden, Dresden, Germany
e-mail: dominik.moest@tu-dresden.de

D. Gunkel
e-mail: david.gunkel@tu-dresden.de

V. Bertsch et al. (eds.), *Advances in Energy System Optimization*,
Trends in Mathematics, DOI 10.1007/978-3-319-51795-7_9

transmission grid, making it currently one of the most discussed topics in the field of energy economics. RES feed-in peaks and the large spatial distances between points of RES generation and demand centers need to be spanned by increases in transmission capacities. A considerable amount of literature has been published on grid extensions at the European level within the context of nuclear and carbon phase-out scenarios. The German transmission system operators (TSO) suggest extensions as a policy response in [1] and calculate the required investments based on the assumption that every available unit of RES has to be integrated in the system. This approach is likely to lead to overinvestment since the investments are leveled by the RES feed-in peaks. Reference [12] generally show that RES supply curtailment can reduce extension needs. Reference [5] investigate investments in additional lines, gas-fired power plants and storage units within the German transmission grid considering different levels of fixed curtailment rates across RES technologies. In this paper, different RES integration pathways and their impact on the need for grid extensions are explored. To this end, current subsidized direct marketing (DM) rules for RES with priority feed-in in Germany and their influence on grid extensions are analyzed. We present findings as to whether DM should be updated in the future to reduce grid investments in Germany. The combination of renewable integration and an optimal grid expansion requires the development and implementation of an advanced model. In order to ensure that the optimization problem is solvable, the Benders Decomposition (BD) approach is applied.[1] Instead of solving a non-linear sub-problem and using the marginal of line capacity fixation as discussed in [2], the marginal can be calculated by means of an alternative method. The paper is organized as followed: input data and scenarios (Sect. 2), methodology (Sect. 3), results (Sect. 4), critical appraisal (Sect. 5) and conclusion (Sect. 6).

2 Input Data and Scenarios

2.1 Scenarios of Different RES Integration

For this analysis, a set of scenarios concerning different RES feed-in design options for Germany are listed in Table 1. Consistent with the economic rationale of DM under the German Renewable Energy Act (EEG), RES generators feed their energy into the grid up until negative prices emerge at a certain level. This level is determined by the respective feed-in tariffs of the RES. It is assumed that this tariff is set by technology-specific levelized costs of electricity (LCOE). RES producers would not feed-in their energy into the grid, if the negative price falls below their tariffs to avoid financial losses. They curtail the supply and do not use their priority feed-in status. In line with this approach, the *REF* scenario considers the individual LCOE of every RES technology. Beside the *REF* scenario, four further scenarios with more flexible RES integration are defined. All further scenarios share the feature that the curtailment rule explained above is weakened. The RES generator can not fully use

[1] A comprehensive literature about BD and other methods of grid extensions are provided in [10].

Table 1 Applied scenarios for the analysis

Scenario	Description
REF	DM for all RES technologies
All	PMI for all RES technologies
Off	PMI only for offshore wind
On	PMI only for onshore wind
PV	PMI only for photovoltaic

the DM. It is suspended for an amount of surplus RES. This amount is set to 1% of the annual RES supply and makes the RES integration more flexible.[2] This could foster a cost-minimal design for the future grid since peaks of supply are cut. The approach is referred to as a partial market integration (PMI) of RES for the remainder of the analysis. In contrast to PMI, full market integration represents an allocation of RES to the market at marginal costs of nearly zero. RES generators feed in their electricity as long as the price is above zero. This option is not considered within the scope of this analysis. The flexible RES integration scenarios are broken up into one with individual fluctuation technologies and one with flexible curtailment that includes all of them. The values of LCOE in 2030 for the *REF* scenario are based on [14]. These cost rates are comparable with their minimal fixed reference feed-in tariff, which creates incentives for further RES installations. It can be understood as compensation for avoided feed-in for RES generation plant owners.[3] The cost rates for curtailment influence market prices in hours of curtailment and partly set incentives for grid investments.[4,5]

2.2 Inputdata

The set of conventional power plants consists of fossil-fueled, nuclear and hydro plants with different technological characteristics like efficiency, emission factor and availability. The assumed generation parameters for the considered technologies are taken from [16]. All power generation capacities for 2030 are taken from the ESA^2-project [6].[6] The future capacities for Germany as well as the fuel and carbon

[2]The assumption is related to the hardship ruling in the EEG 2014. It defines, that all lost revenues have to compensated above 1% of annual income of a year.

[3]The individual LCOE as curtailment cost rate are represented with the parameter c_{ren}^{curt}.

[4]The discussion can be read in [12].

[5]From the system view, the load at every node is to be covered at minimal costs provided by RES. For this intention new transmission capacities are required. This leads to the trade-off between building a new line for transferring RES energy to other regions or curtail regional surplus supply. The non-sold energy is valuated with the LCOE of the individual generators. So the overall costs have to be rectified considering this amount.

[6]As part of the ESA^2-project, an alternative road-map for European energy system transformation to a low carbon economy was calculated. The outcome of the project was based on synergies arising

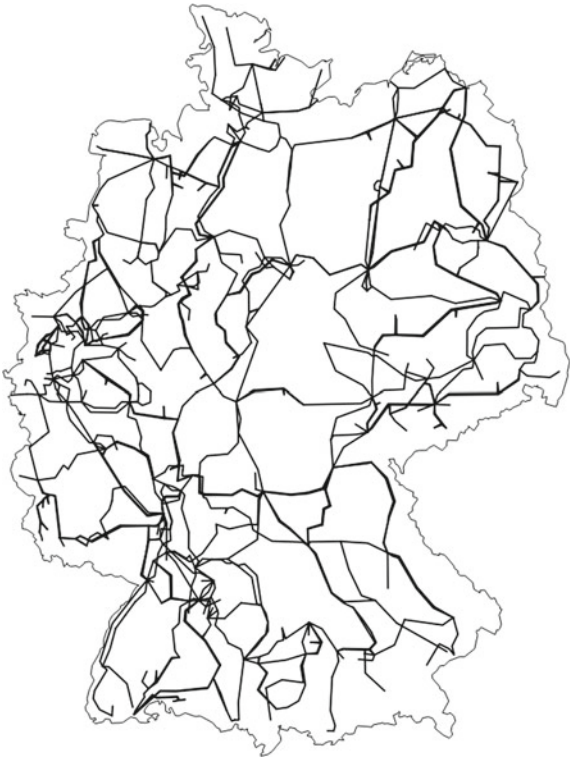

Fig. 1 Illustration of the German transmission grid without extensions

prices are obtained from [19]. The local distribution of capacities are based on the installed capacities in 2014 published in [3]. The German transmission grid, with its aggregated neighboring countries, consists of 418 nodes and 665 lines (see Fig. 1) based on data from 2012 provided by [7].[7] It is assumed that grid extensions are only possible within the German transmission grid, which is bound by a total number of four circuits. Using a temporal resolution of 8760 hours per year in such a large-scale problem entails a tremendous computing capacity. Hence, a reduction of the time set is required to obtain results. The public available data set from German TSOs for demand, photovoltaic (PV) and wind feed-in from 2012 is clustered into 64 weighted time subgroups, which are representative for the whole year of 2012.

(Footnote 6 continued)
from coupled and highly specified models for calculating the demand, investment in power plants and generation dispatch on a time horizon up to 2050. The EU27+ countries were considered. It is assumed for this paper that the capacities of the neighboring countries will develop according to a similar path presented in the EU Roadmap. The central assumptions are analogical. The complete report is available at researchgate.net.

[7] To cope with network security requirements like the n-1-criterion, a transmission reliability margin of 20% is assumed.

Table 2 Measurements of transmission capacity increase and its individual investment costs

Measurements	Specific costs
Line upgrade	125 kEUR/km [13]
Installation of a new	
220 kV transmission line	535 kEUR/km [13]
380 kV transmission line	1000 kEUR/km [13]
HVDC line	1500 kEUR/(km MW) [17]
HVDC converter	295 kEUR/MW [17]

3 Optimal Transmission Extensions Using Benders Decomposition

3.1 Sequential Transmission Capacity Increase

The TSO has the following options for increasing the transmission capacity of its grid as an assumption within this analysis:

1. Line upgrade (up): A shift of the voltage level from 220 to 380 kV is equal to a capacity increase of a factor of around 3.5.
2. Line extension (exp): Adding up to four further identical lines respectively circuits to an existing branch.
3. Constructing a HVDC-connection (HVDCadd) from the north respectively the middle to the south of Germany.

For computational reasons, these three options are sequentially analyzed in three-part models (line upgrade, line extension, HVDC-line installation) instead of a simultaneous, integrated calculation. The results of the prior-gained grid investments denote the starting grid configuration for the next step. The final grid is based on all chosen options to increase the transmission capacity. The possibility of linking prior non-directly connected nodes in the AC grid is neglected for reasons of simplification. The starting and end node of newly constructed HVDC-lines is given by [1].[8] The investment costs of different capacity increase measurements are presented in Table 2.

3.2 Configuration of the Global Model

The analysis is based on the deterministic bottom-up electricity model ELMOD (for further details see [15]) focused on the German transmission grid with all lines l,

[8]The demolition or downgrading of existing lines is assumed to be impossible. The TSO can use these existing transmission capacities for transmission reliability measurements.

grid nodes n and power plants p as well as RES units r and time t. The power flows through the transmission lines are based on the DC approximation of AC load flows as presented in [20, 21].[9] The global objective function for the component models extension are formulated as a MINLP-problem as followed[10] (see nomenclature at the end):

$$\begin{aligned} C^{total} = & \sum_{p \in P} \sum_{t \in T} c_p^{gen} \cdot G_{p,t} \cdot \tau_t \\ & + \sum_{ren \in REN} \sum_{t \in T} \begin{pmatrix} c_{ren}^{curt} \cdot \tau_t \\ \cdot \left(g_{ren}^{inst} \cdot r_{ren,t}^{max} \cdot a_{ren,t} - G_{ren,t} \right) \end{pmatrix} \\ & + \sum_{n \in N} \sum_{t \in T} c^{VoLL} \cdot \left(ENS_{n,t} + ART_{n,t}^{load} \right) \cdot \tau_t \\ & + I \rightarrow \min \end{aligned} \tag{1}$$

annualized investment costs for adding further lines

$$I^{exp} = \sum_{lef \in LEF} \left(EF_{lef} - exist_{lef} \right) \cdot c_{lef}^{exp} \tag{2}$$

with the subject of:
energy balance

$$\begin{aligned} demand_{n,t} = & \sum_{p \in P} G_{p,t} - \sum_{sto \in STO} PUMP_{sto,t} \\ & - NI_{n,t} + \left(ENS_{n,t} - ART_{n,t}^{load} \right) \\ & | \lambda = price_{n,t};\ \forall\, n \in N,\ \forall\, t \in T \end{aligned} \tag{3}$$

power generation restriction

$$G_{p,t} \leq g_p^{inst} \cdot a_{p,t};\ \forall\, p \in P,\ \forall\, t \in T \tag{4}$$

PMI with flexible curtailment of $\zeta = 1\%$

$$\begin{aligned} \sum_{t \in T} \tau_t \cdot \begin{pmatrix} g_{ren}^{inst} \cdot r_{ren,t}^{max} \cdot a_{ren,t} \\ -G_{ren,t} \end{pmatrix} \leq \zeta \cdot \sum_{t \in T} \begin{pmatrix} \tau_t \cdot g_{ren}^{inst} \\ \cdot r_{ren,t}^{max} \cdot a_{ren,t} \end{pmatrix} \\ \forall\, ren \in REN \subseteq P \end{aligned} \tag{5}$$

[9] An assumption of the model is the application of nodal price system in Germany. It is assumed that this is going to be implemented by 2030.

[10] The line upgrade component model contains binary decisions referring to voltage increase. This method is similar to the extension component model and therefore not demonstrated here.

storage and reservoir restrictions

$$PUMP_{sto,t} \leq pump_{sto}^{inst} \quad \forall\, sto \in STO \subseteq P,\ \forall\, t \in T \tag{6}$$

$$\sum_{t \in T} \left(PUMP_{sto,t} \cdot \tau_t \cdot \eta_{sto}\right) = \sum_{t \in T} \left(G_{sto,t} \cdot \tau_t\right) \quad \forall\, sto \in STO \subseteq P \tag{7}$$

$$\sum_{t \in T} \left(G_{rese,t} \cdot \tau_t\right) \leq g_{rese}^{inst} \cdot flh_{rese} \quad \forall\, rese \in RESE \subseteq P \tag{8}$$

updating the transfer matrix $H_{l,n}$

$$H_{lef,n} = \frac{REF_{lef}}{exist_{lef}} \cdot h_{lef,n}^{exist};\ \forall\, lef \in LEF \subseteq L \tag{9}$$

$$H_{lfx,n} = h_{lfx,n};\ \forall\, lfx \in LFX \subseteq L \tag{10}$$

updating the system sensitivity matrix $B_{n,nn}$

$$B_{n,nn} = \sum_{lfx \in LFX} inci_{lfx,nn} \cdot h_{lfx,n} + \sum_{lef \in LEF} inci_{lef,nn} \cdot H_{lef,n} \quad \forall\, n, nn \in N \tag{11}$$

definition of the net injection

$$NI_{n,t} = \sum_{nn \in N} B_{n,nn} \cdot \Delta_{nn,t} \cdot \beta;\ \forall\, n \in N,\ \forall\, t \in T \tag{12}$$

definition of the load flow

$$LF_{lef,t} = \sum_{n \in N} H_{lef,n} \cdot \Delta_{n,t} \cdot \beta \quad \forall\, lef \in LEF \subseteq L,\ \forall\, t \in T \tag{13}$$

$$LF_{lfx,t} = \sum_{n \in N} h_{lfx,n} \cdot \Delta_{n,t} \cdot \beta \quad \forall\, lfx \in LFX \subseteq L,\ \forall\, t \in T \tag{14}$$

limitation of the load flow of transmission lines

$$LF_{lef,t} \leq \frac{REF_{lef}}{exist_{lef}} \cdot p_{lef}^{max} \quad (15)$$
$$\forall\, lef \in LEF \subseteq L,\ \forall\, t \in T$$
$$-LF_{lef,t} \leq \frac{REF_{lef}}{exist_{lef}} \cdot p_{lef}^{max} \quad (16)$$
$$\forall\, lef \in LEF \subseteq L,\ \forall\, t \in T$$
$$LF_{lfx,t} \leq p_{lfx}^{max} \quad (17)$$
$$\forall\, lfx \in LFX \subseteq L,\ \forall\, t \in T$$
$$-LF_{lfx,t} \leq p_{lfx}^{max} \quad (18)$$
$$\forall\, lfx \in LFX \subseteq L,\ \forall\, t \in T$$

limitation of the load flows on HVDC-lines

$$HVDCF_{hvdc,t}^{pos}, HVDCF_{hvdc,t}^{neg} \leq phvdc_{hvdc}^{max} \quad (19)$$
$$\forall\, hvdc \in HVDC,\ \forall\, t \in T$$

extension cap

$$exist_{lef} \leq EF_{lef} \leq exist_{lef} + ef_{lef}^{max} \quad (20)$$
$$\forall\, lef \in LEF \subseteq L$$

non-negativity condition

$$0 \leq ART_{n,t}^{load}, ENS_{n,t}, G_{p,t}, PUMP_{sto,t} \quad (21)$$
$$\forall\, n \in N, \forall\, sto \in STO \subseteq P,\ \forall\, t \in T$$
$$0 \leq HVDCF_{hvdc,t}^{pos}, HVDCF_{hvdc,t}^{neg} \quad (22)$$
$$\forall\, hvdc \in HVDC,\ \forall\, t \in T.$$

Due to the lumpiness of line investment and the product of variables in Eqs. (12) and (13), the global problem becomes a highly complicated MINLP.[11]

3.3 Benders Decomposition (BD)

In the steps upgrade and line extension, the global MINLP problem is further decomposed by the BD method [4, 8] into a master-problem (investment decision) and a sub-problem (dispatch decision) due to the high computational burden resulting in

[11] The installation of a further line additionally influences the corridor's line parameters like series conductance and series susceptance which are summarized in H.

long computing times. The master-problem (MP) has a linear mixed-integer character, which has an adequate solvability. The bi-linearity of Eqs. (12) and (13) characterize the sub-problem (SP) as a NLP. Both problems are solved iteratively. In this way, they exchange information. Initially, the MP must be solved. It decides the line investments and delivers the updated grid topology to the SP. The objective value of the MP determines the lower bound. The process delivers information from the SP to the MP about required capacity additions by using the shadow price of the fixed line capacity decision. Subsequently, the upper bound can be calculated using the investment and operational costs of the corresponding Benders iteration.[12] The application of the BD methodology is representatively illustrated for the line extension model. The method for the line upgrade component model is similar.

Master-problem (MP): The Eq. (25) determines the Benders cuts. During the iteration process, further values for $\lambda_{lef}^{(k)}$, $C_{SP}^{(k)}$ and $ef_{lef}^{(k)}$ are calculated generating additional constraints for the MP for iteration k.

$$C_{Exp}^{MP(k)} = \sum_{lef \in LEF} \left(EF_{lef} - exist_{lef}\right) \cdot c_{lef}^{exp} + \alpha \tag{23}$$

subject to the constraint (20) and:

$$\alpha \geq C_{SP}^{(k)} + \sum_{lef \in LEF} \lambda_{lef}^{(k)} \cdot \left(EF_{lef} - ef_{lef}^{(k)}\right) \tag{24}$$

$$\alpha \geq \alpha^{down} \tag{25}$$

Sub-problem (SP): The corresponding SP is constituted in the following:

$$\begin{aligned} C_{Exp}^{SP(k)} = & \sum_{p \in P} \sum_{t \in T} c_p^{gen} \cdot G_{p,t} \cdot \tau_t \\ & + \sum_{ren \in REN} \sum_{t \in T} \left(\cdot \left(g_{ren}^{inst} \cdot r_{ren,t}^{max} \cdot a_{ren,t} - G_{ren,t} \right) \right) \\ & + \sum_{n \in N} \sum_{t \in T} c^{VoLL} \cdot \left(ENS_{n,t} + ART_{n,t}^{load}\right) \cdot \tau_t \rightarrow \min \end{aligned} \tag{26}$$

The SP is equipped with the constraints (3)–(19), (21) and (22) defined in Sect. 3.2. Additionally, the fixation of the extensions decision is:

[12] If the difference between the upper and lower bound falls below a tolerance level of 6%, the iteration process will stop. The level was chosen after applying different sensitivities. A reduction of this level only leads to longer computational times. Due to the high non linearity (see e.g. Eqs. (12) and (13)) the obtained solution has no global optimality evidence. The process gains at least a local optimum.

$$REF_{lef} = EF_{lef}^{(k)};\ \forall\ lef \in LEF \subseteq L \tag{27}$$

3.4 Karush–Kuhn–Tucker-System (KKT-system) for Derivation of the Marginals

The KKT-system allows for determining the marginals for all constraints of the SP. For the actual BD process the marginals of the fixed extensions decision $\lambda_{lef}^{(27)}$ is important. The KKT-system with its relevant parts are:

$$\begin{aligned}
L =& C_{Exp}^{SP(k)} + \ldots \\
&+ \sum_{lef \in LEF} \sum_{n \in N} \lambda_{lef,n}^{(9)} \cdot \left(H_{lef,n} - \frac{REF_{lef}}{exist_{lef}} \cdot h_{lef,n}^{exist} \right) \\
&+ \sum_{lfx \in LFX} \sum_{n \in N} \lambda_{lfx,n}^{(10)} \cdot \left(H_{lfx,n} - h_{lfx,n} \right) \\
&+ \sum_{n \in N} \sum_{nn \in N} \lambda_{n,nn}^{(11)} \cdot \begin{pmatrix} B_{n,nn} \\ -\sum_{lfx \in LFX} inci_{lfx,nn} \\ \cdot h_{lfx,n} \\ -\sum_{lef \in LEF} inci_{lef,nn} \\ \cdot H_{lef,n} \end{pmatrix} \\
&+ \sum_{n \in N} \sum_{t \in T} \tau_t \cdot \lambda_{n,t}^{(12)} \cdot \begin{pmatrix} NI_{n,t} \\ -\sum_{nn \in N} B_{n,nn} \cdot \Delta_{nn,t} \cdot \beta \end{pmatrix} \\
&+ \sum_{lef \in LEF} \sum_{t \in T} \tau_t \cdot \lambda_{lef,t}^{(13)} \cdot \begin{pmatrix} LF_{lef,t} \\ -\sum_{n \in N} H_{lef,n} \\ \cdot \Delta_{n,t} \cdot \beta \end{pmatrix} \\
&+ \sum_{lfx \in LFX} \sum_{t \in T} \tau_t \cdot \lambda_{lfx,t}^{(14)} \cdot \left(\ldots \right) \\
&+ \sum_{lef \in LEF} \sum_{t \in T} \tau_t \cdot \lambda_{lef,t}^{(15)} \cdot \begin{pmatrix} LF_{lef,t} \\ -\dfrac{REF_{lef}}{exist_{lef}} \cdot p_{lef}^{max} \end{pmatrix} \\
&+ \sum_{lef \in LEF} \sum_{t \in T} \tau_t \cdot \lambda_{lef,t}^{(16)} \cdot \begin{pmatrix} -LF_{lef,t} \\ -\dfrac{REF_{lef}}{exist_{lef}} \cdot p_{lef}^{max} \end{pmatrix} \\
&+ \sum_{lef \in LEF} \lambda_{lef}^{(27)} \cdot \left(REF_{lef} - EF_{lef}^{(k)} \right) \\
&+ \ldots
\end{aligned} \tag{28}$$

3.5 Parallel SP for Determing the KKT-marginals

The original NLP-SP is related to a parallel LP-SP since the extensions decision EF_{lef} is fixed and replaced by a constant parameter set by every iteration. The results of the NLP-SP and the parallel LP-SP will be identical. The marginals of the fixed extensions decision are necessary for the BD algorithm. These marginals can alternatively be derived by applying the following method.

The parallel LP-SP is equipped with the objective function (26) and its identical constraints (3)–(18) formulated above, whereas $B_{n,nn}$, $H_{lef,n}$, REF_{lef} are replaced by constant parameters. The altered constraints are listed below:

$$NI_{n,t} = \sum_{nn \in N} b_{n,nn} \cdot \Delta_{nn,t} \cdot \beta \qquad (29)$$
$$\forall\, n \in N,\ \forall\, t \in T$$

$$LF_{lef,t} = \sum_{n \in N} h_{lef,n} \cdot \Delta_{n,t} \cdot \beta \qquad (30)$$
$$\forall\, lef \in LEF \subseteq L,\ \forall\, t \in T$$

$$LF_{lef,t} \leq \frac{ef_{lef}^{fix}}{exist_{lef}} \cdot p_{lef}^{max} \qquad (31)$$
$$\forall\, lef \in LEF \subseteq L,\ \forall\, t \in T$$

$$-LF_{lef,t} \leq \frac{ef_{lef}^{fix}}{exist_{lef}} \cdot p_{lef}^{max} \qquad (32)$$
$$\forall\, lef \in LEF \subseteq L,\ \forall\, t \in T.$$

The transfer matrix can be set by $h_{lef,n} = \dfrac{ef_{lef}^{fix}}{exist_{lef}} \cdot h_{lef,n}^{exist}$ with $ef_{lef}^{fix} = EF_{lef}$. The net sensitivity matrix is derived from the updated transfer matrix of all potential extended lines $h_{lef,n}$ and the lines without an extension option $h_{lfx,n}$ formulated as:

$$b_{n,nn} = \sum_{lef \in LEF} inci_{lef,nn} \cdot h_{lef,n} + \sum_{lfx \in LFX} inci_{lfx,nn} \cdot h_{lfx,n} \qquad \forall\, n, nn \in N.$$

The marginals $\lambda_{lef,t}^{(31)}$ and $\lambda_{lef,t}^{(32)}$ are revealed after solving the parallel LP-SP. The constraints (31) and (32) comply with the constraints (15) and (16). Hence, the marginals are the same ones. Consequently, it can be expressed as $\lambda_{lef,t}^{(31)} = \lambda_{lef,t}^{(15)}$ and $\lambda_{lef,t}^{(32)} = \lambda_{lef,t}^{(16)}$. The marginals $\lambda_{lef,n}^{(9)}$ corresponding to the updated variable transfer matrix $H_{lef,n}$ have to be calculated which subjects to REF_{lef} and is part of load flow definition (13) and network sensitivity matrix definition (11)

$$\lambda_{lef,n}^{(9)} - \sum_{t \in T} \tau_t \cdot \Delta_{n,t} \cdot \lambda_{n,t}^{(13)} - \sum_{nn \in N} inci_{lef,nn} \cdot \lambda_{n,nn}^{(11)} = 0. \tag{33}$$

The voltage angel $\Delta_{n,t}$ is given by the parallel SP. The Eq. (13) of the original NLP-SP conforms with (30). Hence, it can be formulated as: $\lambda_{lef,n}^{(13)} = \lambda_{lef,n}^{(30)}$. The marginals $\lambda_{n,nn}^{(12)}$ are unknown. They can be determined by deriving of the KKT-system after $B_{n,nn}$. The constraints (11) and (12) contain the variable $B_{n,nn}$. This leads to related the row of the KKT-system:

$$\lambda_{n,nn}^{(11)} - \sum_{t \in T} \tau_t \cdot \Delta_{nn,t} \cdot \lambda_{n,t}^{(12)} \cdot \beta = 0. \tag{34}$$

The restriction (12) of the original NLP-SP is equivalent to (29) of the parallel-SP, resulting in: $\lambda_{n,t}^{(12)} = \lambda_{n,t}^{(29)}$. Consequently, all required marginals of the KKT-system row (35) are known for calculating the marginals $\lambda_{lef}^{(27)}$ of the fixed extension decision. Using $\frac{\partial L}{\partial REF_{lef}} = 0$ results for the related row:

$$\begin{aligned} &\sum_{n \in N} \left(-\lambda_{lef,n}^{(9)} \cdot \frac{h_{lef,n}^{exist}}{exist_{lef}} \right) + \sum_{t \in T} \tau_t \cdot \left(-\lambda_{lef,t}^{(15)} \cdot \frac{p_{lef}^{max}}{exist_{lef}} \right) \\ &+ \sum_{t \in T} \tau_t \cdot \left(-\lambda_{lef,t}^{(16)} \cdot \frac{p_{lef}^{max}}{exist_{lef}} \right) + \lambda_{lef}^{(27)} = 0. \end{aligned} \tag{35}$$

By inserting variables and rearranging the solution for the KKT-system can be obtained:

$$\begin{aligned} &\sum_{t \in T} \left(\tau_t \cdot \sum_{n \in N} \left(\begin{array}{c} \Delta_{n,t} \cdot \lambda_{n,t}^{(30)} \\ + \sum_{nn \in N} inci_{lef,nn} \cdot \Delta_{nn,t} \cdot \lambda_{n,t}^{(29)} \end{array} \right) \cdot \frac{h_{lef,n}^{exist}}{exist_{lef}} \cdot \beta \right) \\ &+ \sum_{t \in T} \left(\tau_t \cdot \lambda_{lef,t}^{(31)} \cdot \frac{p_{lef}^{max}}{exist_{lef}} \right) + \sum_{t \in T} \left(\tau_t \cdot \lambda_{lef,t}^{(32)} \cdot \frac{p_{lef}^{max}}{exist_{lef}} \right) \\ &= \lambda_{lef}^{(27)};\ \forall\ lef \in LEF \subseteq L \end{aligned} \tag{36}$$

The calculation of the sought after marginals does not require a solution from a further system of equations. The voltage angle $\Delta_{n,t}$ is only variable which influences the marginals of the fixation $\lambda_{lef}^{(27)}$. The optimal value is given by the solution of parallel SP and is the same as in the original NLP-SP. Due to the linear constraints of the parallel SP, it can be solved by applying a solver for LP, which significantly reduces the computational burden compared to a gradient-based solver for NLP. The same methodology is applied for the first step "line upgrade" with the adaption that

the decision has a binary character and consequently the transfer matrix $H_{l,n}$ and network sensitivity matrix $B_{n,nn}$ are adjusted in the same way.

3.6 Installation of New HVDC Lines

For the last step of the transmission capacity increase, the investment costs are defined as:

$$I^{HVDCadd} = \sum_{hvdcexp \in HVDCEXP} P^{HVDCadd}_{hvdcexp} \cdot c^{HVDCadd}_{hvdcexp} \tag{37}$$

$$HVDCF^{pos}_{hvdcexp,t} \leq P^{HVDCadd}_{hvdcexp} \tag{38}$$

$$-HVDCF^{neg}_{hvdcexp,t} \leq P^{HVDCadd}_{hvdcexp} \tag{39}$$

$$\forall\ hvdcexp \in HVDCEXP \subset HVDC, t \in T$$

The installation of transmission capacities of HVDC lines is possible in 1 GW steps.

4 Impact of Curtailing Different RES Technologies on Grid Extensions, Overall Costs and Curtailed Energy

Length of grid extensions: Figure 2 shows the length of transmission capacity increases for the three different steps of the respective scenarios. The length of transmission lines with an upgrade is determined to be the same in all scenarios; a span of 1186 km. Due to the fact that 220 kV lines with congestion especially run parallel to a 380 kV line, voltage shifting measurements are beneficial. The extent of additional lines differs between scenarios. The fewest additional lines can be observed in the scenario *All* where all RES supply is faced with an amount of curtailed energy without DM. This PMI provides a flexibility to cut the feed-in peaks where extensions of nearly 4310 km is optimal in this scenario. If offshore wind power in Northern Germany is only equipped with a flexibility option, around 1200 km of further lines is additionally needed to transfer the energy to the load centers in the South of Germany. In contrast to this, the flexible cutting of onshore wind energy and PV peaks has no impact on the length of additional line in this analysis. The lengths of new lines are 10,765 km for *On* and *PV* setting which is equal to the reference case since the offshore wind feed-in with the highest LCOE triggers additional transmission capacities. The same development can be observed for the installation of the HVDC connection within Germany. The greatest extent is in the *REF*, *On* and *PV* scenario. However, the lowest level of HVDC lines can be achieved in case of flexible

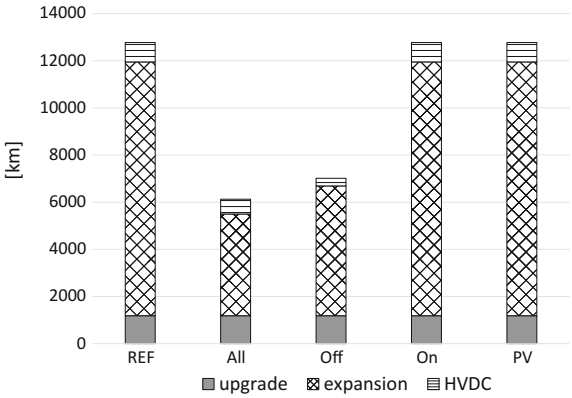

Fig. 2 Lengths of extensions within the German transmission grid in 2030

offshore wind energy cutting with 324 km. The scenario *All* leads to twice as many HVDC lines compared to the *Off* scenario, since it is beneficial to transfer offshore wind energy to Southern Germany and replace expensive gas-fueled power units there. To sum up, the integration of the offshore wind energy has the main impact on the future grid design. Note that the lengths are based on the assumed sequence of voltage increases before adding further lines before HVDC installations and may result in an overestimation of line lengths with voltage increases.

Integration of RES: In the reference case, 1.3 TWh of RES cannot be integrated into the system, which is equal to the *Off* scenario with more flexible curtailing (PMI). The onshore wind farms have a greater distribution in the north and extensions of the grid for the last available unit of wind would be an over-investment. PV is located in the south and additionally provides energy during the midday peak. Thus, its power will be consumed close to load centers as long as offshore wind does not reach its feed-in peak transferred via the additional built transmission lines. The tariffs of PV and onshore wind force their surplus supply out of the system before offshore wind feed-in is cut. This holds across all scenarios. The PMI of offshore wind energy in scenario *All* and *Off* only changes the structure of curtailed RES supply. Its peaks will be curtailed with impact on the grid extensions as discussed above. The annual amount of flexible curtailment is completely utilized and especially more onshore energy can be integrated. Flexible offshore wind curtailing at 1% of the annual supply (*Off*) results in −45% grid extensions compared to *REF*. If all surplus of RES can flexibly be cut (*All*), +6% more RES can be integrated into the system and grid extensions can be reduced by −52% compared to *REF*. In this case, curtailment is less concentrated to few regions, but rather the majority of RES units is chosen for flexible integration and more gas-fueled generation is required in the south during high demand times (Fig. 3).

Overall costs: The obtained results above shall be evaluated by their overall costs (Table 3). The highest annual overall costs with 19.7 billion EUR/a are generated by DM (*REF* scenario). The annualized costs of grid investments are 488 Mio. EUR/a.

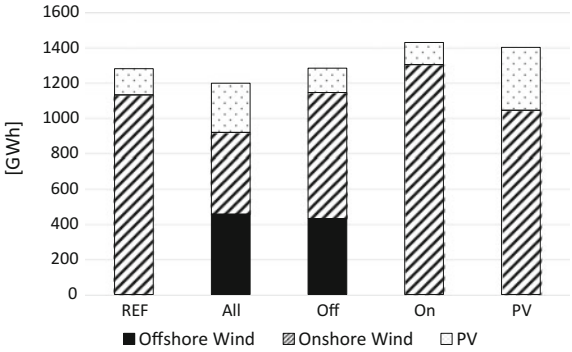

Fig. 3 Amount of curtailed RES supply for different integration scenarios in 2030

Table 3 Adjusted annual overall costs for Germany for different integration scenarios in 2030

Scenario	In billion EUR/a and the difference to *REF*
REF	19.66
All	−0.32(−1.6%)
Off	−0.17(−0.8%)
On	−0.13(−0.6%)
PV	−0.28(−1.4%)

The lowest system costs (−1.6%) can be achieved if all RES units are subject to a partial market integration since line investments can be reduced by −56%. The *Off*, *On* and *PV* scenarios reach a cost reduction of maximal −1.4%. This is caused by reductions in generation costs in the same scale. The most cost-effective way of designing the future transmission grid and increase the RES integration is the partial market integration of RES equipped with flexibility of curtailing the feed-in peaks.

5 Critical Appraisal

The following section provides a critical discussion of the results. The analysis conducted reveals general trends and impacts for the grid planning process being undertaken in Germany and is not to be viewed as an alternative to the national network plan. It is assumed within the scope of the analysis that the electricity market in Germany is based on a locational marginal pricing system (LMP), which does not exist currently. However, it enables the calculation of the optimal grid extensions with high local resolution in a practical manner by applying the established DC load-flow approach in [20]. A general validation of the DC load flow approach can be seen in [18] and for the German case in [11]. Furthermore, the scale of grid extensions could be underestimated since the German electricity market does not rate line congestion within its pricing mechanism. LMP takes congestion into account and thus differences can occur. The future RES capacities for Germany are taken from the reference scenario in [19] and are distributed according to their current relative shares to every

individual grid node. For the sake of simplification, interactions between the adjusted levels of remuneration and curtailment of RES are not explored.[13] The implementation of decentralized storage units and demand-side measures is not integrated as an option to reduce power grid expansion measures.[14] The structure of future generation plants and prices are also assumed to be uncertain. The portfolio for Germany calculated in [19] represents the most probable development in Germany. The optimal results are based on set of 64 time slices. The utilization of 8760 hours allows for examining all RES feed-in and load situations in a year. However, a load flow and dispatch problem with 8760 hours and the size of the German transmission grid is currently not computationally possible and thus necessitates a representative number of hours.[15] Finally, the time horizon of analysis is the year 2030. According to the German RES target (share of 80% in 2050), further lines could be required to achieve the given targets.

6 Conclusion

This paper presents a methodology for analyzing large scale power grid extension problems. The global grid extension problem is divided by the BD into an extension and a dispatch problem. The latter is translated into a KKT-system resulting in less computational effort by using the favorable conditions. The model was applied for the analysis of different RES integration principles (current DM and a possible PMI) and their impact on transmission grid extensions, RES integration and overall costs for Germany in 2030. PMI is defined as flexible curtailing of RES surplus in the amount of 1% of the available supply for all RES. The core message for policy makers is that PMI goes along with significantly less grid investments and increases RES integration. If at least offshore wind can be partially curtailed by PMI, the extent of grid investments can be reduced. However, the energy not integrated into the system is equal to the case with DM. The greatest effect on costs, grid extensions and RES integration is obtained if all RES provide their energy with more flexibility beyond the DM. From a political perspective, the principal recommendation can be drawn: An integrated planning of transmission grid extensions with respect to RES integration principles are needed. Furthermore, the introduction of more flexible RES integration is cost-efficient and calls into question the current design of DM for RES.

[13] As discussed in [12], the curtailment compensation can influence the location of further RES plants. If the compensation is not capable of covering the RES investment, the financial risk of additional RES installations will increase since revenues decline.

[14] The influence of decentralized storages are investigated in [9].

[15] The calculated time slices consider different combinations of wind, photovoltaic feed-in and inelastic demand. Every time slice is weighted by the frequency of similar situations during a year. The authors have verified the adequate level of representation of the used snapshot of 8760h a by successfully meeting the annual conventional and intermittent generation of the reference year 2012.

7 Nomenclature

Sets:

$hvdcexp$	= optional HVDC line: $hvdcexp \in HVDCEXP \subset HVDC$
$lef \in LEF \subseteq L$	= subset of corridors with option for adding further lines
$lfx \in LFX \subseteq L$	= subset of corridors without option for adding lines
$n \in N$	= grid nodes
$p \in P$	= generation plants
$ren \in REN \subseteq P$	= subset of RES generation units
$sto \in STO \subseteq P$	= subset of storage units
t	= time step

Parameters:

$a_{p,t}$	= availability of power plants
$b_{n,nn}$	= network sensitivity matrix
c_{ren}^{curt}	= costs for curtailing RES feed-in
c_{lef}^{exp}	= specific investment costs for line extensions
c_{p}^{gen}	= plant specific generation costs
$c_{hvdcexp}^{HVDCadd}$	= specific investment costs for voltage increase
c^{VoLL}	= value of lost load
$demand_{n,t}$	= inelastic demand
$exist_{lef}$	= original number of circuits of lef
flh_{rese}	= full load hours of reservoir power plants
g_{p}^{inst}	= installed generation capacity
$h_{l,n}$	= transfer matrix
$inci_{l,n}$	= incidence matrix
p_{l}^{max}	= maximal transmission capacity
$pump_{sto}^{inst}$	= installed pump capacity
$r_{ren,t}^{max}$	= time dependent feed-in factor for RES
β	= conversion factor for p.u.
$\lambda_{lef}^{(k)}$	= marginal on extension fixation in iteration k
τ_t	= weighting for reference time steps

Variables:

$ART_{n,t}^{load}$	= dummy consumer to ensure the energy balance
$B_{n,nn}$	= network sensitivity matrix
C^{total}	= total system costs
$EF_{lef} \in \mathbb{N}$	= extension factor
$ENS_{n,t}$	= energy not supplied
REF_{lef}	= relaxed extension factor
$G_{p,t}$	= electric Generation
$H_{lef,n}$	= variable transfer matrix
$HVDCF_{hvdc,t}$	= HVDC load flow
I^{exp}	= annualized investment costs for extensions
$NI_{n,t}$	= net injection
$PUMP_{sto,t}$	= pump storage charging
$\Delta_{n,t}$	= voltage angle

References

1. 50Hertz Transmission GmbH; Amprion GmbH; TenneT TSO GmbH; TransnetBW GmbH (2015) Netzentwicklungsplan 2015. Tech. Rep. April 2014, Berlin; Dortmund; Bayreuth; Stuttgart
2. Binato S, Pereira M, Granville S (2001) A new Benders decomposition approach to solve power transmission network design problems. IEEE Transactions on Power Systems 16(2):235–240
3. Bundesnetzagentur (2014) Kraftwerksliste Bundesnetzagentur zum erwarteten Zu- und Rückbau 2014 bis 2018.
4. Conejo AJ, Castillo E, Minguez R, Garcia-Bertrand R (2006) Decomposition Techniques in Mathematical Programming: Engineering and Science Applications. Springer
5. Egerer J, Schill WP (2014) Power System Transformation toward Renewables: Investment Scenarios for Germany. Economics of Energy & Environmental Policy 3(2):29–43
6. Energy System Analysis Agency (ESA2) (2013) Shaping our energy system - combining European modelling expertise. Tech. rep., Energy System Analysis Agency (ESA2), Brussels
7. ENTSO-E (2013) Data. URL https://www.entsoe.eu/data/
8. Geoffrion AM (1972) Generalized Benders Decomposition 1. JOURNAL OF OPTIMIZATION THEORY AND APPLICATIONS 10(4):238–260
9. Gunkel D, Möst D (2015) Netzausbau unter Beachtung von dezentralen Speichersystemen in Deutschland im Jahr 2030. In: 9. Internationale Energiewirtschaftstagung an der TU Wien I, Wien
10. Hemmati R, Hooshmand RA, Khodabakhshian A (2013) State-of-the-art of transmission expansion planning: Comprehensive review. Renewable and Sustainable Energy Reviews 23:312–319
11. Hinz F, Möst D (2014) Opportunity cost of reactive power provision - Development and backtesting of a techno-economic AC load flow model. In: 14th IAEE European Conference, Rome, pp 1–15
12. Klinge Jacobsen H, Schröder ST (2012) Curtailment of renewable generation: Economic optimality and incentives. Energy Policy 49:663–675
13. Klobasa M, Erge T, Wille-Haussmann B (2009) Integration von Windenergie in ein zukünftiges Energie- system unterstützt durch Lastmanagement. Tech. rep., Fraunhofer-Institut für System- und Innovationsforschung ISI; Fraunhofer-Institut für Solare Energiesysteme ISE, Karlsruhe; Freiburg
14. Kost C, Schlegl T, Thomsen J, Nold S, Mayer J (2013) Studie Stromgestehungskosten Erneuerbare Energien. Tech. rep., Fraunhofer-Institutfür Solare Energiesysteme ISE, Freiburg
15. Leuthold FU, Weigt H, Hirschhausen C (2010) A Large-Scale Spatial Optimization Model of the European Electricity Market. Networks and Spatial Economics 12(1):75–107
16. Müller, T, Gunkel, D, Möst D (2013) How Does Renewable Curtailment Influence the Need of Transmission and Storage Capacities in Europe? In: 13th European IAEE Conference, Düsseldorf
17. Oswald BR, Hofmann L (2010) Wirtschaftlichkeitsvergleich unterschiedlicher Übertragungstechniken im Höchstspannungsnetz anhand der 380-kV-Leitung Wahle-Mecklar. Tech. rep., Leibniz Universität Hannover, Hannover
18. Overbye TJ, Cheng X, Sun Y (2004) A comparison of the AC and DC power flow models for LMP calculations. Proceedings of the Hawaii International Conference on System Sciences 37(C):725–734, 10.1109/HICSS.2004.1265164
19. Schlesinger M, Hofer P, Kemmler DA, Kirchner DA, Koziel S, Ley A, Lindenberger D, Knaut A, Malischek R, Nick S, Panke T, Paulus S, Tode C, Wagner J, Piégsa DA, Seefeldt F, Straß burg S, Weinert K, Lutz C, Lehr U, Ulrich P (2014) Entwicklung der Energiemärkte - Energiereferenzprognose. Tech. Rep. 57, Prognos AG; EWI - Energiewirtschaftliches Institut an der Universität zu Köln; GWS - Gesellschaft für wirtschaftliche Strukturforschung, Basel; Köln; Osnabrück

20. Schweppe FC, Tabors RD, Caraminis MC, Bohn RE (1988) Spot pricing of electricity
21. Stigler H, Todem C (2005) Optimization of the Austrian Electricity Sector (Control Zone of VERBUND APG) by Nodal Pricing. Central European Journal of Operations Research 13:105–125

Simulation of Distribution Grid Expansion Costs and the Impact of Load Shifting

Thomas Eberl

Abstract The increasing electricity generated by the renewable energy generation units connected to the distribution grid can lead to the allowed level of voltage range and current rating in the lines being exceeded. One option to prevent this from happening is line extension. This article describes a method of quantifying the line extension, its costs and the impact of load shifting which can be used in electricity system models. The region considered is the state of Baden-Württemberg in Germany. The operation of the distribution grid is simulated based on region-specific electricity demand and electricity generation. In order to use the voltage range of 10% (based on DIN EN 50160) completely, the countrywide installation of regulated distribution transformers is assumed. The allowed level of voltage and current rating is mainly exceeded in regions with a high supply of photovoltaic electricity at the low voltage level. With the modelled assumptions and the extension of renewable energy under consideration, an expense of about 760–880 million Euros in Baden-Württemberg will be required by the year 2030 to ensure that the operation complies with the technical restrictions. By using load shifting, the expense can be reduced by 140–220 million Euros.

Keywords Distributed generation · Renewable energy · Energy policy · Distribution grid · Electricity system · Photovoltaic · Wind power · Voltage range derivation · Regulated distribution transformer · Load shifting

1 Introduction

In its latest energy concept, the German Government has set the goal of meeting 50% of the total electricity demand with renewable energy by the year 2030 [1]. Nearly all plants are installed in the distribution grid. The photovoltaic plants are mainly located in the low voltage (LV) level, whereas the wind plants are mainly installed

T. Eberl (✉)
Institute of Energy Economics and Rational Energy Use, University of Stuttgart, Stuttgart, Germany
e-mail: te@ier.uni-stuttgart.de

V. Bertsch et al. (eds.), *Advances in Energy System Optimization*,
Trends in Mathematics, DOI 10.1007/978-3-319-51795-7_10

in the medium voltage (MV) and the high voltage (HV) level. Due to the increased generating power in the distribution grid, a reverse of the load flow can occur. This can lead to voltage range and current in the lines being exceeded. The distribution grid operator is required to prevent this from happening by using adequate measures. By installing regulated distribution transformers on all stations between the medium and low voltage level and through line extension, voltage range violation caused by Feed-in tariff (FIT) plants can be prevented [2]. Using a regulated distribution transformer allows the regulation of the voltage of the LV-grid regardless of the voltage in the MV grid. Therefore, the use of the voltage range in accordance with DIN EN 50160 is possible without considering the load in the MV grid. If this is not sufficient for the integration of the renewable energy plants, a line extension or load shifting can be carried out. The grid topology has to be known to determine the costs. It is very heterogeneous and the data has not been published. Several studies have been conducted to analyze the line extension based on typical example grids for several typical regions or by using many of the available grid topologies [3, 4]. Furthermore in several studies an optimization of the grid expansion planning of example grids by using for example generic algorithms is conducted [5, 6]. The following simulation allows the determination of the need for line extension by using aggregated data without knowing the real topology of the grid. Therefore, simulating representative topologies for large geographic regions is relatively straightforward. The following methodology allows the simulation of a representative topology and the necessary line extension. The cost for the grid expansion, consisting of line extension and regulated distribution transformers, is calculated on the basis of this analysis for Baden-Württemberg, a federal state of Germany. Furthermore, the potential to reduce line extension by using load shifting, which can be implemented by shifting either demand or supply, is simulated.

2 Simulation of the Distribution Grid System in Baden-Württemberg

The grid in Baden-Württemberg is subdivided into 30 regions. High-voltage grids with attached medium and low-voltage grids are simulated for every region, as schematically shown in Fig. 1. In every simulation run, the topology of the grid, the electricity demand/supply and the necessary line extensions are simulated. To achieve the necessary line extension or load shifting of representative grid systems, under consideration of the heterogeneity of the single distribution grids, a Monte-Carlo simulation with several runs is executed. The topology, the allocation of the electricity demand and supply are thus varied and around 1,00,000 single grids are simulated. This allows the determination of the cost for line extension in every modeled region based on representative distribution grid systems.

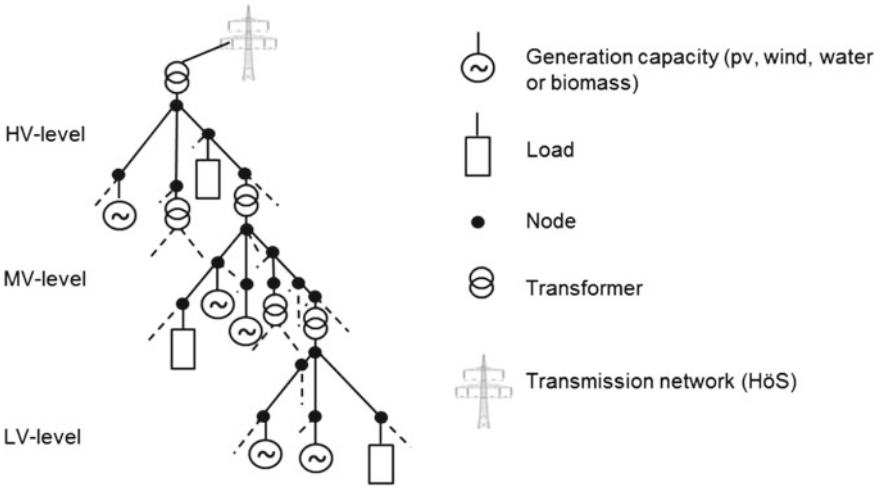

Fig. 1 Schematic extract of the distribution model

2.1 Regions

Baden-Württemberg is subdivided geographically in 30 regions, which account for around 1/8 of the total length of Germany's distribution grid. These correspond to the supply areas of substations between the transmission and the distribution grid. The location, the electrical power and the connecting voltage level of the photovoltaic, wind, biomass and water plants are published in the "EEG-Anlagenregister" [7]. By considering their geographic location, every plant will be allocated to a substation of the transmission grid by considering geographical and technical restrictions.[1] The area and the population can be determined on the basis of the "Amtlichen Gemeindeschlüssel (AGS)". The installed capacity of the "EEG-Anlagenregister" in the year 2010 is shown in Fig. 2. There are an especially large number of photovoltaic plants in Baden-Württemberg for example, the capacity in the Region Eichstetten, with 4,000 km^2 surface and about one million inhabitants, is around 230 MW, which corresponds to about 210 GWh per year.[2]

[1] By considering their geographic location, every plant will be allocated to a substation of the transmission grid. A FIT plant is allocated to a substation in the same district. If no substation is located, the geographically closest one is chosen. One further restriction is that plants can't be allocated to areas which are separated galvanically in the high voltage level.

[2] Assumption for full load hours: 940 (pv); 1770 (wind); 6220 (biomass); 4100 (running water).

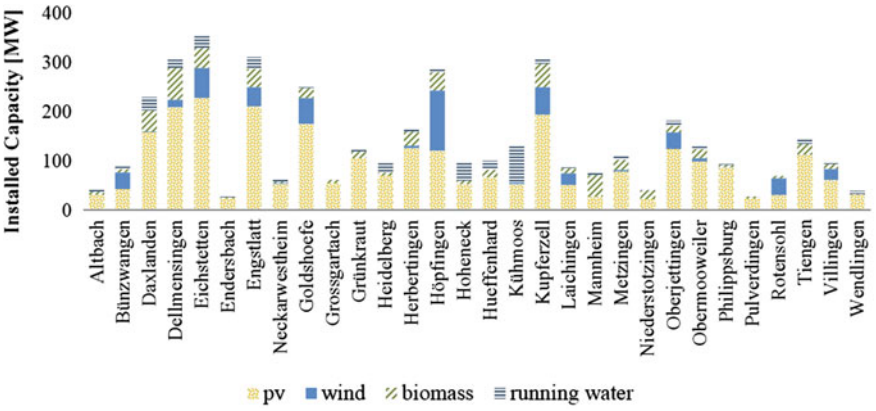

Fig. 2 Installed capacity of renewable energy in the model regions in Baden-Württemberg in the year 2010

2.2 Grid Topology

The grid topology is modeled as a graph. Starting with the first node, the grid is successively enlarged by lines, nodes and transformers connecting the grid levels. It is assumed that the grids are radial at every voltage level, and consist of nodes in the lines to link them.[3] Furthermore, it is assumed that the length of the lines of the high voltage grid is direct proportional to the population [8]. The length of the lines of the medium and low voltage grid and the node density match average values in Germany[4] [9]. To simulate the heterogeneous structure of the distribution grid, data of published example grids is used. Therefore, the quantity of direct successor for every node are counted to derive a probability distribution of the quantity of the succeeding nodes [10, 11]. The quantity of branch connections can be simulated using this as a basis. The distribution of the length between nodes is derived from example grids to obtain the length of the lines between nodes. After scaling it to the node density of the analyzed regions in every voltage level, the topology of the distribution grids in Baden-Württemberg can be simulated. This methodology allows the simulation of a specific distribution grid at the voltage levels considered in any of the 30 simulated regions in Baden-Württemberg. These grids are assembled to one distribution grid per region, which consists of grids of every voltage level.[5] Before the line extension,

[3] Nominal voltage of the grid levels: Low voltage (LV) $\widehat{=}$ 400 V; Medium voltage (MV) $\widehat{=}$ 10–30 kV; High voltage (HV) $\widehat{=}$ 110 kV.

[4] Average length of the lines = length of all lines in Germany/number of transformers in Germany.

[5] To reduce the complexity, it is possible to reduce the number of different generated distribution grids at a specific voltage level. This allows the speed of the simulation to be increased.

all the simulated grids have a length of around 2,10,000 km (1,40,000 km in the LV level, 60,000 km in the MV level and 10,000 km in the high voltage level).[6]

2.3 Electricity Demand and Generation

The electricity demand of one model region is derived from the electricity demand in Germany (488 TWh), and the hourly load profile for one year is derived from historical consumption data of Germany [12]. Therefore, it is assumed that the electricity demand is proportional to the population in the model region. Consequently, regions with a high population have a high electricity demand. The distribution of the electricity demand over the different voltage levels is based on data of the "EnergieDienst GmbH", one of the biggest distribution grid operators in the south of Baden-Württemberg [13]. The distribution of the electricity demand over the nodes of a grid is again derived from example grids. The generating plants in one region are distributed randomly to the nodes until the capacity of a region is reached. The resulting power on a node is the sum of demand and generation, which is simulated hourly and is based on historical profiles. To get the resulting power of the high and medium voltage grids, it is necessary to add the resulting power of the downstream grids.

2.4 Load Flow

In order to analyze the consequences of distributed generation on the operation of the distribution grid, it is particularly important to determine the voltage angle and the thermal resistance. The calculation of the voltage is based on a linear procedure [14]. The relative change to the nominal voltage on the connecting node is shown in Eq. (1).

$$\Delta u = \frac{S \cdot (R \cos \Phi + X \sin \Phi)}{U^2} \tag{1}$$

Φ: Phase angle of the unit on the connection node
S: Apparent power on the connection node
R: Resistance on node x
X: Reactance on node x
U: Nominal voltage

The connection of a generation plant, or the load on a node, changes the voltage of both the successor and the predecessor node. The relative voltage change on

[6]For comparison: the length of the lines in Germany is about 12,00,000 km at the LV level, 5,00,000 km in MV level and 80,000 km at the HV level [7].

a predecessor node Δu_w equals the ratio of the impedance of the lines between the predecessor node Z_{1v} and the local grid station to the impedance of the lines between the connecting node and the local grid station Z_{1x}. The formula is shown in Eq. (2). The relative voltage change of the successor equals the relative voltage on the connecting node.

$$\Delta u_v = \Delta u_x \cdot \frac{Z_{1v}}{Z_{1x}} \tag{2}$$

Δu_v: relative voltage change at the predecessor node v
Δu_x: relative voltage change at the successor node x
Z_{1v}: Impedance of the line from the transformer station to the successor node v
Z_{1x}: Impedance of the line from the transformer station to the connection node x

By connecting several generation units or loads, the relative voltage changes are summed up as a resulting relative voltage change. This procedure has been validated by comparing it to a typical MV grid of CIGRE (Council International des Grands Reseaux Electriques) [15]. The voltage level in every node has been modeled using the "Integral7" software [16]. The average divergence of the voltage level was less than 0.09% and will therefore be ignored. The current I_x in the lines is calculated by using Eq. (3).[7]

$$I_x = \frac{P_x}{\sqrt{3} \cdot U_x} \tag{3}$$

I_x: Current on node x
P_x: Active power on node x
U_x: Voltage on node x

The voltage level on every node and the current between them can be determined with this formula. A deviation of the voltage of more than 10% causes a violation of the voltage range in accordance with DIN EN 50160. A decoupling of the grid levels by using regulated distribution generators is necessary to use the entire range. This means they have to be adjusted so that the secondary side nominal voltage is reached. In order to avoid the violation of current rating in the lines, a maximum current of 735 A in the HV lines and 462 A/265 A in the MV/LV lines is assumed [17, 18]. The resistance is 0.060, 0.161 and 0.642 Ω/km in the HV, MV and LV lines. The reactance corresponds to 0.191, 0.110 and 0,083 Ω/km.

[7] To reduce complexity the phase angle is assumed to be zero.

2.5 Line Extensions

Violation of the voltage range and current rating can be avoided by a line extension. It leads to a decrease in the voltage and an increase in the current rating. The following procedures are used to determine the necessary line extension.

2.5.1 Line Extension Because of Voltage Range Deviation

The line extension decreases resistance and reactance of the connections. In the simulation this is achieved by installing parallel lines. Equation (4) describes the change of the resistance of a connection after line extension. The determination of reactance is accomplished similarly. To quantify the line extension, every grid is first searched for voltage range deviations starting at the nodes which are closest to the local grid station. If the algorithm detects an exceedance, lines will be expanded until the voltage reaches the allowed level again. Thus the connecting line with the shortest distance to the local grid station will be expanded first. If there is still a violation, the line which is next to the local grid station which has not been expanded, will be expanded next. By first expanding the lines next to the local grid station, the voltage will drop on several further nodes. Therefore it is a very efficient procedure.

$$R_{new} = \frac{R_{old}}{k+1} \tag{4}$$

R_{new}: Resistance of the connections after line extension
R_{old}: Resistance of the connections before line extension
k: Number of lines before extension.

2.5.2 Line Extension Because of Exceedance of the Current Rating

An exceedance of the current rating leads to an extension of only those lines which are affected. This procedure is repeated until no violation of the current rating is detected in the grid anymore. The maximum current in the line is shown in Eq. (5).

$$I_{new} = I_{old} \cdot k \tag{5}$$

I_{new}: Current after line extension
I_{old}: Current rating after line extension
k: Number of lines before extension.

2.6 Use of Load Shifting to Prevent Line Extension

Load shifting can be used to prevent line extension. Thus, the load from an hour where the aforementioned technical restrictions are not followed has to be transferred to a period with no restrictions. The developed algorithm enlarges capacity for load shifting on any node in the grid, as long it has a positive impact on either the current rating or the voltage range deviation. The algorithm starts by enlarging the load shifting at the node next to the transformer to minimize the capacity which has to be transferred to a different hour.

3 Scenarios

In order to analyze the impact of renewable energies, especially photovoltaic and wind power, on the necessary line extension, the following four scenarios will be considered. The assumed electricity generation based on renewable energies is shown in Fig. 3 (right ordinate). Scenario "2010" represents the situation in Baden-Württemberg 2010. The distribution of the electricity generation in the different regions has been shown in Sect. 2.1. In the other scenarios, the distribution will be scaled to the entire generation in Baden-Württemberg. Scenario "2030" is based on a scenario of the "Federal Ministry for the Environment, Nature Conservation and Nuclear Safety", which shows a significant increase in electricity generation based on photovoltaic to 11 TWh. The government of Baden-Württemberg aims to increase the share of electricity generated by wind power to 10% by the year 2020 [19]. Based on this directive, the electricity generation based on wind power in scenario "2030W" increases to 8 TWh. Scenario "2030P" assumes an increase in electricity generation based on photovoltaic to 13 TWh. This corresponds to an increase of the share from 15% in the electricity demand in scenario "2030" to 17.5% in scenario "2030P". The share of electricity generation based on renewable energy in electricity demand in the different scenarios is shown in Fig. 3 (left ordinate).

4 Required Line Extension

Based on the assumptions made, line extension is necessary to not exceed technical restrictions. In the scenario "2030", as shown in Fig. 4, a line extension of around 4,200 km in the LV grid, 74 km in the MV grid and 69 km in the HV grid is necessary in Baden-Württemberg. When considering additional wind plants in the MV and HV level in the scenario "2030W", the required line extension rise to 89 km at the MVlevel and 171 km at the HV level. In the scenario "2030P" the line extension

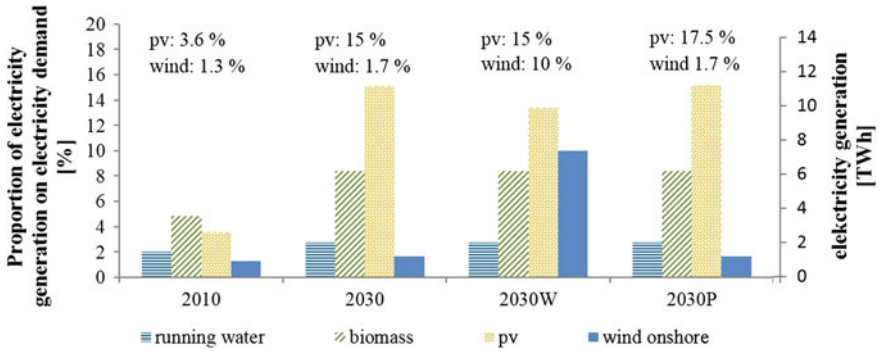

Fig. 3 Share of electricity generation in the electricity demand

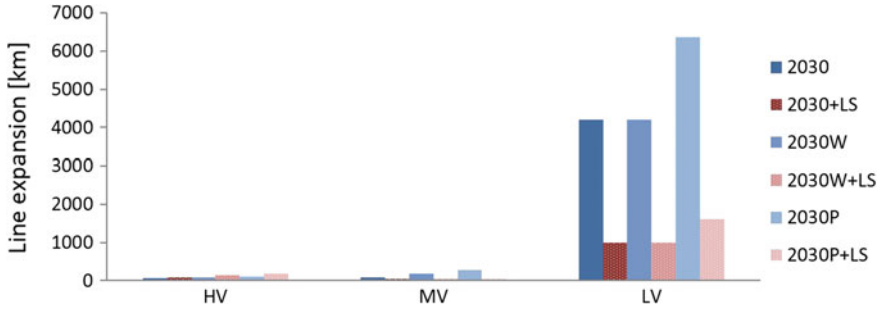

Fig. 4 Necessary line extension in the different scenarios in different voltage levels without and with load-shifting (LS)

rises at the LV level to 6,360 km and in the MV level to 277 and 106 km at the HV level. The line extension thereby primarily affects the LV grid. The current in the LV level rarely exceeds the current rating; the main reason is the violation of the voltage range in accordance with DIN EN 50160. Violation of the current rating in the upstream grid level causes a relatively small extent of line extension. Using load-shifting reduces the need for line extension, especially in the LV level, to around 1,000 km in the scenario 2030 as well as in scenario 2030W, and 1,600 km in scenario 2030P. Only a few kilometers have to be installed at the MV level, and the need for line extension is comparable to the scenarios without load shifting at the HV level. The distribution of the line extension in the model regions in the Scenario "2030" is shown in Fig. 5. In regions with a high installed capacity of FIT-plants, for example Eichstetten, a line extension of up to 870 and 340 km, respectively, with load shifting can be necessary (see Fig. 5).

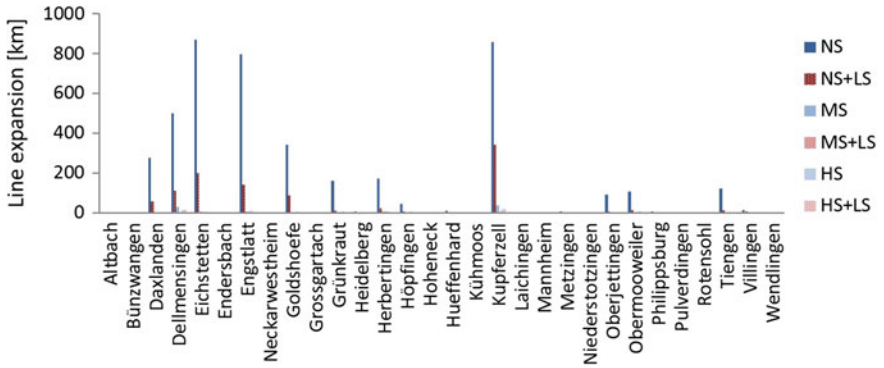

Fig. 5 Necessary line extension in different network levels in scenario "2030"

5 Costs of the Grid Extension

To quantify the costs of the network extension, the statewide installation of regulated distribution transformers has to be evaluated. In Baden-Württemberg, around 78,000 local grid stations need to be considered. The modification of a local network station is possible by investing €7,000 per station [20], which amounts to €550 million in Baden-Württemberg.[8] The costs of a line extension in the LV grid are €45,000/km [21], €65,000/km in the MV grid, and €2,20,000/km in the HV grid [21, 22]. Therefore, an expense of €209 million is necessary to upgrade the distribution grid in scenario "2030". The cost rises to €220 million in scenario "2030W" and to €327 million in scenario "2030P". By using load shifting, the costs drop to €62 million in the scenario "2030" and respectively to €79 million and €110 million in the 2030W and 2030P scenarios. In Fig. 6, the costs in the different voltage levels are shown. It is obvious that the LV level is the most affected, especially in scenario "2030P", where there is a high supply of photovoltaic. The overall costs of the grid extension are shown in Fig. 7. In scenario "2030" and "2030W" around €760 million have to be invested. In scenario "2030P" the costs rise to €880 million, which can be reduced by load shifting to €660 million. Furthermore, it becomes clear that the costs for the regulated distribution transformer account for the lions' share.

6 Critical Review

Some assumptions are used to keep the calculation computable or to substitute publicly unavailable data. Although these assumptions may cause uncertainties, they are needed for a representative calculation but some of them can be specified in more

[8]The extension of the transformers between HV and MV level will not be considered but will be examined in further publications.

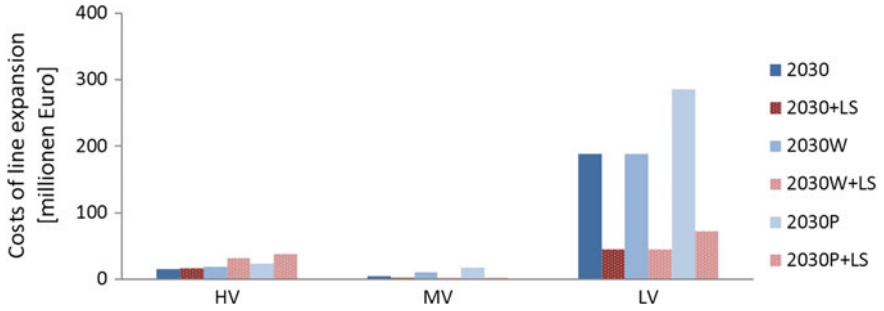

Fig. 6 Costs of the line extension in the different scenarios and different voltage levels

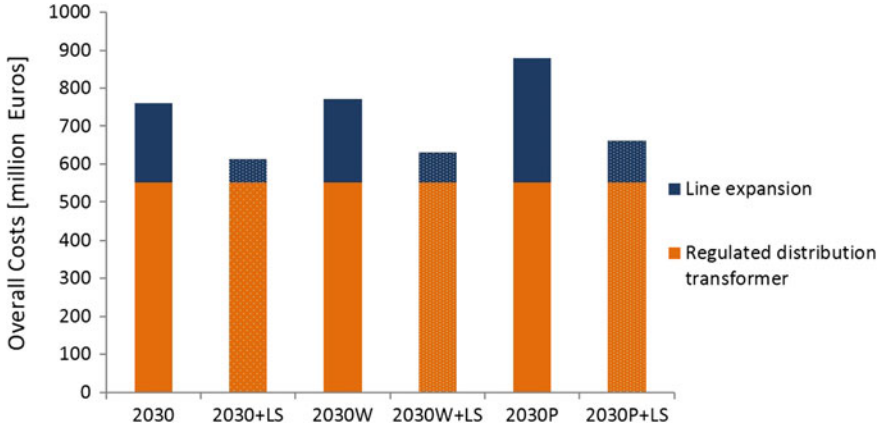

Fig. 7 Overall costs (not discounted) for grid extension in the different scenarios

detail in further analysis. The topologies of the grids are generated numerically and are therefore representative and do not correspond to a existing structure. The grids are radial at every voltage level, which means that they are not operated intermeshed. Furthermore, the countrywide installation of regulated distribution transformers is assumed to allow a deviation of the voltage range of 10%. To comply with the technical restrictions the connection of a single renewable energy plant is expected to change the voltage range less than 3% which is also not examined [23]. It must also be mentioned that substations between the medium and high voltage level are neglected in this analysis. In addition, technical restrictions are simplified, for example no system operation devices are regarded and a simplified computation of the load flow is chosen. Due to lack of data, for example the length of the lines of the high voltage grid and the electricity demand being direct proportional to the population is assumed. For this reason, distortion occurs because the influence, for example of demand of the industry is neglected. The distribution of the length of the lines between nodes, the distribution of the amount of successors of a node and the distribution of the electricity demand over the nodes of a grid are based on the data of published

example grids. To expand the variety of the heterogeneous distribution grids, the data of further example grids could be integrated in the analysis. However the validation of the load flow calculation could be expanded to further grids in different voltage levels. Furthermore average values and historical data of Germany, for example grid length, are used in the calculation and the cost assumptions can vary significantly.

7 Conclusion and Outlook

The methodology used allows the quantification of the distribution grid extension based on a simulation of the distribution grid. This allows the heterogeneity of the grid structure and further region specific parameters in different regions in Baden-Württemberg to be simulated. The analysis shows, that with modelled assumptions under consideration by investing around €760–880 million in regulated distribution transformers and line extension, the electricity generation based on renewable energy can be integrated in Baden-Württemberg by the year 2030 in the scenarios considered, which shows that decoupling of the voltage by using regulated distribution transformers is insufficient for that purpose. For a line extension, an additional sum of between €210 million and 330 million is necessary. The grid extension in the LV grid accounts for the majority of these additional costs. This means the costs are mainly caused by the photovoltaic plants installed in the LV grid. The installation of wind plants at the MV and HV level requires relatively low investment costs. Furthermore, the analysis shows that the grid costs could be reduced by up to €220 million by using load shifting, depending on the scenario. These costs have to be compared with the costs for implementing load shifting to minimize grid extension.

References

1. Bundesministerium für Umwelt, Naturschutz und Reaktorsicherheit (BMU), Bundesministerium für Wirtschaft und Technologie (BMWi), Energiekonzept für eine umweltschonende, zuverlässige und bezahlbare Energieversorgung, Berlin, 2010
2. Brückl O, Hinz A, Vielhauer A, Basmann R, Der Regelbare Ortsnetztransformator zur Steigerung des Integrationspotentials von Erneuerbaren Energien- Ergebnisse aus Simulationen und Felderprobungen, “Internationaler ETG-Kongress”, Würzburg, 2010
3. Deutsche Energie- Agentur (Dena), Dena-Verteilnetzstudie, Berlin, 2012
4. Gutachten im Auftrag des BDEW Bundesverband der Energie- und Wasserwirtschaft e.V., Abschätzung des Ausbaubedarfs in deutschen Verteilungsnetzen aufgrund von Photovoltaik- und Windeinspeisungen bis 2020, Aachen/Bonn, 2010
5. Borges C, Martins V, Multistage expansion planning for active distribution networks under demand and Distributed Generation uncertainties, Rio de Janeiro, 2010
6. Miranda V, Ranito J, Proenca L, Genetic algorithms in optimal multistage distribution network planning, Porto, 1994
7. Informationsplattform der deutschen Übertragungsnetzbetreiber (EEG/KWK-G), 2012
8. Statistisches Bundesamt, Statistisches Jahrbuch 2012 - Gesellschaft und Staat, Wiesbaden, 2012

9. Deutscher Bundestag, Entwurf eines Gesetzes über Maßnahmen zur Beschleunigung des Netzausbaus Elektrizitätsnetze, 2010
10. Herold I, Stifter M, Bletterie B, Brunner H, DG DemoNet Validation, Increasing the DER Hosting Capacity of Distribution Networks -Voltage Control from Simulation to Field Test, 2nd European Energy Conference - E2C, Maastricht, 2012
11. Schwab A, Elektroenergiesysteme: Erzeugung, Transport, Übertragung und Verteilung elektrischer Energie, 2. Auflage, Springer Verlag, Berlin, Heidelberg, 2009
12. European Network of Transmission System Operators for Electricity (ENTSO-E), https://www.entsoe.eu/db-query/consumption/mhlv-a-specific-country-for-a-specific-month/, 2011
13. Energie Dienst Netze GmbH, http://www.energiedienst-netze.de/cms/netznutzung/veroeffentlichungspflichten, 2011
14. Heuck K, Dettmann K D, Elektrische Energieversorgung, Vieweg Verlag, Wiesbaden, 2005
15. Rudion K, Orths A, Styczynski Z A, Design of Benchmark of Medium Voltage Distribution Network for Investigation of DG Integration. IEEE PES Conference, Montreal, 2006
16. Forschungsgemeinschaft für elektrische Anlagen und Stromwirtschaft e.V. (FGH), Interaktives Grafisches Netzplanungssystem 7 (INTEGRAL 7), 2012
17. Spring E (Prof.), Elektrische Energienetze. VDE Verlag GmbH, Berlin, 2003
18. Pundt H. et. al. (Prof.), Wissensspeicherheft, Dresden, 1997
19. Landtag von Baden-Württemberg, Antrag der Abg. Manfred Groh u.a. CDU und Stellungnahme des Ministeriums für Verkehr und Infrastruktur, Ausbau der Windenergie in Baden-Württemberg, 2013
20. Estimation for future production costs based on informations given by A. Hinz, (Maschinenfabrik Reinhausen GmbH), 2012
21. Bundesverband der Energie- und Wasserwirtschaft BDEW, Abschätzung des Ausbaubedarfs in deutschen Verteilnetzen aufgrund von Photovoltaik und Windeinspeisungen bis 2020, Bonn/Aachen, 2011
22. Bundesverband WindEnergie e.V., Netzverstärkungs-Trassen zur Übertragung von Windenergie: Freileitung oder Kabel?, Rheinberg, 2004
23. Verband der Elektrizitätswirtschaft (VDEW), Eigenerzeugungsanlagen am Niederspannungsnetz, Richtlinie für Anschluss und Parallelbetrieb von Eigenerzeugungsanlagen am Niederspannungsnetz, VWEW Energieverlag GmbH, Frankfurt am Main, 2001

Part VI
Data Provision for Power Grid Modeling

Structure Analysis of the German Transmission Network Using the Open Source Model SciGRID

Carsten Matke, Wided Medjroubi, David Kleinhans and Sebastian Sager

Abstract High voltage transmission networks play a crucial role in the ongoing transformation from centralized power generation in conventional power plants to decentralized generation from renewable energy sources (RES). The rapid expansion of RES requires a structural rearrangement of the entire power system to ensure the current level of supply security. Scientific approaches to the characterization and improvement of power transmission networks, however, often lack the availability of reliable and appropriate data on the networks' structure. Using SciGRID, which was recently released open source, we generate a topological grid model for Germany using open data provided by OpenStreetMap. Starting from this particular grid model we characterize the structure of the German transmission grid by means of graph-theoretical decomposition approaches to complexity reduction. Our procedure aims to identify key features and characteristics complementing the grid's electrotechnical properties; it is for example used to characterize the SciGRID approach and validate the resulting models against other (potentially not open source) transmission network models. In addition, it paves the way for networks with reduced complexity, which might be beneficial in optimization problems addressing system design and operation.

Keywords Open model · Transmission network · Structural analysis · OpenStreetMap

C. Matke (✉) · W. Medjroubi · D. Kleinhans
NEXT ENERGY, EWE Research Centre for Energy Technology, Oldenburg, Germany
e-mail: carsten.matke@next-energy.de

W. Medjroubi
e-mail: wided.medjroubi@next-energy.de

D. Kleinhans
e-mail: david.kleinhans@next-energy.de

S. Sager
Institute for Mathematical Optimization, Otto-von-Guericke University Magdeburg, Magdeburg, Germany
e-mail: sager@ovgu.de

V. Bertsch et al. (eds.), *Advances in Energy System Optimization*,
Trends in Mathematics, DOI 10.1007/978-3-319-51795-7_11

1 Introduction

Since the pioneering contributions by Euler, theoretic investigations of networks have become increasingly relevant in Mathematics and Physics. With the increased availability of (structured) data, network theory has experienced a comeback in recent decades [5], with widespread applications such as human mobility patterns [6, 10] and in social networks [7, 11, 12].

Power grids were used as one example in the seminal work by Watts and Strogatz [18], resulting in an increased interest in their theoretical characterization [2–4]. However, many of the contributions at least on European grids reveal a lack in the availability of reliable data on power grids, potentially impeding the relevance of the results from a technical perspective and their application to network design and operation. Since reliable recommendations are urgently required in political and strategical decision making processes, a sufficiently detailed representation of transmission grids would be desirable [1].

The project SciGRID [14], started in October 2014, is intended to face the problem of power data availability. Using the open geo-database available from OpenStreetMap[1] (OSM) the objective of SciGRID is to develop an open source dataset of the European transmission grids for scientific applications. A first official version of a dataset for Germany together with the SciGRID documentation and source code was released in June 2015 [14].

The goal of the present work is to characterize a "realistic" and georeferenced German transmission network obtained by using the SciGRID dataset. A realistic and georeferenced network is important for studies dealing with network expansion, congestion management, and cross-border flows. This characterization permits a better understanding of the transmission network topology and structure. Hence, better modeling tools from network theory can be applied. Using such tools can contribute into reducing the complexity of such networks and the computational time of transmission network and energy systems simulations. Moreover, by using the open source dataset, comparison of our findings with other models is made possible. This provides a unique opportunity to stimulate and enrich the debate about energy modeling in general and modeling transmission networks in particular.

In this contribution, we start with a brief introduction to SciGRID and the dataset of the German transmission grid. The core of this contribution is to use this dataset to characterize the transmission grid and its intrinsic structure. For this purpose, prior mathematical approaches used to characterize networks are revisited and applied to the data of the German transmission network. We demonstrate that these methods reveal relevant features of the underlying network and can be used for the decomposition of the transmission into relevant sections. Thus, the network theory can contribute to a better understanding of key features of power grids and can improve the integration of grid aspects in large scale energy system models.

[1] http://www.openstreetmap.org.

2 Power Data in OSM and the SciGRID Model

In this section, we first introduce OSM and describe the power data available therein. We then briefly describe the SciGRID approach to derive a topological network using OSM power data. Finally, the derived German network obtained using SciGRID is presented.

2.1 OpenStreetMap

OpenStreetMap (OSM), is a "free [and] editable map of the whole world that is being built by volunteers largely from scratch and released with an open-content license".[2] OSM was founded in 2004 by Steve Cost and is at present one of the best sources of Volunteered Geographic Information [15]. The aim of OSM is to build a free geographic database of the whole planet. OSM data is made available under the Open Database License 1.0 (ODbL),[3] a share alike license allowing users to share, modify and use the data if retaining the same rights for derived data.

OSM includes *geo-referenced* data about streets, roads, buildings, power plants, power lines, and many more geographic features. The data is mainly collected by volunteers, although some government and commercial institutions contribute to OSM. Mappers, as the volunteers are often called, collect data about geographical features and paths e.g. using Global Positioning System (GPS) receivers. The information is used to construct points, lines, and polygons and export them to OSM using editing applications.

Small extracts of OSM data can be downloaded directly from the OSM webpage. However, there are several tools to download large OSM extracts.[4] OSM data has its own particular data model with XML as default format. Data in OSM is represented using three data types or "primitives" which are hierarchically organized and are called *nodes*, *ways*, and *relations*. *Nodes* are points in space defined with their geographic coordinates (longitude and latitude). An ordered list of nodes represents *ways* which can be linear paths (e.g. highway roads) or closed areas (e.g. footprints of buildings). Finally, *relations* are ordered lists of nodes, ways, and even other relations. All OSM data primitives mostly have *tags* providing information about the geographical features they represent. In the context of power grids, the tag *power* is typically used and nodes can represent a power tower, ways can represent a transmission line as linear path or a transmission substations as a closed area.[5] Finally, relations with a tag *power* are typically used either to represent complex

[2] http://wiki.openstreetmap.org/wiki/About.

[3] http://opendatacommons.org/licenses/odbl.

[4] http://wiki.openstreetmap.org/wiki/Downloading_data.

[5] http://taginfo.openstreetmap.org/.

geographic features as large power plants including, e.g. substations, generators and transformers, or representing the route of power circuits, e.g. from one substation to another one.

2.2 The SciGRID Model

This article uses power-related data from OSM. Of particular interest for the analysis of transmission grids is the information on individual power transmission circuits, which are typically represented in OSM by power *relations*. Since the OSM database is available under an open license and continuously updated and improved, using power relations for the derivation of open models of the transmission grids represents a sustainable and traceable method.

The transmission network used here, is obtained using the SciGRID model [14], which is solely based on OSM power data and power relations. These relations representing power circuits are mainly two types: relations with two substations and one/or more transmission lines, and relations with more than two substations and one/or more transmission lines. The relations with more than two substations contain T-junctions of the transmission lines.

The transmission network is build as follows: the power data are filtered and extracted from the OSM database. The substations contained in the power relations are abstracted to their geometrical centre and represent the vertices of the network. The transmission lines in a relation are abstracted to a straight line and represent the links between vertices of the transmission network. Thus, links represent abstracted relations. The resulting network model is an abstracted or topological network consisting of geo-referenced vertices and links with their individual lengths derived from its relation. The data also includes additional information about the vertices and links e.g. the voltage level and the number of cables if available from OSM. In the special case of relations containing T-junctions [17], the relations are abstracted using the T-junctions as additional auxiliary vertices in the network.

2.3 The German Transmission Network

In this contribution, the German extra-high voltage transmission network generated with SciGRID is used; i.e. only voltage levels of 220 kV and above are considered. The dataset represents a snapshot of the transmission network represented in OSM as of 12th of July 2015 and is depicted in Fig. 1. In this dataset the transmission network is composed of 462 vertices (including 37 auxiliary vertices for T-junctions) and 759 links connecting vertices.

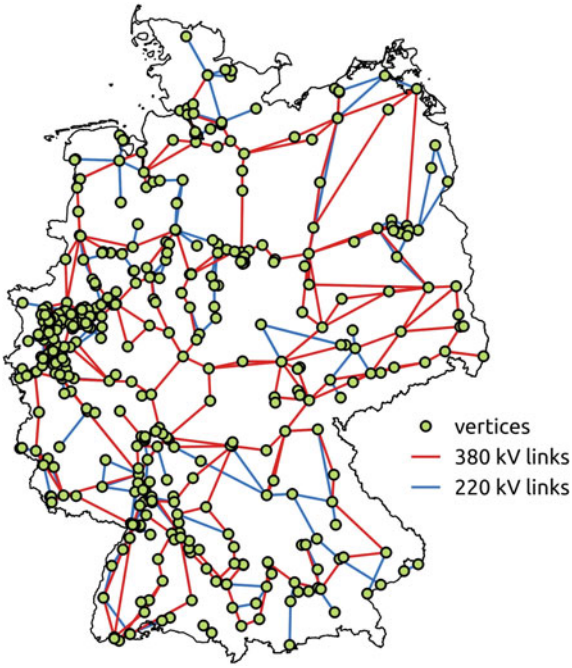

Fig. 1 Topological transmission network for Germany as of 12th of July 2015

3 Structure of the German Transmission Grid

In this section, we present the analysis of fundamental properties of the German network as described above. Two processing steps precede the main analysis of the German network.

1. Since electrical networks must fulfill the $n - 1$ criteria in Europe [8, 9], multiple links exist between two vertices. These multiple links are assigned to different relations in OSM. Since the German power network is based on a three phase system, links with more than 3 cables are divided so that every resulting link has an equal number of 3 cables. In the dataset we use, 26 OSM power related relations had no information about the number of cables. For these cases, we assumed links to have 3 cables. The result of this step is a graph with 462 vertices and 833 links.
2. In a second step, the largest set of connected vertices is determined and the analysis is restricted to this largest set. The resulting graph G has 454 vertices and 826 links.

We compare our results to an analysis of a dataset on the western US grid, provided by Watts and Strogatz [18]. This dataset has 4941 vertices and 6594 links, but lacks any information on the geographical locations of the vertices or electro-technical properties of the links.

For several standard approaches from networks theory and a comparison with the western US network, we analyse the graph $G = (V, L)$ with the set V of vertices v_i and the set L of links $l_{ij} = \{v_i, v_j\}$ with $v_i, v_j \in V$. Note, that for the graph G multiple links between vertices are not considered. Before the comparison, the terminologies *adjacent*, *degree*, *path*, *diameter*, *local clustering coefficient* are defined. Two vertices v_i and v_j are *adjacent*, if there exists a link l_{ij} between them. The *degree* of a vertex v_i expresses the number of links that connect v_i with adjacent vertices $v_j \neq v_i$. A *path* is a sequence of adjacent vertices with a length defined as the number of links associated to the path. The shortest path length between two vertices is defined as the minimal number of links connecting these two vertices. The shortest path between two vertices in a network with the highest length is called the *diameter* of the graph. In our analysis, we also use the definition of *local clustering coefficient* provided in [18], where it is stated that small values for shortest path lengths and high clustering coefficients are characteristic for electrical networks, e.g. the western US grid. The local clustering coefficient quantifies how close a vertex v_i and its adjacent vertices are to be complete connected by links among themselves. Thus, the local clustering coefficient of a vertex $v_i \in V$ is the proportion of the number of existing links divided by the number of links that could combinatorially exist between them:

$$c_i = \frac{2\,|\{l_{mn} : v_m \in A_i \wedge v_n \in A_i\}|}{n_i(n_i - 1)}, \tag{1}$$

where $A_i = \{v_j : l_{ij} = \{v_i, v_j\} \in L\}$ and $n_i = |A_i|$.

In our instance, G has a diameter of 23, an average shortest path length of 9.880, an average degree of 3.639, and the average of all c_i from Eq. (1) is 0.142. For comparison, the network of the western US grid has a diameter of 46, an average shortest path length of 18.989, an average degree of 2.669, and the average of all c_i from Eq. (1) is 0.080. The smaller numbers of vertices, links, and diameter of the German network indicate that there exist less tuples of vertices with long shortest paths and thus, decrease the average path length. The higher average degree of vertices in the German network indicates that there exist more adjacent vertices for each vertex. Since the local clustering coefficient assigns higher values if adjacent vertices are more densely connected, the average local clustering coefficient is higher for the German network than for the western US network.

Considering that both networks have different sizes, the German network has a smaller value of the average path length and a higher average local clustering coefficient Eq. (1) compared to the western US network. However, the two networks share the so called *small-world property* [18] which describes the combination of small values for shortest path length and a high average local clustering coefficient. In other words, both networks have few links that behave like shortcuts which causes short paths and high clustering. In the following section, we are interested in finding those shortcuts in the German transmission network by means of graph theoretical approaches.

3.1 Complexity Reduction

Typically, real networks contain parts in which vertices are more dense connected within each other than to the rest of the network. In the following, these subsets of vertices are called *clusters*. One option for the determination of clusters in a network is to identify a small number of particularly *central* links connecting clusters. The removal of these links then causes a degeneration of G into a number of clusters [13]. Finding these small sets of critical links is useful to characterize networks and provides more insight into the structure of the network.

Here, we present results of a decomposition method applied to the German transmission network. Different centrality measures on links were calculated and the links in each case were ordered with respect to their centrality. These links were then consecutively removed from the graph G and the clustering of the resulting graph was investigated. The analysis was performed with methods available in the python-igraph package version 0.7.0.[6] The results presented here refer to the *betweenness centrality* measure for links, which appeared to be a particularly promising candidate for a decomposition of the network. The *betweenness centrality* of a link $l_{ij} = \{v_i, v_j\} \in L$ is defined as

$$b_{ij} = \sum_{v_s \neq v_i, v_j \neq v_t} \frac{\sigma_{st}(l)}{\sigma_{st}}, \tag{2}$$

where σ_{st} is the total number of shortest paths from vertex v_s to vertex v_t and $\sigma_{st}(l)$ is the number of those paths that pass through the link l.

For the betweenness centrality, links are weighted according to their presence in shortest paths between all combinations of tuples of vertices of G. The more often links are present in shortest paths, the higher values are assigned as weights for them.

The result of the decomposition by means of a consecutive removing of links in the German and western US network is shown in Fig. 2. The blue color is assigned to clusters with less than 9 vertices. The order of removed links is obtained by the sorted list of betweenness values starting with the link with the highest betweenness value. The colors red and yellow are alternated for clusters with 9 or more vertices.

In addition to the visual investigation of the graph decomposition, the *modularity* Eq. (3) as defined by Newman and Girvan [16] provides a quantitative measure for the strength of the decomposition of a graph. For a graph with adjacency matrix $A_{v_i v_j}$ and a decomposition into clusters $V_i \subset V, i = 1, \ldots, c$ with $V_i \cap V_j = \emptyset, i \neq j$ the modularity is defined as:

$$Q = \sum_{i=1}^{c} (e_{ii} - a_i^2), \tag{3}$$

where

[6] http://igraph.org.

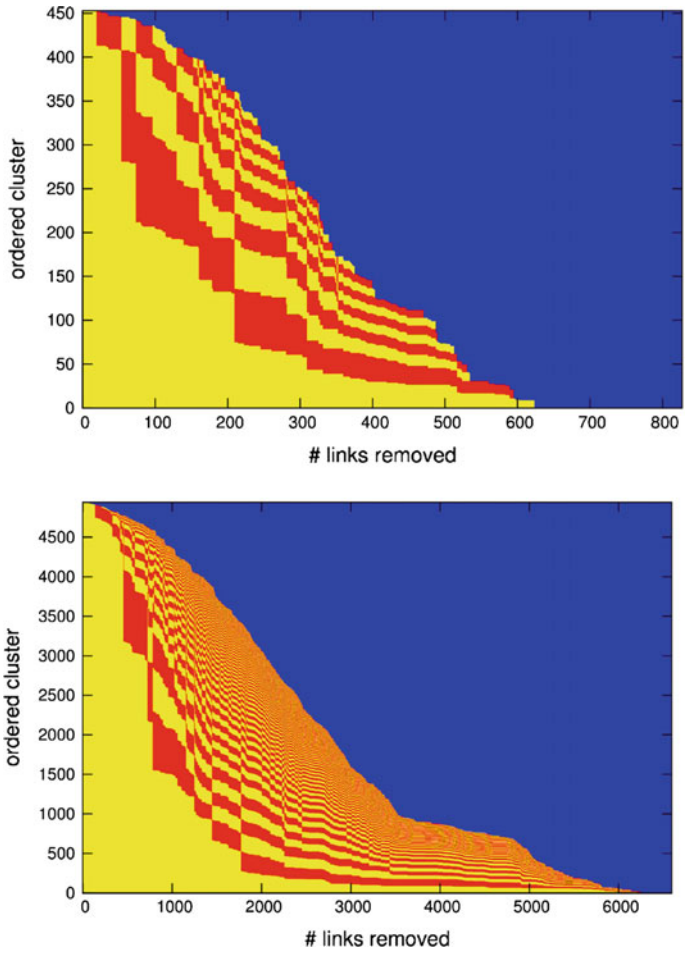

Fig. 2 Network decomposition by consecutive removal of links according to their *betweenness centrality* Eq. (2) calculated from the initial graph G for the German (*top panel*) and US (*bottom panel*) grid model, ordered by size. The absolute number of removed links is indicated on the x axis. In each column changes in color indicate the border between clusters. Clusters smaller than 9 vertices are not colored individually but plotted in *blue*

$$e_{ij} = \sum_{\{v_k, v_l\} \in L} \frac{A_{v_k v_l}}{2|L|} \mathbb{1}_{v_k \in V_i} \mathbb{1}_{v_l \in V_j}$$

is the fraction of links with both ends in cluster V_i and $a_i = \sum_j e_{ij}$ is the fraction of ends of links that are attached to vertices in cluster V_i.

The modularity determines how "well" the decomposition is, with higher values indicating stronger separation between the different clusters. The maximum of the modularity is 1. The development of the modularity with the iterative decomposition

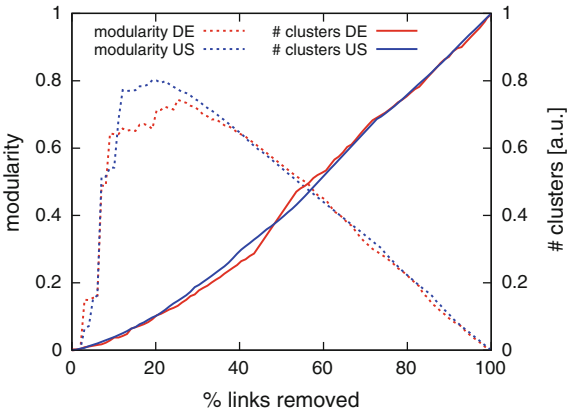

Fig. 3 Modularity Eq. (3) and rescaled number of clusters as a function of the fraction of links removed from the initial graph G, plotted for the dataset on the German grid (*red*) and the reference dataset of the US grid (*blue*). A rather good relative agreement of the results is evident

is shown both for the German and the western US network in Fig. 3, where the overall number of clusters is also plotted. Both curves show strong similarities between the two networks, confirming the small world property of the German transmission grid. Moreover, Figs. 2 and 3 show strong similarities between both networks in terms of the amount of clusters and cluster sizes. One cause for the higher maximum of modularity in the western US network may be the absence of multiple links, which causes the lower maximal modularity observed for the German network. Another reason could be the lack of electrical details about the western US network, as different voltage levels in power networks have an impact on the network properties.

From Fig. 3, the number of links resulting in an optimal decomposition of the grids can be calculated as the share of removed links leading to a maximum modularity. For the German transmission grid, this maximum is achieved at a removal of 25% of the links (i.e. 209 links). A snapshot of the resulting graph when the maximum number of links is removed (shown in gray in the Figure) is depicted in Fig. 4. From this Figure the effect of the decomposition (removing the links with the highest betweenness values) is that we observe the appearance of 13 clusters in the German transmission network.

3.2 Discussion

In this section, the limitations of the German and US network data are introduced and discussed. Suggestions about how these limitations can be overcome are also presented.

The SciGRID data used in this contribution has a very good coverage of the German transmission network. However, due to the fact that SciGRID is build on using OSM data, some issues can be raised concerning the accuracy of the power data used. As introduced in Sect. 2.1, OSM is a voluntary project. There exist no

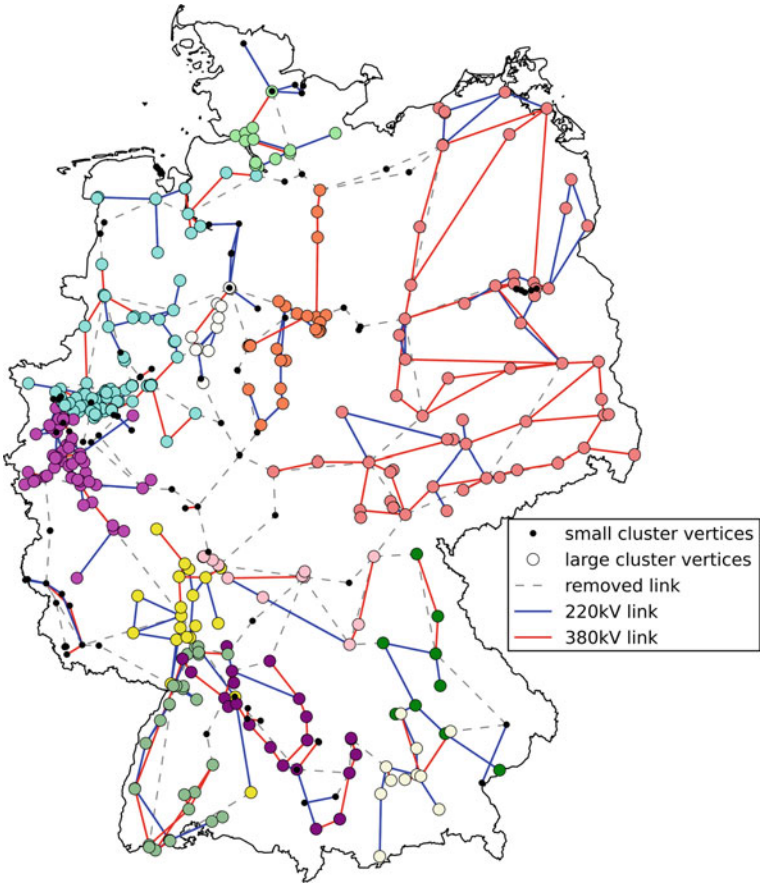

Fig. 4 Decomposition of the German network into 13 large clusters after removing 209 links with highest betweenness values. Different clusters are represented by colored vertices and removed links by *gray dashed lines*

authority which verifies the accuracy of OSM data which is mapped. However, there are quality assurance tools available contributing to verify the accuracy of the data and to detect errors. The inaccuracies and mapping errors can then corrected by OSM users.[7]

As stated in Sect. 3.1, differences were observed in the network decomposition and the modularity between the German and western US network. These differences may have there origin in the presence of multiple links in the German network or the difference in the voltage levels of both networks. However, this assumption cannot be verified here, due to the lack of details on the US network. Therefore, further investigations are needed for an in-depth comparison of the two networks on the

[7] http://wiki.openstreetmap.org/wiki/Quality_assurance.

electrical level. Another way to address this limitation is to build a model of the US transmission network from OSM using SciGRID. This will be possible when the power relations have a better coverage of the US power network.

4 Conclusions

In this contribution we presented an analysis of the German transmission network model derived from open data available in OpenStreetMap using the open source tool SciGRID. Our approach aims to characterize the German transmission network and to investigate its optimal decomposition into a number of clusters. The results are compared with a dataset of the western US power grid.

Although the size of the German network is smaller than the size of the western US network, we could show that the "small-world" property by Watts and Strogatz [18] describing small values for shortest path length and a high average local clustering coefficient is maintained for this network.

The proposed grid model provides sufficient data to characterize and explore the fundamental properties of the German transmission network. We propose to use graph-theoretical approaches as this leads to a better understanding of the network structure. In particular we identified clusters that may be beneficial in reduced models for optimization problems addressing system design and operation.

Acknowledgements Funding for SciGRID by the German Federal Ministry of Education and Research (BMBF) through the funding initiative "Zukunftsfähige Stromnetze" (funding code 03SF0471) is acknowledged by C. Matke, W. Medjroubi, and D. Kleinhans. Sebastian Sager gratefully acknowledges funding from the European Research Council (ERC) under the European Union's Horizon 2020 research and innovation programme (grant agreement No 647573) and from the German BMBF under grant 05M2013—GOSSIP.

References

1. Ahlhaus P, Stursberg P (2013) Transmission capacity expansion: An improved transport model. In: ISGT Europe, IEEE, pp 1–5, URL http://dblp.uni-trier.de/db/conf/isgteurope/isgteurope2013.html#AhlhausS13
2. Albert R, Barabási AL (2002) Statistical mechanics of complex networks. Reviews of modern physics 74(1):47
3. Amaral LAN, Scala A, Barthelemy M, Stanley HE (2000) Classes of small-world networks. Proceedings of the national academy of sciences 97(21):11,149–11,152
4. Barabási AL, Albert R (1999) Emergence of scaling in random networks. science 286(5439):509–512
5. Boccaletti S, Latora V, Moreno Y, Chavez M, Hwang DU (2006) Complex networks: Structure and dynamics. Physics reports 424(4):175–308
6. Brockmann D, David V, Gallardo AM (2009) Human mobility and spatial disease dynamics. Reviews of nonlinear dynamics and complexity 2:1–24
7. Butts CT (2001) The complexity of social networks: theoretical and empirical findings. Social Networks 23(1):31–72

8. Codes EEN (2015) Network code on operational security. http://networkcodes.entsoe.eu/category/requirements-within-the-code/?p=operational-security
9. ENTSO-E (2015) Entso-e continental europe operation handbook. https://www.entsoe.eu/publications/system-operations-reports/operation-handbook/Pages/default.aspx
10. Gonzalez MC, Hidalgo CA, Barabasi AL (2008) Understanding individual human mobility patterns. Nature 453(7196):779–782
11. Hazy JK (2012) Leading large: emergent learning and adaptation in complex social networks. International Journal of Complexity in Leadership and Management 14 2(1–2):52–73
12. Johnson M, Paulusma D, van Leeuwen EJ (2015) Algorithms for diversity and clustering in social networks through dot product graphs. Social Networks 41:48–55
13. Kramer L (2013) Modeling price formation in a multi-commodity market - a graph-theoretical decomposition approach to complexity reduction. PhD thesis, University of Heidelberg, URL http://www.ub.uni-heidelberg.de/archiv/16013
14. Medjroubi W, Matke C, Kleinhans D (2015) SciGRID - An Open Source Reference Model for the European Transmission Network (v0.1). http://www.scigrid.de
15. Neis P, Zielstra D, Zipf A (2013) Comparison of volunteered geographic information data contributions and community development for selected world regions. Future Internet 5(2):282, DOI 10.3390/fi5020282, URL http://www.mdpi.com/1999-5903/5/2/282
16. Newman MEJ, Girvan M (2004) Finding and evaluating community structure in networks. Phys Rev E 69(2):026,113, DOI 10.1103/PhysRevE.69.026113, URL http://link.aps.org/doi/10.1103/PhysRevE.69.026113
17. Sivanagaraju S (2008) Electric power transmission and distribution. Pearson Education India
18. Watts D, Strogatz S (1998) Collective dynamics of 'small-world' networks. Nature 393(6684):440–442

Modeling of the Transmission Grid Using Geo Allocation and Generalized Processes

Simon Köppl, Felix Böing and Christoph Pellinger

Abstract Feasible scientific usage of transmission grid data requires a node-edge-model with georeferenced information (location of substations or positioning of power lines) and specific electric parameters of each included element. The paper summarizes available data sets for existing and future line sections of the European transmission grid. The developed process model shows a suitable, transparent approach for integration of varying data into one coherent model. The resulting structure provides a consistent transmission grid model for scientific research in simulations.

Keywords Transmission grid · Process model · Grid model

1 Introduction

The rising integration of renewable energies in Europe leads to a growing spatial discrepancy between power generation and consumption. Therefore, cost efficient and optimized scheduling of power plants and the future grid load are topics of high research interest today which require besides highly resolved demand and generation data detailed information about the transmission grid. This paper focuses on the acquisition of grid data. For detailed information on the renewable generation and the demand data, it is referred to the short description in Sect. 4.1 and to [1–3]. The quality and availability of the grid data are highly influencing the results of scientific studies. In many cases, the ENTSO-E Grid Map [4] is used as a source for the

S. Köppl (✉) · F. Böing · C. Pellinger
Research Center for Energy Economics (Forschungsstelle Für Energiewirtschaft), Munich, Germany
e-mail: SKoeppl@ffe.de

F. Böing
e-mail: FBoeing@ffe.de

C. Pellinger
e-mail: CPellinger@ffe.de

V. Bertsch et al. (eds.), *Advances in Energy System Optimization*, Trends in Mathematics, DOI 10.1007/978-3-319-51795-7_12

European grid data due to the unavailability of other consistent and comprehensive data sets (see [5–7]).

The ENTSO-E Grid Map contains simplified information about the voltage and the number of circuits of the European transmission grid but no exact electrical parameters (e.g. maximal current, reactance or resistance). Such specific information is occasionally provided by the TSOs, but never comprehensively throughout Europe. The purpose of this paper is to describe a transparent approach for the construction of a comprehensive grid model of the existing and the future transmission grid which integrates the most suitable available data sets and additionally portrays the remaining European transmission grid in a sufficiently precise manner with the use of appropriate assumptions.

The developed model focuses on the energy system of Germany and Austria but the transmission grid of the neighboring countries should be considered in a proper way as well. Initially in this paper, possible data sets for the existing and the future grid are described. The following explanation of the process model shows an approach to standardize the different data sets and to integrate grid data into dispatch models. The paper ends with a critical review of the model and the scope of application.

2 Public Grid Data Sets

For a sufficiently precise simulation of the transmission grid, a variety of grid data sets can be used which vary in covered region, voltage level, date/period of publishing, integrity of covered instances, contained elements (only lines or also transformer/substation data) and level of accuracy. The usage and the integration in a coherent data set require specific properties:

Technical parameters For lines and for substations, relevant electrical parameters have to be given. Possible electrical properties of lines are resistance, capacity and reactance. Additionally, the thermal limits power and the current load capacity are important information to evaluate the maximum transfer capacity of a transmission line.

Geographical position of lines and stations Every device has to be allocated to an exact geographical location. For substations, the voltage levels which are connected in the station are also essential to factor possible power flows from the transmission into the lower level distribution grid within the computational models.

Possibility of validation The collected data has to be validated to ensure its correctness and to identify possible incorrect entries. Reliable grid data is provided by e.g. the transmission system operators or official associations, for example national regulation authorities e.g. the German Federal Network Agency (BNetzA) or international federations like the ENTSO-E. If open source data is used, the validation especially for regions where no reliable reference source is available requires the

comparison with other open source data and a careful examination of the gathered data.

2.1 Data Sets of Existing Transmission Lines

To capture the existing transmission grid, a convenient database is published by the transmission system operators (TSO). Because of transparency reasons, the CWE region, defined by the ENTSO-E (Belgium, France, Germany, Luxembourg and the Netherlands), publishes directly static grid models of their transmission system (e.g. [8–10]). A static grid model mostly consists of a simplified map, a comprehensive illustration excluding correct geographical information or specific electrical information and a list of all line sections with relevant electric parameters, e.g. voltage U, maximum current I, resistance R or reactance X (see Table 1).

The availability of all electric parameters for each line allows the use of the TSOs' static grid models in scientific simulations like load flow calculations. In Germany, the BNetzA is legally bound by Energiewirtschaftsgesetz Sect. 12f (2) Sentence 1 to publish the "Impedanzen und Kapazitäten von Leitungen und Transformatoren an Dritte" (*the impedances and capacities of lines and transformers for third parties*) on request [11]. This data set offers the same electric level of detail (LoD) as the static grid model of the TSOs but it contains only the short names/abbreviations of the substations. This fact essentially complicates the integration of the data set into the requested structure and requires a significant amount of manual revision of the data. Furthermore, for the rest of Europe, the ENTSO-E annually releases the "Interconnected Network Grid Map" of the ENTSO-E member TSOs [4]. Similar to the grid maps of the TSOs, the ENTSO-E Grid Map only roughly displays the position of lines/substations and provides only reduced electric information (voltage and number of circuits for lines). In addition, the usage of open source data like Open Street Map (OSM) is also a possibility to complete the grid model [12]. OSM includes a large number of entries regarding the electric grid, though the included technical parameters could hardly be validated. In this paper, OSM is only used for geographical referencing of the substations. Other research projects like SciGrid revise and edit the transmission line data in OSM to build an open source data set of the transmission grid [13]. A first version of the SciGrid model was released in June 2015 and will be considered in the further development of the model. Figure 1 gives an overview of the most import attributes of the used data sets.

Table 1 Sample data of a static grid model

ID Station 1	ID Station 2	U	I	R	X
137	138	380	2300	1.11	15.5
138	139	220	800	4.5	34.1

	Grid models TSO	BNetzA data set	Open Street Map	ENTSO-E Grid Map
Covered region	Supplied area of the TSO	Germany and Europe reduced	Varying coverage in Europe	Member countries of the ENTSO-E
LoD of lines	Lines (>220 kV) with el.parameter	Lines (>220 kV), transformers, busbars with el.parameter	Varying coverage, lines with the parameters „voltage“, „cables“ & „wires“	Lines (>220 kV) with no. of ciruits
Geometry	Full names of substations, no geometry	No geo information	Geometries for every elements	Comprehensive illustration

Fig. 1 Data basis for the transmission grid

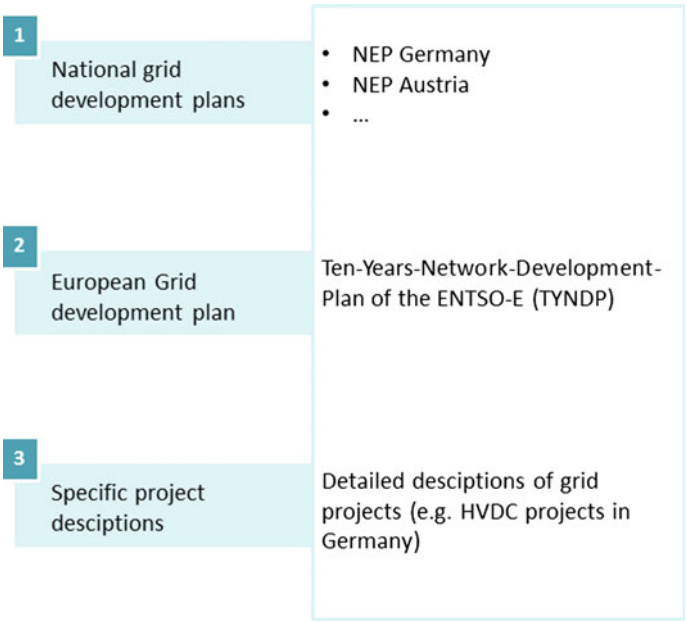

Fig. 2 Data basis for future grid projects

2.2 Future Grid Projects

The acquisition of future projects deals with the same requirements on the level of detail as the modeling of the existing transmission lines. Figure 2 shows possible data basis for national and European projects.

National grid development plans like the German NEP (Netzentwicklungsplan) display a list of projects which were identified by the TSOs in order to provide a future transmission grid without congestion [14]. Projects with a high significance on the European and not only national energy systems are published in the TYNDP of the ENTSO-E [15]. Especially for long-term projects in an early planning phase, the informational content of the description does not always meet the requirements for a direct integration into the final structure (e.g. TYNDP investment 40.A29 "New connection with neighbor(s) either 220 kV or 400 kV" [15]). In this case, the available information has to be completed with typical values and proper assumptions which will be described later.

2.3 Geo Allocation and Merging into Standardized Lists

Subsuming, a variety of different data sets have to be integrated into one consistent node-edge-model. The nodes list represents the relevant substations with the following parameters:

- ID of the station
- Name (optional spelling if necessary)
- Voltage levels
- Geographical position

The acquisition of the exact location of a grid node, which represents mostly a real existing substation, can be done in different ways and is based on the public geo data base OSM [12]:

- If an automated matching of the OSM substation with the node from the nodes list above is possible, the coordinates of the OSM substations can be used directly.
- In some cases, OSM and the static grid models of the TSOs use different spellings for the same substation. In these cases, a manual assignment of the gathered nodes to OSM data is necessary.
- If a node cannot be matched with an OSM substation (e.g. for future projects which are not yet constructed), the coordinates are set manually according to available information like grid maps or project descriptions.

The line list contains the transmission lines which connect the substations. Every line has to be described with specific parameters. Table 2 shows an example data set with necessary parameters as needed for the final model:

Generally, it is possible to assign concrete corridors for every line to achieve a more realistic visualization of the transmission lines. For load flow calculations and dispatch models, an adequate display of a transmission line is a simple connection between two substations. If the used data set does not contain the required information, a method to complete the missing entries has to be developed. A suitable approach to integrate different types of data into one coherent data structure by the usage of generalized processes is described in the following.

Table 2 Sample entries of the line list

ID Line	ID Stat. 1	ID Stat. 2	U	I	R	X	C
4000080	205	232	380	2720	1,41	13,26	0,35
2000376	91	252	380	3216	2,00	21,70	1,30
2008763	395	410	380	2580	4,98	42,85	1,35
5000104	339	659	380	2240	1,28	18,58	1,35

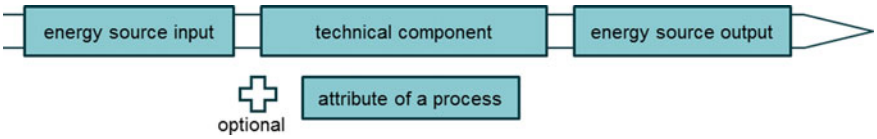

Fig. 3 Definition of a process

3 Process Model

In the projects MOS 2030 [1] and MONA 2030 [16],[1] a process model was developed to combine different data regarding the energy system in one consistent approach. This method is not only suitable for the aggregation of grid data, but also for a structured acquisition of data sets for e.g. consumption, power plants or storage systems. In addition to that, the process model is used for dispatch modeling of an energy system in form of a process network (see Chap. 5).

3.1 Definition of a Generalized Process

Generally, every device of the energy system can be described by a well-defined process (see Fig. 3).

A process consists of three obligatory elements: the energy source input, the technical component and the energy source output. Both, the input and output energy source, as well as the process attribute can occur separately or in combination. E.g. the energy source output of a CHP unit is "electrical energy, alternating current" and "heat". A technical component describes the technical function of a device. Technical components of grid devices are e.g. "power line", "transformer" or "reactive power compensation". In some cases, the same combination of these three elements occurs in different technical design. For example the combination "380 kV AC – AC power line – 380 kV AC" could include the attribute "underground cable" or "overhead line".

[1]The projects MOS 2030 (funding code 03ESP110A) and MONA 2030 (funding code 03ET4015) are co-funded by German Federal Ministry of Economic Affairs and Energy through the funding initiatives "Energiespeicher" and "Zukünftige Stromnetze". More information on the projects can be found on ffe.de/mos2030 and ffe.de/mona.

This requires a further distinction of the process. Therefore, the optional "attribute of a process" (see Fig. 3) is introduced. In both cases, the transportation task "transferring energy from station1 to station2" is similar, but the manner of transferring energy and its characteristics like construction costs, losses or transfer capacities differ and require the usage of different processes.

3.2 General Approach

Management and classification of input data in a database environment is a major challenge in the projects MOS and MONA. Due to the claim of implementing a numeric model of the energy system and grid, an extensive recording and process-labeling of all involved devices (e.g. power plants, transmission lines) and parameters has to be done. Therefore, processes have to be formed and placed in a hierarchic structure. As shown in Fig. 4 the level of detail increases the farther right the process is located.

Depending on the information content of the raw data, processes can be aggregated on different levels in the hierarchic structure. The complexity of the tree is set by the given problem, the information on existing devices and the available parameters.

3.3 Modification for the Integration of Grid Processes

The validity of simulation results is highly linked to the quality of input data. With the aim to reflect the properties of certain grid devices as exact as possible, a list of process attributes is prepared. Typical attributes are shown below:

- Cable type, e.g. 264-Al1/31St1A or 562-AL1/St1An
- No. of circuits
- Laying of the line: Overhead lines, underground cable, sea cable

Implementing a grid model within an energy system model using linear optimization sets further requirements for the design of processes. One modification is the introduction of the attribute "bidirectional grid process". This information is relevant for the automated model generation. It says that the device like a typical AC line can be used in both directions unlike standard processes that are valid only in one direction. Simulating and optimizing grid development demands the attributes "symmetric grid process" or "asymmetric grid process". The building of a standard AC power line is symmetric, because the transfer capacities are equal in both directions. In contrast, grid supporting measures can be asymmetric if the transfer capacity is not equally increased in both directions, e.g. for specific HVDC or cross border lines.

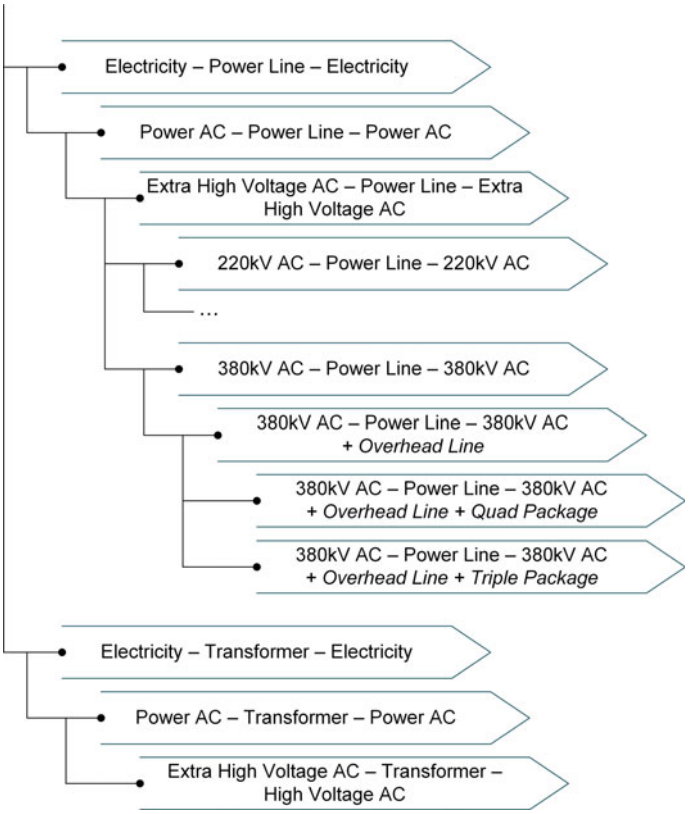

Fig. 4 Hierarchic structure of the process model in extracts

3.4 Assumptions for Grid Processes

Due to the varying structure, completeness and level of detail of the different input sources a data preparation has to be done. This step is necessary to implement a working model. Two classes of data are distinguished: device data and parameter data. Device data contain all device specific information of real existing devices (e.g. a specified power line) and consist of values like "year of commissioning", "starting substation". If some of the relevant information (e.g. the resistance) is not given, the missing data is assigned to a device using the information of the process. Generalized data for the process IDs is valid for certain processes and for this reason regardless of individual devices. To illustrate this principle Table 3 shows an exemplary extract of device data and Table 4 a selection of parameter data.

Each parameter is stored with a Process-ID, Region-ID and year reflecting its validity. This allows the subsequent addition of more detailed values for one certain parameter.

Table 3 Description of different grid devices

ID line	Process ID	Grid nodes	Year
35487	5642	123–134	1970
35847	6874	123–145	1978
20154	4653	145–134	1999

Table 4 Electric parameters of grid processes (sample data)

ID	Process ID	Valid	Region	Parameter	Value
1	4571	1960–1980	EU	R	2.00
2	5642	1980–2010	EU	X	23.80
3	4653	1990–2050	D	C	1.27

3.5 Implementation in a Database Environment

Using an SQL-database enables the implementation of an assignment algorithm. This algorithm assigns the most appropriate parameters to one device. Thereby the process, the year of validity and the regional resolution are considered. By the use of the hierarchic structure in Fig. 4, parameters on a lower level of detail can be assigned to devices on a higher level. Therefore, so called "universal parameters" can be stored on a very low level of detail. These parameters are used when no precise ones exist. Figure 5 shows the use of the different LoDs for the integration of projects of the TYNDP which are described in a very heterogeneous way. The result of this allocation algorithm is an input dataset on the highest available level of detail for each parameter. The use of this structure also enables flexible expansion of the parameter database, resulting in a steady improvement of the input data of simulation runs.

4 Integration of Grid Data in Energy System Models

After the definition of relevant processes and their parameters, the process model can assign values to devices with an under-determined process. With this approach, every present and future line section of the grid model is described with pertinent technical and economic parameters.

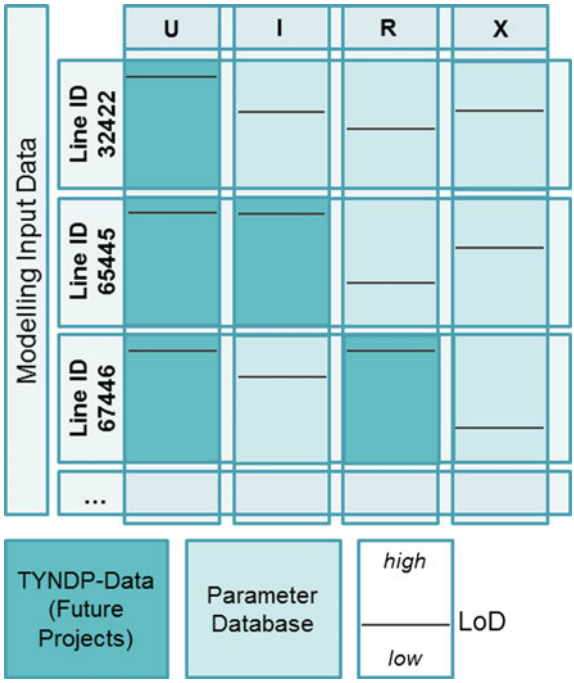

Fig. 5 Result of the allocation algorithm (schematic)

4.1 Nodal Allocation of Load and Production Data

In scientific computational models, it is crucial to calculate the residual load for every grid node. Therefore, every consumer unit and every energy production unit has to be allocated to one grid node. The load on a node is aggregated as the sum of all these single load profiles. By analogy, the production of renewable energies is calculated depending on geo and weather data and added up for each node. With the FREM, the FfE Regionalized Energy System Model – a comprehensive, spatially and temporally highly resolved energy system model – it is possible to answer a variety of complex energy technology and energy economics related questions [2]. This regionalized energy system model has been developed in the last years at the Research Center for Energy Economics in Munich. It combines heterogeneous data from a wide range of technical and statistical sources into a flexible and consistent data basis at all aggregation levels (see Fig. 6).

By this approach, the FREM can provide geographically and temporally highly resolved generation and demand data which can be used as input data for transmission grid modeling. The regional distribution and the construction of demand and generation profiles are described in various publications and will not be explained in detail in this paper (see [1–3]). Furthermore, the incorporation of the exact geographical location of lines and substations allows integrating the electric grid data into the FREM and to assign the load and production data points to the corresponding grid

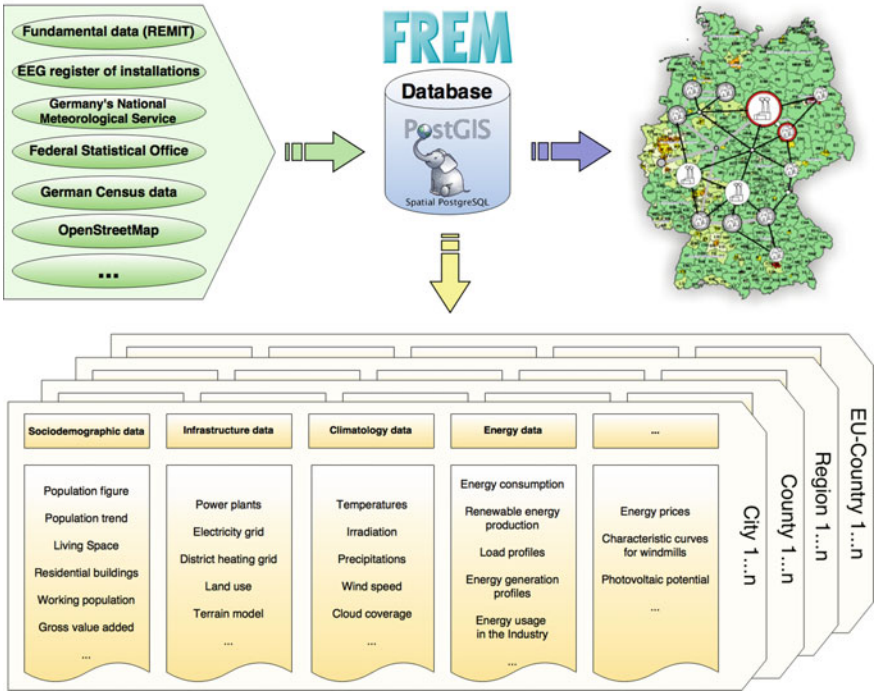

Fig. 6 Structure of the FREM

nodes. Beyond energy system simulations, the usage of a PostGIS database in the FREM opens up a great variety of possible energy related geoanalysis.

4.2 Virtual Network in Peripheral Regions

This allocation method is only possible for regions where the load and production data is available in a high spatial resolution. In the projects MOS and MONA, the main focus are the energy systems of Germany and Austria which are defined as one market zone and which can be modeled with detailed data. Especially for the neighboring countries, load and production data is often available in a low spatial resolution, e.g. in nationwide statistics. For those regions, there is most commonly no detailed data available. Hence, for the peripheral regions a reduced and simplified network is implemented to consider possible loop flows. Virtual dummy transmission lines connect the centroids of the countries with specific process definition and assume the transmission grid within a country as a "copper plate". The transfer capacity of these connections is figured as the sum of all cross border lines between the countries (see Fig. 7). The constructed reduced network facilitates the simulation of power flows

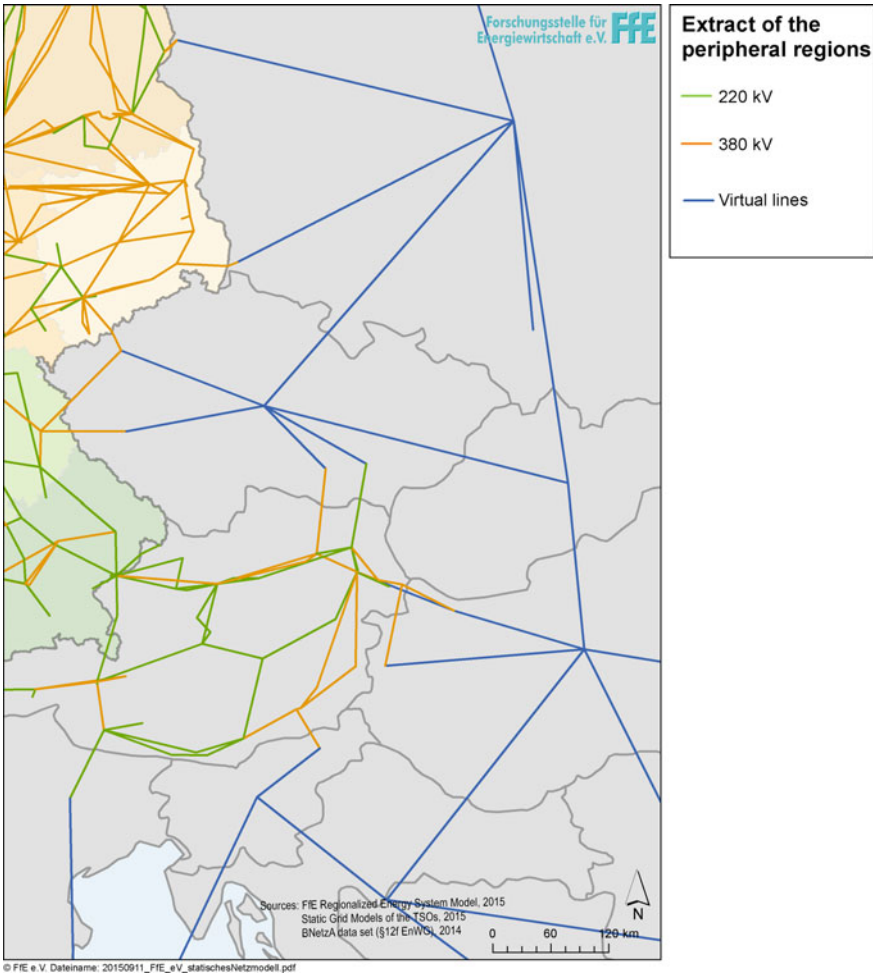

Fig. 7 Virtual transmission network in the peripheral regions

outside Germany and Austria in a proper way but does not represent power flows in the actual transmission grid in the rest of Europe. Moreover, a geographically exact reproduction of the transmission grid is only possible for Germany and Austria.

As a general rule, it can be determined that the grid has to be shaped in a similar spatial resolution as the load and production data. On the analogy of the peripheral region, the process model easily enables the addition of missing lines which are not part of the integrated grid data.

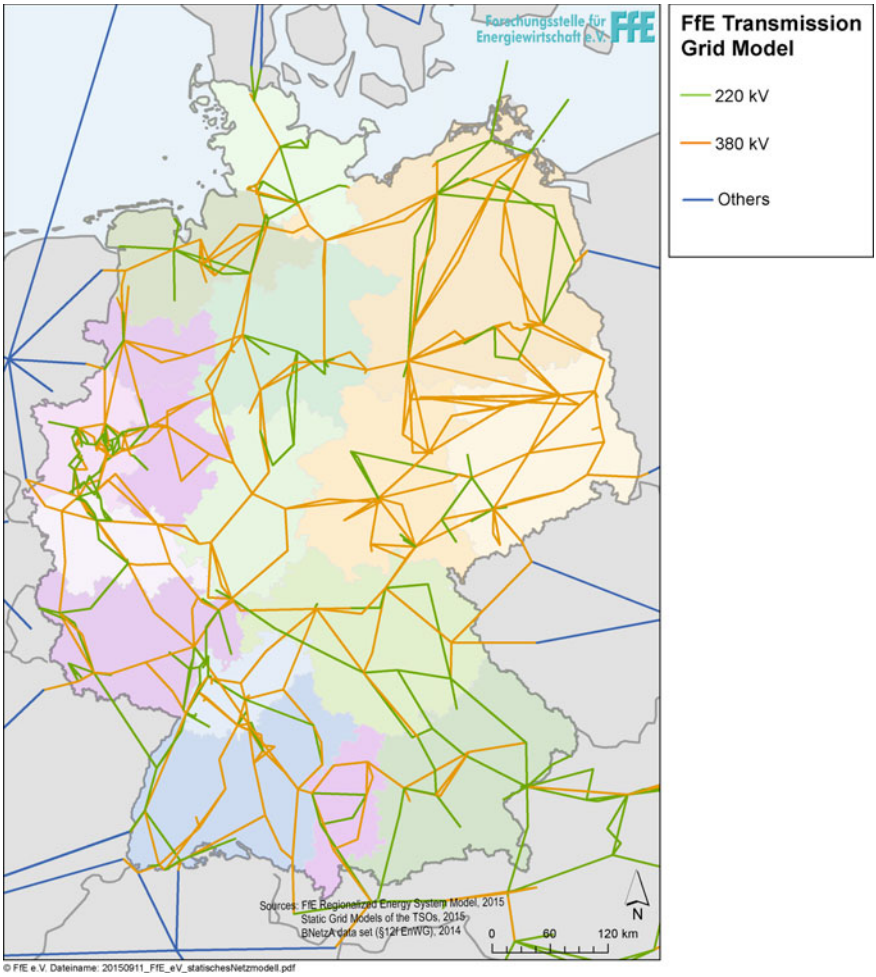

Fig. 8 Extract of the grid model

5 Resulting Transmission Grid Model

The resulting model unifies the data sets of existing transmission lines, the virtual network for the peripheral regions and the manually added lines into one coherent model. By the use of the process model, all line sections regardless of the quality of the input parameter are described with definite electrical values. The definition of scenarios and reference years enables the modeling of future transmission structure according to the project requirements. Figure 8 shows an extract of the final grid model with transmission lines as simplified connections between the grid nodes.

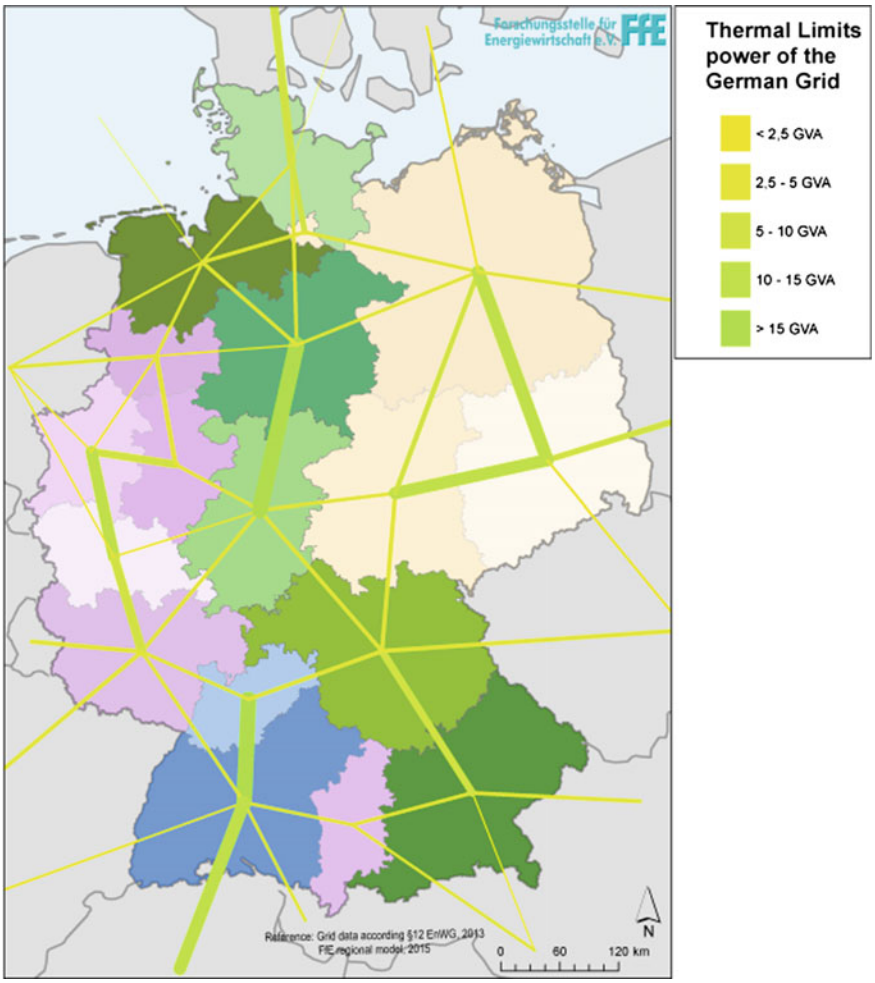

Fig. 9 Aggregated transmission capacities between regions

The so designed grid structure allows static load flow calculation or isolated researches, e.g. on transmission capacities between regions (see Fig. 9).

Another significant application of the process model is the use in dispatch models. In this context a process not only defines different types of power plants or lines. The entire optimization model is built dynamically, depending on the available processes and their geo information. The energy system is modeled as a network of processes. This enables flexible selection of the relevant energy system elements while maintaining the numeric functionality of the model. The spatial resolution of input data is not affecting the general composition of the mathematical problem. Thus, a calculation can take place on different voltage levels or considers several levels as shown in Fig. 10 (Appendix).

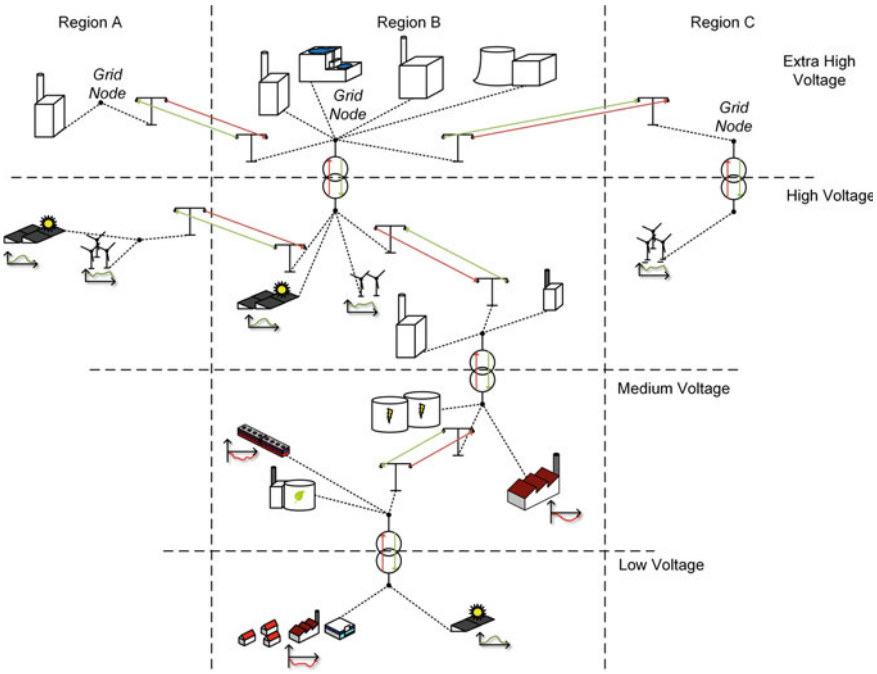

Fig. 10 Schematic visualization of an energy system model

6 Critical Review

The described model shows one possible approach of merging different types of grid data sets into one grid model. One of the weaknesses of the model depicts the availability of grid data. Additional data which provides added value in comparison of e.g. the ENTSO-E Grid Map is occasionally provided by TSOs, but never comprehensively. Furthermore, the used data sets vary in publishing dates, which makes temporal consistency of data another weak spot of the model. The varying and not clear designations for substations complicate the precise geo allocation and may be looked at critically, which has to be done manually in most cases. Due to the lack of a transmission grid reference data set, the possibility to validate data is problematic. A rough validation of the number of circuits and the voltage of lines is possible with the ENTSO-E Grid Map, albeit not for exact electrical parameters.

7 Conclusion and Outlook

The process model amalgamates several data sets into one coherent transmission grid, using a transparent approach which is also suitable for other elements of the energy system. With appropriate simplifications and assumptions, missing specific values

of elements are complemented to attain a consistent model with entire electrical information content. The resulting transmission grid model provides basic data on scientific evidence for dispatch models or studies on transmission capacities. In the further project course it is planned to reduce the complexity and number of nodes of the developed model by network decomposition, which can be realized by geometric operations or the evaluation of load flow calculations. In the project MONA 2030, the FfE evaluates and analyzes existing and future optimizing measures for a foresighted and holistic grid planning. The described grid model is used for the construction of the future energy system scenarios and the cost-optimized ranking of the measures.

Appendix

See Fig. 10

References

1. Pellinger, Christoph et al., Merit-Order der Energiespeicherung im Jahr 2030. Forschungsstelle für Energiewirtschaft e.V., Munich (2012)
2. Forschungsstelle für Energiewirtschaft e.V.: The FfE Regionalized Energy System Model (FREM). Forschungsstelle für Energiewirtschaft e.V., Munich (2014)
3. Carr, Luis et al., Erneuerbare Energien - Potenziale und ihre räumliche Verteilung in Deutschland in: Flächennutzungsmonitoring V - Methodik Analyseergebnisse Flächenmanagement. Leibniz-Institut für ökologische Raumentwicklung e. V., Forschungsstelle für Energiewirtschaft e.V., Dresden, Munich (2013)
4. ENTSO-E, Interconnected network of ENTSO-E. Brussels (2014)
5. Egerer, Jonas et al., Electricity Sector Data for Policy-Relevant Modeling - Data Documentation and Application to the German and European Electricity Markets. DIW - Deutsches Institut für Wirtschaftsforschung, Berlin (2014)
6. Ackermann, Thomas et al., European Grid Study 2030/2050. energynautics GmbH, Langen (2011)
7. Viljanen, Ari et al., DC description of power grids - EURISGIC technical note in: The EURISGIC EU/FP7 project. Neurospace, Limhamm (2012)
8. TenneT TSO GmbH, Static Grid model: https://www.tennettso.de/site/en/Transparency/publications/static-grid-model/static-grid-model. TenneT TSO GmbH, Bayreuth (2015)
9. Amprion GmbH, Static grid model: http://www.amprion.net/en/static-grid-model. Amprion GmbH, Dortmund (2015)
10. Netzentwicklungsplan 2014 für das Übertragungsnetz der Austrian Power Grid AG (APG) - Planungszeitraum: 2015 - 2024. Austrian Power Grid AG, Vienna (2014)
11. Bundesnetzagentur, Daten nach 12f Abs.1 EnWG. Bundesnetzagentur, Bonn (2014)
12. OpenStreetMap, United Kingdom (UK): https://www.openstreetmap.org/about (2015)
13. Medjroubi, Wided et. al., SciGRID - An Open Source Reference Model for the European Transmission Network (v0.1). NEXT ENERGY, Oldenbourg (2015)
14. Feix, Olivier et al., Grid Development Plan 2014 - first draft. 50Hertz Transmission GmbH, Amprion GmbH, TransnetBW GmbH, TenneT TSO GmbH, Stuttgart (2014)
15. ENTSO-E, 10-Year Network Development Plan 2014. ENTSO-E, Brussels (2014)
16. Samweber, Florian et al., Merit Order des Netzausbaus im Jahr 2030. Forschungsstelle für Energiewirtschaft e.V., Munich (2014)

Regionalizing Input Data for Generation and Transmission Expansion Planning Models

Viktor Slednev, Manuel Ruppert, Valentin Bertsch, Wolf Fichtner, Nico Meyer-Hübner, Michael Suriyah, Thomas Leibfried, Philipp Gerstner, Michael Schick and Vincent Heuveline

Abstract To support decision making in the context of restructuring the power system, models are needed which allow for a regional, long-term operation and expansion planning for electricity generation and transmission. Input data for these models are needed in a high spatial and temporal granularity. In this paper, we therefore describe an approach aimed at providing regionalized input data for generation and transmission expansion planning models. We particularly focus on a dynamic

V. Slednev (✉) · M. Ruppert · V. Bertsch · W. Fichtner
Institute for Industrial Production, Karlsruhe Institute of Technology, Karlsruhe, Germany
e-mail: viktor.slednev@kit.edu

M. Ruppert
e-mail: manuel.ruppert@kit.edu

V. Bertsch
e-mail: valentin.bertsch@kit.edu

W. Fichtner
e-mail: wolf.fichtner@kit.edu

N. Meyer-Hübner · M. Suriyah · T. Leibfried
Institute of Electric Energy Systems and High-Voltage Technology,
Karlsruhe Institute of Technology, Karlsruhe, Germany
e-mail: nico.meyer-huebner@kit.edu

M. Suriyah
e-mail: michael.suriyah@kit.edu

T. Leibfried
e-mail: thomas.leibfried@kit.edu

P. Gerstner · M. Schick · V. Heuveline
Engineering Mathematics and Computing Lab, Heidelberg University, Heidelberg, Germany

P. Gerstner · M. Schick · V. Heuveline
Heidelberg Institute for Theoretical Studies, Heidelberg, Germany
e-mail: philipp.gerstner@h-its.org

M. Schick
e-mail: michael.schick@h-its.org

V. Heuveline
e-mail: vincent.heuveline@h-its.org

V. Bertsch et al. (eds.), *Advances in Energy System Optimization*,
Trends in Mathematics, DOI 10.1007/978-3-319-51795-7_13

assignment of renewable energy sources and electrical load to potential buses of the transmission grid. Following a bottom up approach, we model the existing and potential distributed generation and load at the lowest possible spatial resolution based on various databases and models. Besides large power plants, which are directly connected to the transmission grid, a decentralized grid connection is modeled on the distribution grid level based on Voronoi polygons around the corresponding substations. By simplifying the load flow over the distribution grid to a shortest path problem, we model the feed-in into the transmission grid as a variable, depending on the nearest available transmission grid connection. As a result, the connection to the buses at transmission grid level is kept variable in case of grid expansion measures at substation level.

Keywords Regionalization · Generation and transmission expansion planning

1 Introduction

The rapid expansion of decentralized renewable energy sources (RES) in many European countries necessitates an extensive structural rearrangement of the power system. In particular, since many of these new RES facilities will be located far from the load centres (in particular new wind parks), an expansion of the transmission grid is necessary to meet the resulting transport capacity requirements. To support decision making in this context, models are needed which allow for a long-term, regional operation and expansion planning for electricity generation and transmission. The consideration of grid constraints in energy systems models therefore becomes increasingly important. In turn, this means that input data for these models are needed in a high spatial and temporal granularity.

In general, the following four categories of input data are needed to analyze long-term electricity generation and transmission expansion developments: First, transmission grid data is required, in particular the technical characteristics and geographical information of all buses and lines. Second, conventional power plant data including their geographical location and assignment to the buses of the transmission grid are required. Third and fourth, RES generation profiles and electricity demand profiles are needed - each in high temporal and spatial granularity, allowing for an assignment to the buses of the transmission grid.

Although the fields of transmission network expansion planning (TNEP) and generation expansion planning (GEP) are well established in research as shown by several exhaustive reviews available [6, 7, 10], the application in the context of large-scale, long-term energy systems models is quite rare. Furthermore, the provision of adequate data models for this special task of a combined TNEP and GEP is often neglected. Especially, the challenge of modeling a grid expansion within the complex network topology of mature power systems and its implications on the data model are hardly investigated so far. In Germany, for instance, the national power grid development plan also includes dismantling of lines besides expansion plans or the construction of new transformer stations. While modeling approaches which consider

the number of buses and the structure of the grid topology as dynamic variables are well established in the context of the distribution network expansion planning (DNEP) and substation expansion planning (SEB) [2, 4, 8], their application in the context of TNEP within energy systems analysis (ESA) is rare. Obviously, the first best solution of including the grid restrictions on the power flow from the source to the sink over each voltage level is computationally infeasible in the context of expansion planning of large energy systems. Therefore, flexible data models are needed, which allow a dynamic assignment of RES generation and electricity demand profiles to the potential buses of the transmission system.

The remainder of this paper is structured as follows. Section 2 provides an overview of selected literature related to TNEP and GEP problems for power systems planning regarding the underlying models for the provision of regionalized input data. In Sect. 3, we present our approach for a dynamic assignment of generator and load variables to a variable electrical transmission network. The main contribution of this paper is the subsequent demonstration of the approach, including the presentation of a data model for providing regionalized input data for the analysis of the German power generation and transmission system, in Sect. 4. Finally, we summarize our main findings and indicate future research needs in Sect. 5.

2 Selected Approaches in Power Generation and Transmission Planning and Their Handling of Regionalized Input Data

As mentioned above, the distribution of generation and load in energy systems modeling may have a crucial impact on the results, especially when modeling grid constraints. In this section, we review relevant, existing literature focusing on the representation of geo-referenced data in the context of generation and transmission expansion planning approaches.

Because of this paper's focus on the application to transmission grid expansion planning, we neglect models which primarily focus on the generation expansion or are restricted to a single node or a pure transhipment problem. Thus, we follow the categorization of Ventosa et al. [17] who distinguish between so-called single node models (not considering the grid at all), transhipment models (considering the grid in a simplified way, but ignoring Kirchhoff's voltage law) as well as linearized DC models and nonlinear AC models (considering both of Kirchhoff's laws) within electricity market modeling.

Despite the restriction to DC and AC models, the reviews of Hemmati et al. [6] and Latorre et al. [10] still show a broad range of modeling approaches, which may be categorized according to their methodological approach used, their application in regulated or deregulated markets or the coordination of the GEP and TNEP problem for instance. While many of these approaches address issues such as reliability

and uncertainty, their application is often limited to artificial benchmark networks or strongly simplified power systems. Thus, they mainly neglect the data-related challenges on the input side of modeling network expansion measures within real networks. A condensed review of existing co-optimization tools which are applied in long-term investment planning in the power sector is given by Krishnan et al. [9], while a more detailed review may be found in the underlying study for the Eastern Interconnection States' Planning Council [11]. Besides characterizing different approaches it is notable that the authors provide a synopsis of the data needs of co-optimization problems. In total they differentiate between five different categories:

(i) historical conditions (e.g., hourly load and generation data, fuel prices),
(ii) existing and planned infrastructure (e.g., AC-network topology, fossil and renewable data),
(iii) resource options (e.g., generation, storage),
(iv) transmission options (e.g., AC or DC lines, transformers) and
(v) future conditions.

While no further information about the approach for handling the data within a modeling environment is provided, Liu et al. [11] give a detailed description of the data sources (for the US market) and many remarks on the requirements from the data. Furthermore, an overview of selected approaches considering grid restrictions in energy systems analysis, partially including grid expansion, with a focus on Europe can be found in Nolden et al. [13].

In the context of distribution network expansion planning, both the handling of georeferenced data and the detailed representation of grid expansion options, including substation expansion, are addressed frequently in literature (see [1, 5, 8, 12]). Applications of this level of detail in the field of TNEP, however, are rare or applied to power systems with a low complexity and number of elements. For instance, the approach of Cebeci et al. [2] for optimizing size and location of new transmission substation (TS) investments with the expansion of high and medium voltage lines is only applied to a small and simple system.

In summary, the above literature review shows that, while being common in DNEP, so far, transmission expansion planning under high topological variability has not been of particular interest in long-term, large scale energy systems analysis (TNEP in ESA).

3 The Developed Approach for a Dynamic Assignment of Generation and Load Data to Varying Topologies of the Transmission Grid

The following approach addresses the restructuring of transmission networks in mature power markets with a dense electrical network connecting all sources and sinks of electricity. In typical TNEP approaches within ESA, the relation between the

transmission network and the generators and loads is assumed to be fixed. In case of a variable expansion and dismantling of busbars within substations or even of entire substations, however, a fixed indexing of generators and loads through the buses of the transmission grid is no longer possible. Therefore, a variable grid connection of generators and loads directly connected to the transmission grid or indirectly through the distribution grid is needed. Besides the challenge of modeling a variable grid connection, an accurate load flow analysis in the context of the TNEP with decentralized generators and loads would require to extend the load flow calculation from the transmission grid level to the distribution grid level. In large-scale power systems, however, such an approach is computationally highly challenging, especially in the context of a long-term capacity expansion planning. In order to reduce the complexity of the problem, a reduction of the electrical network to an equivalent but less complex system is often applied in TNEP and GEP. Given our focus on the transmission network expansion planning, a reduction of the distribution network could be an obvious solution. In literature, many approaches for a network reduction may be found, ranging from classical ward-type equivalents or REI equivalents or more advanced optimal power flow (OPF) based network aggregation techniques [3, 16]. Furthermore, improved bus aggregation techniques based on the power transfer distribution factor (PTDF) were recently published, which allow to overcome the typical drawback of the set-point dependency of conventional equivalent techniques [14, 15]. However, to our knowledge, these approaches are not capable of dealing with a variable grid connection under varying topologies of the transmission grid while all of them require a detailed knowledge of the network parameters, which might not always be given, especially in the distribution grid.

Due to the high variability of the transmission grid, we propose to model the task of a grid connection of generators and loads endogenously through a binary assignment graph. The basic idea for the computation of the assignment graph follows the approach of Di Shi et al. [16] by moving generators comprehensively to the buses of the retained network such that the weights of constituent branches are minimized. In order to deal with the uncertainty related to the number of buses and substations in the transmission grid, the approach of Di Shi et al. [16] is extended in a way such that all paths are computed until the next static transmission grid substation is found, including all transmission grid buses as potential solutions of the assignment graph. For simplicity, the resulting shortest path problems are also solved for loads, resulting in a network reduction which is less eligible of preserving the original load flows but may be flexibly adapted to varying network topologies. The detailed procedure for computing the assignment graph for generators and loads to potential buses of the transmission grid in the further TNEP is shown in Fig. 1. The nomenclature is summarized in Table 1.

Generally, the proposed approach results in a static assignment of central units to their predefined buses and of decentral units to the next boundary bus of the TG/DG network, if the corresponding buses of the transmission grid are static. In case of variable buses, the next static substation is determined, including all potential next buses to the solution vector. Depending on the knowledge of the network parameters of the distribution grid, the weights for the shortest path problem might be either chosen by

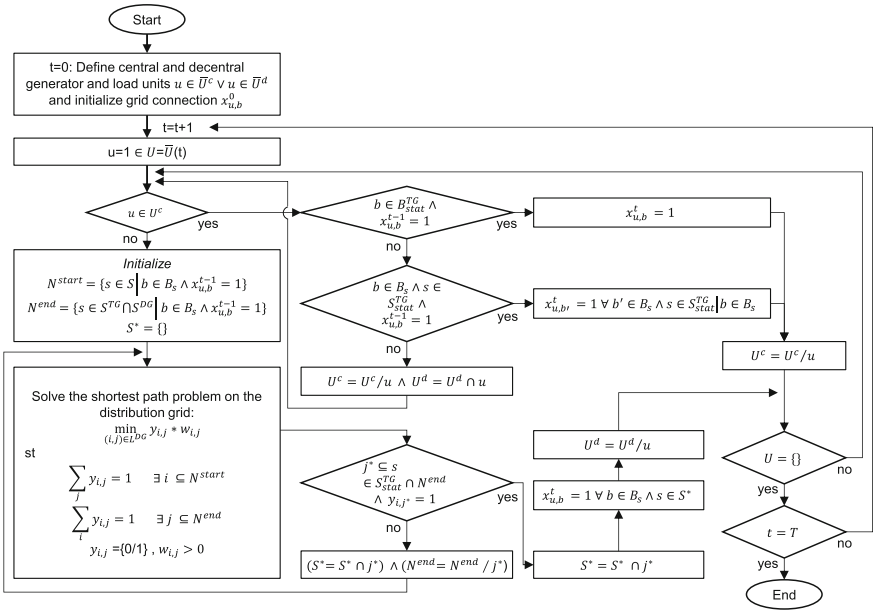

Fig. 1 Procedure for generating an assignment graph for a dynamic grid connection

Table 1 Nomenclature

Sets	
T	Set of years
$\bar{U}$	Master set of units
U^c, U^d	Set of centralised / decentralised units
B	Set of buses
S	Set of substations
B_S	Subset of buses which are element of substation S
B^{TG}_{stat}	Static buses of the transmission grid (TG)
S^{TG}, S^{DG}	TG, DG substations
N, N^{start}, N^{end}, $S^\star$	Subset of substations for the shortest path problem
L^{DG}	Set of lines in the DG
Variables	
$x^{t-1}_{u,b}$	Assignment of unit u to bus b in year t
$y_{i,j}$	Binary variable of the shortest path problem

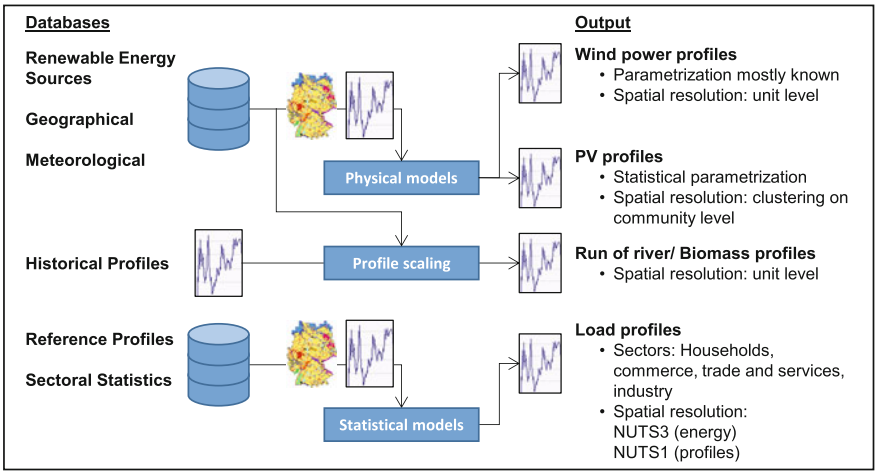

Fig. 2 Schematic overview of our regionalization approach

the squared sum of the branch resistance and reactance following Di Shi et al. [16], or if these parameters are not known, by the line length. The main advantage of this approach is its flexible and consistent handling of various assignment problems. For instance, even the challenge of a decommissioning of a substation with initially connected generators, in the end results in a similar assignment problem as the voltage switching problem within a transmission grid substation. Finally, it should be noted that in most applications with a comparatively large number of static transmission grid buses in comparison to the variable ones, most generators and loads remain statically assigned. Especially, most large scale generators and consumers, which are directly connected to the transmission grid are often not affected by grid expansion measures. Therefore, the increase in complexity resulting from including generators and loads through a binary assignment graph within the TNEP remains manageable.

4 Case Study: Regionalization of Input Data for the Transmission Network Planning in Germany

Following the previously described approach, our goal for providing regionalized input data for the TNEP is the assignment of all relevant generators and loads to the substation level of the distribution and transmission grids and the modeling of their conditions on this level. In this case study, we apply our approach to the German transmission grid. The prerequisite for such an application on the transmission grid level is the availability of a transmission grid data model, containing all relevant geographical information of all buses and lines. Based on various data sources for

Germany, among others the static network models provided by the transmission system operators (TSO), the network expansion plan as well as open street map (OSM), we developed a model containing data of 559 substations and 1290 buses, connected to each other via 1760 lines and 1047 transformers. For the long-term investment planning within an energy systems model, all topological changes according to the network expansion plan 2014 are integrated in addition to the technical characteristics of the grid infrastructure. On the distribution grid level, we developed a data model of the topology of the German high voltage distribution grid based on OSM data. In Germany, the high voltage grid (110 kV) is the highest grid level below the transmission grid (220 and 380 kV).

Based on the geographical location and the often known actual substations, the assignment of conventional generators and large-scale RES from our power plant data model is achieved. In order to connect decentralized consumers and renewables to the distribution grid level, Voronoi polygons around these substations are used to define a consistent reference area. In case that the exact location of the decentralized units is available, the assignment is trivial. However, the modeling of consumption and renewable generation profiles and their potential is often referenced to varying areas, such as postal code areas, municipalities or the NUTS 3 level, depending on the data availability. In these cases, the overlay with the Voronoi polygons allows a consistent assignment to the distribution grid level. In this way, profiles as well as potentials within a polygon are assigned to the corresponding 110 kV substation while overlying referenced profiles and potentials are proportionally distributed according to the land use.

For the modeling of the conditions of centralized or decentralized generation and consumption, a consistent parametrization is of high relevance. Especially, for the modeling of weather dependent components, such as the (domestic) electricity consumption and renewable energy availability (wind, PV, hydro), spatially and temporally consistent data are needed in order to preserve the interregional and intertemporal dependencies and correlations. By choosing historical weather years and modeling at the lowest available spatial resolution, these challenges can be met. An overview of our regionalization approach can be found in Fig. 2.

A further challenge consists in the modeling of the future conditions of generators and load. Especially for RES, the potential for expansion planning and its exploitation need to be taken into account. In our approach, this is realized through a linear programming optimization for the wind power and PV development, while other RES are considered by basic scaling. In case of the future development of wind power, our approach also takes into account repowering at unit level. One problem, which is often observed in practical applications of regionalization is the low availability of highly resolved spatial input data.

While the modeling approach provides the ability to generate load profile data on a NUTS 3 level, we are facing the challenge of distributing these profiles on the distribution grid level, where demand is mainly connected to the grid. In such cases, available statistical data, for instance on the municipality level, can be used to break down the profiles to a lower level. Especially in rural areas, the load on the distribution grid level can be aggregated from the multiple municipalities within

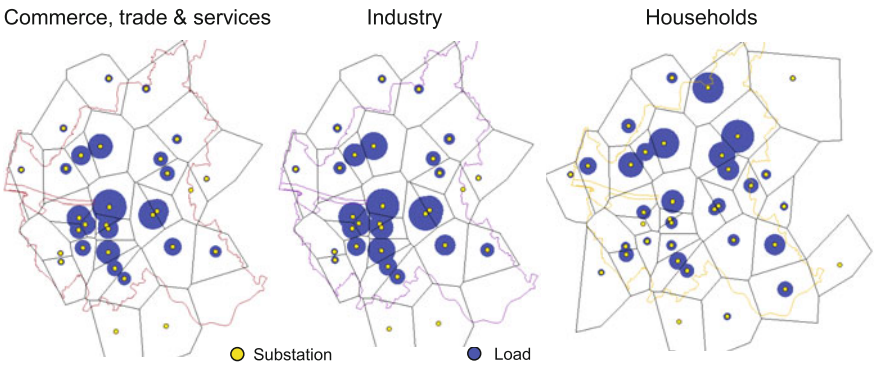

Fig. 3 Example of regionalization approach for the yearly load on the 110 kV level in Hamburg

the polygons of the 110 kV substations. In some cases, however, this is not possible since the municipality corresponds to the NUTS 3 classification. Figure 3 shows the regionalization of the yearly load on the 110 kV level for the example of the city state Hamburg, demonstrating the suitability of our approach also on this level. In detail, we chose a raster approach and analyzed the land use in Voronoi polygons at a resolution of 1 ha. In order to show the yearly impact of the resulting distribution, the yearly load by sector (households, commerce, trade and services, industry) is represented at each 110 kV node in Fig. 3. It can be seen that this approach allows a significant differentiation between the different load types on the distribution grid level and doesn't lead to a uniform distribution as it would be expected from a simple regionalization approach.

Figure 4 shows the results of the assignment approach for the load in the reference case of the year 2012 over the entire area of Germany both on the 110 kV level and the transmission grid level. The previously discussed distribution of load data in the case of Hamburg also shows a clear impact on the transmission grid level as the aggregation to the transmission grid nodes does not lead to a unification of shares per demand type. Rather, we observe that the inhomogeneous structure which was determined at the distribution grid nodes remains.

Compared to the high concentration of the demand at certain load centres, the generation from renewable energy sources on the 110 kV level shows a much higher distribution in the reference case of 2012. On the transmission grid level, however, a concentration of the RES feed-in to a limited number of buses may be observed. In relation to the homogeneous structure of the input values, the assignment results of RES turn out to deviate even more from a unification approach.

Finally, following the network expansion plan of the German TSOs and their reference scenario for 2025, the modeled future distribution of renewables on the DG and TG level is shown in Fig. 5. In the first place, a further concentration of the RES feed-in on the TG level might be observed, partly resulting from a higher concentration on the DG level. Note that, without the expansion of new transmission grid substations in this reference case, the concentration effect of RES would be even

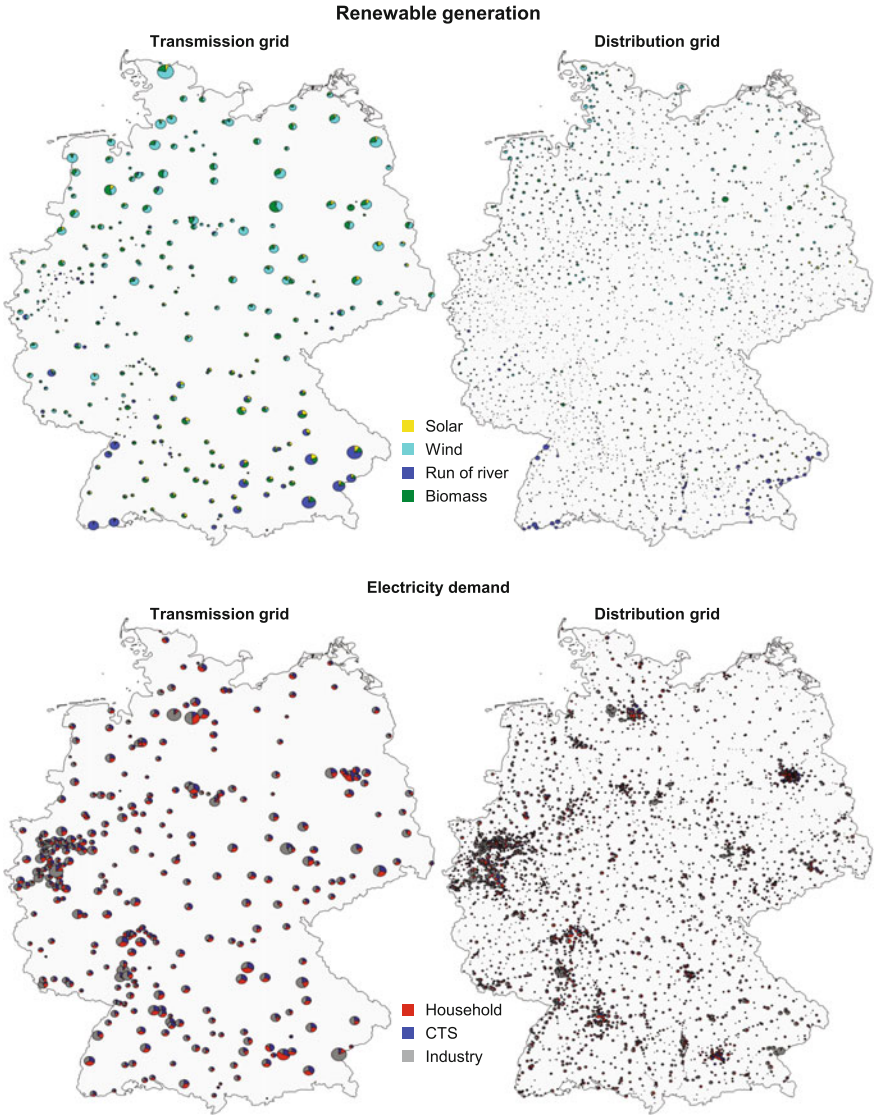

Fig. 4 Assignment results for the load in the reference case of the year 2012

more prominent. Contrary to the common trend, however, the expansion of transmission grid substations in some areas of the northern and eastern part of Germany even resulted in a reduction of the assigned RES feed-in at some nodes due to the reassignment from the 110 kV level.

Critically reflecting the presented approach, note that the proposed assignment approach is very sensitivity to the structure of the distribution grid. The concentration

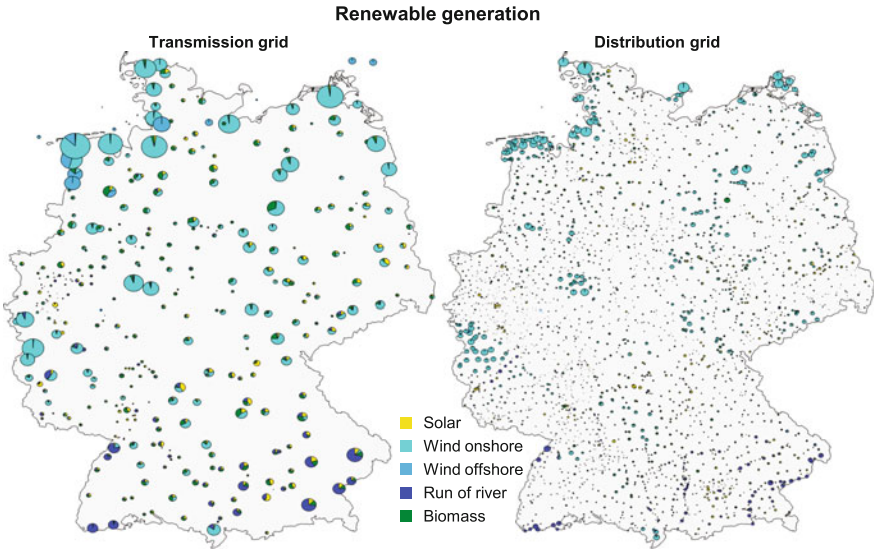

Fig. 5 Assignment results for renewables in the reference grid expansion scenario of the year 2025

of the RES feed-in apart from centres with a high transmission grid node density as well as the differences between the feed-in into neighbouring transmission grid nodes are both indicators of this limitation (see Fig. 4). Moreover, this approach includes the implicit assumption that the topology of the distribution grid is known in advance. In reality, however, the distribution grid is also subject to expansion measures. Consideration of these would further increase the accuracy of the used assignment method. Finally, please note that the cost-optimal expansion of wind power, ignoring all acceptance related issues, is expected to deviate from wind power expansion in reality and may overestimate concentration effects of RES expansion.

5 Conclusions and Outlook

In literature dealing with network expansion problems, regionalization of input data is generally not paid much attention. Consequently, most energy system models do not include a regionalization of input data to the extent required for the utilization in a combined GEP and TNEP model in large-scale ESA. In this paper, we presented an approach which can be applied for a dynamic grid connection of large-scale as well as distributed units. We have applied the approach to the distribution and transmission grids of Germany, using consistent datasets for the years 2012 and 2025. Our results show that regional differences can be observed on a large-scale, legitimating the increasing complexity of a dynamic connection of distributed load and generation.

There is further potential for improving the model by considering the distribution grid in more detail, which is currently not possible using a graph-based approach. This includes taking grid topologies determined by the areas of different distribution system operators into account or even extend load flow calculations to the distribution grid level.

Acknowledgements The content of this paper is closely related to research carried out within the project HE 4760 / 8-1, funded by the Deutsche Forschungsgemeinschaft (DFG). The authors wish to thank the DFG for their financial support.

References

1. Carvalho PM, Ferreira LA, Lobo FG, Barruncho LM (1997) Distribution network expansion planning under uncertainty: a hedging algorithm in an evolutionary approach. In: 20th International Conference on Power Industry Computer Applications, IEEE, pp 10–15
2. Cebeci ME, Eren S, Tor OB, Giiven N (2011) Transmission and substation expansion planning using mixed integer programming. In: North American Power Symposium (NAPS), 2011, IEEE, pp 1–5
3. Deckmann S, Pizzolante A, Monticelli A, Stott B, Alsac O (1980) Studies on power system load flow equivalencing. IEEE Transactions on power Apparatus and Systems 6(PAS-99):2301–2310
4. Franco JF, Rider MJ, Romero R (2015) Robust multi-stage substation expansion planning considering stochastic demand. IEEE Transactions on Power Systems PP(99):1–10
5. Govender K, Meyer A, Dwolatzky B (2001) The automatic clustering of uniformly distributed loads for the use in rural electrification planning. In: Transmission and Distribution Conference and Exposition, 2001 IEEE/PES, IEEE, vol 1, pp 450–455
6. Hemmati R, Hooshmand RA, Khodabakhshian A (2013a) Comprehensive review of generation and transmission expansion planning. Generation, Transmission & Distribution, IET 7(9):955–964
7. Hemmati R, Hooshmand RA, Khodabakhshian A (2013b) State-of-the-art of transmission expansion planning: Comprehensive review. Renewable and Sustainable Energy Reviews 23:312–319
8. Hemmati R, Hooshmand RA, Taheri N (2015) Distribution network expansion planning and dg placement in the presence of uncertainties. International Journal of Electrical Power & Energy Systems 73:665–673
9. Krishnan V, Ho J, Hobbs BH, Liu AL, McCalley JD, Shahidehpour M, Zheng QP (2016) Co-optimization of electricity transmission and generation resources for planning and policy analysis: review of concepts and modeling approaches. Energy Systems 7(2):297–332
10. Latorre G, Cruz RD, Areiza JM, Villegas A (2003) Classification of publications and models on transmission expansion planning. IEEE Transactions on Power Systems 18(2):938–946
11. Liu A, Hobbs B, Ho J, McCalley J, Krishnan V, Shahidehpour M, Zheng Q (2013) Co-optimization of transmission and other supply resources. Prepared for the Eastern Interconnection States Planning Council, NARUC
12. Luchmaya A, Dwolatzky B, Meyer A (2001) Using terrain information in an electrification planning tool. In: Transmission and Distribution Conference and Exposition, 2001 IEEE/PES, IEEE, vol 1, pp 456–460
13. Nolden C, Schönfelder M, Eßer-Frey A, Bertsch V, Fichtner W (2013) Network constraints in techno-economic energy system models: towards more accurate modeling of power flows in long-term energy system models. Energy Systems 4(3):267–287

14. Oh H (2010) A new network reduction methodology for power system planning studies. IEEE Transactions on Power Systems 25(2):677–684
15. Shi D, Tylavsky DJ (2012) An improved bus aggregation technique for generating network equivalents. In: Power and Energy Society General Meeting, 2012 IEEE, IEEE, pp 1–8
16. Shi D, Shawhan DL, Li N, Tylavsky DJ, Taber JT, Zimmerman RD, Schulze WD (2012) Optimal generation investment planning: Pt. 1: network equivalents. In: North American Power Symposium (NAPS), 2012, IEEE, pp 1–6
17. Ventosa M, Baıllo A, Ramos A, Rivier M (2005) Electricity market modeling trends. Energy Policy 33(7):897–913

Part VII
Convex Versus Nonconvex Approaches for Power Flow Analysis

Convexity/Nonconvexity Certificates for Power Flow Analysis

Boris Polyak and Elena Gryazina

Abstract Optimal Power Flow problem is considered as minimization of quadratic performance function subject to linear and quadratic equality/inequality constraints, AC power flow equations specify the feasibility domain. Similar quadratic problems arise in discrete optimization, uncertainty analysis, physical applications. In general they are nonconvex, nevertheless, demonstrate hidden convexity structure. We investigate the "image convexity" property. That is, we consider the image of the space of variables under quadratic map defined by power flow equations (the feasibility domain). If the image is convex, then original optimization problem has nice properties, for instance, it admits zero duality gap and convex optimization tools can be applied. There are several classes of quadratic maps representing the image convexity. We aim to discover similar structure and to obtain convexity or nonconvexity certificates for the individual quadratic transformation. We also provide the numerical algorithms exploiting convex relaxation of quadratic mappings for checking convexity. We address such problems as membership oracle and boundary oracle for the quadratic image. Finally the results are illustrated through some examples of 3-bus systems, namely, we detect nonconvexity of them.

Keywords Power flow · Hidden convexity · Quadratic maps

1 Introduction

Various formulations of the Optimal Power Flow problem (OPF) can be found in recent publications [1–3]; numerous references are given in the survey [4]. From mathematical point of view most of them (if transformed into real space) can be

B. Polyak (✉) · E. Gryazina
Institute for Control Sciences, Moscow, Russia
e-mail: boris@ipu.ru

E. Gryazina
e-mail: gryazina@gmail.com

B. Polyak · E. Gryazina
Center for Energy Systems,
Skolkovo Institute of Science and Technology, Moscow, Russia

V. Bertsch et al. (eds.), *Advances in Energy System Optimization*,
Trends in Mathematics, DOI 10.1007/978-3-319-51795-7_14

described as optimization problems with quadratic (or partially linear) objective and constraints. Thus OPF can be considered in the framework of quadratic programming with quadratic constraints. The same class of optimization problems arises in discrete optimization, uncertainty analysis, various physical applications. It is well known that such problems are typically nonconvex and NP-hard. However the special quadratic structure often exhibits so called "hidden convexity" properties, see, e.g. [5, 6]. On the other hand quadratic problems admit efficient techniques of convex relaxation, see [7, 8]; for OPF problems convex relaxation was used in [1, 3]. In what follows we treat OPF as particular case of quadratic optimization. Moreover we proceed from optimization problems to more general setting of images of quadratic maps.

In Sect. 2 we formulate the problem of convexity of quadratic transformations and refer to known results for particular classes of quadratic functions. Power Flow equations do not fit directly to any of the known classes, thus our approach is different — we try to check convexity/nonconvexity of an individual quadratic map. Such certificates of convexity/nonconvexity will be provided in Sect. 3; we also develop efficient algorithms to obtain the certificates. The algorithms exploit convex relaxation technique and so called "boundary oracle" for convex domains. Section 4 contains results on numerical simulation. Conclusions and directions for the future work can be found in final Sect. 5.

2 Convexity of Quadratic Transformations

We consider AC power flow model. The network is characterized by complex admittance matrix

$$Y \in \mathbb{C}^{(\mathcal{N}-1)\times(\mathcal{N}-1)},$$

where $\mathcal{N}$ is the total number of buses (including slack bus with fixed voltage magnitude and phase). Power injections defined by Kirchhoff's laws can be written through matrix Y and complex voltages V_i:

$$s_i = V_i(YV)_i^*, \quad i = 1, \ldots, \mathcal{N}-1.$$

Typical OPF problem is to minimize linear or quadratic cost $c(V)$ subject to quadratic constraints $\underline{s_i} \le s_i \le \overline{s_i}$. We treat all $V \in \mathbb{C}^{\mathcal{N}-1}$ feasible while the constraints are stated in the space of quadratic image of V. Introducing real vector $x = [\mathrm{Re}(V)^T,\ \mathrm{Im}(V)^T]^T$ active and reactive powers are real-valued quadratic functions of x. Further we deal with quadratic transformations in the general setting.

We consider multidimensional quadratic mapping $f : \mathbb{R}^n \to \mathbb{R}^m$ of the form

$$f(x) = (f_1(x), f_2(x), \ldots, f_m(x))^T$$
$$f_i(x) = (A_i x, x) + 2(b_i, x), \quad i = 1, \ldots, m \le n,$$

then

$$E = \{f(x) : x \in \mathbb{R}^n\}$$

is the image of the space of variables x under this quadratic map. We do not assume that matrices A_i are sign-definite; nevertheless E sometimes occur to be convex ("hidden convexity" property). Let us mention some known results of this sort.

- For $m = 2$ and $b_i \equiv 0$ E is convex. This is the pioneering result by Dines [9]. For $m = 2$, $b_i \neq 0$ and $c_1 A_1 + c_2 A_2 \succ 0$ (the matrix combination is positive definite for some c) E is convex as well [10].
- For $m = 3$ E is convex if there exists a positive-definite linear combination of matrices A_1, A_2, A_3 and $b_i \equiv 0$. This is proved in [11] and in [10].
- If $b_i \equiv 0$ and matrices A_i commute, then E is convex [12].
- If A_i have positive off-diagonal entries, then "positive part of E" is convex (i.e. $E + R^m_+$ is convex) [13].

Consider the image of a ball $F = \{f(x) : ||x|| \leq \rho\}$.

- For $m = 2$ and $b_i \equiv 0$ F is convex [14].
- If matrix B with columns b_i is nonsingular and ρ is small enough, then F is convex for all $m, n \geq 2$ ("small ball" theorem [15]).

There are some other classes of quadratic transformations with convex images, however typically E (or F) is nonconvex; numerous examples will be provided later.

3 Certificates of Convexity/Nonconvexity

We remind some known facts on convex relaxations for quadratic optimization and on convex hull for quadratic image.

The idea of convex relaxations for quadratic problems goes back to [16]; recent results and references can be found in [7, 8]. Similar ideas and technique give the convex hull of the image set E, see also [17].

Notation For symmetric matrices $\langle X, Y\rangle = \mathrm{trace}(XY)$, and $X \succeq 0$ denotes nonnegative definite matrix X.

Theorem 1 *The convex hull for the feasibility set E is*

$$G = conv(E) = \{\mathcal{H}(X) : X \succeq 0, X_{n+1,n+1} = 1\},$$

where $X = X^T \in \mathbb{R}^{(n+1)\times(n+1)}$,
$\mathcal{H}(X) = (\langle H_1, X\rangle, \langle H_2, X\rangle, \ldots, \langle H_m, X\rangle)^T$
$H_i = \begin{pmatrix} A_i & b_i \\ b_i^T & 0 \end{pmatrix}$.

Hence we can provide simple sufficient conditions for *membership oracle*, i.e. checking if a particular point $y \in \mathbb{R}^m$ is feasible (belongs to E). Indeed, it is necessary to

have $y \in G$, that is to solve corresponding linear matrix inequality (LMI) [18]. Alternatively, introduce the variable $c \in \mathbb{R}^m$ and construct matrix $A = \sum c_i A_i$, vector $b = \sum c_i b_i$ and block matrix $H(c) = \begin{pmatrix} A & b \\ b^T & -(c, y) \end{pmatrix}$, then the sufficient condition for $y \notin G$ has the form:

Theorem 2 *If there exists c such that for a specified y*

$$H(c) \succ 0,$$

then y is not feasible.

Indeed if the LMI is solvable, there exists the separating hyperplane, defined by its normal c that strictly separates y and $G = conv(E)$, hence y does not belong to E. Now we can proceed to a nonconvexity certificate.

Theorem 3 *Let $m \geq 3$, $n \geq 3$, $b_i \neq 0$, and for some $c = (c_1, c_2, \ldots, c_m)^T$, the matrix $A = \sum c_i A_i \succeq 0$ has a simple zero eigenvalue $Ae = 0$, and for $b = \sum c_i b_i$ we have $(b, e) = 0$. Denote $d = -A^+ b$, $x^\alpha = \alpha e + d$, $f^\alpha = f(x^\alpha) = f^0 + f^1\alpha + f^2\alpha^2$. If $|(f^1, f^2)| < \|f^1\| \cdot \|f^2\|$, then E is nonconvex.*

Geometrically the condition implies that the linear function (c, f) attains its minimum on E at points f^α only. But parabola f^α is nonconvex, thus the supporting hyperplane touches E on a nonconvex set.

Now the main problem is to find c (if exists) which satisfies Theorem 1 and hence discovers nonconvexity of the feasible set. For this purpose let us construct so called *boundary oracle* for G. For given $y^0 \in E$ and the arbitrary direction $d \in \mathbb{R}^m$ the following Semidefinite Program (SDP) [18] with variables $t \in \mathbb{R}$, $X = X^T \in \mathbb{R}^{(n+1)\times(n+1)}$ specifies the boundary point $y^0 + td$ of the convex hull:

$$\begin{aligned} \max\ & t \\ \mathcal{H}(X) &= y^0 + td \\ X &\succeq 0 \\ X_{n+1,n+1} &= 1. \end{aligned} \tag{1}$$

If we obtain $\operatorname{rank}(X) = 1$ for the solution of (1) we claim that the obtained boundary point is on the boundary of E. Otherwise, the boundary point of the convex hull does not belong to E.

On the other hand the dual problem to (1) gives us normal vector c for the boundary point:

$$\begin{aligned} \min\ & \gamma + (c, y^0) \\ (c, d) &= -1 \\ H &= \begin{pmatrix} \sum c_i A_i & \sum c_i b_i \\ \sum c_i b_i^T & \gamma \end{pmatrix} \succeq 0 \end{aligned} \tag{2}$$

This is SDP problem with variables c, γ.

Equipped with boundary oracle technique (which provides both a boundary point of G and the normal vector c in this point) we are able to generate vectors c to identify nonconvexity as in Theorem 1. Thus we arrive to

Algorithm

1. Take arbitrary $x^0 \in \mathbb{R}^n$, calculate $y^0 = f(x^0)$ and fix some N.
2. Generate N random directions d^i on the unit sphere in $\mathbb{R}^m$.
3. For every random direction d^i solve SDP (2). If the obtained c satisfies Theorem 1, we identifyed nonconvexity.

At the first glance, simpler approach can be applied. Take $c \in \mathbb{R}^m$ and minimize (c, y) on G (given by lemma 1) if such minimum exists. If $A = \sum c_i A_i \succ 0$ the minimum is unique and obtained at rank-1 matrix xx^T, $x = A^{-1}b$, $b = \sum c_i b_i$, and x gives a boundary point of the feasibilty set E. However to identify nonconvexity we should find c such that A is singular. The probability of this event is zero if we sample c randomly. In our approach (when we generate directions d) the probability of finding a boundary point on a "flat" part of the boundary of G (which correspond to nonconvex E) is positive. In simulation results nonconvexity was identified in all examples, where it has been recognized by other methods.

To conclude it is the strong support of the convexity assumption if our algorithm does not meet nonconvexity after large number of iterations N for various y^0.

4 Numerical Results

In this section we apply the proposed routine for several test maps. The first one is artificially constructed while the others describe power flow feasibility region for 3-bus networks. Starting form a specified feasible y^0 and $N = 10^4$ we run the algorithm to obtain vector c such that the supporting hyperplane (c, y) touches the image $y(x)$ in more than one point and thus certifies its nonconvexity. We distinguish nonconvexities discovered by different vectors c and examine the portion of random directions d resulted in every c. The results are summarized in Table 1.

Table 1 Numerical results for discovering nonconvexity of test mappings

Source	Map	Number of nonconvexities	Portion of d's per nonconvexity
Artificial	$\mathbb{R}^3 \to \mathbb{R}^3$	3	0.04 0.13 0.03
[19]	$\mathbb{R}^3 \to \mathbb{R}^3$	1	0.02
[20]	$\mathbb{C}^2 \to \mathbb{R}^4$	1	0.06
[21]	$\mathbb{C}^2 \to \mathbb{R}^4$	2	<0.001 <0.001

Artificial system We start with the artificially constructed quadratic mapping $\mathbb{R}^3 \to \mathbb{R}^3$ with

$$A_1 = \begin{pmatrix} 1 & 1 & 1 \\ 1 & 2 & 0 \\ 1 & 0 & 2 \end{pmatrix}, \qquad A_2 = \begin{pmatrix} 3 & -1 & 0 \\ -1 & 0 & -1 \\ 0 & -1 & 1 \end{pmatrix}, \qquad A_3 = I$$
$$b_1 = \begin{pmatrix} 1 & 1 & 1 \end{pmatrix}^T, \qquad b_2 = \begin{pmatrix} 1 & 0 & -1 \end{pmatrix}^T, \qquad b_3 = \begin{pmatrix} 0 & 0 & 0 \end{pmatrix}^T.$$

Note that A_1 is positive semidefinite thus $c^1 = (1, 0, 0)^T$ specifies the supporting hyperplane (c, y) touching the image in more than one point. For this map we obtain two other critical $c^2 = (1, 0.5, -1)^T$ and $c^3 = (1, 4.75, 1.38)^T$. For $y^0 = (0, 1, 1)^T$ the portion for every c is given in Table 1. We analytically justify that there is no other c specifying nonconvexity for this map and plot several 2-D sections of the image in $\mathbb{R}^3$ (Fig. 1). For fixed $0 \le y_3 \le 1/3$ the section appears to be convex and for $y_3 = 4$ we visualize all three nonconvexities.

Constant power loads [19] This example is borrowed form [19], where feasible points of E are addressed as equilibria of system with constant power loads. The map of interest has the form:

$$P_1(x) = x_1^2 - 0.5x_1x_2 + x_1x_3 - 1.5x_1$$
$$P_2(x) = x_2^2 - 0.5x_1x_2 - x_2x_3 + 0.5x_2$$
$$P_3(x) = x_3^2 - 2\epsilon x_3(x_1 + x_2) - x_3, \quad \epsilon = 0.01.$$

For $P^0 = (0.5, 0.5, 0.25)^T$ we obtain a single $c = (1, 2.9021, 0.7329)^T$ identifying nonconvexity. It means that the supporting parabola

$$f^\alpha = \begin{pmatrix} -0.5442 \\ 0.0022 \\ -0.0339 \end{pmatrix} + \alpha \begin{pmatrix} 0.5043 \\ 0.0400 \\ -0.8463 \end{pmatrix} + \alpha^2 \begin{pmatrix} -0.0022 \\ -0.1991 \\ 0.7912 \end{pmatrix}$$

provides boundary points for the image $P(x)$, $x \in \mathbb{R}^3$ but the convex combination of two boundary points $\lambda f^{\alpha_1} + (1 - \lambda) f^{\alpha_2}$ is infeasible for $0 < \alpha < 1$, $f^{\alpha_1} \ne f^{\alpha_2}$.

3-bus [20] Consider tree unbalanced 3-bus system (1 slack, 2 PQ-buses) with the admittance matrix

$$Y = \begin{pmatrix} -1 & 1 & 0 \\ 1 & -2 - i & 1 + i \\ 0 & 1 + i & -1 - i \end{pmatrix}.$$

The feasibility region in the space of P_2, Q_2, P_3, Q_3 is known to be nonconvex [20]. Here P_i and Q_i denote active and reactive power at the i-th bus,

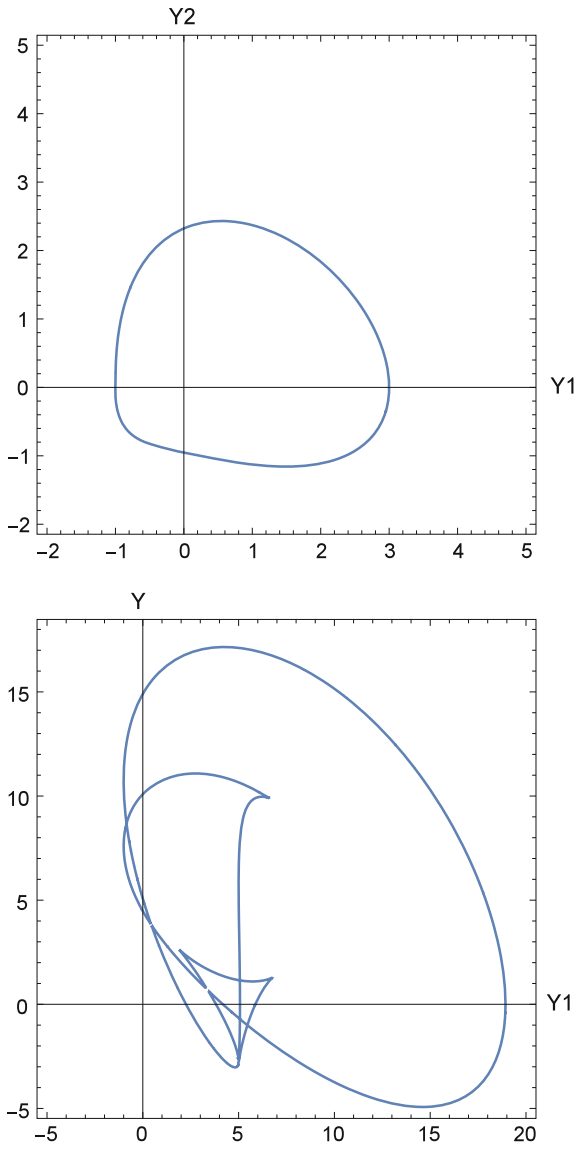

Fig. 1 Two sections of the feasibility domain: first we fix $y_3 = 1/3$ and obtain convex section, then for $y_3 = 4$ the section is nonconvex

$y = (P_2, Q_2, P_3, Q_3)^T$. For $y^0 = (0, 0, 1, 1)^T$ our numerical routing obtains the single c generating nonconvexity for approximately 6% of random directions.

3-bus [21] This example of 3-bus cycle network with slack, PV and PQ-bus is borrowed from [21] (Fig. 2).

Power flow equations take the form

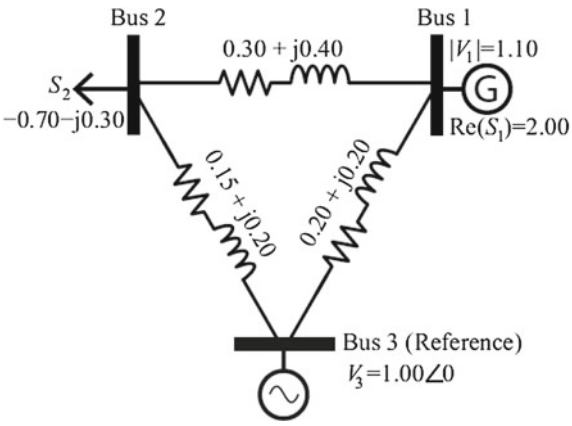

Fig. 2 Three-bus system

$$
\begin{aligned}
P_1 &= x^T \begin{pmatrix} 3.7 & -0.6 & 0 & -0.8 \\ -0.6 & 0 & 0.8 & 0 \\ 0 & 0.8 & 3.7 & -0.6 \\ -0.8 & 0 & -0.6 & 0 \end{pmatrix} x + \\
&\quad + 2((-1.25, 0, 1.25, 0)^T, x), \\
V_1 &= x_1^2 + x_3^2, \\
P_2 &= x^T \begin{pmatrix} 0 & -0.6 & 0 & 0.8 \\ -0.6 & 3.6 & -0.8 & 0 \\ 0 & -0.8 & 0 & -0.6 \\ 0.8 & 0 & -0.6 & 3.6 \end{pmatrix} x + \\
&\quad + 2((0, -1.2, 0, 1.6)^T, x), \\
Q_2 &= x^T \begin{pmatrix} 0 & -0.8 & 0 & -0.6 \\ -0.8 & 4.8 & 0.6 & 0 \\ 0 & 0.6 & 0 & -0.8 \\ -0.6 & 0 & -0.8 & 4.8 \end{pmatrix} x + \\
&\quad + 2((0, -1.6, 0, -1.2)^T, x).
\end{aligned}
$$

We remind that $x = (\mathrm{Re}V_1,\ \mathrm{Re}V_2,\ \mathrm{Im}V_1,\ \mathrm{Im}V_2)^T$ and $V_3 = 1$ for slack bus. Starting at the given operation regime $P_1 = 2$, $V_1^2 = 1.21$, $P_2 = -0.7$, $Q_2 = -0.3$ we obtain at least two vectors c identifying nonconvexity but it requires more computational effort than in previous examples. Although our routine is capable to catch nonconvexity with probability one we are not sure that obtained vectors describe all the nonconvexities for this system.

The example may look artificial since the line resistances are as high as the reactances. We run our algorithm for the five times larger line reactances to model transmission grid and still discover nonconvexity of the image.

Remark We do not propose any routine to solve power flow equation, and we do not pretend to compete with any power flow solvers, neither DC equations nor iterative methods. Our method is focused on the certification and numerical description of nonconvexities of the image that is the reason for inexactness of convex relaxation for OPF.

5 Conclusions and Future Work

The paper addresses power flow analysis in the framework of quadratic transformations geometry. We provide some conditions which guarantee convexity of a quadratic image and numerical tools to identify nonconvexity. Simulation confirms that the technique works for low-dimensional examples. We plan to apply the analysis for medium-dimensional and large-dimensional problems in future. For instance IEEE-14-bus test is one of the first candidates.

The key question is how to deal if nonconvexity is identfied. There are some promising ideas for this case, for instance, based on [22] cutting plane approach can be introduced to specify convex parts of the feasibility region. The proposed algorithm could be potentially improved by finding appropriate y^0, incorporating other algorithms for boundary walk, efficient algorithms for solving arising SDP. All the issues mentioned above establish the future research plan.

Acknowledgements The authors are thankful to Anatoly Dymarsky and Prof. Steven Low for rising our interest to power flow analysis and to Prof. Janusz Bialek who gave us opportunity working together. The collaboration between Institute for Control Sciences RAS and Center for Energy Systems of Skolkovo Institute of Science and Technology is gratefully acknowledged.

References

1. S. Low, Convex Relaxation of Optimal Power Flow Part I: Formulations and Equivalence *IEEE Trans. Control of Network Systems*, 1(1), 15–27, (2014), Part II: Exactness, 1(2): 177–189, (2014)
2. S. Low, Mathematical Methods for Internet Congestion Control and Power System Analysis, Lecture Notes (in press).
3. J. Lavaei and S. Low, Zero Duality Gap in Optimal Power Flow Problem *IEEE Transactions on Power Systems*, 27(1), 92–107, (2012)
4. S. Frank, I. Stepanovice and S. Rebennack, Optimal Power Flow: A Bibliographic Survey, *Energy Systems*, 2012, 221–289, (2012)
5. A. Ben-Tal and M. Teboulle, Hidden convexity in some nonconvex quadratically constrained quadratic programming, *Mathematical Programming*, 72(1), 51–63, (1996).
6. J.-B. Hiriart-Urruty, M. Torki, Permanently going back and forth between the "quadratic world" and the "convexity world" in optimization, *Appl. Math. and Optim.*, 45, 169–184, (2002)
7. Luo, Z. Q., Ma, W. K., So, A. M. C., Ye, Y., and S. Zhang. Semidefinite relaxation of quadratic optimization problems, *IEEE Signal Processing Magazine*, 27(3), 20–34. (2010)
8. S. Zhang, Quadratic optimization and semidefinite relaxation, *Mathematical Programming*, 87, 453–465, (2000)

9. L.L. Dines, On the mapping of quadratic forms *Bull. Amer. Math. Soc.*, 47, 494–498, (1941).
10. B.T. Polyak, Convexity of quadratic transformations and its use in control and optimization *Journal of Optimization Theory and Applications*, 99, 553–583, (1998)
11. E. Calabi, Linear Systems of Real Quadratic Forms, *Proceedings AMS*, 84(3), 331–334, (1982)
12. A. L. Fradkov, Duality Theorems for Certain Nonconvex Extremum Problems, *Siberian Mathematical Journal*, 14, 247–264, (1973)
13. S. Kim, M. Kojima, Exact Solutions of Some Nonconvex Quadratic Optimization Problems via SDP and SOCP Relaxations, *Computational Optimization and Applications*, 26, 143–154, (2003)
14. L. Brickman, On the field of values of a matrix, *Proc. Amer. Math. Soc.*, 12, 61–66, (1961).
15. B.T. Polyak, Convexity of nonlinear image of a small ball with applications to optimization, *Set-Valued Analysis*, 9(1/2), 159–168, (2001)
16. N.Z.Shor, Quadratic Optimization Problems, *Soviet J. of Computer and Syst. Sci.*, 25(6), 1–11, (1987)
17. A. Beck, On the convexity of a class of quadratic mappings, *J. of Global Opt.*, 39(1), 113–126, (2007)
18. S. Boyd, L. El Ghaoui, E. Feron, and V. Balakrishnan, Linear Matrix Inequalities in System and Control Theory, Volume 15 of Studies in Applied Mathematics Society for Industrial and Applied Mathematics, SIAM, (1994)
19. N. Barabanov, R. Ortega R.Grino and B. Polyak, On existence and stability of equilibria of linear time-invariant systems with constant power loads, *IEEE Transactions on Circuits and Systems IRegular papers*, 63(1), 114–121, (2016)
20. A. Dymarsky and K. Turitsyn, Convex partitioning of the power flow feasibility region, (2014).
21. S. Baghsorkhi and S. Suetin, Embedding AC Power Flow with Voltage Control in the Complex Plane: The Case of Analytic Continuation via Pade Approximants, arXiv:1504.03249.
22. A. Dymarsky, On the Convexity of Image of a Multidimensional Quadratic Map, *Linear Algebra and its Applications*, 488, 109–123, (2016)

A Convex Model for the Optimization of Distribution Systems with Distributed Generation

Mariana Resener, Sérgio Haffner, Panos M. Pardalos and Luís A. Pereira

Abstract This work presents a convex model to be used in the analysis and optimization of power distribution systems with distributed generation (DG). The steady-state operation point is calculated through a linearized model of the network, which makes it possible to calculate the branch currents and bus voltages through linear expressions. The optimization model proposed to optimize the operation of capacitor banks and DGs uses a linear objective function, along with linear constraints, binary and continuous variables. The model can be applied to problems related to the operation and expansion of smart grids. A study case using real distribution system data is presented, comparing the results with the solution of the nonlinear load flow.

Keywords Distribution systems optimization · Distributed generation · Distribution system modeling · Mixed integer linear programming

1 Introduction

The problem of power systems expansion and operation planning is a mixed integer problem by its nature [15]. One of the goals when planning a power distribution system (PDS) is the power losses minimization, which is essentially nonlinear and, therefore, usually modeled as a mixed integer nonlinear programming problem [4]. This problem can be non-convex with many local minima, challenging the global minimum solution achievement. Furthermore, this is a large scale combinatorial

M. Resener (✉) · S. Haffner · L.A. Pereira
Federal University of Rio Grande do Sul, Porto Alegre, Brazil
e-mail: mariresener@gmail.com

S. Haffner
e-mail: haffner@ieee.org

L.A. Pereira
e-mail: lpereira@ufrgs.br

P.M. Pardalos · M. Resener
University of Florida, Gainesville, FL, USA
e-mail: pardalos@ufl.edu

V. Bertsch et al. (eds.), *Advances in Energy System Optimization*,
Trends in Mathematics, DOI 10.1007/978-3-319-51795-7_15

problem in which the options to be analyzed increase with the size of the PDS, becoming even more difficult to solve when different load levels are considered, since the operation of automatic equipment, such as a capacitor bank (CB), must be optimized too. Heuristics are often employed to solve such problems, as the solution is a challenging computational process [10].

The connection of distributed generation (DG) in PDS brought new technical issues to be analyzed when planning and operating the network. From the point of view of network operation, this transition from passive to active networks has impacts on voltage profiles and energy losses, as power injections from DGs modify network power flows, besides changing the maintenance and system restoration practices [12]. The implications are technical and economical [2], and depend strongly on the amount of generated power. The extent of the impacts also depends on the specific characteristics of the PDS, the location of the DG along the feeder and the type of output (firm or variable) [9].

In this context, the definition of the operation mode of control and protection devices becomes more complex, as it needs to take into account all the modes that DGs will be authorized to operate. Thus, a model for verifying the impacts of the inclusion of DG units in PDS becomes very important and useful to allow the formulation and solution of problems related to the optimal planning of operation and expansion of these systems [5–7].

The complexities related to DG presence in distribution systems are difficult to incorporate into an optimization model for improvement of voltage profile and energy loss minimization, and still represent a challenge [9]. Also, the presence of smart grids makes it possible to operate the PDS in a more efficient way, specially when there are DGs connected, since the number of controls available in this case is greater than in conventional networks. This potential advantage can be more explored so as to optimize the operation of PDS [9]. Several studies have been realized to evaluate energy losses and voltage profile in PDS with DG. The optimal DG allocation problem has been extensively explored, and is in general associated to heuristic methods [1, 14]. Other authors analyzed the reactive power control strategy for the DGs and its impacts on power losses [11] and proposed a planning methodology to better explore the DG reactive power dispatch capability [3].

Since the load behavior presents many uncertainties and varies along the day, it is impossible to obtain a model capable of exactly representing a PDS. Even detailed models can show significant differences with respect to what is really happening on the system, since it is difficult to determine the individual behavior of the consumers. In this context, a linearized model is developed and applied in this work, which gives a satisfactory representation of the network and allows the solution of PDS optimization problems using classical optimization techniques. Moreover, using a linear approach it is easy to incorporate linear constraints, without turning the model more difficult to solve.

In this work, the proposed model is applied to evaluate and determine the best operation mode for the DGs, aiming to minimize energy losses and voltage violations, besides optimizing the operation of automatic CBs. This flexibility represents an advantage with respect to the conventional load flow methodology, where a gen-

erator bus has to be previously defined as a PV or PQ bus and it is not allowed to automatically adjust the voltage or the injection power to attend a specific objective, as the power losses minimization.

The proposed optimization model uses a linear objective function, along with linear constraints, binary and continuous variables. Therefore, the optimization problem can be represented as a mixed integer linear programming problem (MILP). The objective function to be minimized represents the total operation costs, which are related to the energy losses and violation of voltage limits. To represent the absolute value of the violation of voltage limits, auxiliary variables and linear constraints are applied. Thus, it is not necessary to impose limits to the voltage magnitudes at the buses, avoiding the problem to become unfeasible if the violation of voltage limits cannot be eliminated. This situation can occur when handling with problems related to the optimization of PDS operation, in which no investment is considered.

2 Steady-State Representation of PDS

The behavior of the feeders at steady-state is obtained using a linearized model, with the following characteristics:

- the system is divided into buses, at which loads and sources are concentrated, and branches, which connect buses and represent the feeder route;
- the load variation is represented by discrete load levels (hereinafter a load level is referred as LL);
- each bus has three variables related to each LL: voltage magnitude, real and imaginary part of the demanded current;
- each branch has five variables related to each LL: real and imaginary part of the current, square of the real and the imaginary part of the current, and power losses;
- the power losses are calculated using an approximation for both the squared real part and the imaginary part of the branch current;
- fixed CBs operate at all LLs, while automatic CBs operate when necessary;
- voltage violations are evaluated for all buses with load and for all LLs;
- the objective function corresponds to the minimization of the operational costs.

2.1 Representation of Voltage Violation

In this model, the voltage violations are calculated for each loaded bus and for all load levels through the following expression:

$$z_{i,j} = \begin{cases} V_{i,j} - V_i^{\max} & \text{if } V_{i,j} > V_i^{\max} \\ V_i^{\min} - V_{i,j} & \text{if } V_{i,j} < V_i^{\min} \\ 0 & \text{otherwise} \end{cases} \quad (1)$$

where $V_i^{\min}$ and $V_i^{\max}$ are the minimum and maximum voltage limits, respectively, at bus i, and $V_{i,j}$ is the voltage at bus i and load level j. The piecewise linear function (1) is replaced by an equivalent linear programming model as follows:

$$\begin{aligned} \min \quad & z_{i,j} \\ \text{subject to} \quad & z_{i,j} \geq V_{i,j} - V_i^{\max} \\ & z_{i,j} \geq V_i^{\min} - V_{i,j} \\ & z_{i,j} \geq 0 \end{aligned} \tag{2}$$

2.2 Representation of Power Losses

The power losses are estimated through linear expressions in which the magnitude of a branch current flow can take positive or negative values. The current flow in a branch i for a load level j is defined as follows:

$$f_{i,j} = f_{i,j}^{\text{Re}} + j f_{i,j}^{\text{Im}} \tag{3}$$

where $f_{i,j}^{\text{Re}}$ and $f_{i,j}^{\text{Im}}$ represent, respectively, the real and the imaginary part of the current in branch i for the load level j. The square of the magnitude of $f_{i,j}$ is calculated from the following expression:

$$\left| f_{i,j} \right|^2 = (f_{i,j}^{\text{Re}})^2 + (f_{i,j}^{\text{Im}})^2 \tag{4}$$

Using (4), the active power losses in branch i and load level j can be obtained from:

$$P_{i,j}^{\text{loss}} = R_i \left| f_{i,j} \right|^2 = R_i (f_{i,j}^{\text{Re}})^2 + R_i (f_{i,j}^{\text{Im}})^2 \tag{5}$$

where R_i is the real part of the impedance of the branch i.

The terms $(f_{i,j}^{\text{Re}})^2$ and $(f_{i,j}^{\text{Im}})^2$ can be approximated by $f_{i,j}^{2\text{Re}}$ and $f_{i,j}^{2\text{Im}}$, respectively, using a set of linear expressions [13]. These expressions are defined as:

$$\left(f_{i,j}^{\text{Re}}\right)^2 \approx f_{i,j}^{2\text{Re}} \geq a_k f_{i,j}^{\text{Re}} + b_k \tag{6}$$

$$\left(f_{i,j}^{\text{Im}}\right)^2 \approx f_{i,j}^{2\text{Im}} \geq a_k f_{i,j}^{\text{Im}} + b_k \tag{7}$$

where $k = 1, 2, \ldots, N^{LC}$, a_k and b_k are constants and N^{LC} is the number of linear constraints. So, the squared terms of (5) are approximated by simple linear equations. Figure 1 shows the linear constraints for $\left(f_{i,j}^{\text{Re}}\right)^2$, considering $N^{LC} = 10$. The a_k and b_k coefficients values are presented in Table 1.

Additionally, heed that it is necessary to include the terms $f_{i,j}^{2\text{Re}}$ and $f_{i,j}^{2\text{Im}}$ into the objective function to ensure that the approximation remains valid. These terms are

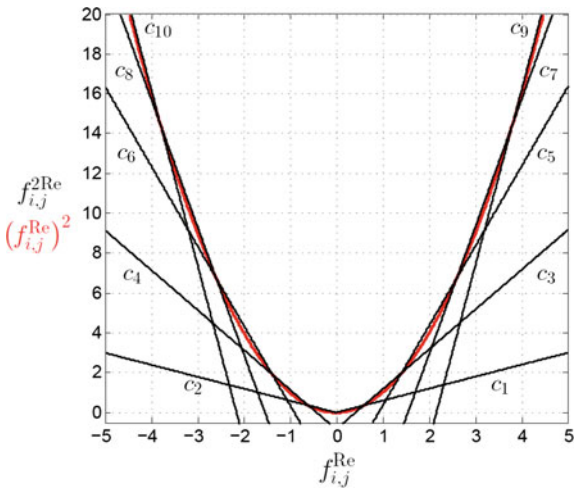

Fig. 1 Linear approximation of the square of the real part of the current

Table 1 Coefficients for the estimation of power losses

k	a_k	b_k	k	a_k	b_k
1	0.6	0	6	−4	−3.64
2	−0.6	0	7	6.4	−9.88
3	2	−0.84	8	−6.4	−9.88
4	−2	−0.84	9	8.8	−19
5	4	−3.64	10	−8.8	−19

minimized when the optimization problem is solved. By increasing N^{LC}, the exact value can be closely attained.

2.3 Representation of Generators

The buses with generation capacity (substation or distributed generation) are represented by current injections, with real and imaginary components. One bus is selected to close the current flow balance and the others can operate in distinct ways. In general, every bus with generation capacity must operate within these limits:

$$V_{i,j}^{\min} \leq V_{i,j} \leq V_{i,j}^{\max} \tag{8}$$

$$g_{\min,i,j}^{\mathrm{Re}} \leq g_{i,j}^{\mathrm{Re}} \leq g_{\max,i,j}^{\mathrm{Re}} \tag{9}$$

$$g_{\min,i,j}^{\mathrm{Im}} \leq g_{i,j}^{\mathrm{Im}} \leq g_{\max,i,j}^{\mathrm{Im}} \tag{10}$$

where, for the bus i and LL j, $V_{i,j}^{\min}$ and $V_{i,j}^{\max}$ represent the minimum and maximum voltage limits, $g_{\min,i,j}^{\mathrm{Re}}$, $g_{\max,i,j}^{\mathrm{Re}}$, $g_{\min,i,j}^{\mathrm{Im}}$ and $g_{\max,i,j}^{\mathrm{Im}}$ represent the limits for the real and imaginary current injections.

Therefore, using simple linear expressions it is possible to define the operation mode of the generators, or even determine the optimal mode. For example, by properly defining the limits of the expressions (8)–(10) it is possible to represent three different operation modes:

PQ bus The active and reactive current injections are known. In this case, the voltage is calculated and the constraints (9) and (10) are defined as:

$$g_{\min,i,j}^{\mathrm{Re}} = g_{\max,i,j}^{\mathrm{Re}} = g_{\mathrm{sp},i,j}^{\mathrm{Re}} \tag{11}$$

$$g_{\min,i,j}^{\mathrm{Im}} = g_{\max,i,j}^{\mathrm{Im}} = g_{\mathrm{sp},i,j}^{\mathrm{Im}} \tag{12}$$

where $g_{\mathrm{sp},i,j}^{\mathrm{Re}}$ and $g_{\mathrm{sp},i,j}^{\mathrm{Im}}$ are the specified values for the real and the imaginary current injections.

Power factor (PF) range In this case, the reactive current injection can vary according to a specified PF range. To represent this operation mode, the following limits are defined:

$$g_{\min,i,j}^{\mathrm{Im}} = -(g_{i,j}^{\mathrm{Re}})\sqrt{\frac{1}{(\mathrm{PF}_{\mathrm{sp},i}^{\mathrm{ind}})^2} - 1} \tag{13}$$

$$g_{\max,i,j}^{\mathrm{Im}} = \ (g_{i,j}^{\mathrm{Re}})\sqrt{\frac{1}{(\mathrm{PF}_{\mathrm{sp},i}^{\mathrm{cap}})^2} - 1} \tag{14}$$

where $\mathrm{PF}_{\mathrm{sp},i}^{\mathrm{cap}}$ and $\mathrm{PF}_{\mathrm{sp},i}^{\mathrm{ind}}$ represent, respectively, the capacitive and inductive PF limits of bus i. Note that the active current injection or the voltage can be either optimized or constrained using (8) and (9).

Voltage controlled bus (PV bus) In this operation mode both the active current injection and the voltage are specified. The active current injection limits can be defined as in (11) and the voltage limits as follows:

$$V_{i,j}^{\min} = V_{i,j}^{\max} = V_{i,j}^{\mathrm{sp}} \tag{15}$$

being $V_{i,j}^{\mathrm{sp}}$ the specified voltage for bus i during LL j.

3 Optimization Model

In this work, the objective function accounts for the network operation costs, which are related to the costs of violation of voltage limits and energy losses. These costs are weighted by the duration of each LL. The total operation costs are given by:

$$C^{\text{oper}}(\mathbf{z}, \mathbf{p}) = \sum_{j=1}^{LL} C_j^v(\mathbf{z}_j) + \sum_{j=1}^{LL} C_j^l(\mathbf{p}_j) \tag{16}$$

$$C_j^v(\mathbf{z}_j) = \Delta T_j \sum_{i \in \Psi^D} CV_i z_{i,j} \tag{17}$$

$$C_j^l(\mathbf{p}_j) = C^{\text{kWh}} \Delta T_j S_{\text{base}} \sum_{i \in \Psi^B} P_{i,j}^{\text{loss}} \tag{18}$$

where the variables represent:

$\mathbf{z}$	vector of voltage violations for all LLs [pu];
$\mathbf{p}$	vector of power losses for all LLs [kW];
$C_j^v(\cdot)$	daily cost of voltage violation at LL j [US$];
$C_j^l(\cdot)$	daily cost of energy losses at LL j [US$];
LL	number of load levels;
$\mathbf{z}_j$	vector of voltage violations at LL j [pu];
$\mathbf{p}_j$	vector of power losses at LL j [pu];
ΔT_j	daily duration of LL j [hour];
S_{base}	base power [kVA];
CV_i	cost of the voltage violation [US$];
$z_{i,j}$	voltage violation at bus i and LL j [pu];
C^{kWh}	energy cost per kWh [US$/kWh];
$P_{i,j}^{\text{loss}}$	power losses of branch i and LL j [pu];
Ψ^D	set of buses with load;
Ψ^B	set of branches.

3.1 Constraints

The constraints used in this model are obtained from the Kirchhoff's Laws and the operational limits of equipment. The loads, sources (substation and distributed generation), and shunt compensation units (usually capacitors) are represented by current injections, which have two components: a real component, related to the active power, and an imaginary component, related to the reactive power. Applying the Kirchhoff's Current Law to all buses and all LLs ($\forall j = 1, 2, \ldots, LL$), it is possible to show that:

$$\mathbf{Sf}_j^{\text{Re}} + \mathbf{g}_j^{\text{Re}} = \mathbf{d}_j^{\text{Re}} \tag{19}$$

$$\mathbf{q}^F + \mathbf{Q}^A \mathbf{y}_j^A + \mathbf{Sf}_j^{\text{Im}} + \mathbf{g}_j^{\text{Im}} = \mathbf{d}_j^{\text{Im}} \tag{20}$$

where:

$\mathbf{S}$	bus-branch incidence matrix of the system;
$\mathbf{f}_j^{\text{Re}}$,$\mathbf{f}_j^{\text{Im}}$	vector of real and imaginary branch currents at LL j [pu];
$\mathbf{g}_j^{\text{Re}}$,$\mathbf{g}_j^{\text{Im}}$	vector of real and imaginary current injections at LL j [pu];
$\mathbf{d}_j^{\text{Re}}$,$\mathbf{d}_j^{\text{Im}}$	vector of real and imaginary load currents at LL j [pu];
$\mathbf{q}^F$	vector of current injections related to fixed CBs;
$\mathbf{Q}^A$	matrix of current injections related to automatic CBs;
$\mathbf{y}_j^A$	vector of operation variables related to automatic CBs at LL j.

Equation (20) considers the contribution of both fixed and automatic CBs in operation at the respective load level.

Applying the Kirchhoff's Voltage Law to all branches ($\forall i \in \Psi^B$) and to all LLs ($\forall j = 1, 2, \ldots, LL$) yields:

$$K_{i,j} R_i f_{i,j}^{\text{Re}} - X_i f_{i,j}^{\text{Im}} + [\mathbf{S}']_{\text{line i}} \mathbf{V}_j = 0 \tag{21}$$

where X_i is the imaginary part of the branch impedance, and where the superscript $'$ indicates the transposed matrix. The adjustment factor $K_{i,j}$ is calculated for all branches and for all LLs for a given base case of the system, so that the solution obtained with the approximated model equals the exact solution obtained through a load flow procedure, for a given neighborhood of the operation point. The factor $K_{i,j}$ is calculated by:

$$K_{i,j} = \frac{\Delta V_{i,j}^{\text{LF}} + X_i f_{i,j}^{\text{Im}}}{R_i f_{i,j}^{\text{Re}}} \tag{22}$$

where $\Delta V_{i,j}^{\text{LF}}$ is the voltage drop in branch i, obtained from a conventional load flow procedure. The $K_{i,j}$ factors are calculated for the base case and then used to calculate the voltage drops using Eq. (21).

Regarding the current capacity of the conductors, from (4), (6), and (7), it is possible to define linear constraints to limit the current in branches as follows:

$$f_{i,j}^{2\text{Re}} + f_{i,j}^{2\text{Im}} \leq \left| f_i^{\max} \right|^2 \tag{23}$$

where $f_i^{\max}$ is the current capacity of the conductors of the branch i.

4 Tests and Results

The proposed model for the PDS optimization problem was written in the mathematical programming language OPL [16] and solved using the solver CPLEX (called with default options) [8], using a workstation with an Intel $i7$-2640M processor.

The model was tested in a test feeder based on real distribution system data from a brazilian energy company. The 155-bus distribution system, illustrated in Fig. 2,

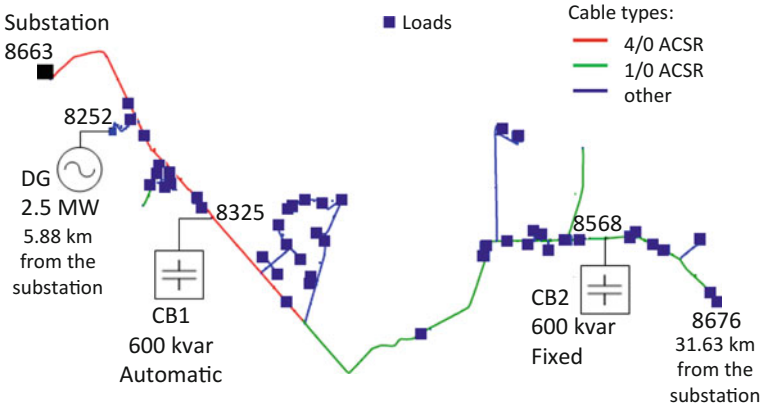

Fig. 2 System diagram

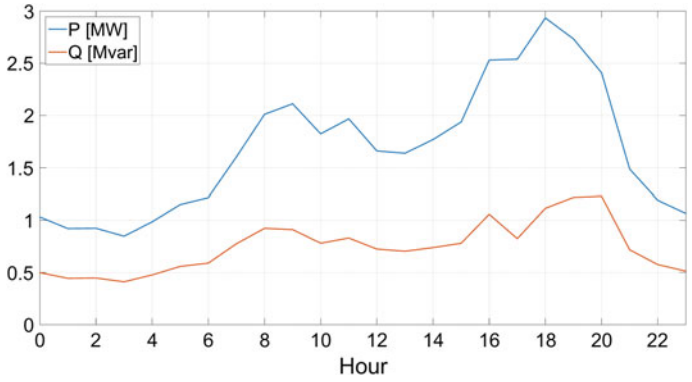

Fig. 3 Load profile

operates at 13.8 kV and is supplied by a 50 MVA 138/13.8 kV substation. The system has a total line length of 57.6 km and feeds 56 load buses. The line data is presented in the Appendix section. One 600 kvar automatic CB is connected at bus 8325 (CB1) and one fixed 600 kvar CB is connected at bus 8568 (CB2), as shown in Fig. 2. Also, a synchronous distributed generator is connected at bus 8252, delivering 2.5 MW to the grid.

Regarding the load behavior, a typical daily load curve with 24 load levels was considered, each level with a duration equal to 1 h. Figure 3 presents the load profile of the feeder, obtained by the summation of the active and reactive power of the loads. The maximum load demand is equal to $2934.07 + j1115.226$ kVA, while the minimum load demand is $848.115 + j411.04$ kVA. The loads have distinct consumption profiles, as well as a varying power factor during the day. In order to illustrate the time variability of the loads, Table 2 presents the maximum and minimum apparent

Table 2 Load data

Bus	Maximum		Minimum		Average	Standard
	Demand (kVA)	Hour	Demand (kVA)	Hour	Demand (kVA)	Deviation (kVA)
8315	785.37	18	143.10	5	399.45	222.00
8635	138.50	20	25.63	6	56.10	27.78
8804	175.70	19	65.52	4	106.79	32.00
8965	54.00	17	8.76	2	23.66	12.62
8337	0.48	20	0.07	6	0.18	0.10

power of some loads, as well as the load level (hour of the day) at which they occur. It is also presented the average and the standard deviation values.

In order to illustrate the characteristics and advantages of the proposed formulation, in this section it is applied to some test cases, varying the operation mode of the DG connected at bus 8252. Three scenarios were considered: (i) the DG operates as a PV bus, with a voltage reference equal to 1 pu; (ii) the DG operates as a PQ bus, with unity power factor; (iii) the DG voltage reference is determined in order to obtain a lower operation cost. In the first two cases the substation voltage was limited to 1 pu, and in the last case it was determined using the proposed formulation. During the optimization process, the automatic CB unit operation is also optimized.

The results obtained with the proposed linear formulation were compared to those obtained through the solution of the nonlinear load flow. For the nonlinear load flow solution, the CBs were modeled as 100% constant impedance, the loads as 50% constant power and 50% constant impedance and the DG as 100% constant power. The voltage violation cost was considered to be $CV_i = 10$ US$, $\forall i \in \Psi^D$ and the energy cost $C^{\text{kWh}} = 0.11$ US$/kWh. The voltage limits for the loaded buses were defined as $V_i^{\min} = 0.93$ pu and $V_i^{\max} = 1.05$ pu.

4.1 DG as a PV Bus

In this test case, the DG was considered to be operating with a fixed voltage reference equal to 1 pu. The DG reactive power limits were accounted too, with a corresponding power factor of 0.8 (capacitive or inductive). The optimization process found a solution of US$ 221.37 in 56.5 s.

The results obtained using the linearized model (LM) are presented in Table 3. The optimal solution indicates that the automatic CB at bus 8325 needs to be turned on between 18 and 20 h, and off during the other load levels. To compare the results from the LM and the nonlinear model, the optimal solution obtained through the LM was verified using the nonlinear load flow, being the results presented in the column indicated by LF in Table 3.

Table 3 Optimization results - Case 1

Results	LM	LF
$\sum_{i,j} z_{i,j}$ (pu)	0.1256	0.2392
Energy losses (kWh/day)	2001.04	1971.79
C^{oper} (US$)	221.37	219.29

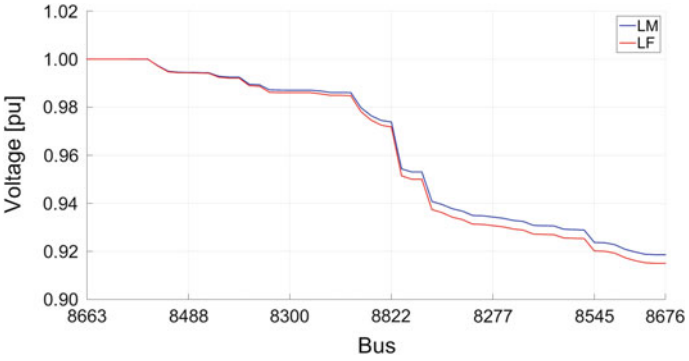

Fig. 4 Voltage profile

From Table 3 it is possible to observe a good agreement between the results obtained with the LM and with the nonlinear load flow. Regarding the total operation costs, a divergence of less than 1.0% is found, taking the LF value as basis. With respect to the bus voltages, the greatest divergence is 0.0036 pu and occurs at the load level corresponding to 18 h. Figure 4 presents the voltage profile from the substation bus (8663) to the bus 8676, for the 18 h load level, where it is possible to observe an excellent agreement between the voltage values obtained with LM and with the nonlinear load flow.

4.2 DG as a PQ Bus

Considering the DG operating as a PQ bus with unity power factor, the optimization problem was solved in order to optimize the operation of the automatic CB unit. The optimization process found a solution of US$ 193.63 in a time of 56.4 s. The results are presented in Table 4, where the optimal solution indicates that the automatic CB at bus 8325 must be turned on between 18 and 20 h, and off during the other LLs.

Table 4 shows a good agreement between the results obtained with the LM and with the nonlinear load flow method. The percent error in the total operation costs is 2.27% taking the LF value as basis. The greatest divergence between the voltage values is 0.0047 pu.

Table 4 Optimization results - Case 2

Results	LM	LF
$\sum_{i,j} z_{i,j}$ (pu)	0.0663	0.1476
Energy losses (kWh/day)	1754.23	1707.74
C^{oper} (US$)	193.63	189.33

Table 5 Optimization results - Case 3

Results	LM	LF
$\sum_{i,j} z_{i,j}$ (pu)	0.0000	0.0053
Energy losses (kWh/day)	1744.40	1686.87
C^{oper} (US$)	191.88	185.61

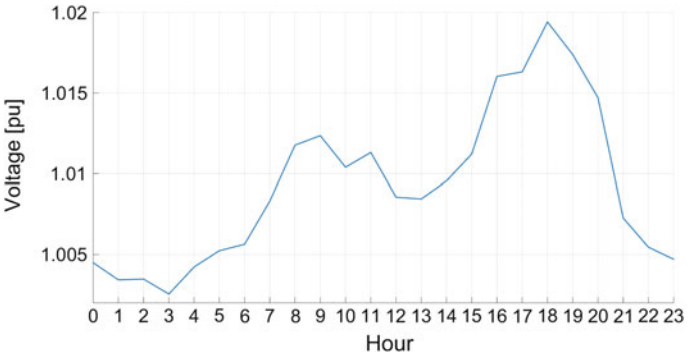

Fig. 5 Substation voltage

4.3 Determination of the DG Operation Point

In this test case, the optimization problem was solved considering $V^{\min} = 0.93$ pu and $V^{\max} = 1.05$ pu as voltage limits at the connection point of the DG (bus 8252). A constraint was used in order to impose the same DG voltage reference for all 24 LLs, although it would have been possible to obtain a different value for each LL. This constraint assumes an automatic voltage regulator with just one value for the voltage reference. Furthermore, in this test case the substation voltage limits were defined as $V^{\min} = 0.95$ pu and $V^{\max} = 1.05$ pu, instead of being fixed at 1.0 pu as in the previous cases.

The optimization process found a solution in a time of 56.7 s, equal to US$ 191.88, being the results presented in Table 5. The optimal solution indicates that the automatic CB at bus 8325 remains turned off during all LLs. Also, the DG voltage reference was determined as being 1.0217 pu and the substation voltage for each LL varies between 1.0026 pu and 1.0194, as shown in Fig. 5.

According to Table 5, the energy losses decreased in comparison to the losses obtained for a DG voltage reference and a substation voltage of 1.0 pu (see Table 3). Moreover, a reduction of 13.32% in the total operation costs resulted. As in the preceding cases, a good agreement was verified between the results from the LM and from the solution of the nonlinear load flow. The error in the total costs is approximately 3.38%, while the greatest divergence between the voltage values is 0.0028 pu.

5 Conclusions

A mixed integer linear programming model (MILP) for the optimization of distribution systems with DG was presented. Using a MILP approach, there are sufficient conditions that guarantee the optimality of a given feasible solution, besides allowing the solution to be obtained by classical optimization methods. The proposed formulation represents an alternative to the usual approach that uses the nonlinear load flow equations in conjunction with heuristic methods to solve PDS optimization problems.

Balanced three-phase systems and loads are assumed, although the formulation can be easily extended to consider single-phase and two-phase systems, besides unbalanced loads. The test results demonstrated a close agreement between the results obtained with the linearized model and with the nonlinear load flow, considering different load levels and including DG. Furthermore, it was considered just one daily load curve, although it would have been possible to consider different load curves, applying the formulation to different operation planning horizons.

The application of the proposed formulation to solve expansion planning problems of PDS is presented in [17].

Acknowledgements M. Resener thanks CAPES for the research support associated with grant 0411/15-9. P. M. Pardalos is partially supported by LATNA Laboratory, NRU HSE, RF government grant, ag. 11.G34.31.0057. S. Haffner and L. A. Pereira thank the CNPq for the research support associated with grants 303650/11-7 and 140357/13-0.

Appendix

Table 6 presents the line data of the system used in the test cases. The impedance equal to zero stands for a branch where there is a switch.

Table 6 Line data

Bus from	Bus to	R (Ω)	X (Ω)	Max (A)	Bus from	Bus to	R (Ω)	X (Ω)	Max (A)	Bus from	Bus to	R (Ω)	X (Ω)	Max (A)
8663	8313	0.0003	0.0008	419	8330	8331	0.0446	0.0202	113	8640	8635	0.0376	0.0252	138
8313	8667	0.0009	0.0022	419	8333	8422	0.8056	0.3653	113	8644	8640	0.0648	0.0595	195
8667	8668	0.0010	0.0024	419	8336	8337	0.0693	0.0314	113	8644	8774	0.0000	0.0000	–
8668	8665	0.0003	0.0008	419	8342	8455	0.0182	0.0167	195	8649	8336	0.5473	0.2482	113
8665	8765	0.0092	0.0149	293	8348	8293	0.0718	0.0660	195	8693	8676	0.2167	0.1993	195
8765	8406	0.0013	0.0021	293	8348	8354	0.4367	0.2056	101	8701	8702	0.0000	0.0000	–
8406	8233	0.6106	0.9880	293	8354	8620	0.2403	0.1131	101	8702	8728	0.0490	0.0222	113
8233	8493	0.5862	0.7236	282	8354	8874	0.0505	0.0238	101	8709	8701	1.8086	0.8202	113
8493	8487	0.1496	0.1846	282	8360	8264	0.1827	0.1680	195	8709	8311	0.0000	0.0000	–
8487	8488	0.0064	0.0080	282	8379	8380	0.0000	0.0000	–	8715	8709	0.3157	0.1431	113
8488	8486	0.0420	0.0518	282	8380	8867	0.0272	0.0336	282	8728	8333	1.1721	0.5315	113
8486	8208	0.0431	0.0532	282	8397	8314	0.0000	0.0000	–	8729	8989	0.3262	0.1479	113
8208	8811	0.1608	0.1984	282	8400	8644	0.0359	0.0330	195	8774	8773	0.0476	0.0308	150
8811	8970	0.0415	0.0513	282	8400	8775	0.0000	0.0000	–	8775	8772	0.0919	0.0417	113
8970	8969	0.0000	0.0000	–	8402	8507	0.1940	0.0880	113	8784	8700	0.0134	0.0123	195
8969	8477	0.3480	0.4296	282	8402	8494	0.6941	0.3147	113	8784	8804	0.3118	0.2867	195
8477	8968	0.0494	0.0609	282	8405	8616	0.2242	0.2062	195	8786	8277	0.1060	0.0975	195
8968	8404	0.5480	0.6765	282	8415	8566	0.0066	0.0063	184	8787	8786	0.0277	0.0254	195
8404	8207	0.0185	0.0228	282	8422	8432	0.7346	0.3331	113	8788	8822	0.0847	0.0779	195
8207	8300	0.0086	0.0107	282	8432	8433	0.1996	0.0905	113	8797	8282	0.3341	0.3073	195
8300	8250	0.0006	0.0009	293	8455	8405	0.0125	0.0115	195	8804	8797	0.2314	0.2128	195
8250	8227	0.0051	0.0083	293	8455	8476	1.6991	1.5626	195	8809	8784	0.1285	0.1182	195
8227	8379	0.0879	0.1085	282	8477	8415	0.0000	0.0000	–	8811	8966	0.0000	0.0000	–
8379	8598	0.1620	0.2000	282	8494	8268	0.0302	0.0137	113	8822	8360	2.7636	2.5415	195
8598	8600	0.0000	0.0000	–	8497	8787	0.3453	0.3175	195	8822	8305	0.0000	0.0000	–
8600	8325	0.0200	0.0246	282	8499	8503	0.2603	0.2394	195	8841	8211	0.8684	0.3938	113
8325	8585	0.8192	1.0112	282	8503	8497	0.1882	0.1731	195	8841	8837	0.5473	0.2482	113
8585	8593	0.4403	0.5435	282	8503	8505	0.0000	0.0000	–	8841	8334	0.5451	0.2472	113
8593	8788	0.2660	0.3284	282	8505	8962	4.8429	2.1961	113	8874	8878	0.2563	0.1207	101
8968	8549	0.0022	0.0036	293	8507	8847	0.9989	0.4530	113	8883	8885	0.0000	0.0000	–
8549	8550	0.0018	0.0030	293	8515	8499	0.1802	0.1657	195	8885	8886	0.0017	0.0011	150
8207	8249	0.0047	0.0058	282	8545	8809	0.0162	0.0149	195	8886	8884	0.0323	0.0217	138
8208	8209	0.0021	0.0019	195	8546	8972	0.0068	0.0110	293	8905	8906	0.1449	0.0657	113
8209	8990	0.1547	0.1423	195	8549	8546	0.0000	0.0000	–	8905	8914	0.0000	0.0000	–
8211	8402	0.3128	0.1418	113	8566	8400	0.0614	0.0565	195	8906	8918	0.1354	0.0614	113
8263	8515	1.7526	1.6117	195	8568	8572	0.1274	0.1172	195	8906	8916	0.0000	0.0000	–
8264	8263	0.0000	0.0000	–	8568	8889	0.0185	0.0124	138	8912	8905	1.2862	0.5833	113
8277	8568	0.1274	0.1172	195	8571	8342	0.2358	0.2168	195	8916	8910	0.0650	0.0295	113
8277	8779	0.0151	0.0139	195	8572	8571	0.0646	0.0594	195	8918	8920	0.0408	0.0185	113
8282	8649	0.7794	0.3534	113	8585	8586	0.0000	0.0000	–	8962	8330	0.7122	0.3230	113
8282	8693	0.7954	0.7315	195	8586	8587	0.0008	0.0010	282	8962	8912	0.0053	0.0024	113
8293	8883	0.0715	0.0480	138	8587	8841	0.5556	0.2520	113	8966	8965	0.0242	0.0162	138
8293	8601	0.4093	0.3764	195	8615	8630	0.0332	0.0306	195	8968	8860	0.0068	0.0084	282
8493	8303	0.0142	0.0095	138	8616	8615	0.0214	0.0197	195	8990	8397	0.0498	0.0458	195
8303	8882	0.0449	0.0204	113	8620	8873	0.4044	0.1904	101	8990	8994	0.1193	0.1142	184
8305	8319	1.8214	0.8260	113	8630	8545	0.8419	0.7742	195	8994	9006	0.0000	0.0000	–
8311	8310	0.4125	0.1871	113	8632	8581	0.0718	0.0482	138	9002	9007	0.0042	0.0040	184
8314	8315	0.0421	0.0387	195	8632	8634	0.0067	0.0045	138	9006	9002	0.2229	0.2133	184
8317	8327	0.3102	0.1407	113	8635	8639	0.1306	0.0877	138	9007	9008	0.0006	0.0006	184
8319	8715	2.0702	0.9388	113	8639	8389	0.0834	0.0798	184	9008	8252	0.0460	0.0493	370
8319	8317	0.0051	0.0023	113	8640	8348	0.2250	0.2069	195					
8319	8729	0.0000	0.0000	–	8640	8632	0.0477	0.0320	138					

References

1. Bagheri A, Monsef H, Lesani H (2015) Integrated distribution network expansion planning incorporating distributed generation considering uncertainties, reliability, and operational conditions. International Journal of Electrical Power & Energy Systems 73:56–70
2. Delfanti M, Falabretti D, Merlo M (2013) Dispersed generation impact on distribution network losses. Electric Power Systems Research 97:10–18
3. Donadel C, Fardin J, Encarnao L (2015) Electrical distribution network operation with a presence of distributed generation units in a pre smart grid environment using a clustering-based methodology. Energy Systems pp 1–23
4. Gallego R, Monticelli A, Romero R (2001) Optimal capacitor placement in radial distribution networks. Power Systems, IEEE Transactions on 16(4):630–637
5. Ganguly S, Sahoo N, Das D (2010) A novel multi-objective pso for electrical distribution system planning incorporating distributed generation. Energy Systems 1(3):291–337
6. Haffner S, Pereira L, Pereira L, Barreto L (2008) Multistage model for distribution expansion planning with distributed generation part i: Problem formulation. Power Delivery, IEEE Transactions on 23(2):915–923
7. Haffner S, Pereira L, Pereira L, Barreto L (2008) Multistage model for distribution expansion planning with distributed generation part ii: Numerical results. Power Delivery, IEEE Transactions on 23(2):924–929
8. ILOG I (2009) IBM ILOG CPLEX V12.1 User's Manual for CPLEX. IBM
9. Ochoa L, Harrison G (2011) Minimizing energy losses: Optimal accommodation and smart operation of renewable distributed generation. Power Systems, IEEE Transactions on 26(1):198–205
10. Pardalos P, Resende M (2002) Handbook of Applied Optimization. Oxford University Press
11. Persaud S, Fox B, Flynn D (2000) Impact of remotely connected wind turbines on steady state operation of radial distribution networks. Generation, Transmission and Distribution, IEE Proceedings- 147(3):157–163
12. Quezada V, Abbad J, Roman T (2006) Assessment of energy distribution losses for increasing penetration of distributed generation. Power Systems, IEEE Transactions on 21(2):533–540
13. Resener M, Haffner S, Pereira LA (2013) Representação aproximada de sistemas de distribuição em problemas de otimização. In: X Latin-American Congress on Electricty Generation and Transmission (CLAGTEE)
14. Singh A, Parida S (2015) Allocation of distributed generation using proposed dmsp approach based on utility and customers aspects under deregulated environment. International Journal of Electrical Power & Energy Systems 68:159–169
15. Sorokin A, Rebennack S, Pardalos P, Iliadis N, Pereira M (2012) Handbook of Networks in Power Systems I. Energy Systems, Springer Berlin Heidelberg
16. Van Hentenryck P, Lustig I (1999) The OPL Optimization Programming Language. Computing in Musicology; 11, MIT Press
17. Mariana Resener, Sérgio Haffner, Luís A. Pereira, Panos M. Pardalos (2016) Mixed-integer LP model for volt/var control and energy losses minimization in distribution systems. Electric Power Systems Research 140:895–905. http://dx.doi.org/10.1016/j.epsr.2016.04.015